The Mechanistic Link Between Type 2 Diabetes and Colorectal Cancer

Hannah L Thompson

Submitted in partial fulfilment of the requirements of the Degree of Doctor of Philosophy

Barts and The London School of Medicine and Dentistry

Queen Mary University of London

Primary Supervisor – Professor Andrew Silver

Secondary Supervisor – Dr Cleo Bishop

Contents

Statement of Originality

I, Hannah Thompson, confirm that the research included within this thesis is my own work or that where it has been carried out in collaboration with, or supported by others, that this is duly acknowledged below and my contribution indicated. Previously published material is also acknowledged below.

I attest that I have exercised reasonable care to ensure that the work is original, and does not to the best of my knowledge break any UK law, infringe any third party's copyright or other Intellectual Property Right, or contain any confidential material.

I accept that the College has the right to use plagiarism detection software to check the electronic version of the thesis.

I confirm that this thesis has not been previously submitted for the award of a degree by this or any other university.

Signature: Hannah Thompson

Date: 31 May 2018

Abstract

Compared to non-diabetics, type 2 diabetics (T2D) have a 30% increased risk of colorectal cancer (CRC), which exhibits more serious histopathological features and has an increased risk of recurrence. Cell stress following hyperglycaemia or hypoxia reduces fumarate hydratase (FH) activity promoting increased intracellular fumarate. Fumarate irreversibly modifies cysteine residues by succination to form 2-succino-cysteine (2-SC) which can inactivate proteins.

A significant increase in 2-SC staining was found in CRC compared to matched normal tissue and in tumours from T2D individuals compared to non-diabetics. Tumours positive for *KRAS* or *BRAF* mutation showed elevated staining, which was higher in T2D patients. Adenomas also showed 2-SC staining. The 2-SC staining was non-uniform across tumours, underlining metabolic heterogeneity of CRC.

Paradoxically, tumours showed intense cytoplasmic FH staining. In a mouse model of polyposis and diabetes, overexpression of cytoplasmic FH in the gut led to larger polyps. In CRC cells, fumarate increased and gene expression altered after mitochondrial stress *via* treatment with 25mM glucose and 0.2% oxygen: FH was active and increased in cells cultured without glucose; its activity inversely correlated with fumarate. Mitochondria function was higher in CRC cells without glucose, but cells retained their ability to utilise glucose metabolism pathways.

Separately, oxaliplatin therapy led to *DUOX2* transcription mediated by STAT1, whereas cetuximab treatment inhibited STAT1 activation, oxaliplatin-induced DUOX2 upregulation, and ROS generation. This may explain why CRC patients on oxaliplatin alone have a better prognosis than those treated with a combination of oxaliplatin and cetuximab.

This work has increased our understanding of CRC and aspects linked indirectly to mitochondria: diabetes mediating altered metabolism and potentially altered protein function. Dysregulated metabolism, as typified by FH dysfunction in CRC developing in the context of T2D, is significant and requires further investigation including identification of succinated proteins, which may give insights into improved therapies.

Publications arising from this work

Valeria Santoro, Ruochen Jia, **Hannah Thompson**, Anke Nijhuis, Rosemary Jeffery, Konstantinos Kiakos, Andrew R. Silver, John A. Hartley, Daniel Hochhauser. Role of Reactive Oxygen Species in the Abrogation of Oxaliplatin Activity by Cetuximab in Colorectal Cancer. Journal of the National Cancer Institute, 2016 June 1;108(6): djv394. doi.org/10.1093/jnci/djv394.

Publications in preparation

Hannah Thompson, Julie Adam, Kathryn Lynes, Amy Lewis, Hayley Davies, Rosemary Jeffery, Liliane Eleid, David Propper, Roger Feakins, Neel Sengupta, Anil Ghosh, Simon Leedham, Mohammed Thaha, Tomoyoshi Soga, Norma Frizzell, Dmitri Mouradov, Oliver M. Sieber, Ian Tomlinson Cleo Bishop, Andrew Silver. Heterogeneous epigenetic changes are influenced by type 2 diabetes in colorectal adenomas and cancers.

Other publication

Anke Nijhuis, **Hannah Thompson**, Julia Adam, Alexandra Parker, Luke Gammon, Amy Lewis, Jake Bundy, Tomoyoshi Soga T, Aleshi Jalaly, David Propper, Rosemary Jeffery, Nirosha Suraweera, Sarah McDonald, Mohammed Thaha, Roger Feakins, Robert Lowe, Cleo Bishop, Andrew Silver. Remodelling of microRNAs in colorectal cancer by hypoxia alters metabolism profiles and 5-fluorouracil resistance. Hum Mol Genet. 2017 Apr 15;26(8):1552-1564. doi: 10.1093/hmg/ddx059.

Sarah-Jane Walton, Amy Lewis A, Rosemary Jeffery, **Hannah Thompson**, Roger Feakins, Eleni Giannoulatou, Christopher Yau, James Lindsay, Susan Clark, Andrew Silver. Familial adenomatous patients with desmoid tumours show increased expression of miR-34a in serum and high levels in tumours. Oncoscience. 2016 Jun 30;3(5-6):173-85. doi: 10.18632/oncoscience.312.

Acknowledgements

This thesis would not be the same without the care and attention paid by my supervisors Professor Andy Silver and Dr Cleo Bishop as well as Dr Julie Adam. I'd like to thank Andy for giving me such a novel and exciting research topic as well as tirelessly looking over my written work. I'd like to thank Cleo for her help with absolutely everything when required, but especially Chapter 5. I have learnt a lot from Cleo's approach to experimental work. I'd like to thank Julie for allowing me to be part of this exciting field of work and for letting me learn as much as possible in my time alongside her at Oxford Centre for Diabetes, Endocrinology and Metabolism in Oxford for the experimental work presented in Chapter 3.

I'd like to thank the members of the Silver lab. Especially Dr Anke Nijhuis for teaching me the ins and outs of The Blizard Institute and being a fantastic friend. Dr Amy Lewis for helping with various analysis problems. Dr Sham Mehta for reminding me that if he can complete a PhD with small kids and a consultant position, then so can I! Rosemary Jeffery for teaching me histological techniques and inspiring me to travel the world even more. I'm also grateful to two of my fantastic students, Liliane and Anthony who contributed to this thesis and who allowed me to practise explanations of my work on them!

There's also other members of The Blizard Institute who helped me along my journey. Dr Luke Gammon thanks for teaching me how to use the InCell. Professor Tom Vuilliamy and Professor Denise Sheer thanks for critically assessing the progress of my PhD at 9 and 18 months. And to the rest of the PhD students I interacted with either through socials, lunch club, in the lab or at start-up competitions - Heather, Emma, Ellie, Kasia, Ngoc, Deb, Maddi, Debbie, Joanna, Inva, Stef, Paul, Harry, Amy, Chris, Lisa, Farrell and more – thank you! Ofcourse I can't forget the Nucleus café staff for providing me with a baked potato for most of my lunches and the post room guys for being so friendly. All of you helped with the everyday life of my PhD.

I'd also like to put a special mention to Kimberley Freeman, Public Engagement Manager at QMUL who gave me many opportunities to speak about my research, and is the catalyst for my following success with stand-up comedy about science.

My family and friends have also been a source of support throughout my PhD. Special mention to other members of the Talent Factory (science communication and performance development programme). As well as my work colleagues at Cambridge Cancer Genomics who have been very understanding.

Finally, I'd like to thank the Constance Travis Trust for financially supporting my PhD. It has been a pleasure to meet with Tony and Peta over the course of my PhD to hear their stories and get to know them.

List of figures

List of tables

Table of abbreviations

Abbreviation	Description
2-SC	2-succino cysteine
20AARs	20 amino acid repeats
5-FU	5-fluorouracil
5-mC	5-methylcytosine
AFAP	attenuated FAP
ALDH4	aldehyde dehydrogenase 4
AML	acute myeloid leukaemia
APC	adenomatous polyposis coli
ATP	adenosine triphosphate
AXIN2	axis inhibition protein 2
BMI	body mass index
BMPR1A	bone morphogenetic protein receptor type 1A
BSA	bovine serum albumin
CA	carbonic anhydrase
CA 19-9	carbohydrate antigen
CAPOX	capecitabine with oxaliplatin
CBP	CREB binding protein.
CD	Crohn's disease
CE-TOF/MS	capillary electrophoresis time of flight mass spectrometry
CEA	carcinoembryonic antigen
CI	confidence intervals
CIMP+	CpG island methylator phenotype positive
CIN	chromosomal instable
CK1	casein kinase 1
CKO	conditional knock out
COX	cytochrome C oxidase
CpG	5'—C—phosphate—G—3'
CRC	colorectal cancer
CT	computerised tomography
DAB	3,3-diaminobenzine
DCC	deleted in colorectal carcinoma
DM	Diabetes mellitus
DMEM	Dulbecco's modified Eagle's Medium
DMT	dimethylfumarate
DNA-PK	DNA-dependent protein kinase
DPX	distyrene plasticiser xylene

DUOX	dual oxidase
Dvl	dishevelled homolog DVL-1
EGFR	epidermal growth factor receptor
EMT	epithelial to mesenchymal transition
ENU	ethylnitorsourea
EPOC	Eloxatin Peri-Operative Chemotherapy
ERK	extracellular signal-regulated kinase
ETC	electron transport chain
FAD	flavin adenosine dinucleotide
FAP	familial adenomatous polyposis
FBS	fetal bovine serum
FBXW7	F-box and WD repeat domain containing 7
FFPE	formalin fixed paraffin embedded
FH	fumarate hydratase
FOBT	faecal occult blood test
FOLFIRI	5-FU with irinotecan
FOLFOX	5-FU with oxaliplatin
GAPDH	glyceraldehyde 3-phosphate dehydrogenase
GLUT	glucose transporter
GSH	glutathione
GTP	guanosine triphosphate
H_2O_2	hydrogen peroxide
HIF	hypoxia inducible factor
HK	hexokinase
HLRCC	hereditary leiomyomatosis and renal cell cancer
HNPCC	hereditary non-polyposis colorectal cancer
HRE	hypoxia response elements
HRP	horseradish peroxidase
IBD	inflammatory bowel disease
IDH	isocitrate dehydrogenase
IDMM	insulin-dependent diabetes mellitus
IGF	insulin-like growth factor
IHC	immunohistochemistry
IL	interleukin
ISCU	iron-sulphur cluster assembly enzyme
ISH	in situ hybridisation
JAK	janus kinase
KDM	lysine demethylase

KEAP	kelch-like ECH-associated protein
KRAS	Kirsten rat sarcoma
LB	large bowel
LDH	lactate dehydrogenase
lef	lymphoid enhancer factor
LOH	loss of heterozygosity
LPR	lipoprotein receptor
LS	Lynch syndrome
LSL	lox-stop-lox
MACS	microsatellite and chromosomal stable
MAP	MUTYH-associated polyposis
MAPK	mitogen activated protein kinase
MAX	MYC-associated protein X
MCT	monocarboxylate transporter
MEF	myocyte enhancer
MEFs	mouse embryonic fibroblasts
MEX3C	mex-3 homolog C
Min	multiple intestinal neoplasia
miRNA	micro RNA
MLH1	MutL homolog 1
MMR	mismatch repair
MMT	mono-methyl fumarate
MRI	magnetic resonance imaging
MS	multiple sclerosis
MSH	MutS homolog
MSI	microsatellite instable
mtDNA	mitochondrial DNA
mTOR	mammalian target of rapamycin
MX11/MAD2	MAX interactor 1
MXD1/MAD	MAX dimerisation protein
MYC	v-myc avian myelocytomatosis viral oncogene homolog
NADH	nicotinamide adenine dinucleotide
NADPH	nicotinamide adenine dinucleotide phosphate
NBF	neutral buffered formalin
NF-kB	nuclear
NFκB	nuclear factor κB
NHS	National Health Service
NOX	NADPH oxidase
NRF2	nuclear factor (erythroid-derived 2)-like 2

OGDD	oxoglutarate dependent dioxygenases
OXPHOS	oxidative phosphorylation
PAI	plasminogen activator inhibitor
PBS	phosphate buffered saline
PBS-T	PBS Tween
PCR	polymerase chain reaction
PDK	pyruvate dehydrogenase kinase
PET	positron emission tomography
PGAM	Phosphoglycerate Mutase
PHD	prolyl hydroxylase domain-containing protein
PI3K	phosphatidylinositol 3-kinase
PIGN	phosphatidylinositol glycan anchor biosynthesis class N
PKC	protein kinase c
PLC	phospholipase C
PMS	post-meiotic segregation
POLD1	DNA polymerase delta
POLE	DNA polymerase epsilon
PTEN	Phosphatase and tensin homolog
RBFOX1	fox-1 homolog 1
ROS	reactive oxygen species
RR	relative risk
RT	reverse transcription
SB	small bowel
SDH	succinate dehydrogenase
SEER	Epidemiology and End Results
SMAD	Smooth mothers against decapentaplegic homolog
SNP	single nucleotide polymorphism
Sp1	specificity protein 1
SRC	cellular Src kinase
STAT	signal transducer and activator of transcription
STK11	serine threonine kinase 11
SUR	sulfonylurea receptor
T1D	type 1 diabetes
T2D	type 2 diabetes
TAZ	tafazzin
TCA	tri-carboxylic acid
tcf	T-cell factor
TCGA	the cancer genome atlas

TET	ten-eleven-translocation
TGFß	transforming growth factor ß
TGFßR2	transforming growth factor ß receptor 2
TIGAR	TP53 Induced Glycolysis Regulatory Phosphatase
TNF-a	tumour necrosis factor alpha
TP53	tumour protein 53
UC	ulcerative colitis
US	united states
VEGF	vascular endothelial growth factor
VHL	von Hippel-Lindau
WHO	World Health Organisation
ZNF516	zinc finger protein 516

Chapter 1 – Introduction

1.1. Colorectal cancer background

Colorectal cancer (CRC) is a malignant epithelial tumour arising from the large intestine, which comprises the colon and rectum (Figure 1.1). In 2015, the office for national statistics found that CRC was the third most common cancer for both males and females in the UK; there were 34,729 cases, with 19,178 for males and 15,551 for females[1].

Worldwide, CRC is the third most common cancer and the fourth most common cancer cause of death[2]. In total, CRC accounts for 9% of cancer-related deaths worldwide, of which 90% are from metastasis[3]. In developed countries, almost half of the population will develop at least one benign intestinal tumour (adenoma) during their lifetime[2]. Although CRC survival has increased year on year since the 1960's[4], survival rates are still poor with no significant difference in mortality between male and female cases (Table 1.1).

The most obvious symptoms of CRC are blood in the faeces, a change in bowel habit and abdominal pain[5] although these are often associated with other conditions, such as infection and inflammatory bowel disease (IBD), leading to problems with CRC diagnosis.

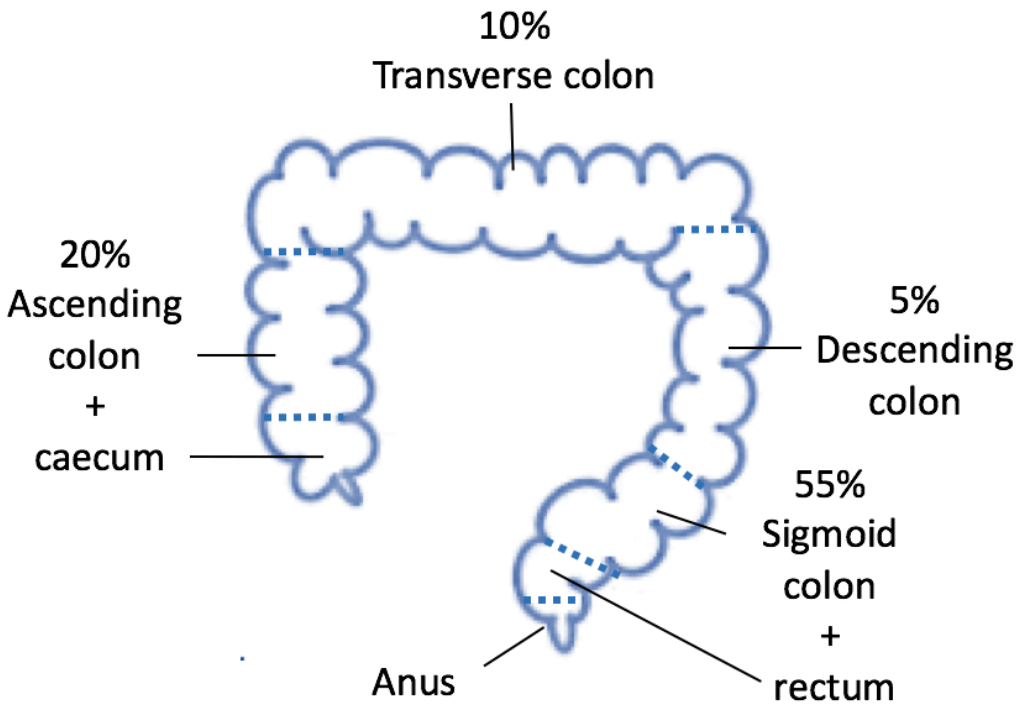

Figure 1.1. CRC incidence per large bowel section. Fifty five percent of CRC tumours are located in the recto-sigmoid section, 20% in the caecum and ascending colon, 10% in the transverse colon and 5% in the descending colon[6,7](10% undescribed location).

Table 1.1. Bowel cancer statistics. Survival statistics for patients up to 10 years post CRC diagnosis. Figures from Cancer Research UK 2010-2011[8].

	Survival (%)		
Years post-diagnosis	**All adults**	**Men**	**Women**
0	100	100	100
1	75.7	77.4	73.9
2	67.9	69.5	66.3
3	63.2	64.5	61.9
4	60.4	61.2	59.5
5	58.7	59.2	58.2
6	57.7	57.5	58.0
7	57.1	57.2	57.1
8	56.8	56.6	57.0
9	56.6	56.3	57.1
10	56.6	56.0	57.2

1.2. Molecular genetics of colorectal cancer

The epithelium of the large bowel consists of tens of millions of crypts which are home to intestinal stem cells that multiply to renew the crypt every three to six days. A model of CRC progression, which was initially proposed in 1990 by Fearon and Vogelstein, where CRC results from the progressive accumulation of genetic and epigenetic alterations in colonic epithelium, remains a basic paradigm for the molecular genetics of CRC to date[9] (Figure 1.2). Sequential mutations in adenomatous polyposis coli (*APC),* Kirsten rat sarcoma *(KRAS)* and smooth mothers against decapentaplegic homolog (*SMAD) 2/4* lead to transitions through early, intermediate and late adenoma, respectively. A loss of function mutation in tumour protein 53 (*TP53*) transforms the adenoma into a carcinoma. Subsequent genetic mutations occur which promote carcinogenesis and metastasis (Figure 1.2).

Large scale sequencing of CRC tissue has demonstrated the presence of tens of thousands of somatic mutations in intestinal cancer cells, although only a handful of these are considered essential or "drivers" for tumourigenesis; the true impact of the many genes identified in the development of CRC remains incomplete[10–12].

APC is mutated in the majority (>80%) of sporadic CRC[13]. APC is a key protein in the Wnt signalling pathway where it acts as a negative regulator, controlling β-catenin levels in the cell (Figure 1.3.A). Constitutive activation of Wnt signalling within the crypts of the colon promotes extensive proliferation of the stem cells and the subsequent development of tumours[14,15]. This is due to the actions of β-catenin as a co-ordinator of cell–cell adhesion and gene transcription (Figure 1.3.B)[16]. Interestingly, genetic alterations in *APC* do not lead to a complete loss of APC protein function[17]. Mutations in *APC* are usually bi-allelic and occur at non-random positions with respect to each other[18]. *APC* mutations cluster in codon 1282-1581 to produce truncated proteins which retain 1-3 of the 20 amino acid repeats (20AARs) that are critical functional domains for binding of β-catenin (Figure 1.3.C)[19]. Proximal CRC tumours show enrichment for mutations which retain 2-3 20AARs whereas distal cancers predominantly have *APC* mutations which retain 0-1 20AARs indicating selection of distinct Wnt/β-catenin signalling which is favourable for tumour progression dependent on location, as described by the "just-right" theory[19,20]. When *APC* is mutated, β-catenin is able to translocate to the nucleus where it binds to other

transcription factors to form a complex, which leads to the transcription of Wnt target genes involved in proliferation and differentiation pathways[21]. Mutations in other key players of the Wnt pathway, such as axis inhibition protein 2 (AXIN2) and β-catenin, are also common in CRC[22].

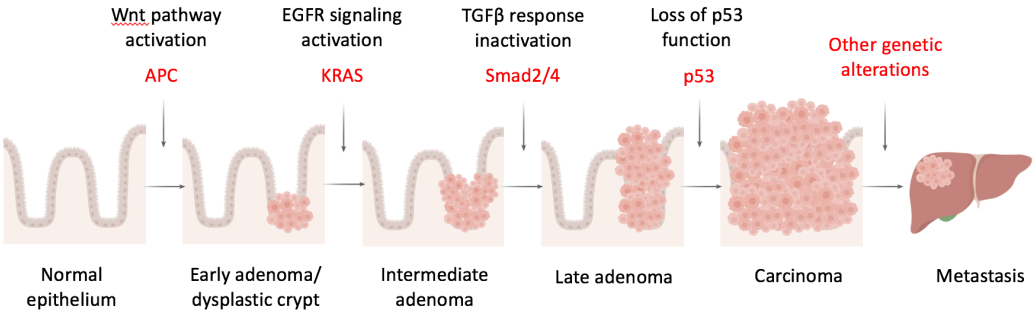

Figure 1.2. Fearon and Vogelstein model of CRC progression. First, a mutation in *APC* leads to activation of the Wnt pathway, which leads to an early adenoma. Next, a mutation in *KRAS* leads to activation of the EGFR pathway, promoting transformation to an intermediate adenoma. Then, mutations in *Smad 2/4* lead to TGFß pathway inactivation and transformation to a late adenoma. A loss of function mutation in *p53* then leads to carcinoma formation, with additional genetic mutations occurring which promote metastasis[23]. APC, adenomatous polyposis coli; KRAS, Kirsten rat sarcoma; EGFR, epidermal growth factor receptor; SMAD, mothers against decapentaplegic homolog; TGFß, transforming growth factor ß.

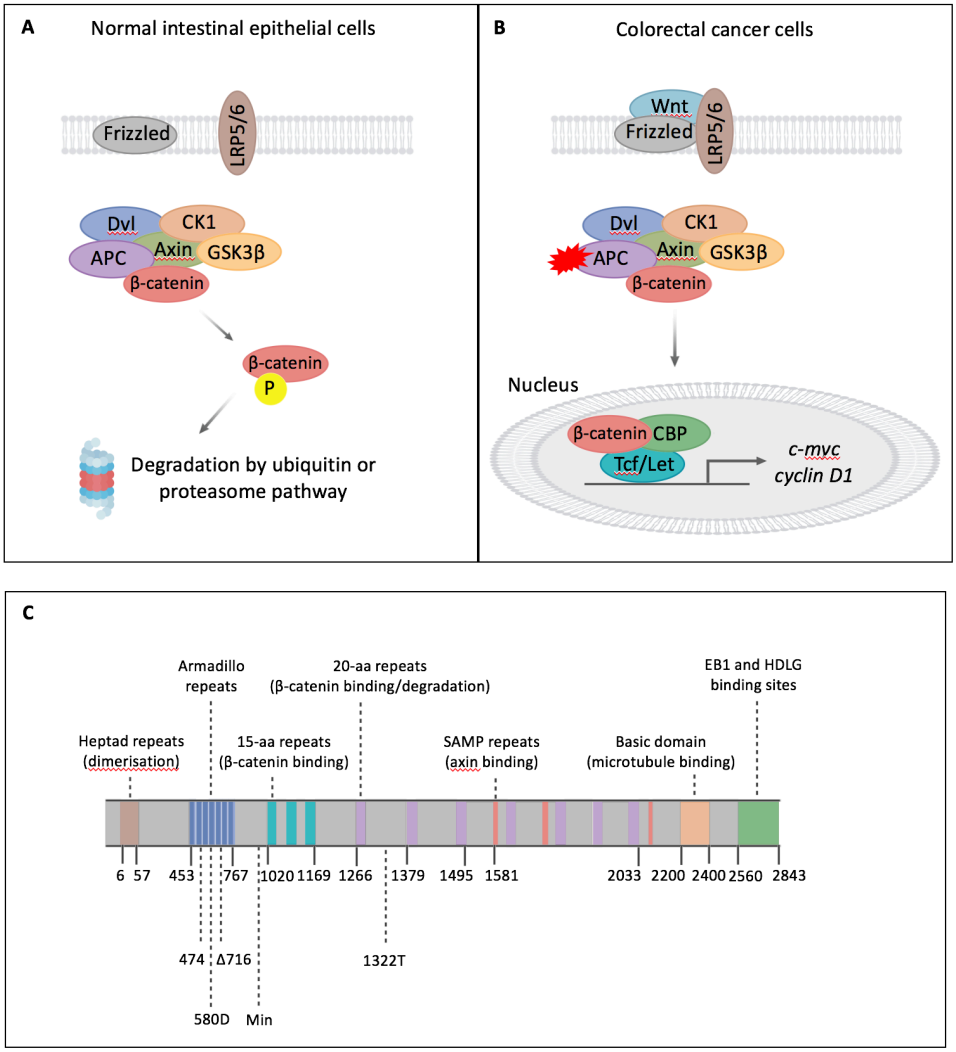

Figure 1.3. The Wnt pathway and APC mutations in CRC. (**A**) The Wnt signalling pathway which controls β-catenin levels in the cell. (**B**) A mutation in APC leads to changes in cell proliferation, cell polarity, cell migration and cell fate due to the actions of β-catenin as a co-ordinator of cell–cell adhesion and gene transcription (**C**) *APC* mutations cluster in codon 1282-1581 to produce truncated proteins which retain 1-3 of the 20AARs that are critical functional domains for binding of β-catenin, adapted from Pollard *et al* 2009[15]**.** APC, adenomatous polyposis coli; 20AARs, 20 amino acid repeats; LRP, lipoprotein receptor; Dvl, dishevelled homolog Dvl-1; CK1, casein kinase 1; GSK, glycogen synthase; CBP, CREB binding protein; Tcf, T-cell factor; Lef, lymphoid enhancer factor; myc, v-myc avian myelocytomatosis viral oncogene homolog.

Approximately 54% of all CRC cases harbour mutations in tumour protein 53 (*TP53)* which is commonly known as the "The guardian of the genome"[24]. *TP53* is the most frequently mutated tumour suppressor gene (TSG) in all human cancers[25]. A *TP53* mutation is a late event in the adenoma-carcinoma sequence[26]. DNA damage and genotoxic stress results in induction of oncogenic TP53 which leads to cell proliferation[27].

The third most frequent mutation in CRC is the *KRAS* oncogene which is mutated in 40% of CRC tumours, and only found alongside an *APC* mutation[28]. The RAS protein is an on/off switch for the epidermal growth factor receptor (EGFR) pathway. Another member of the EGFR pathway, BRAF is mutated in 10% of CRC tumours[29]. Mutations in *RAS* and *RAF* result in a permanent activation of the EGFR pathway (Figure 1.4), resulting in cell proliferation.

Additional genetic alterations are observed in 70% of CRCs[23]. Some examples are loss of the 18q chromosome segment which harbours a number of key genes including deleted in colorectal carcinoma (*DCC*)[30], *SMAD*2[31] and *SMAD4* [32]. Both SMAD2 and 4 mediate the transforming growth factor beta (TGF-β) pathway, which in turn regulates cell growth and differentiation. Recent studies have identified three genes encoded on the 18q chromosome which are lost in 79% of CRC tumours: phosphatidylinositol glycan anchor biosynthesis class N (*PIGN*); mex-3 homolog C (*MEX3C*); and zinc finger protein 516 (*ZNF516*)[33].

Intra-tumour heterogeneity results in therapy resistance as well as disease recurrence across all cancers[34]. Although CRCs are largely a result of clonally derived cell populations from a smaller number of long-lived lineages from the crypt[35,36] (Figure 1.2), sub-clonal expansion is also found[37,38].

Despite tumour heterogeneity, the majority of CRCs (~80%) can be divided into three groups by their distinctive genetic alterations: chromosomal instable (CIN), microsatellite instable (MSI) tumours and microsatellite and chromosomal stable (MACS) tumours[33,39,40].

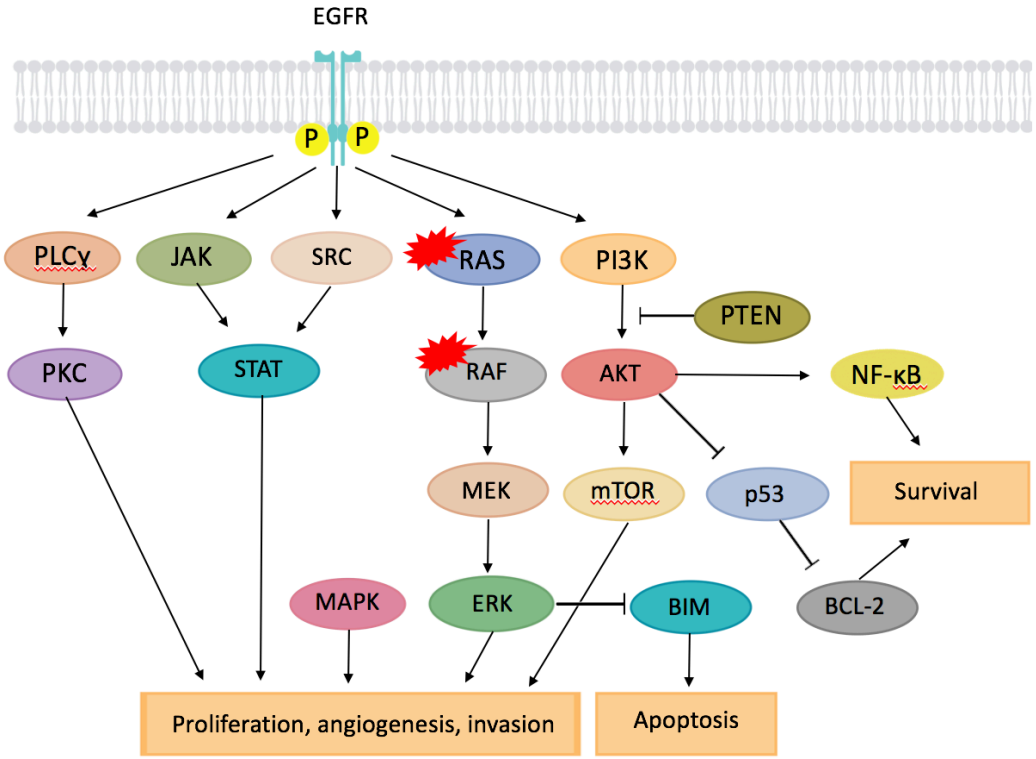

Figure 1.4. The epidermal growth factor receptor pathway. This pathway regulates cell survival, proliferation, angiogenesis, invasion and apoptosis. Mutations in RAS and RAF lead to permanent activation of the pathway, resulting in uncontrolled cell growth and therefore tumour promotion[41]. EGFR, epidermal growth factor receptor; PLC, phospholipase C; JAK, janus kinase; SRC, cellular Src kinase; PI3K, phosphatidylinositol 3-kinase; PKC, protein kinase C; STAT, signal transducer and activator of transcription; PTEN, phosphatase and tensin homolog; NF-κB, nuclear factor κB; MEF, myocyte enhancer; mTOR, mammalian target of rapamycin; MAPK, mitogen activated protein kinase; ERK, extracellular signal related kinase; BIM, Bcl-2 like protein 11; BCL-2, B-cell lymphoma 2.

1.2.1. Chromosomal Instability

CIN develops in the large majority (~60%) of CRC cases and is characterised by an accelerated rate of allelic gains or losses and gross chromosomal abnormalities. CIN tumours therefore have an imbalance in chromosome number (aneuploidy) and a high frequency of loss of heterozygosity (LOH) where an entire gene and the surrounding chromosome region are lost. Frequently mutated genes in CIN tumours are *APC*, *TP53* and *KRAS* [33]. CIN tumours have recently been divided into two groups depending on telomere length. Near-tetraploid CIN tumours have significantly longer relative telomere length compared to CIN- and aneuploidy tumours, whereas CIN tumours with larger numbers of chromosome breaks have significantly shorter relative telomere length[42].

1.2.2. Microsatellite Instability

MSI occurs in around 15% of all CRC cases, of which 3% are associated with Lynch syndrome (LS, also known as Hereditary Non-Polyposis Colorectal Cancer (HNPCC)) and 12% are sporadic. MSI is characterised by overall genetic hyper mutation as a result of functional loss of DNA mismatch repair (MMR) genes[43]. The MMR system consists of six genes: MutL homolog 1 (*MLH1*), MutS homolog (*MSH*) 2, *MSH3*, *MSH6*, post-meiotic segregation (*PMS*)-1 and *PMS2*[44]. When the MMR system is impaired, genome-wide mutations accumulate during DNA replication, usually within microsatellites (repetitive DNA sequences such as (A)n or (CA)n repeats), giving rise to MSI and eventually cancer. Cancers with high MSI have better clinical outcome then low or non-MSI tumours[39] but are also shown to be more resistance to first line drug treatments such as 5-fluorouracil (5- FU)[45].

A subgroup of MSI tumours are 5'—C—phosphate—G—3' (CpG) island methylator phenotype positive (CIMP+), due to hyper methylation in the promoter of the MMR gene *MLH1*[46]. CIMP+ cancers are more frequently observed in the proximal colon compared to distal colon and rectal cancers[47].

1.2.3. Microsatellite and chromosome stable

A third subgroup of tumours that are neither CIN nor MSI was first described in 1999 by Georgiades and colleagues[48]. MACS tumours are more likely to develop in younger patients[49] and are localised to the distal colon as well as being poorly differentiated and more invasive at the time of diagnosis[40]. This subgroup has stable, near-diploid chromosomes and stable microsatellites.

1.3. Cell lines as a model for human CRC

As described above there are a variety of CRC molecular phenotypes observed in patients. It is essential that cell lines represent the spectra of mutations and DNA copy-number aberrations in primary tumours, and that these are known. Whole-exome sequencing and single nucleotide polymorphism (SNP) microarray analysis of 70 CRC cell lines established that overall cell lines represent primary tumours at the genomic level[50].

In a recent paper by Sieber *et al*. the proteomes of CRC cell lines have also been found to represent primary tumours; proteomic analysis was performed on 44 CRC cell lines and compared to 95 primary CRCs[51].

1.4. Risk factors for CRC

Countries with the highest incidence rates of CRC include Australia, New Zealand, Canada, the United States, and parts of Europe, whereas the countries with the lowest risk include China, India, and parts of Africa and South America[52]. The variation in incidence could be due to available diagnostic and treatment options[2] as well as several genetic and environmental risk factors that increase a person's chance of developing CRC. These are described below.

1.4.1. Age

CRC is predominantly a disease of the elderly population, with an average age at diagnosis of 70 years old. Almost nine out of 10 patients diagnosed in the UK are over 60[53]. However, the average age of onset is decreasing and more people under the age of 50 are being diagnosed[53]. The United States National 1987-2006 Surveillance, Epidemiology and End Results (SEER) data showed increased colon and rectal cancer incidence in individuals

between 20 and 49 years, with the largest increase seen in the 40-44 years old bracket (10.7 per 100,000 population in 1988 and 17.9 per population in 2006)[54]. This is worrying as currently all diagnostic screening in the UK is carried out in people 55 years and above.

1.4.2. Inherited CRC syndromes

Around 75% of all CRCs occur sporadically with no obvious inherited gene mutation or notable family history. The remaining CRC cases are hereditary CRC syndromes with specific genetic mutations (2-6%) or familial CRC (~20%), where at least one blood relative has CRC without a specific germline mutation[55]. Hereditary CRC syndromes (Table 1.2) are highly penetrant and passed on to offspring in a Mendelian manner. The most common form of hereditary CRC is LS, which is an autosomal dominant condition where individuals harbour mutations in DNA MMR genes, most commonly in *MSH2*, *MLH1*[56], *MSH6* and *PMS2*[57]. These patients have a cumulative risk of developing CRC of 60-70% in men and 30-40% in women[58,59]. LS patients also have an increased risk of developing other cancers such as endometrial and stomach cancers[60–62]. Familial adenomatous polyposis (FAP) is the second most common hereditary CRC syndrome and is well characterised; patients develop many precancerous colonic polyps in their mid-teens. FAP patients carry a mutation in one *APC* allele[63,64]. The location of the 'second hit' mutation which causes progression to FAP in linked to the location of the initial mutation. FAP patients with germline *APC* mutations within codons 1194-1392 show allelic loss in their colorectal adenomas in contrast to FAP patients whose 'second hits' occur by truncating mutations in the mutation cluster region[17]. Disease severity has also been linked to the site of the germline *APC* mutation: patients with a deletion at codon 1309 have significantly more colorectal polyps at colectomy than age and sex matched FAP controls[65]. Nearly all FAP patients will go on to develop CRC by the time they reach 40 years of age. The recommended management for germ-line positive members of families with FAP is early surveillance with endoscopy and genetic tests to identify individuals who have inherited an *APC* germline mutation. Total resection of the colon is advised for patients that test positive for FAP usually during their late teens[66].

Attenuated FAP (AFAP) is a subtype of FAP[67]. AFAP patients develop polyps after 40 years which is much later than FAP patients, and the polyp number in AFAP patients is less than 100, much lower than FAP patients where there can be up to 5,000[67].

Table 1.2. Hereditary and hamartoma CRC syndromes. Hereditary CRC syndrome features and associated genetic mutations.

Syndrome	Features	Genetic mutation(s)	References
Lynch syndrome	Early onset, multiple colorectal polyps, ~80% penetrance	*MSH2, MSH6, MLH1, PMS2*	[57,59,62]
Familial adenomatous polyposis	100-5000 adenomatous colorectal polyps, 100% penetrance	*APC*	[64,68]
MUTYH-associated polyposis	Multiple adenomatous colonic polyps (10- 100)	*MUTYH*	[69,70]
Peutz-Jeghers	Hamartomatous GI polyps (5-100), ~40% penetrance	*Serine threonine kinase 11 (STK11)*	[71,72]
Juvenile polyposis	Early onset, Hamartomatous GI polyps (50-200), 10-40% penetrance	*SMAD4, bone morphogenetic protein receptor type 1A (BMPR1A)*	[73]
Polymerase proofreading-associated polyposis	Early onset, multiple adenomas, dominant inheritance	*DNA polymerase epsilon (POLE), DNA polymerase delta 1 (POLD1)*	[74]

Other hereditary CRC syndromes are MUTYH-associated polyposis (MAP) and the more recently described polymerase proofreading-associated polyposis. Hamartoma syndromes such as Peutz-Jeghers and Juvenile polyposis are also associated with an increased risk of developing cancer. See Table 1.2 for more details.

1.4.3. Other bowel disorders

There is an increased risk of CRC for those with severe prolonged active IBD such as Ulcerative Colitis (UC) and Crohn's disease (CD), where the large bowel can be inflamed for a long period of time and/or where there are recurrent cycles of inflammation and repair[75]. Inflammation is a well-known hallmark of cancer, contributing to proliferation and survival of malignant cells[76,77]. One consequence of inflammation in the gut is increased risk of field cancerisation where the normal cell population is replaced by a histologically non-dysplastic but pro-tumourigenic cell population[78,79]. IBD can also directly result in dysplasia, an abnormal collection of cells in the lining of the colon or rectum that can progress to cancer. As a result, UC and CD patients are screened for dysplasia and CRC more frequently and at an earlier age.

1.4.4. Racial and ethnic background

Incidence rates of CRC are highest for black people and lowest for American Indian/Alaska Native people[80]. Mortality rates are highest for black people and lowest for Asian/Pacific Islander persons[80]. As for worldwide populations, countries with a high-income economy have a higher incidence of CRC which suggests a significant environmental influence on the development of CRC.

Jews of Eastern European descent (Ashkenazi Jews) are a distinct population with one of the highest CRC risks of any ethnic group in the world[81]. Several gene mutations have been found in this group, which lead to an increased risk of CRC; the most common is the I1307K *APC* mutation[81].

A study in Tower Hamlets, UK found that although British Bangladeshi patients have a low prevalence of CRC at 27/100,000 compared to British Caucasians at 342/100,000, 61% of British Bangladeshi patients that present with CRC are less than 40[82]. This is defined as

early onset CRC and a link to a high frequency of somatic mutations in RNA binding protein, Fox-1 homolog 1 (*RBFOX1)* has been made, but not yet characterised[83].

1.4.5. Diet

A diet high in red and processed meat is linked to increased CRC development[84]. One study estimated the risk of CRC to increase by 29% for every 100 g/day increase in red meat and by 21% for every 50 g/day increase in processed meat consumed[85]. The heme iron present in red meat generates oxidative stress in cells and is a contributor to CRC progression[86]. Diets high in vegetables, fruits and whole grains are linked to a decreased risk of CRC[87].

1.4.6. Intestinal Microbiota

Many changes in the intestinal microbiota have been reported in CRC with some species of bacteria identified to have a role in CRC progression including *Streptococcus bovis, Helicobacter pylori, Bacteroides fragilis, Enterococcus faecalis, Clostridium septicum, Fusobacterium* spp. and *Escherichia coli*[88–91]*.* Recent evidence suggests that altered gut microbiota is present in patients with adenomas[92] suggesting that an imbalance in intestinal microbiota promotes the early stages of CRC. More research is necessary to determine correlations between changes in intestinal environment and microbiota homeostasis.

1.4.7. Smoking

Long-term smokers are 2.14 times more likely than non-smokers to develop CRC[93]. In total, smoking has been attributed as the cause of 12% of all CRC[94] and is associated dramatically with poorer prognosis after diagnosis: meta-analyses yielded random-effects hazard ratio estimates (95% confidence intervals (CI)) for all-cause mortality of 1.26 (1.15–1.37) for current and former smokers compared with 1.11 (0.93–1.33) for never smokers[95]. Tobacco smoke contains at least 50 carcinogenic compounds, exposure of the bowel epithelium to these chemicals via the blood circulation or after ingestion of saliva contaminated by tobacco smoke may be a possible mechanism of CRC promotion[96].

1.4.8. Alcohol intake

A meta-analysis by Fedirko *et al*. highlighted that those who have a high intake of alcohol (+4 drinks/day or +50g ethanol/day) are more likely to develop CRC[97]. The relative risk

(RR) for moderate intake (2-3 drinks per day or 12.6-49.9g ethanol/day) was 1.21 (95% CI 1.13-1.28) and 1.52 (95% CI 1.27-1.81) for heavy alcohol intake. The RR for moderate alcohol intake, compared with non-/occasional alcohol intake, was stronger for men (RR = 1.24, 95% CI 1.13-1.37) than for women (RR = 1.08, 95% CI 1.03-1.13). The mechanism by which alcohol promotes CRC remains controversial. A metabolite of alcohol, acetaldehyde, has been proven to be cytotoxic as it can react with proteins such as tubulin and collagen, to form stable and unstable products[98].

1.4.9. Weight

The risk and incidence of CRC increases with body mass index (BMI)[99]. Those with class 2 obesity (BMI 35-39.9) are the most commonly diagnosed and treated for colorectal as well as other cancers. A study by Daniel *et al*. found that patients over 50 with local or locally advanced CRC and either class 1 (BMI 30-34.9) or class 2 obesity were associated with a two-fold to five-fold increased risk of death as compared to overweight patients (BMI 25-29.9)[100]. Severe obesity (BMI>40) was also associated with a more than two fold risk of death from CRC[100]. Chronic inflammation is a phenotype of obesity which contributes to the progression of CRC[101]. Adipose tissue releases pro-inflammatory cytokines including interleukin (IL)-8, IL-6, IL-2 and tumour necrosis factor alpha (TNF-α)[102].

1.4.10. Physical Inactivity

Those who have a high level of physical activity have a 27% reduced risk of developing CRC[103] compared to those with a low level of physical activity. Unfortunately, studies do not always report intensity, timing or domain of physical intensity so it is hard to define high and low levels of physical activity. Biological mechanisms of CRC prevention by exercise include: increase in gut motility with exercise, boosting the immune system, decreasing insulin and insulin-like growth factor levels, decreasing obesity and boosting free radical scavenger systems[104].

1.4.11. Type 2 diabetes

Type 2 diabetes is the commonest form of diabetes. The function of β-cells in the pancreas is impaired and/or response to insulin is compromised, leading to hyperglycaemia. Major risk factors are excess body weight and physical inactivity.

Patients with type 2 diabetes (T2D) have an increased risk of developing CRC due to confounding risk factors of obesity, lack of exercise and smoking[105–110]. Nevertheless, even when confounders are removed, those with T2D still have a 34% increased risk of CRC as well as more serious histopathological features and a higher chance of recurrence[111]. The mechanisms linking T2D to CRC remain unknown.

1.5. Diagnosis of colorectal cancer

Methods of CRC diagnosis vary between countries. In the UK, there is a bowel cancer screening service which uses two methods used to detect CRC in its earliest stage. The first is a one-off bowel scope screening for 55 year olds[112]. Polyps in the bowel are indicative of CRC risk: adenomatous polyps are a pre-cancerous polyp with the potential to transform into cancer whereas hyperplastic and inflammatory polyps are not currently considered pre-cancerous[113]. In the United States (US), patients are screened from the earlier age of 50. Screening in the US has been credited as the main reason for the 6% decline in cases, between 2005 and 2014[114]. The second diagnostic test available in the UK is a faecal occult blood test (FOBT) for those between 60 and 74. Blood in a stool sample is indicative of CRC. FOBT has a specificity of 95% and has reduced CRC-associated mortality by 15-33%[115], but its usefulness in clinics is limited due to poor sensitivity and false negatives, as not all CRC tumours bleed[116]. Quantitative immunological detection of human haemoglobin (i-FOBT), offers a higher sensitivity as it eliminates contamination of sample with sources other than human haemoglobin, like diet. Unfortunately, this technique is more expensive so is not widely used[117].

Once a lesion is suspected, the next step is a flexible sigmoidoscopy or a colonoscopy. Both permit the removal of adenomas at the same time, reducing cancer incidence. Biopsy samples removed during the procedure are sent for histopathological assessment and genetic testing can be undertaken to provide further information. However, endoscopic procedures require bowel preparation, carry a risk of complications, such as bowel perforation, are expensive and the results only give a snapshot of information about the tumour at the biopsy site and time point. Alongside an endoscopic procedure, other tests are completed, such as blood tests to detect an elevation in carcinoembryonic antigen (CEA) and carbohydrate antigen (CA 19-9) which is indicative of CRC, however, these can be unreliable due to high levels of false positives as well as false negatives[118].

Current methods of diagnosis employed in the UK often fail to distinguish between high- and low-risk patients because there are no current prognostic or predictive markers for CRC that are easy to use and accurate. An easy to perform, non-invasive, inexpensive and accurate test, such as a blood test, which can detect the disease at an early stage is still desperately needed.

1.6. Staging of colorectal cancer

The most common system for pathological staging of CRC is called TNM: T (1-4) represents primary tumour and how far it has penetrated into the lining of the bowel and nearby tissues; N (0-2) represents the spread of the cancer to regional lymph nodes; and M (0-2) represents the presence of metastases to other organs (Figure 1.5). A simplified version is outlined in Table 1.3. There are also three grades of bowel cancer which are described in Table 1.4. Grade is based on how closely the cancer looks like normal CRC tissue under a microscope.

To determine the clinical stage of the tumour, clinicians use a variety of imaging tests which help to identify small tumours. One imaging technique is computerised tomography (CT), but this method has a staging accuracy of 45-77%. Another imaging technique called magnetic resonance imaging (MRI) has a better staging accuracy of 73%[119] and positron emission tomography (PET) scans can identify small metastases well[120]. Imaging techniques are combined with physical examination, combined with information from endoscopic procedures, surgical resection and pathological assessment.

At diagnosis, approximately 25% of patients will have metastatic disease and almost 50% of CRC patients will develop metastasis[121]. The main sites of CRC metastases are liver, lung and peritoneum. Recent evidence suggests that *KRAS* mutant tumours are associated with lung, brain and bone metastases, whilst *BRAF* mutant tumours are associated with peritoneal and distant lymph node metastases[122,123].

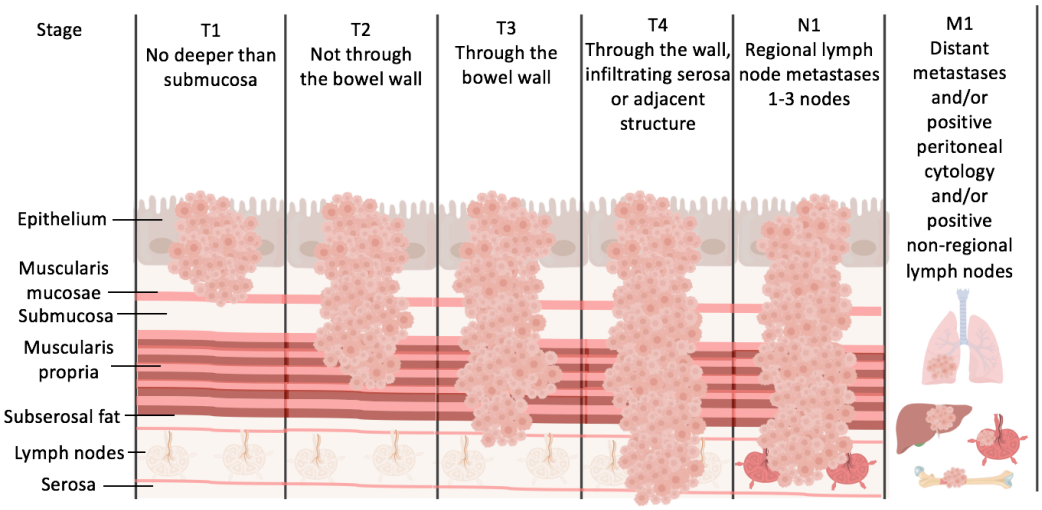

Figure 1.5. TNM staging of CRC. T represents the primary tumour and the level of penetration into the lining of the bowel and nearby tissues in more severe cases; N represents the spread of the cancer cells to regional lymph nodes; and M represents the presence of secondary tumour or metastases to other organs[124]. Each is given a score between 0 and 4, with 4 being most severe.

Table 1.3. TNM staging. T - primary tumour penetration; N - spread to regional lymph nodes; and M - presence of metastases to other organs (Figure 1.5).

Stage	Description
1	**T1-2, N0, M0:** The cancer has spread beyond the layer of muscle surrounding the bowel and may have penetrated the surface covering the bowel. No nearby organs, lymph nodes or distant sites have been reached.
2a	**T3, N0, M0:** The cancer has spread into the outermost layers of the colon or rectum. No nearby organs, lymph nodes or distant sites have been reached.
2b	**T4a, N0, M0:** The cancer has grown through the wall of the colon or rectum. No nearby organs, lymph nodes or distant sites have been reached.
2c	**T4b, N0, M0:** The cancer has grown through the wall of the colon or rectum and is attached to or has penetrated nearby tissues or organs. No nearby lymph nodes or distant sites have been reached.
3a	**T1-2, N1-2a, M0:** The cancer has spread beyond the mucosa into the submucosa or the muscularis propria. No nearby organs have been reached. It has spread to 1-3 (N1) or 4-6 (N2a) nearby lymph nodes. No distant sites have been reached.
3b	**T3-4a, N1-2a/b, M0:** The cancer has grown into the outermost layers or through the visceral peritoneum. No nearby organs have been reached. It has spread to 1-3 (N1) or 4-6 (N2a) or 7+ (N2b) nearby lymph nodes. No distant sites have been reached.
3c	**T3-4a/b, N2a/b, M0:** The cancer has grown into the outermost layers or through the visceral peritoneum. No nearby organs have been reached (T3/4a). The cancer has spread to nearby organs (T4b). It has spread to 1-3 (N1) or 4-6 (N2a) or 7+ (N2b) nearby lymph nodes. No distant sites have been reached.
4a	**Any T, Any N, M1a:** The cancer may or may not have penetrated the wall of the rectum or the colon, and it may or may not have spread to nearby lymph nodes. It has reached one distant organ or tissue.
4b	**Any T, Any N, M1b:** The cancer may or may not have penetrated the wall of the rectum or the colon, and it may or may not have spread to nearby lymph nodes. It has reached one or more distant organs or tissue.

Table 1.4. Grades of CRC. Description of the grades of CRC.

Grade	**Description**
1	A cancer growing slowly with a low chance of spreading beyond the bowel.
2	A cancer growing moderately with a medium chance of spreading beyond the bowel.
3	A cancer growing rapidly with a high chance of spreading beyond the bowel.

1.7. Treatment of colorectal cancer

Surgery, chemotherapy and radiotherapy all have key roles in the treatment of CRC dependent on stage. Surgery is the main treatment for all stages of rectal cancer and the early stages (T1-2) of colon cancer, when the cancer remains localised, are often considered curative. During surgery, nearby lymph nodes are also removed to prevent recurrence.

Chemotherapy remains the standard of care for the 50% of patients that develop advanced metastatic disease. Selecting the appropriate therapy for patients with metastatic CRC is complex because the treatment options are diverse. Patients are usually treated with a combination of cytotoxic and targeted therapeutics, dictated by therapy toxicity. The cytotoxic chemotherapy gold standard remains one of three options: 5-FU with oxaliplatin (FOLFOX); capecitabine with oxaliplatin (CAPOX); or 5-FU with irinotecan (FOLFIRI). Newer targeted agents include antibodies against tumour antigens that are used depending on the patient's mutation profile[125–128]. Patients with *RAS* mutant tumours (mutation in *KRAS,* usually codon 12 and 13*,* or *NRAS* exon 2, 3 and 4) are treated with Bevacizumab (anti-vascular endothelial growth factor (VEGF)-A antibody) whereas RAS wild-type patients receive Bevacizumab, Cetuximab or Panitumumab (anti-EGFR antibodies)[126].

Tumour response to therapy is often transient and many patients develop resistant cell populations resulting in treatment failure or cancer recurrence. Biomarkers of response to therapy are needed for more reliable stratification of patients for proper clinical management. However, second-line therapeutics are available: Regorafenib a non-specific kinase inhibitor, is approved for the refractory setting; and aflibercept and ramucirumab, which both target VEGF, are approved for oxaliplatin-resistant patients[129–131]. More clinical trials are necessary to determine the optimum regimen for combining the newer biologics and traditional chemotherapy.

Recently, the new Eloxatin Peri-Operative Chemotherapy (EPOC) study of combination therapy of cetuximab with FOLFOX for CRC showed a disadvantage in overall survival combined with an increase in tumour burden[132]. Work by Prof. Daniel Hochhauser's group at University College London in collaboration with Prof. Andrew Silver's group at Queen

Mary University of London found that reactive oxygen species (ROS) (Chapter 1, Section 1.8) generated by dual oxidase (DUOX)-2 as a result of cetuximab treatment reduced oxaliplatin activity[133] (detailed in Chapter 6). DUOX2 is a 175kDa enzyme which is part of the nicotinamide adenine dinucleotide phosphate (NADPH) oxidase (NOX) family. The NADPH oxidase family of enzymes consists of NOX1-5 which produce superoxide and DUOX1 and 2 which produce the carcinogen hydrogen peroxide (H_2O_2)[134]. DUOX2 was first described as a H_2O_2-producing enzyme in the thyroid with an important role in thyroid hormone biosynthesis[135]. DUOX2 is now also recognised as an important part of the host defence system of the airway epithelium and the human gastrointestinal tract[136–139]. DUOX proteins are found in the apical membrane and in the enterocytes of the human colon[140]. It is known that hypoxia increases the expression of DUOX2 in the gut[139]. High levels of DUOX2 have been observed in the colonic epithelium of IBD patients and in colonic and pancreatic cancers[141]. Recently, DUOX2 has been shown to be regulated by a signal transducer and activator of transcription (STAT)-dependent janus kinase (JAK) independent pathway[142].

Radiation therapy is also a treatment arm for rectal cancer. Radiation works by damaging the cell's DNA leading to cell death. Radiation is often given alongside chemotherapy before and/or after surgery to remove any remaining cancerous cells. This type of therapy is also used to treat metastases, mainly those that have spread to the bones[143].

There are a variety of clinical trials underway and others completed recently for CRC treatment. For primary CRC, the focus is on improving screening accuracy and surgical techniques. For metastatic CRC, there are a variety of targeted therapies, which have been trialled in other cancers previously. These are being tested alongside traditional chemotherapy.

1.8. Hypoxia in colorectal cancer

Hypoxia is defined as a lack of oxygen in tissues. Healthy tissues in the body experience 2-9% oxygen[144] whereas hypoxic areas in solid tumours experience less than 2% oxygen[145]. The diffusion limit for oxygen is ~100-200μm, therefore for adequate oxygenation cells must be within this radius[146,147]. The gradients of hypoxia are functional, they allow for appropriate cell and tissue development and function. For example, during foetal development, hypoxia represents a positive and necessary stimulus that is required for patterning and function of most organs[148]. However, it is clear that the cellular effects of exposure to low-oxygen tensions represent a malignant stage of many diseases such as dementia[149], cardiovascular disease[150], diabetes[151] and cancer[152].

Formation of vessels in tumours is not carefully co-ordinated like normal physiological angiogenesis, leading to vascular leakiness, chaotic architecture, non-laminar blood flow[147] and dynamic fluctuations in blood flow called 'cycling hypoxia'[153]. Hypoxic areas in tumours are formed as a consequence of the metabolic demands of proliferating cancer cells and/or functionally limited vasculature[154]. There is often heterogeneity in tumour oxygenation with hypoxic and necrotic areas characteristically observed towards the centre of the tumour. Experimental evidence demonstrates steep gradients of oxygen partial pressure that are close to zero when cells are distant from vessels[155], with an oxygen diffusion limit of 235μm[156]. Poor vascularisation in hypoxic areas makes drug delivery difficult and is one reason why hypoxic areas in solid tumours, such as CRC are naturally more resistant to radiation and chemotherapy[157,158].

The cellular response to hypoxia is mediated by the O_2-labile transcription factors hypoxia inducible factors (HIF)-1 and -2[144]. The HIFs consist of O_2 sensitive α subunits and constitutively expressed β subunits[159]. In normoxic conditions, HIF-1α has a half-life of five minutes due to continuous degradation by the ubiquitin-proteasome pathway (Figure 1.6) where HIF-1α is regulated by von Hippel-Lindau protein (VHL)[159]. As the oxygen tension lowers, as is often seen in solid tumours[158], VHL is downregulated, HIF-1α is stabilised and dimerises with HIF-1β to bind hypoxia response elements (HRE) within the genome (Figure 1.6). This leads to transcriptional activation of more than 30 genes which promotes

aberrant cell survival alongside a switch in cellular metabolism to anaerobic glycolysis enabling disease progression[160]. These genes include glucose transporter (*GLUT*)-1 which facilitates cellular glucose uptake; hexokinase (*HK*)-2 and lactate dehydrogenase (*LDH*)-A which regulate anaerobic metabolism; carbonic anhydrase (CA)-9 helps to maintain intracellular pH in a hypoxic environment; and VEGF which leads to vascularisation of the tumour mass, a phenomenon which was first reported in 1908[161]. HIF-1α overexpression is associated with increased chemoresistance, metastasis and mortality in various human cancers including bladder, breast, lung, ovary, pancreas, stomach and colon[162]. High expression of HIF-1α in CRC correlates with increased tumour invasion, tumour stage, lymphatic invasion and liver metastasis and a poorer prognosis[163].

ROS are thought to increase in hypoxia. ROS are radicals, ions or molecules that have an unpaired electron in their outer shell which makes them highly reactive. ROS can cause DNA damage and subsequent genomic instability and result from increased metabolic activity, mitochondrial dysfunction and oncogene activity. Cancer cells also express an increased level of antioxidant proteins to neutralise ROS, suggesting a delicate balance of ROS is necessary for cancer cell function[164].

To maintain cell viability mitochondria quench ROS by generating glutathione and thioredoxin redox couples. Under aerobic conditions, cells express cytochrome C oxidase (COX4) subunit 4-1-regulatory subunit within the COX complex. However, in hypoxia HIF-1 increases the expression of COX4-2 subunit as well as mitochondrial lon protease which leads to degradation of the COX4-1 subunit[165,166]. This is hypothesised to aid the efficiency of complex IV of the electron transport chain under hypoxia and to prevent generation of ROS in hypoxia.

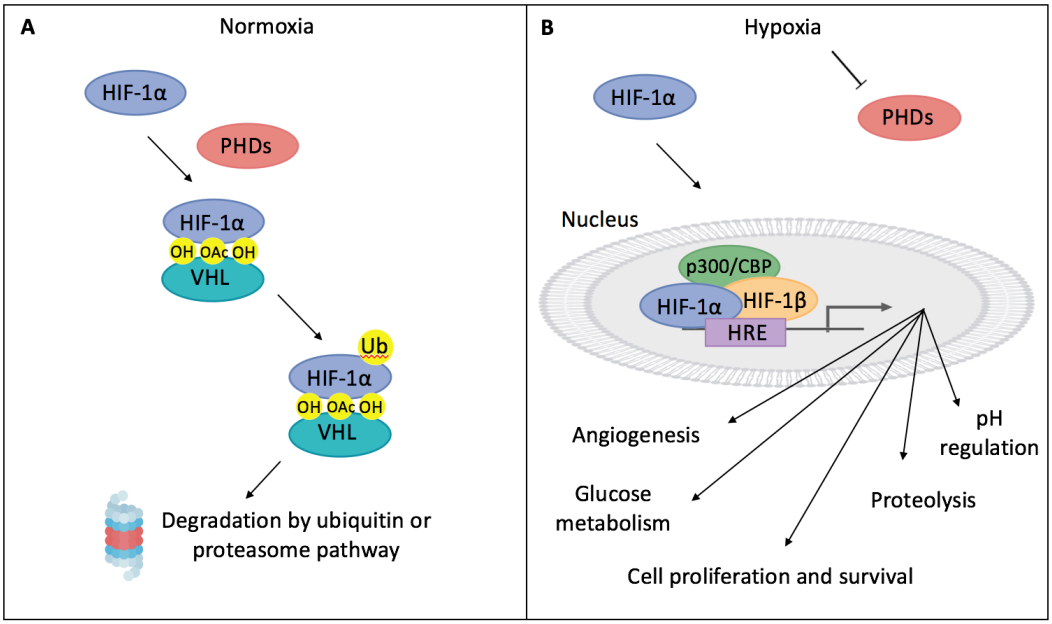

Figure 1.6. Stabilisation of HIF-1α during hypoxia. (**A**) In normoxic conditions, HIF-1α is regulated by VHL leading to continuous degradation by the ubiquitin-proteasome pathway. (**B**) In hypoxic conditions, VHL is downregulated. HIF-1α is stabilised and free to dimerise with HIF-1β which then binds as a complex to HRE within the genome, promoting transcription of genes involved in cancer cell survival[167]. VHL, von Hippel-Lindau; HIF, hypoxia inducible factor; HRE, hypoxia response elements; PHD, prolyl hydroxylase; CBP, CREB binding protein; OAc, acetoxy group.

1.9. Metabolism in colorectal cancer

Physiologically, normal cells have a low rate of glycolysis with most energy efficiently generated by oxidative phosphorylation in the mitochondria. In general cancer cells mainly use glycolysis to generate adenosine triphosphate (ATP).

Glycolysis takes place in the cytoplasm, where glucose is broken down to pyruvate, producing 2 ATP molecules per glucose molecule (Figure 1.7). Pyruvate is then converted into acetyl-CoA by pyruvate dehydrogenase in the mitochondria (Figure 1.8). Acetyl-CoA enters the tri-carboxylic acid (TCA) cycle (also known as the citric acid cycle or the Krebs cycle) where it is broken down via nine further enzymatic steps to oxaloacetate[168] (Figure 1.8). Cells can also metabolise glutamine using the TCA cycle, which can be another useful source of energy for cancer cells[169] (Figure 1.8). During the TCA cycle nicotinamide adenine dinucleotide (NADH) is produced which then serves as an electron donor in the electron transport chain (ETC), where 30-36 molecules of ATP are produced for each glucose molecule via oxidative phosphorylation (OXPHOS) in the inter-membrane space of mitochondria[168] (Figure 1.9). Oxygen is used as an electron acceptor for OXPHOS. In the absence of oxygen (hypoxia) or functioning mitochondria, non-malignant cells rely on glycolysis for ATP generation. It has also been recently shown that cancer cells can use intracellular glycogen as a means of maintaining cell viability and proliferation[170] and in response to acute hypoxia, cancer cells can increase glycogen storage[171]. This is consistent with the previously described glycogen shunt in a number of other cell types[172].

Interestingly, even when oxygen is plentiful, rapidly growing cancer cells have glycolytic rates of 200 times that of a normal cell[173]. Cancer cells in general are metabolically adapted to grow and proliferative rapidly under conditions of low pH and oxygen tension with limited nutrients[174] where non-transformed cells would struggle to grow[175]. An important study by Sonveaux *et al*. in 2008[176] showed that normoxic tumour areas can oxidise lactate as a significant carbon source, sparing glucose and allowing it to diffuse further away from the tumour vasculature into hypoxic areas where anaerobic metabolism was used to metabolise the glucose to lactate, which was then used by the normoxic areas.

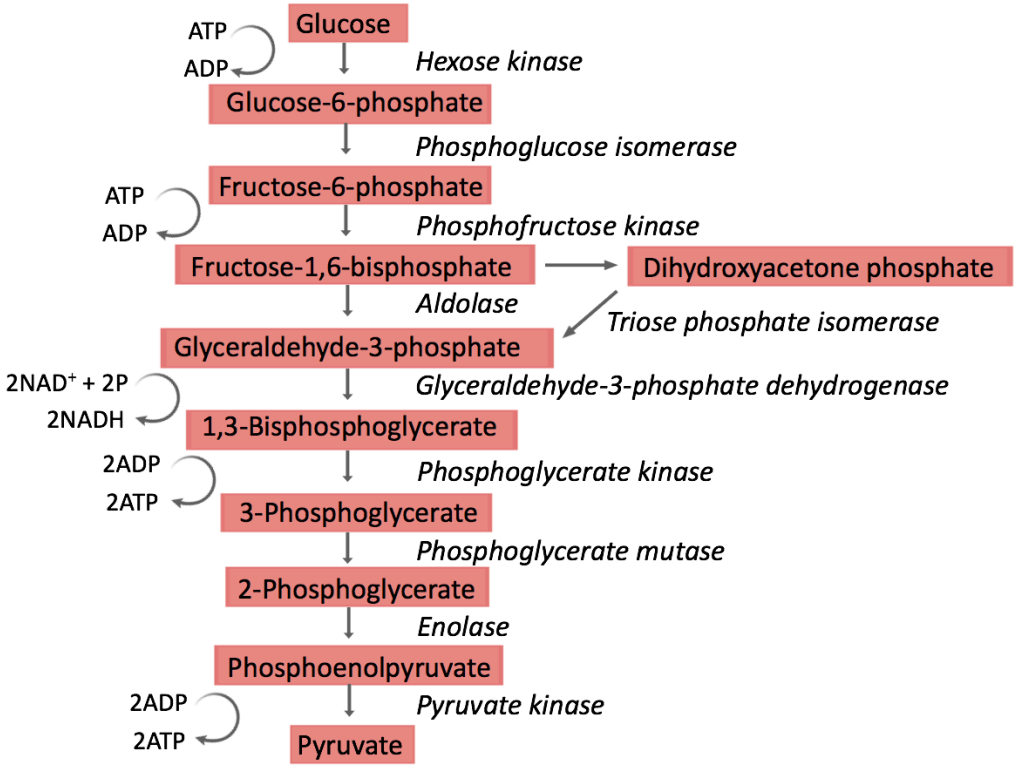

Figure 1.7. Glycolysis. The breakdown of glucose by enzymes into pyruvate, ATP and NADH in the cytosol[173]. ATP, adenosine triphosphate; ADP, adenosine diphosphate; NAD, nicotinamide adenosine dinucleotide.

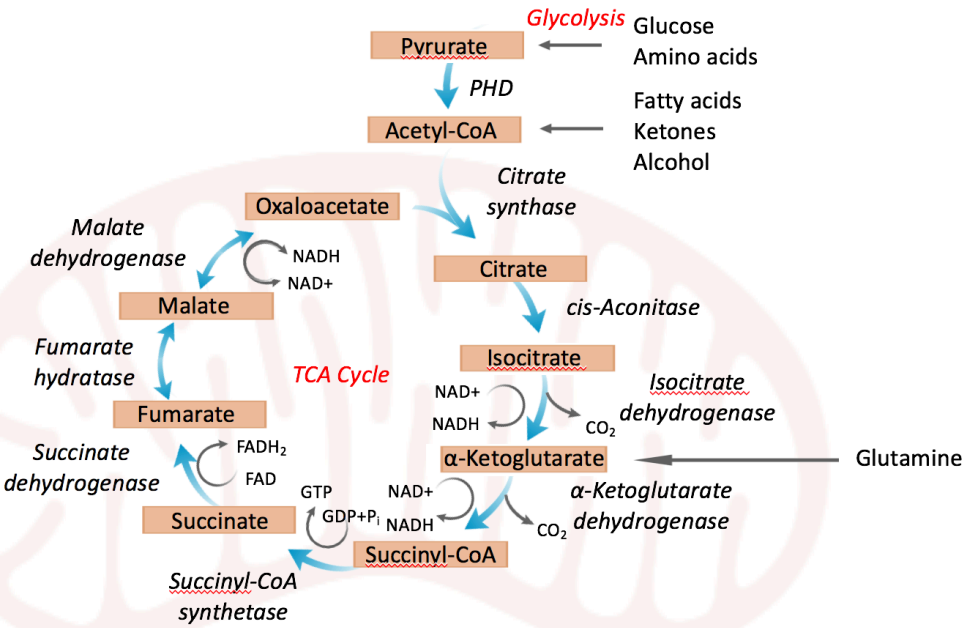

Figure 1.8. The tri-carboxylic acid cycle. Acetyl-CoA enters the TCA cycle in the mitochondria where it is broken down via nine further enzymatic steps to oxaloacetate[168]. Glutamine can also enter the TCA cycle. TCA, tricarboxylic acid cycle; PHD, prolyl hydroxylase, NAD, nicotinamide adenosine dinucleotide; GTP, guanosine triphosphate; FAD, flavin adenosine dinucleotide.

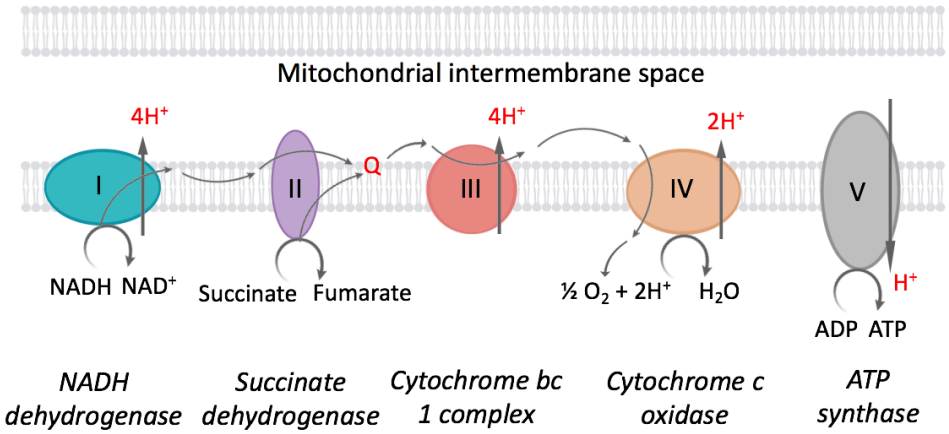

Figure 1.9. The electron transport chain. Electrons from the reduced NADH and succinate generated by the TCA cycle are transferred through a chain of protein complexes embedded in the inner mitochondrial membrane[177]. The oxidation steps lead to protons moving from the inner matrix to the intermembrane space, creating a hydrogen concentration gradient which produces both an electrical potential and a pH potential. This leads to the conversion of ADP to ATP by ATP synthase. These coupled reactions are also referred to as OXPHOS. ETC, electron transport chain; NADH, nicotinamide adenine dinucleotide; TCA, tricarboxylic acid cycle; ADP, adenine di-phosphate; ATP, adenine tri-phosphate; OXPHOS, oxidative phosphorylation.

The exact reason for the switch in glucose metabolism pathways in cancer cells is not known, although there are a number of theories: 1) an inherent feature of the malignant phenotype, called the Warburg effect[178,179]; 2) as a consequence of a hypoxic tumour microenvironment[167], or 3) the existence of a pseudo-hypoxic tumour metabolic profile[173].

Otto Warburg was the scientist who discovered the 'oxidative glycolytic' phenotype of cancer cells. In these cells, glycolysis is uncoupled from the mitochondrial TCA cycle and OXPHOS, and is consequently characterised by excess production of lactate leading to an acidic extracellular environment[178]. Warburg hypothesised that this metabolic reprogramming confers a survival advantage to cancer cells that will inevitably reside in a hypoxic environment if the tumour outgrows the vascularisation. The acidic extracellular environment does favour the survival of cancer cells, especially those that have lost wild type TP53 function, over normal cells and may promote invasion, as well as preventing apoptosis upon detachment (anoikis) facilitating metastasis[180]. This is highly relevant for the colonic epithelium as over 75% of human colonic tumours have lost functional wild type TP53 activity[181]. Analysis of CRC patient samples has identified high levels of GLUT-1, monocarboxylate transporter (MCT)-1 and HIF-1α which indicates increased glycolytic metabolism and lactate production[182]. In CRC, LDHA5, which converts pyruvate to lactate, is linked to activation of the HIF pathway as well as an aggressive phenotype[183–185]. Elevated levels of lactate also correlate with poor patient prognosis and overall survival in cervical and ovarian cancers[186,187].

Warburg also hypothesised that these metabolic changes occurred due to mitochondrial defects, however this topic remains controversial. Evidence is mounting to suggest that damaged mitochondria are not the cause of the increased aerobic glycolysis exhibited by most tumour cells, but that the primary functions of activated oncogenes and inactivated tumour suppressors are to reprogram cellular metabolism (reviewed in[188]). Carbon labelling metabolic studies have identified that in solid tumours, where glucose supply can be low[189], glutaminolysis, the TCA cycle, the pentose phosphate pathway and nucleotide biosynthesis as well as glycolysis are all enhanced in tumour cells[190]. Nevertheless, the mitochondrial genome is susceptible to mutations because of the large amount of ROS they generate, coupled with a low level of DNA repair[191].

There is some evidence to suggest that mitochondria are damaged in CRC. One study showed that mitochondrial microsatellite instability is an early and independent event in colorectal precancerous lesions which occurs in 30% of CRC patients and is linked to poor prognosis[192]. Patients with lower mitochondrial DNA (mtDNA) copy number show higher TNM stages and poorer differentiation[193]. CRC cell lines including DLD1, HCT116, SW837 and HT29 have been shown to have mutations in mtDNA leading to a subtle elevation in ROS[191]; low levels of ROS are highly mitogenic, whereas high levels of ROS are toxic[194]. It has also been shown that HCT116 CRC cells treated with 1% oxygen for at least 20 passages, have larger mitochondrial mass, but decreased mtDNA and reduced sensitivity to 5-FU[193].

Hypoxia is a feature of solid tumours (Chapter 1, Section 1.8) and can lead to expression of many genes, via HIF-1α, that have a role in metabolism such as GLUT-1, HK2 and LDHA, all which have been shown to be relevant in CRC tumorigenesis and linked to poor prognosis[182,195] (Figure 1.10). HIF-1 also promotes the expression of pyruvate dehydrogenase kinase (PDK)-1 expression[162] which acts to block conversion of pyruvate to acetyl-CoA, effectively blocking the TCA cycle and OXPHOS, forcing the cell to use glycolysis for ATP generation. Upregulation of PDK1 also protects cells from ROS damage. There is evidence to suggest that HIF-1 down regulates mitochondrial biogenesis[162] by inducing microRNA (miRNA)-210 transcription resulting in a reduction of iron-sulphur cluster assembly enzyme (ISCU) and COX10, two important elements of the mitochondria electron transport chain and the TCA cycle[196].

HIF transcription factors have also been shown to affect the function and stability of other genes which influence cellular metabolism; the best characterised examples are v-myc avian myelocytomatosis viral oncogene homolog (MYC) and p53. MYC binds E-boxes in the promoter of target genes when associated with MYC-associated protein X (MAX) as a heterodimer[197]. MAX is itself regulated by binding of MAX dimerisation protein (MXD1/MAD) and MAX interactor 1 (MX11/MAD2)[198]. MX11 binding to MAX inhibits binding of MYC:MAX to E-boxes. HIF-1α can also interfere with the MYC:MAX heterodimer; through upregulation of MX11, increasing competition for MAX[199] and by direct binding of MAX to displace MYC. Conversely, HIF-2α binds and stabilises the MYC:MAX heterodimer to promote MYC associated transcriptional changes[200]. HIFα can

be outcompeted in tumours with high expression levels of MYC[201], therefore, HIF-2α interaction with the MYC:MAX heterodimer is more likely to influence the hypoxia-induced metabolic transformation in non-MYC-amplified tumours. There are no known mutations of *MYC* in CRC. However, *MYC* is frequently amplified in CRC; Soga *et al*. recently implicated amplification of *MYC,* which is commonly seen in CRC, leads a change in expression of 121 metabolic genes and 39 transporter genes in CRC promoting metabolic reprogramming[202].

The relationship between TP53 and hypoxia is controversial; hypoxia has been shown to induce TP53 stability in some conditions, but not in others[203,204]. It appears that lower oxygen tensions elicit strong stabilisation of TP53, through DNA damage-response mechanisms[205]. Stabilisation of TP53 increases the entry of glycolytic intermediates into the pentose phosphate and folate pathway by modulation of key enzymes[206,207]. In this way, TP53 can increase antioxidant production, although at the expense of ATP production. Expression of TP53 is also important for the assembly and function of COX in the ETC. Loss of TP53 in normoxia results in a similar phenotype observed in hypoxia as the malate-aspartate shuttle ceases to function effectively[208].

Pseudo-hypoxia is the activation of the hypoxia response pathway under non-hypoxic conditions which is commonly seen in cancers[209], although this has not been reported specifically in CRC to date. Defects in some TCA cycle enzymes lead to decreased hydroxylation of HIFα subunits and trigger the pseudo-hypoxia response[210]. Isocitrate dehydrogenase (IDH) is mutated in glioma and acute myeloid leukaemia (AML); succinate dehydrogenase (SDH) and fumarate hydratase (FH) are mutated in pheochromocytoma, para-ganglioma, leiomyoma, and renal carcinoma[188]. There are no known mutations in these enzymes in CRC[211].

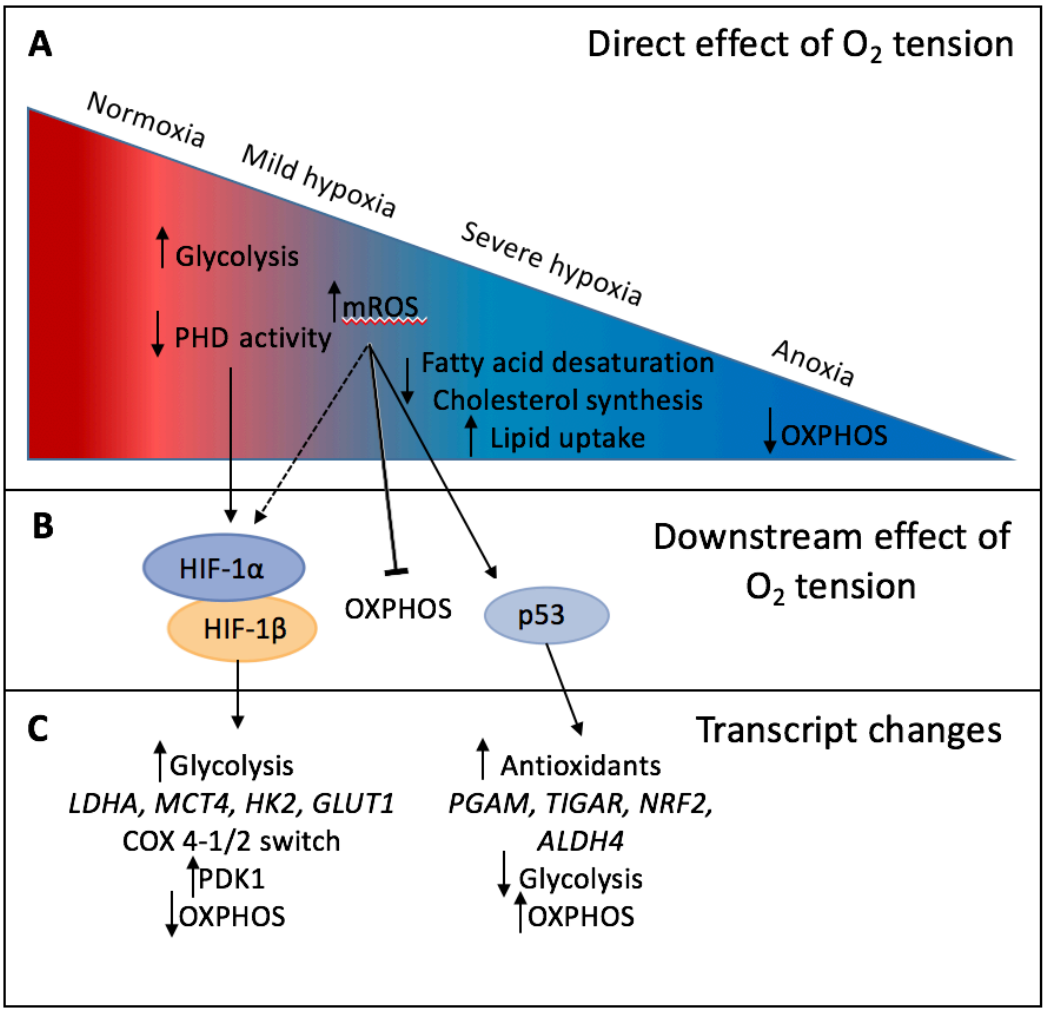

Figure 1.10. Cellular effects of change in O_2 tension. As a result of changes in O_2 tension there are; (**A**) Changes in pathways as a result of changes in O_2 tension, (**B**) changes in specific proteins as a result of changes in O_2 tension and (**C**) changes in transcript expression[152]. ROS, reactive oxygen species; PHD, prolyl hydroxylase domain-containing protein; OXPHOS, oxidative phosphorylation; HIF, hypoxia inducible factor; LDHA, lactose dehydrogenase A; MCT4, mono-carboxylate transporter 4; HK2, hexokinase 2; GLUT1, glucose transporter 1; PGAM, phosphoglycerate mutase; TIGAR, TP53 induced glycolysis regulatory phosphatase; COX, cytochrome C oxidase; ALDH4, aldehyde dehydrogenase 4; PDK1, pyruvate dehydrogenase kinase 1.

1.10. Mouse models of colorectal cancer

Mouse models are often used to explore the influence of genetic changes on the development of CRC as well as effects of therapy. Developing the ideal mouse model for CRC is challenging.

Despite the evolutionary distance between mouse and humans, the genome content has largely been conserved[212] and most cancer pathways operate in both species[213]. The genomes of inbred laboratory mice are well characterised; they are considered homozygous at every locus and are housed in a controlled environment. However, there are some drawbacks. Inbred laboratory mice lack the genetic heterogeneity which is present in the human population; human tumours are more heterogeneous than their mouse counterparts[214,215]. The lack of complexity poses problems when trying to recapitulate faithfully the human disease for pre-clinical studies particularly as the heterogeneity of human tumours results in greater potential for the development of resistance to therapy and for recurrence after surgical resection[216]. Humans also experience a more varied diet and have a different microbiome compared to the mouse, which exposes human intestinal epithelial cells to more exogenous genotoxins[217]. The difference in life span between man and mouse is also a problem. In man, the development of CRC is over a much longer period compared to mouse, and mice often become anaemic as a consequence of polyposis and have to be sacrificed before CRC develops[218]. There are also crucial differences in telomere maintenance and function[219]. Telomeres shorten with each mitotic cell division but are elongated by telomerase. Although telomere sequence is identical in mice and humans, heterozygous telomerase mutations in humans is sufficient to result in cancer development, but laboratory mice lacking telomerase show no phenotype over several generations[219]. This is because laboratory mice telomeres are 5 to 10 times longer than humans but their lifespan is 30 times shorter. It is also well known that the immune system is a very important part in the development of cancer and therefore the use of a whole animal system could be the key to understanding the development of cancer. However, the mouse immune system is not identical to the human immune system and this must be taken into account when interpreting data from mouse models (reviewed in[220]). There is a variety of mouse models

commonly used to investigate polyposis as a benign precursor, these are discussed below.

The first key polyposis mouse model was the multiple intestinal neoplasia (Min) mouse which arose from a random ethylnitorsourea (ENU) mutagenesis screen[221,222]. The *Apc*$^{Min/+}$ mouse was subsequently recognised as a paralog for human FAP syndrome and provided confirmation of the causal gene mutation in sporadic CRCs with 5q21 deletions[223]. The *Apc*$^{Min/+}$ mouse is widely used in research today. More sophisticated knock-in and/or knock-out mouse models enable further functional study of genetic mutations involved in CRC. The cancer genome atlas (TCGA) has identified many genes which are frequently mutated in many different types of malignancy, often referred to as pan-cancer genes, this suggests a role for these genes in the progression of cancer[224]. It is possible to introduce genetic mutations into specific tissues in mice; these models can be used to determine if mutations are passenger or driver mutations[225]. For example, the *Apc*^{1322T} mouse has a mutation in *APC* specifically in the bowel (Figure 1.3). The use of *Apc* mutant mice has increased our understanding of the role of *Apc* in the biology of CRC development, for example, which protein domains and functions of *Apc* are responsible for intestinal tumour initiation and maintenance. Use of a *Cre*-recombinase driven by a specific promoter allows excision of DNA between two *loxP* sites in a given tissue.

Models which manipulate *Apc* alone generate adenomas in the small intestine, particularly the upper part of the small intestine, and relatively few in the colon or rectum which is unfortunately the exact opposite of the human disease. The short lifespan of the *Apc*$^{Min/+}$ and the *Apc*^{1322T} mouse limits the utility of the model. A number of different *Apc* mutant mice were developed, but unlike their human counterparts the mice never develop metastases. To try and recapitulate metastases, *Apc* mutant mice have been crossed to mice with gene mutations found in the later stage of disease including *TP53,* transforming growth factor ß receptor 2 *(TGFßR2),* F-box and WD repeat domain containing 7 *(FBXW7)* and *SMAD2-4,* however, this approach did not yield metastases. At best these compound mutants displayed more adenocarcinomas. However, addition of *KRAS* mutation post *APC* inactivation can lead to metastasis. The *Apc^CKO/CKO -LSL-KRAS* mouse (CKO – conditional knock out, LSL – lox-stop-lox) can develop distant metastases to the liver and other organs[226]. The iKAP mouse which harbours an inducible *KRAS* allele

and conditional null alleles of *APC* and *TRP53* also recapitulates tumour progression to metastases[227].

Xenografts are another type of mouse model. They involve the injection of cell lines or transplantation of primary tissue into immune-deficient mice such as the nude mouse (nu/nu) to prevent rejection. However, the results must be interpreted with caution due to the following points: xenograft mouse models are poor representations of human CRC, as firstly, the host is immune deficient and the role of the immune system is important in the development of CRC. For example, in CRC T-cell infiltrate is predictive of patient survival[228] and mice with deletion of *SMAD4* in T-cells excessively secrete pro-inflammatory cytokines which leads to the development of gastrointestinal tumours[229]. Secondly, few cell lines lead to reliable primary tumour growth and even less produce naturally metastatic CRC[230]. Success rates are highest when using HCT116 and HT29 cell lines but it is not understood why[216]. Thirdly, orthotopic and subcutaneous xenografts show differing sensitivities to chemotherapeutic agents[231,232] and site of injection, mouse age and the genetic background of the mouse all dramatically affect the frequency of lymph-node or liver metastases[230,232,233]. This suggests that the microenvironment is an important determinant of therapeutic response and metastatic potential.

The environment of a subcutaneous xenograft is very different from that of autochthonous tumours and the extent to which mismatch of tumour (human) and stromal (mouse) influences the growth of the tumour is uncertain[216]. Orthotopic xenografts introduce cells to a more natural environment, such as the serosa of the intestine, and these models do result in more reliable liver metastasis[231]. Patient-derived orthotopic xenografts are another option. They avoid natural selection of dominant clones and epigenetic and genetic alterations that occur during long-term cell culture; however, it has been reported that the host cells replace the human stroma which was initially transplanted within 3 weeks[234]. It would be exciting to use this system to predict patient response to therapy and development of resistance. However, this would require the subculture or serial xenografting which is a lengthy process and too long to benefit the patient[235]. The two major limitations of xenograft models are the species mismatch between stroma and tumour and the use of immune-deficient hosts. An allograft model

overcomes both of these issues. Tumour fragments or cell lines derived from them are grafted to a genetically identical inbred, immune competent mouse[236].

1.11. Diabetes

Diabetes mellitus (DM) is a chronic disease caused by dysregulated insulin production from pancreatic β-cells leading to elevated blood glucose (hyperglycaemia). Insulin works to promote the uptake of glucose into cells. Normal homeostatic control maintains a blood glucose concentration of between 4 to 8mM, with tissue levels of glucose commonly below 2.5mM. In a diabetic individual, the pancreatic β-cells are either destroyed culminating in type 1 diabetes (T1D) or their function is impaired and/or the body does not react to insulin correctly creating T2D. A diabetic individual has a blood glucose concentration above and beyond 7mmol/L.

The prevalence of diabetes has been growing for the past three decades. In 2016 the World Health Organisation (WHO) published a global report on diabetes which found that there were 422 million adults living with diabetes in 2014; in 1980 the number of people living with diabetes was 108 million[237] (Table 1.5). The WHO predicts that diabetes will be the 7th leading cause of death by 2030[238]. The overall risk of death of a diabetic person is twice the risk of a non-diabetic person due to its association with a wide range of co-morbidities and complications including Alzheimer's[239], Parkinson's disease[240], cardiovascular disease[241], cancer[242], depression[243], kidney problems[244], liver failure[245] and retinopathy[246].

A study published in the Lancet[247] highlighted the worldwide burden of diabetes; the lowest prevalence of diabetes in 2014 was in Northwestern Europe (5% for women and 5.8% for men). China, India and USA remained the top three countries with the largest number of adults with diabetes in 2014 which is not surprising as they have the largest populations. The Eastern Mediterranean region had the highest percentage prevalence of diabetes in 2014.

Diabetes costs the National Health Service (NHS) in the UK £14 billion a year, 10% of the total budget[248]. The cost of drugs and treatments alone for diabetics in England has risen by 56.3% from £513.9 million in 2005/6 to £803.1 million in 2013/14[249]. Prevention of diabetes, especially T2D, is a global initiative to reduce healthcare costs[250].

1.11.1. Type 1 diabetes

T1D is also known as insulin-dependent diabetes mellitus (IDMM) or juvenile diabetes where the pancreatic β-cells are destroyed by an autoimmune response[251]. T1D often develops suddenly in childhood with symptoms of fatigue and excessive urine excretion. Risk factors are viral infections like German measles, living in a northern climate, genetics and children whose mothers had ill-functioning insulin receptors during pregnancy (gestational diabetes)[252].

T1D patients require lifetime treatment with exogenous insulin, although patients with mutations in the genes encoding the sulfonylurea receptor (SUR)-1 and Kir6.2 subunits of the potassium ion channel that regulates insulin secretion are given sulfonylurea drugs[253]. Newer therapies are emerging such as islet, pancreas-kidney and stem cell transplants, but these therapies are a long way from general clinical use[254].

Sophisticated laboratory tests are required to distinguish between T1D and T2D it is difficult to find accurate global prevalence for each. One study suggests that T1D is most prevalent in Finland (>60 per 100,000/year) and Sweden (47 per 100,000/year), whereas East Asia and native Americans have the lowest prevalence (approximately 0.1–8 per 100,000/year)[255]. Year on year, the average age of onset of T1D is decreasing along with an increase in the numbers of patients diagnosed[256] suggesting that there are also contributing environmental factor(s)[257].

1.11.2. Type 2 diabetes

Most (90%) diabetic patients have T2D, previously called non-insulin-dependent diabetes mellitus (NIDMM) or adult-onset diabetes. T2D was considered a disease of the adult population, but recently many more cases have been identified in children[258].

In T2D, the function of the β-cells is impaired and/or the body's response to insulin is compromised, resulting in hyperglycaemia. Major contributing factors are excess body weight and physical inactivity; over 80% of T2D patients are obese (BMI>30). Other risk factors are high blood pressure, having a close relative with T2D and high cholesterol levels. A diet and exercise plan can offer some control of blood glucose in the short term. However, pharmacological treatment is often needed in the long term. Metformin is first

line therapy for T2D, although further research is necessary to clarify which drugs, or combinations of drugs, have the most durable influence in modulation of blood glucose levels.

Detailed prevalence figures for T2D are hard to come by. The majority of patients with diabetes have T2D it can be suggested at T2D prevalence closely matches worldwide diabetes prevalence figures, shown in Table 1.5 from the latest Risk Factor Collaboration study in 2016[247]. This suggests that the Eastern Mediterranean Region has the highest prevalence and the African Region has the lowest prevalence.

Table 1.5. Estimated prevalence and the number of people with diabetes over 18. The rise in prevalence is thought to be linked to the worldwide population growing and ageing. Adapted from[247].

WHO Region	Prevalence (%)		Number (millions)	
	1980	2014	1980	2014
African Region	3.1	7.1	4	25
Region of the Americas	5	8.3	18	62
Eastern Mediterranean Region	5.9	13.7	6	43
European Region	5.3	7.3	33	64
South-East Asia Region	4.1	8.6	17	96
Western Pacific Region	4.4	8.4	29	131
Total (includes non-Member States)	**4.7**	**8.5**	**108**	**422**

1.12. Mouse models of diabetes

Unfortunately, there is no single animal model which mirrors the human T2D condition fully. The most faithful model would develop insulin resistance, pancreatic dysfunction alongside development of cardiovascular disease. There are, however, mouse models that are relevant to human T2D. Table 1.6 outlines equivalent blood glucose levels needed in human and mice to be classified as normal, pre-diabetic or diabetic.

The first is the *ob/ob* mouse which has mutations in the leptin gene, and the second is the *db/db* mouse which has mutations in the leptin receptor[259,260]. Leptin is a hormone which is important in the control of appetite, it tells the brain when enough food has been consumed relative to demand[261]. The *ob/ob* mouse cannot produce leptin, therefore it has an uncontrolled appetite and rapidly increases in weight compared to a healthy mouse, developing hyperinsulinemia, hyperphagia and insulin resistance at 3-4 weeks[262]. Similarly the *db/db* mouse has an uncontrolled appetite; it becomes hyperinsulinemic within 2 weeks of life and develops obesity by week 3 to 4, followed by β-cell failure and hyperglycaemia at 4-8 weeks[263]. The *db/db* mouse most closely mimics human T2D. These models are most commonly used to assess the effect of obesity on the development of diabetes.

A significant limitation of mouse models is the lack of similarity for islet pathology observed in humans with T2D. In these mouse models, diabetes manifests as a consequence of a failure to adequately increase β-cell mass in response to obesity-induced insulin resistance[264]. In human T2D islet amyloid deposits form and contribute to failure of β-cells[265].

A novel model of diabetes in mice was recently reported by Adam *et al*. which is driven by a knock-out of *Fh1* in the β-cells of the pancreas[266]. This diabetic model used a tissue-specific RipCre promoter to knock out *Fh1* in the β-cells of the pancreas by recombination[267]. Mice lacking *Fh1* in pancreatic β-cells exhibit Hif1α-independent glucose intolerance and show blood glucose levels consistent with those seen in an uncontrolled type 2 diabetic human[268]. Interestingly, mice appear normal for 6-8 weeks, then progressive deterioration of β-cell function and glucose intolerance occurs, resulting

in severe diabetes associated with impaired oxidative metabolism, ATP production, intracellular calcium and cytosolic acidification. This work highlighted a role for FH in T2D.

Table 1.6. Normal, pre-diabetic and diabetic blood glucose values (mmol/L) for human and mouse[269].

Blood glucose	Human (mmol/L)	Mouse (mmol/L)
Normal	5	<8.3
Pre-diabetic	8	8.3-13.9
Diabetic	10	>13.9

1.13. The link between diabetes and colorectal cancer

A positive association between diabetes and cancer has been noted since the early nineteen hundreds[270]. Since then, a significant amount of epidemiological work has been completed, but conclusions remain mixed and the mechanistic links between diabetes and cancer remain unclear. T1D and T2D should be considered as separate diseases with respect to risk as each are linked to different types of cancers.

Whilst T1D and its association with cancer have not been studied in as much detail as T2D, an analysis by Zendenhel et al. of a Swedish cohort found a two-fold increased risk of stomach, cervical and endometrial cancer in patients with T1D[271]. A meta-analysis study using an inclusion criteria of <21 years for T1D found that the risk of cancer was higher for females than males and that patients were three times more likely to get stomach cancer or leukaemia, and five times more likely to get squamous cell skin carcinomas than those without T1D[272]. By contrast, a recent review of all the available epidemiological evidence for T1D and cancer incidence and mortality[273] found no statistically significant link between this type of diabetes and any cancer in case-control studies. Only meta-analyses have found such a link, highlighting the inconsistency of results and the need for further research.

T2D patients have a greater risk of developing cancer compared to patients with T1D which is thought to be due to differences in insulin exposure[274–276]. T2D is most strongly associated with an increased risk of liver and pancreatic cancer[276,277], as well as cancers of the digestive tract[278]. It is plausible that T2D and cancer may be associated without any causal link due to the overlapping nature of both environmental and lifestyle risk factors for both diseases[279–281]. Notably, Yuhara and colleagues suggested that T2D is an independent risk factor for CRC once confounding variables including obesity, smoking and physical exercise are removed[111].

The increased risk of CRC for T2D patients has been highlighted by many meta-analyses[105,110,282–286]. Larsson and colleagues completed a meta-analysis of 15 studies to include over 2.5 million patients to find a 30% increased risk of developing CRC in T2D individuals compared to non-diabetic individuals[282].

Sharma et al. 2005 showed that CRC patients with T2D have more serious histopathological features such as deeper tumour invasion and more advanced staging[124]. Diabetic patients are also at increased risk of CRC recurrence compared to non-diabetics[287]. Conflicting evidence exists regarding disease specific and overall mortality with some studies showing poor survival in diabetics[287] and others showing this apparent mortality increase is in fact due to increased age and co-morbidities[288]. A systematic review on this topic concluded that the current evidence remains inconclusive since most studies fail to account for raised BMI and the effect of co-morbidities[289].

Identification of biological mechanisms that link T2D to the development and/or potentiation of colorectal tumours, could lead to preventative and therapeutic options. Potential mechanistic links between T2D and CRC are discussed below.

1.13.1. Insulin

Insulin resistance and hyperinsulinemia are both common in T2D patients. Insulin resistance occurs when the body is unable to respond to insulin resulting in elevated insulin in the blood. Insulin resistance is the main driver of metabolic syndrome (the medical term for a combination of T2D, obesity and high blood pressure), which is linked to CRC[290]. Hyperinsulinemia is the release of too much insulin relative to the levels of blood glucose[291]. This promotes activation of cellular pathways mediated by insulin and the insulin-like growth factors (IGF)[292] such as Akt, phosphatidylinositol 3-kinase (PI3K) and extracellular signal-regulated kinase (ERK) cascades which have key roles in diabetes and cancer[293].

In 2006, Tran and colleagues showed that hyperinsulinemia alone is associated with an increased risk of CRC; insulin dose dependently promoted proliferation of normal colorectal epithelial cells *in vivo*[292]. There is also a direct correlation between overexpression of insulin and IGF receptors with increased risk of CRC[294] as well as breast[295], lung, and prostate cancer and a polymorphism in the *IGF-1R* gene is associated with advanced CRC[296].

1.13.2. Chronic inflammation

Metabolic abnormalities associated with diabetes lead to an increase in pro-inflammatory molecules which are proven to have cancer promoting roles via the accumulation of DNA damage and mutations[297] such as insulin, fatty acids, IL-6, and plasminogen activator inhibitor (PAI)-1, adiponectin, leptin, TNF-α, free radicals and ROS.

There are many links between inflammation and CRC. For example, CRC cell lines and tumours constitutively express nuclear factor κB (NFκB) and STAT-3[75,298,299]. Also, those that have severe prolonged active IBD, such as UC and CD, have a greater risk of CRC than those without IBD[75], as mentioned in Chapter 1, Section 1.4.3.

1.13.3. Reactive oxygen species and hyperglycaemia

Cancer cells are known to depend on glycolysis for energy production which requires glucose[173]. Therefore, a hyperglycaemic environment is ideal for cancer promotion. Glucose promotes cellular signalling pathways such as proliferation, migration, invasion and recurrence[277,300]. Furthermore, high glucose levels can alter epigenetic modulations of oncogenic pathways and result in prolonged activation of cancer cell proliferation[301]. A significant association between high fasting serum glucose levels and increased risk of CRC has been found in a Korean study[302]. However, when cancer cells *in vitro* are deprived of glucose, most conventional cytotoxic anticancer agents lose their effectiveness[303].

Hyperglycaemia in insulin-independent tissues leads to an increase in substrates for glycolysis as well as the TCA cycle, which in turn increases the propensity for mitochondrial ROS production (Chapter 1, Section 1.8). Therefore, it could be suggested that ROS generated as a result of hyperglycaemia could be linked to CRC in T2D patients.

1.13.4. Impaired mitochondrial function

Defects in mitochondrial morphology, fission, fusion, biogenesis and oxidative phosphorylation are associated with T2D[304]. Studies have been completed on heart[305], skeletal, adipose and renal[306] tissue as these are the most relevant for complications of T2D. Mitochondria in skeletal muscle of T2D compared to non-diabetic individuals are smaller in size, at a lower density and have impaired function[307,308]. In adipose tissue, mitochondrial dysfunction leads to an increase in fatty acid release as well as increased

release of inflammatory cytokines both of which are linked to cancer[309,310]. Adipocyte mitochondrial dysfunction in T2D has been linked to FH as well as succination which will both be explored in later sections (Section 1.13.6) [310,311]. It is interesting to note that in mice, knocking out FH in the β-cells of the pancreas generates a diabetic phenotype[266].

Overall, impaired mitochondrial function generates ROS which can cause genetic instability. Currently, there is no evidence showing mitochondrial dysfunction in the gut of T2D patients.

1.13.5. Fumarate hydratase

FH has previously been linked to both mitochondrial dysfunction and cancer[312]. FH was first discovered by Einbeck in 1919[313], and is conserved from yeast to humans. In human cells, the gene is localised at 1q42.1 and expressed as a homotetramer in mitochondrial and cytosolic compartments, these enzymes are encoded by the same transcript, but are differentially processed[314]. Protein localisation is effected by cleavage of the propeptide into two peptides, one retaining the N-terminal mitochondrial targeting sequence and one that is released into the cytoplasm. In the mitochondria FH participates in the TCA cycle (Figure 1.7), where it catalyses the stereospecific hydration across the olefinic double bond in fumarate to form L-malate. In the cytosol, FH controls the levels of fumarate produced by the urea cycle (Figure 1.11) and amino acid catabolism, by conversion to malate which in turn provides increased substrate for the generation of cytosolic NADPH though the malic enzyme reaction[168]. Cytosolic FH also acts as a DNA damage response protein; upon double strand breaks in DNA, cytosolic FH is recruited into the nucleus to aid with DNA repair[315]. Cytoplasmic FH is present in all tissues except from the brain[314].

FH behaves as a tumour suppressor and, specifically, the cytoplasmic form is considered responsible for this role[315,316]. Loss or inactivation of cytosolic FH causes an increase in fumarate, leading to genomic instability and accumulation of HIF-1α subunits[317,318] (Figure 1.12). A total of 55 mutations have been described to date from work on patients with cutaneous leiomyoma, FH deficiency, hereditary leiomyomatosis and renal cell cancer (HLRCC), Leydig cell tumours, multiple cutaneous and uterine leiomyomas, ovarian mucinous cyrstadenoma, renal cell carcinoma, soft tissue sarcoma, uterine leiomyomas

and uterine leiomyosarcoma[319]. The crystal structure of FH reveals that mutations can be grouped into two distinct classes: 1) affecting structural integrity; or 2) affecting the enzyme active site[319]. The most common mutations in FH are missense (57%), and then frameshift and nonsense (27%), but there are also deletions, insertions and duplications found[319].

Fh1 deficient mice cells were found to use accumulated TCA cycle metabolites to generate haem, which is then degraded to bilirubin, creating mitochondrial NADH to generate ATP by OXPHOS. Recently, Adam et al. have shown that KO of Fh1 in pancreatic ß-cells can generate a diabetic state in mice[266]. It has also been shown that Fh1 deficient cells can use glutamine to generate citrate and malate by performing reductive carboxylation of α-ketoglutarate to isocitrate. This process then provides the anabolic building blocks allowing cell proliferation[320]. Additionally, Fh1 deficient mice and media from FH-deficient cell lines were found to excrete increased amounts of fumarate and arginosuccinate compared to their WT counterparts[321]. This was found to be a result of the reversed activity of the urea cycle enzyme arginosucinnate lyase (Figure 1.11). Concentrations of fumarate of around 10mm in Fh1 deficient cells were recently found to inhibit complex II in OXPHOS by product inhibition[322]. Despite the defects in the respiratory chain, these cells had a high mitochondrial membrane potential and can resist conditions that are unfavourable for mitochondrial function, including hypoxia, which suggests that the loss of FH expression could be selected for during tumour progression.

HLRCC tumours with FH mutation show an upregulation of HIF-1α and associated target genes[317,323,324]. In mice, inactivation of Fh1 (murine FH) causes proliferative renal cyst development and activation of the hypoxia pathway[325]. Using HCT116 CRC cells, Yogev et al., 2010, showed that irradiation induced more cell death with short hairpin RNA (shRNA) lentiviral knock down of FH. In mouse embryonic fibroblasts (MEFs), knock out of Fh1 leads to increased lactate production due to a shift towards glycolysis driven metabolism via upregulation of HIF-1α protein levels and subsequent HIF-1 target gene upregulation (HK2, LDHA, GLUT1), even though there is a reduction of mitochondrial respiration by 80% compared to wild type MEFs[316]. It has recently been shown that FH binding to double strand breaks (DSB) is dependent on DNA-dependent protein kinase (DNA-PK)-regulated phosphorylation of FH and the binding of FH to histone H2A.Z[326]. One paper suggests that

FH acts like an oncogene with elevated enzymatic activity in acute monocytic leukaemia, moderately increased enzymatic activity in acute granulocytic leukaemia, but not significantly elevated in acute lymphocytic leukaemia[327]. Moreover, FH activity was higher in the acute than the chronic phase of all three types of leukaemia. There are no known mutations of FH in CRC patients[328]. Although, one paper found that mRNA levels of FH are reduced in CRC[329].

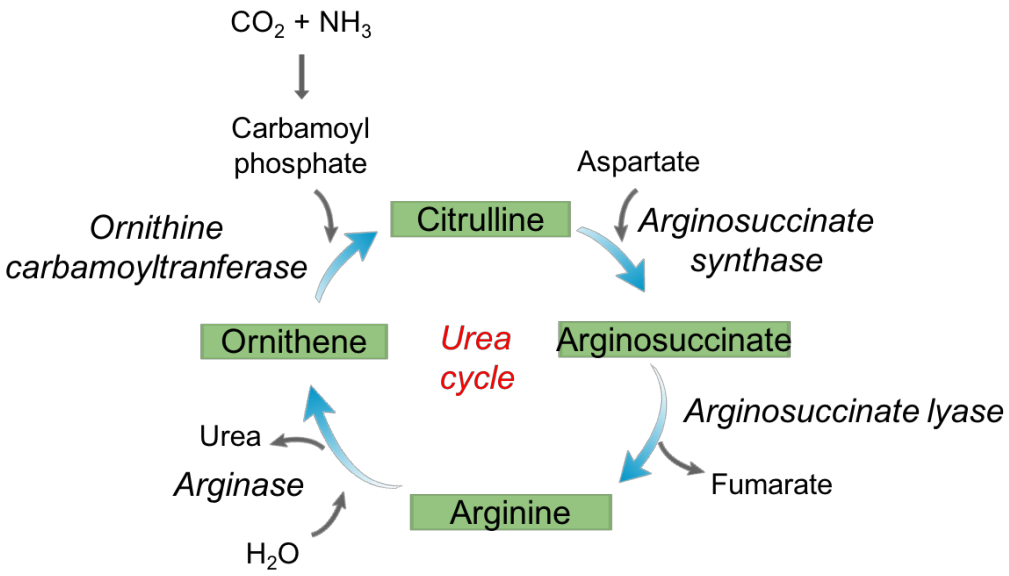

Figure 1.11. Urea cycle. A cycle of biochemical reactions that produce urea from ammonia in the cytosol[330].

1.13.6. Fumarate

Dysregulated metabolism is a designated hallmark of cancer[331] (Chapter 1, Section 1.9). Fumarate is an oncometabolite[332,333] and can accumulate to millimolar levels in FH-deficient tissues[334]. Increased levels of fumarate have been found in CRC patient samples[335], even though there is no evidence of FH mutation(s). Fumarate is a key component of the TCA cycle, where it is converted to malate by FH. Elevated fumarate has multiple cellular consequences (Figure 1.12).

Fumarate inhibits ten-eleven-translocation (TET) 5-methylcytosine (5-mC) dioxygenases which are 2-oxoglutarate dependent dioxygenases (OGDD)[336] . They convert the 5-mC in DNA sequentially to 5-hmC to 5-formylcytocine to 5-carboxylcytocine, leading to DNA methylation. 2-OGDDs other functions are oxygen sensing (via HIF-1α), collagen maturation and regulation of translation. Fumarate, succinate and R-2-hydroxyglutarate are 2-OGDD analogues and competitively inhibit several 2-OGDDs with respect to 2-oxoglutarate. Fumarate competitively inhibits the 2-OGDDs that catalyse HIF prolyl hydroxylation leading to stabilisation of HIF-1α and activation of HIF-dependent pathways including glucose metabolism[332].

Fumarate can modify cysteine residues in proteins via an irreversible process termed 'succination'[333] (Figure 1.12). Alderson et al. 2006 first described the process of succination which is chemical modification of proteins to form S-(2-succino) cysteine (2-SC) by a Michael addition reaction that generates a thioether bond between fumarate and the cysteine sulphydryl group[337].

Succination can have an inhibitory effect e.g., inactivation of glyceraldehyde 3-phosphate dehydrogenase (GAPDH) in muscle of type 1 diabetic rats or preventing the polymerisation and secretion of adiponectin from type 2 diabetic mouse adipose tissue[338,339]. The proteins which undergo succination are identified by mass spectrometry. Some known examples include inactivation of the glycolytic enzyme GAPDH both *in vivo* and *in vitro*[338]; impaired enzymatic activity of mitochondrial aconitase and inhibition of the Kelch-like ECH-associated protein (KEAP)-1 which abrogates its interaction with the transcriptional factor Nuclear factor (erythroid-derived 2)-like 2 (NRF2) resulting in the constitutive activation of the potentially oncogenic NRF2-mediated antioxidant defence

pathway[340]. Fumarate can also succinate glutathione (GSH) to form a compound which depletes intracellular NADPH and enhances oxidative stress leading to cellular senescence in non-transformed cells[341]. The overall effect of 2-SC modifications is currently not understood fully; however, is likely to be cell specific. As succination is an irreversible process the effect on the cell is dependent on the half-life and transcription turnover of the succinated proteins in relation to the level of fumarate, as well as how necessary the proteins affected are for cell function.

It has been shown that 2-SC is significantly increased in adipocytes treated with 30mM glucose versus 5mM glucose[339]. Undifferentiated fibroblasts cultured in the same high glucose media did not exhibit an increase in succination[339] whereas differentiated 3T3 fibroblasts do exhibit increased succination under 30mM glucose[310]. Frizzell et al. showed that 3T3 cells treated with 30mM glucose compared to 5mM showed significant increase in cellular ATP/adenosine diphosphate (ADP), NADH/NAD+, mitochondrial membrane potential, cellular fumarate concentration as well as succination of proteins[310]. This was postulated to be attributed to the inhibition of NAD+-dependent dehydrogenases due to increase in NADH/NAD+ ratio. Chemical uncouplers which reduce the NADH/NAD+ ratio decreased the cellular fumarate concentration and succination. Addition of metformin (an inhibitor of complex I in the ETC) to high glucose caused a further increase in fumarate and succination. The conclusion of the study was that excess nutrients in the form of glucotoxicity creates a pseudo hypoxic environment (high NADH/NAD+) which drives the increase in succination. Subsequent *in vivo* studies indicate that increased succination in adipocytes from db/db and ob/ob mice[342] (two mouse models of human diabetes (Chapter 1, Section 1.12)) and in the skeletal muscle (gastrocnemius) of streptozotocin-induced diabetic rats[333] is associated with glucotoxicity-driven mitochondrial stress[310,343]. Increased succination of KEAP1 and aconitase 2 (ACO2) has been described in renal cell carcinoma models which are derived from FH mutations[344,345].

The role of fumarate in renal disease has been well investigated. The UOK262 cell line was derived from a patient with HLRCC and has an inactive FH and therefore high levels of fumarate[346]. These cells are dependent on glycolysis for survival and display undetectably low mitochondrial oxygen consumption and therefore provide a model for the study of the Warburg effect in human cancer. It was also found in mice that the loss of Fh1 in renal

cells promotes the formation of cysts as a result of increased succination; specifically, the modification of cysteine residues within KEAP1, removing its ability to repress the NRF2 mediated antioxidant response pathway[347]. Normalisation of fumarate levels in the cytosol by re-expression of cytoplasmic-specific Fh1 rescues the defects associated with renal specific Fh1 deletion in the mice[347] suggesting that the addition of Fh1 is enough to quench the succination. Other evidence for the role of succination in disease is found in a mouse model of cardiac disease. Elevated fumarate in Fh1 cardiac knockout mice greatly reduced the amount of heart tissue damage following ischemic-reperfusion injury[348]. This is achieved by diverting amino acids into the Krebs cycle, thus, maintaining ATP levels, stabilising NRF2 and activating the NRF2 antioxidant pathway.

Fumarate has also been proven to have a role as an epigenetic modifier in the context of HLRCC[349]. Fumarate inhibits the Tet-mediated demethylation of a regulatory section of the miRNA cluster *mir-200ba429* which is anti-metastatic, leading to promotion of epithelial to mesenchymal transition (EMT)[349]. This in turn promotes cancer initiation, invasion and metastasis[350].

Interestingly, oral administration of fumarates such as dimethylfumarate (DMT) and mono-methylfumarate (MMF) improve multiple sclerosis (MS) and psoriasis[351]. DMT is Food and Drug Association (FDA) approved for the treatment on MS and psoriasis[352,353]. Ghoreschi et al. 2011 describe a mechanism which results in glutathione (GSH) depletion and leads to induction of type II dendritic cells and reduction of IL-12 and IL-23[354] and therefore improvement of psoriasis and MS symptoms. Later it was found that MMF which is the immediate metabolite of DMT can modify KEAP1, the inhibitor of NRF2 at cysteine residue 151[355]. DMF treatment has also been shown to sensitise cells in hypoxia to radiation treatment[356]. Most recently DMF has been shown to ameliorate pulmonary arterial hypertension and lung fibrosis[357]. Grzegorzewska et al. 2017 suggest that the action of DMF is by inhibition of pro-inflammatory NFκB, STAT3 and cJUN signalling as well as reduction if pro-fibrogenic mediators specificity protein 1 (Sp1), tafazzin (TAZ) and β-catenin[357]. However, a small epidemic of severe contact dermatitis cases in Finland and the UK was attributed to DMF[358]. The effects of DMF in MS, psoriasis, pulmonary arterial hypertension and lung fibrosis are not confirmed as succination. Nevertheless, the link is

possible due to the wide-reaching effects of the drug. It has also been previously shown that DMF and MMF increase succination in adipocytes[359].

The key to understanding these roles of fumarate as either an oncometabolite or as a protective agent may lie in its cellular context, concentration and its compartmentalisation in the mitochondria and cytosol.

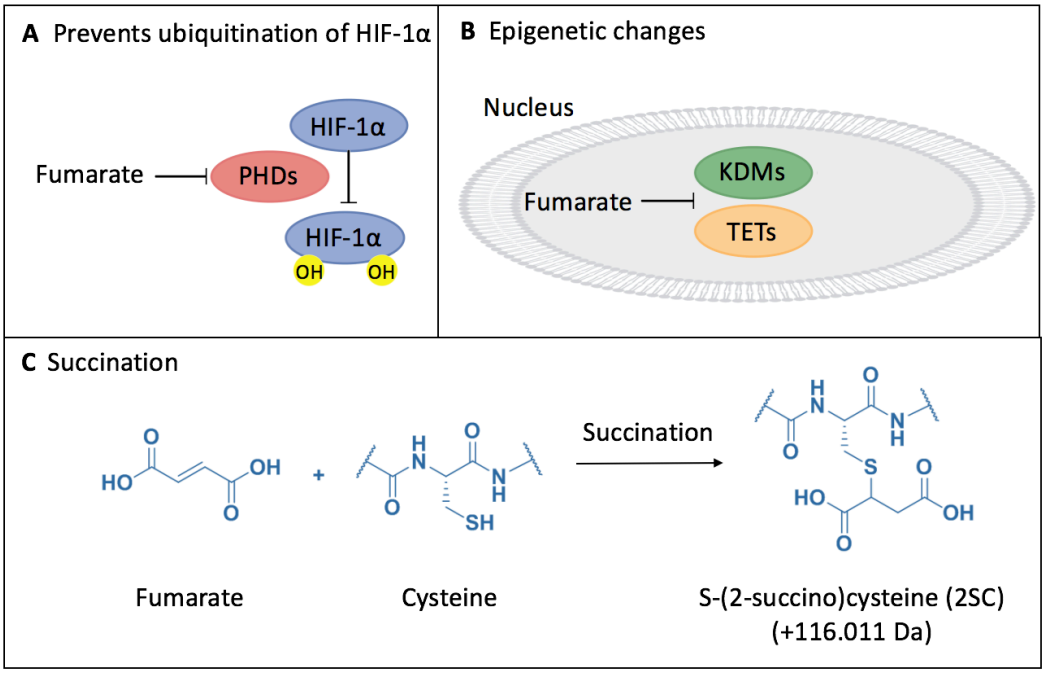

Figure 1.12. Cellular effects of fumarate. (**A**) Preventing ubiquitination of 2-OGDDs such as PHDs leading to stabilisation of HIF-1α and activation of HIF-dependent pathways including glucose metabolism[332]. (**B**) Epigenetic changes. Fumarate can inhibit TETs and KDMs leading to alterations in gene expression[360]. (**C**) Succination. The irreversible generation of a thioether bond between fumarate and the cysteine sulphydryl group to create 2-SC[337]. 2-OGDD, 2-oxoglutarate-dependent dioxygenase; PHD, prolyl hydroxylase; HIF, hypoxia inducible factor; TET, ten-eleven translocation enzyme; KDM, lysine demethylase; 2-SC, S-(2-succino) cysteine.

1.14. Mouse models of colorectal cancer and diabetes

To study the interaction between CRC and T2D in a whole-body system, it is necessary to use animal models to complement findings from human tissues. There are no published models of polyposis, as a benign early lesion of CRC, combined with T2D in mice. There are, however, models of CRC and obesity which can further inform us on the link between T2D and CRC development. Obesity is a major risk factor for T2D, 80% of patients with T2D are obese[361] (Chapter 1, Section 1.4.9). Haha et al. 2011 developed a spontaneous animal model of obesity with adenoma formation in the intestinal tract by crossing the *db/m* mice with $Apc^{Min/+}$ mice, then backcrossing the offspring with *db/m* mice to obtain *db/db*-$Apc^{Min/+}$ mice. They found that the total number of tumours was larger in *db/db*-$Apc^{Min/+}$ mice than *db/m*-$Apc^{Min/+}$ and *m/m*-$Apc^{Min/+}$ mice. Another study[362] used a double-mutant F1 offspring obtained by crossing a mouse model for intestinal tumourigenesis (C57BL/6J-$Apc^{Min/+}$) and a mouse model for obesity (C57BL/6J-$Lep^{ob/+}$) that is heterozygous for the *obese (ob)* mutation in the *leptin (lep).* This compound mutant mouse becomes obese with a homozygous mutation (*ob/ob*) as it lacks functional leptin hormone[363,364] that regulates food intake and energy expenditure. Ob/ob mice exhibit a hyperphagia, a transient diabetes-like syndrome of hyperglycaemia and glucose intolerance, elevated plasma insulin, subfertility, impaired wound healing and increased hormone production from the pituitary and adrenal glands, as well as being hypo metabolic and hypothermic[365]. To study environmentally-induced obesity they fed the F1 mice either a 45% fat diet or a control 10% fat diet as adults. They concluded that homozygous mutation in the *ob* gene significantly increased the number of spontaneous intestinal tumours, suggesting an inherent link between food intake, hyperinsulinemia and polyp formation. A diet of 45% fat also increased the number of tumours in all mice. Prolonged blood glucose levels correlate with the number of tumours.

It is not possible to determine a mechanistic link between T2D and CRC from these studies, as they do not mirror the human situation. An ideal model would mirror the progressive properties of diabetes alongside spontaneous development of CRC in the absence of obesity. However, this is unlikely to be possible due to the inherent short lifespan of mice. Although, generating a model by crossing the $Fh1^{flox/flox\ RipCre\ CAGFH}$ mice[268] (Chapter 1,

Section 1.10) with *Apc*$^{1322T+/-}$ mice[366] (Chapter 1, Section 1.12) may offer some insight into a possible link between polyposis and T2D.

1.15. Hypothesis and aims

My overarching hypothesis was that patients with type 2 diabetes are more likely to go to develop CRC or have a recurrence of CRC due to protein malfunction as a result of succination.

My hypotheses were:

- Increased levels of 2-SC in normal, adenoma and CRC tissue from type 2 diabetic patients compared to non-diabetic patients due to a lack of or inactive FH in this population.
- 2-SC levels would be higher in *KRAS/BRAF* mutant CRC tissue compared to *KRAS/BRAF* WT CRC.
- Mice with diabetes will have more and/or larger polyps compared to non-diabetic mice and mice with overexpression of FH will have fewer and/or smaller polyps.
- Diabetes may alter the cellular profile of the gut.
- Fumarate concentration will be highest in CRC cells held in hypoxia compared to normoxia and cultured in glucose compared to no glucose.
- FH concentration will be highest in CRC cells held in normoxia compared to hypoxia and cultured in no glucose compared to glucose.
- FH activity will be highest in CRC cells held in hypoxia compared to normoxia and cultured in glucose compared to no glucose.
- Expression of genes involved in glycolysis will be highest in CRC cells held in hypoxia compared to normoxia and cultured in glucose compared to no glucose.
- Expression of genes involved in mitochondrial metabolism will be highest in CRC cells held in normoxia compared to hypoxia and cultured in no glucose compared to glucose.
- The number of mitochondria will be highest in CRC cells held in normoxia compared to hypoxia and cultured in no glucose compared to glucose and mitochondrial oxygen consumption rate will be highest in CRC cells held in normoxia compared to hypoxia and cultured in no glucose compared to glucose.
- In a xenograft model of CRC, cetuximab reduces the efficacy of oxaliplatin and that *DUOX2* and *DUOXA2* expression is increased with oxaliplatin treatment, and

reduced with cetuximab treatment and DUOX2 expression is increased with oxaliplatin treatment, and reduced with cetuximab treatment.

- CRC xenografts treated with cetuximab and oxaliplatin would have more proliferating cells.

My aims were:

- To test a panel CRC, adenoma and normal tissue from non-diabetic and T2D individuals for the presence of 2-SC.
- To test a panel CRC, adenoma and normal tissue from non-diabetic and T2D individuals for the presence of FH.
- To examine whether *KRAS/BRAF* mutation in CRC is linked to 2-SC staining score.
- Create and a phenotype a mouse model predisposed to both diabetes and intestinal polyposis.
- Overexpress FH as a rescue of diabetes in the diabetic/polyposis mouse model.
- To generate an *in vitro* model of CRC and T2D and characterise:
    - Concentration of fumarate.
    - Amount and activity of FH.
    - Changes in gene expression.
    - Amount and activity of mitochondria.
- Generate a xenograft mouse model using DLD1 cells. Treat with oxaliplatin and/or cetuximab.
- Analyse *DUOX2* and *DUOXA2* gene expression by RT-PCR, and DUOX2 protein expression by IHC.
- Assess the proliferation and apoptotic status of cells within xenograft tumours using Ki67 and caspase 3 staining.

Chapter 2 – Materials and Methods

2.1 Materials and Methods for Chapter 3

2.1.1 Tissue collection

Human normal gut mucosa and CRC samples were obtained from The Royal London Hospital Pathology Department. Ethical approval for this study was obtained from the local Human Research Ethics Committees (REC reference 13/LO/1271).

2.1.2 Immunohistochemistry to detect succination

Immunohistochemistry (IHC) was carried out using the EnVision kit (Dako). 2-SC was detected with an antibody which is not commercially available (gift from Norma Frizzell, University of South Carolina) and FH with Autogen Bioclear, #NE054. Both were used at 1:2000 following 3 minutes of microwaving with citrate buffer pH6 then 10 minutes in a pressure cooker.

2.1.3 Immunohistochemistry scoring after 2-SC antibody staining

Following IHC with 2-SC antibody (see 2.1.2), stained sections were scored on a numerical scale by Consultant histopathologist Professor Roger Feakins (The Royal London Hospital, Whitechapel, London, UK). RF was blinded to the diabetic status of the patients when scoring the stained sections. Scoring was based on a standard scoring protocol: percentage of epithelial cells at each of three staining intensity levels (1- 3; low, immediate and strong) and a weighted score generated using the formula (1x1 + 2x2 + 3x3). Analysis involved paired matched normal and tumour values. The positive controls were kidney samples from HLRCC patients (positive for 2SC because of loss of FH activity)[334]. There was no non-specific staining observed. Negative controls were primary alone and secondary alone. Reproducibility was tested by conducting repeat 2-SC IHC on 10 cases both N and T (20 sections). No significance difference was identified (N versus, 0.4122; T versus T, 0.4392; t-test) indicating good reproducibility in 2-SC staining.

2.1.4 DNA extraction

DNA was extracted from formalin fixed paraffin embedded (FFPE) sections using QIAamp DNA FFPE Tissue Kit (Qiagen, #56404) according to manufacturer's protocol. Or DNA was

extracted from frozen tissue samples using DNeasy Blood and Tissue Kit (Qiagen, #60504). DNA concentrations were determined using a Nanodrop Technologies spectrophotometer.

2.1.5 PCR for KRAS and BRAF sequencing

Polymerase chain reaction (PCR) was completed using the Qiagen multiplex PCR kit (Qiagen, #206143) with the primers in Table 2.1. PCR product was run out on a 2% agarose (Sigma) gel and imaged using a ChemiDoc (BioRad).

2.1.6 Sequencing

PCR product was cleaned up using ExoSAP-IT^{TM} PCR product clean up reagent (ThermoFisher, #78200.200) and then sent to GATC (UK) for sequencing. FAST Q files were then scored.

2.1.7 Statistics

Unpaired two-tailed t-test and ordinary one-way ANOVA with Bonferroni *post-hoc* test statistics were performed using Prism 7 (GraphPad) analysis software. A P-value of <0.05 was considered statistically significant.

Table 2.1. Primer details for KRAS codon 12 (KRAS exon 12) and BRAF V600 (BRAF exon 15) mutations.

	Forward Primer (5' to 3')	**Reverse Primer (5' to 3')**	**Annealing Temp (°C)**
KRAS exon 12	TTTGATAGTGTATTAACCTTATG	TATTAAAACAAGATTTACCTC	50
BRAF exon 15	TCATAATGCTTGCTCTGATAGG	CCACTGATTAAATTTTTGGCC	60

2.2 Materials and Methods for Chapter 4

2.2.1 Breeding

Julie Adam (Wellcome Trust Centre for Genetics, Oxford) crossed female *Fh1*$^{flox/flox\ RipCre\ CAGFH}$ mice[268] with *Apc*^{1322T} mice[366] and then backcrossed to generate *Fh1*$^{flox/flox}$ *Apc*$^{1322T+/-}$ offspring (see Table 2.2 for breeding details). Female *Fh1*$^{flox/flox\ RipCre\ CAGFH}$ mice had *loxP* sites in both *Fh1* alleles and were RipCre positive; the rat insulin II gene promoter controls cre recombinase creating a conditional knockout of Fh1 in the β-cells of the pancreas. These mice were also globally positive for CAGFH (human cytoplasmic FH, which ensures that the FH is expressed in every cell) to enable females to carry offspring to full term without severe diabetes. Males were heterozygous for the *Apc* ^{1322} allele which predisposes mice to polyps mostly in the small bowel[366]. All mice generated had relevant genotypes for the study (Table 2.2).

2.2.2 Genotyping mice

Tail or ear clips from mice were digested with buffer containing 5% proteinase K overnight at 55°C. DNA was precipitated using iso-propanol and re-suspended in nuclease free water. Amplification for the relevant genes was completed with Taq DNA polymerase (Qiagen) and Taq PCR core kit (Qiagen) with the primers in Table 2.3 and cycling conditions in Table 2.4 using a thermo cycler machine. PCR product was run out on a 2% agarose (Sigma) gel and imaged using BioRad ChemiDoc (Figure 2.1).

The *Mom-1* PCR product was further digested using BamH1 (NEB, #R0136S). *Mom-1*^{S} (susceptible to polyps) will remain as a 500bp product. *Mom-1*^{R} (resistant to polyps) will be cleaved to a 400bp and 100bp product[367–369] (Figure 2.2).

Table 2.2. Mating scheme for *Fh1*$^{flox/flox}$ *Apc*$^{1322T+/-}$ mice.

Round of mating	Parents	Possible Offspring	
1	♀ *Fh1*$^{flox/flox}$*Ripcre*$^{+/-}$ *CAGFH*$^{+/-}$ *Apc*$^{1322T-/-}$ ♂*Fh1*$^{+/+}$*Ripcre*$^{-/-}$ *CAGFH* $^{-/-}$ *Apc*$^{1322T+/-}$	*Fh1*$^{flox/+}$*Ripcre*$^{+/-}$ *CAGFH*$^{+/-}$ *Apc*$^{1322T+/-}$ *Fh1*$^{flox/+}$*Ripcre*$^{+/-}$ *CAGFH*$^{+/-}$ *Apc*$^{1322T-/-}$ *Fh1*$^{flox/+}$*Ripcre*$^{+/-}$ *CAGFH*$^{-/-}$ *Apc*$^{1322T+/-}$ *Fh1*$^{flox/+}$*Ripcre*$^{+/-}$ *CAGFH*$^{-/-}$ *Apc*$^{1322T-/-}$	*Fh1*$^{flox/+}$*Ripcre*$^{-/-}$ *CAGFH*$^{+/-}$ *Apc*$^{1322T-/-}$ *Fh1*$^{flox/+}$*Ripcre*$^{-/-}$ *CAGFH*$^{+/-}$ *Apc*$^{1322T+/-}$ *Fh1*$^{flox/+}$*Ripcre*$^{-/-}$ *CAGFH*$^{-/-}$ *Apc*$^{1322T+/-}$ *Fh1*$^{flox/+}$*Ripcre*$^{-/-}$ *CAGFH*$^{-/-}$ *Apc*$^{1322T-/-}$
2	♀ *Fh1*$^{flox/flox}$*Ripcre*$^{+/-}$ *CAGFH*$^{+/-}$ *Apc*$^{1322T-/-}$ ♂*Fh1*$^{flox/+}$*Ripcre*$^{-/-}$ *CAGFH* $^{-/-}$ *Apc*$^{1322T+/-}$	*Fh1*$^{flox/+}$*Ripcre*$^{+/-}$ *CAGFH*$^{+/-}$ *Apc*$^{1322T+/-}$ *Fh1*$^{flox/+}$*Ripcre*$^{+/-}$ *CAGFH*$^{+/-}$ *Apc*$^{1322T-/-}$ *Fh1*$^{flox/+}$*Ripcre*$^{+/-}$ *CAGFH*$^{-/-}$ *Apc*$^{1322T+/-}$ *Fh1*$^{flox/+}$*Ripcre*$^{+/-}$ *CAGFH*$^{-/-}$ *Apc*$^{1322T-/-}$ *Fh1*$^{flox/+}$*Ripcre*$^{-/-}$ *CAGFH*$^{+/-}$ *Apc*$^{1322T-/-}$ *Fh1*$^{flox/+}$*Ripcre*$^{-/-}$ *CAGFH*$^{+/-}$ *Apc*$^{1322T+/-}$ *Fh1*$^{flox/+}$*Ripcre*$^{-/-}$ *CAGFH*$^{-/-}$ *Apc*$^{1322T+/-}$ *Fh1*$^{flox/+}$*Ripcre*$^{-/-}$ *CAGFH*$^{-/-}$ *Apc*$^{1322T-/-}$	*Fh1*$^{flox/flox}$*Ripcre*$^{+/-}$ *CAGFH*$^{+/-}$ *Apc*$^{1322T+/-}$ *Fh1*$^{flox/flox}$*Ripcre*$^{+/-}$ *CAGFH*$^{+/-}$ *Apc*$^{1322T-/-}$ *Fh1*$^{flox/flox}$*Ripcre*$^{+/-}$ *CAGFH*$^{-/-}$ *Apc*$^{1322T+/-}$ *Fh1*$^{flox/flox}$*Ripcre*$^{+/-}$ *CAGFH*$^{-/-}$ *Apc*$^{1322T-/-}$ *Fh1*$^{flox/flox}$*Ripcre*$^{-/-}$ *CAGFH*$^{+/-}$ *Apc*$^{1322T-/-}$ *Fh1*$^{flox/flox}$*Ripcre*$^{-/-}$ *CAGFH*$^{+/-}$ *Apc*$^{1322T+/-}$ *Fh1*$^{flox/flox}$*Ripcre*$^{-/-}$ *CAGFH*$^{-/-}$ *Apc*$^{1322T+/-}$ *Fh1*$^{flox/flox}$*Ripcre*$^{-/-}$ *CAGFH*$^{-/-}$ *Apc*$^{1322T-/}$
	♀ *Fh1*$^{flox/flox}$*Ripcre*$^{+/-}$ *CAGFH*$^{+/-}$ *Apc*$^{1322T-/-}$ ♂*Fh1*$^{flox/+}$*Ripcre*$^{+/-}$ *CAGFH* $^{-/-}$ *Apc*$^{1322T+/-}$	*Extra genotypes to the above:* *Fh1*$^{flox/+}$*Ripcre*$^{+/+}$ *CAGFH*$^{+/-}$ *Apc*$^{1322T+/-}$ *Fh1*$^{flox/+}$*Ripcre*$^{+/+}$ *CAGFH*$^{-/-}$ *Apc*$^{1322T+/-}$ *Fh1*$^{flox/+}$*Ripcre*$^{+/+}$ *CAGFH*$^{+/-}$ *Apc*$^{1322T-/-}$ *Fh1*$^{flox/+}$*Ripcre*$^{+/+}$ *CAGFH*$^{-/-}$ *Apc*$^{1322T-/-}$	*Fh1*$^{flox/flox}$*Ripcre*$^{+/+}$ *CAGFH*$^{+/-}$ *Apc*$^{1322T+/-}$ *Fh1*$^{flox/flox}$*Ripcre*$^{+/+}$ *CAGFH*$^{-/-}$ *Apc*$^{1322T+/-}$ *Fh1*$^{flox/flox}$*Ripcre*$^{+/+}$ *CAGFH*$^{+/-}$ *Apc*$^{1322T-/-}$ *Fh1*$^{flox/flox}$*Ripcre*$^{+/+}$ *CAGFH*$^{-/-}$ *Apc*$^{1322T-/-}$
	♀ *Fh1*$^{flox/flox}$*Ripcre*$^{+/-}$ *CAGFH*$^{+/-}$ *Apc*$^{1322T-/-}$ ♂*Fh1*$^{flox/+}$*Ripcre*$^{+/-}$ *CAGFH* $^{+/-}$ *Apc*$^{1322T+/-}$	*Extra genotypes to the above:* *Fh1*$^{flox/+}$*Ripcre*$^{-/-}$ *CAGFH*$^{+/+}$ *Apc*$^{1322T+/-}$ *Fh1*$^{flox/+}$*Ripcre*$^{-/-}$ *CAGFH*$^{+/+}$ *Apc*$^{1322T+/-}$ *Fh1*$^{flox/+}$*Ripcre*$^{-/-}$ *CAGFH*$^{+/+}$ *Apc*$^{1322T-/-}$	*Fh1*$^{flox/+}$*Ripcre*$^{-/-}$ *CAGFH*$^{+/+}$*Apc*$^{1322T-/-}$ *Fh1*$^{flox/flox}$*Ripcre*$^{-/-}$ *CAGFH*$^{+/+}$*Apc*$^{1322T+/-}$ *Fh1*$^{flox/flox}$*Ripcre*$^{-/-}$ *CAGFH*$^{+/+}$*Apc*$^{1322T+/-}$ *Fh1*$^{flox/flox}$*Ripcre*$^{-/-}$ *CAGFH*$^{+/+}$*Apc*$^{1322T-/-}$ *Fh1*$^{flox/flox}$*Ripcre*$^{-/-}$ *CAGFH*$^{+/+}$*Apc*$^{1322T-/-}$

Table 2.3. Primer details for genotyping *Fh1*$^{flox/flox}$ *Apc*$^{1322T+/-}$ mice.

Gene	Primer	Primer Sequence (5' to 3')	Annealing temp. for PCR (°C)	Expected band size of product (bp)
1322T	Forward Reverse Reverse	CCCTCCATCAACCAAGAAAC TGGGTTTGGCTCTAGCATTC AAGAGTGCCTCCCAAAATGA	55	WT 430 Target 217
FH^{cyt}	Forward Reverse	AACATGATCGTTGGGATGCAC GCCTCTGCTAACCATGTTCAT	60	510
Fh1	Forward Reverse Reverse	ACCCTGCTAGGTGTCACCAC CCTGGCACTGCAGACTACAA GCTCAGTCACCCATCCAAAT	55	WT 240 Homoflox 470
RipCre	Forward Reverse	TAGCACCAGGCAAGTGTTTG AGGCAAATTTTGGTGTACGG	55	~890
Mom-1	Forward Reverse	GTCCAAGGGAACATTGCG AGAACAGGTGATTTGGCCCC	60	500

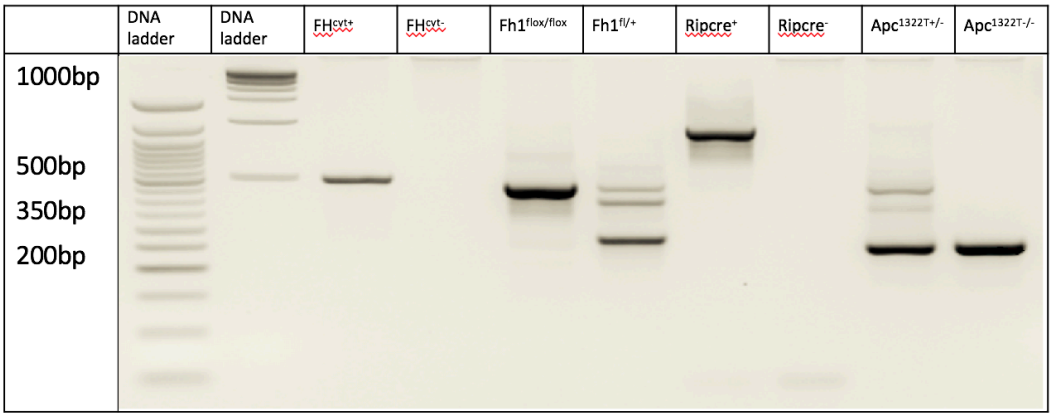

Figure 2.1. Reference gel for genotyping *Fh1$^{flox/flox}$ Apc$^{1322T+/-}$* mice. PCR was performed for CAGFH, Fh1$^{flox/flox}$, RipCre and Apc^{1322T} with primers in Table 2.3 according to details in Table 2.4. PCR product was then run on a 2% agarose gel as shown above. Product sizes are confirmed in Table 2.3.

Table 2.4. PCR reaction conditions.

Step		**Temperature (°C)**	**Time (mins)**
1 - Initial denaturation		95	3
2 - Denaturation	**3-step cycling – repeat 29 times**	95	0.5
3 - Annealing		See Table 2.3	0.75
4 - Extension		72	0.75
5 - End		8	For ever

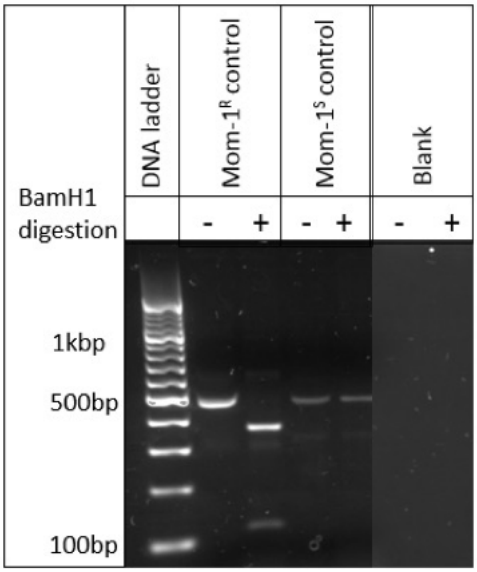

Figure 2.2. *Mom-1* PCR DNA gel example. PCR was performed for *Mom*-1 and then the product was digested with BamH1. There are two forms of the *Mom-1* allele[367] which form different products when incubated with the restriction endonuclease BamH1. The *Mom-1^S* allele is not digested so retains a 500bp length, whereas the *Mom-1^R* allele forms 400bp and 100bp products[367,370].

2.2.3 Tissue collection

Mice were sacrificed *via* a schedule 1 procedure 60-90 days after birth or when symptomatic (anaemic secondary to polyps or suffering rectal prolapse, or high blood sugar). Blood glucose was taken using ACCU-CHEK Aviva machine (Roche) at culling. Gut was removed and divided into four segments in the following fashion: three equal lengths of the small bowel (SB) to give proximal (SB1), middle (SB2), distal (SB3) and then the large bowel (LB). Each segment was flushed with phosphate buffered saline (PBS) and opened longitudinally onto filter paper. Polyps and normal gut were selected from each region of the bowel and snap frozen. Guts were then placed in 10% neutral buffered formalin (NBF) overnight then stored in 70% ethanol until processing.

2.2.4 Quantification of gut length and polyp number

Fixed intestinal tissue was measured using a ruler, then submerged in 0.2% methylene blue (0.5g methylene blue in 15mL glacial acetic acid made up to 500mL with H_2O) for 5 seconds and then placed in PBS. Using a dissection microscope at x3 magnification and polyps were recorded according to size and location. See Figure 2.3 for an example of gut with polyps visible.

2.2.5 Tissue processing for immunohistochemistry

Each gut section was rolled and secured with a pin and placed in a large cassette (Simport, Macrosette, #M512) in the same orientation. Samples were processed for histology using the schedule in Table 2.5 using large moulds (Simport, 11601000 X1000 Base mould disposable 37x24x5mm). Gut rolls were embedded in wax so that each section would present in the same place in all blocks (Figure 2.4).

2.2.6 Immunohistochemistry

H+E stain was carried out by The Royal London Hospital Pathology Department as part of the sectioning service. IHC was carried out using the EnVision kit (Dako). Paneth cells were detected with anti-lysozyme (Dako, #EC 3.2.1.17) used at 1:500 after 5 minutes microwaving in citrate buffer pH6. Goblet cells were detected with alcian blue stain (Sigma, #B8438).

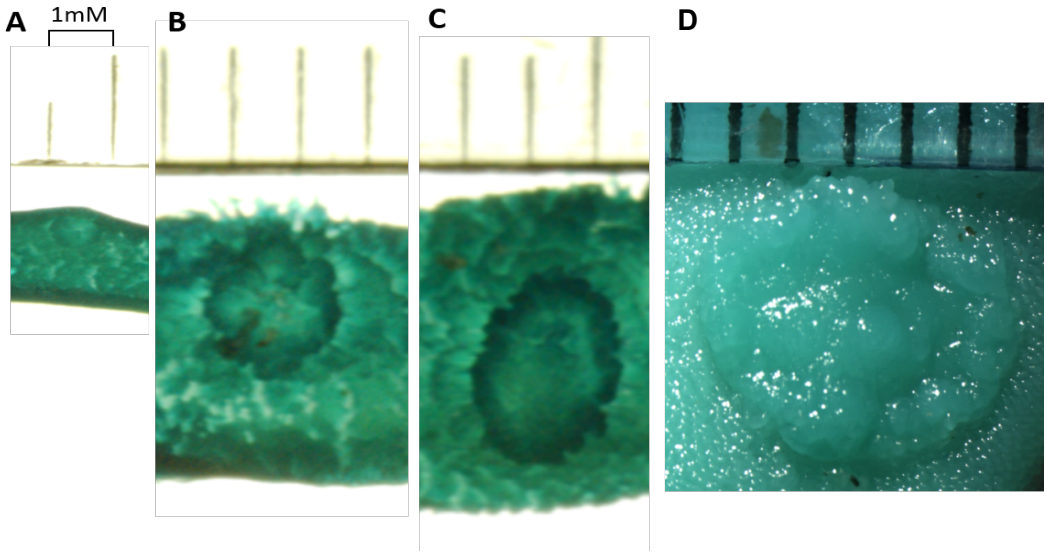

Figure 2.3. Example polyps in mice. Gut was extracted, fixed, and stained with methylene blue. Polyp count was performed using a bright field microscope. There were five categories of polyp size. 0-1mM (A), <1-2mM (B), <2-3mM (C), 3+mM (D).

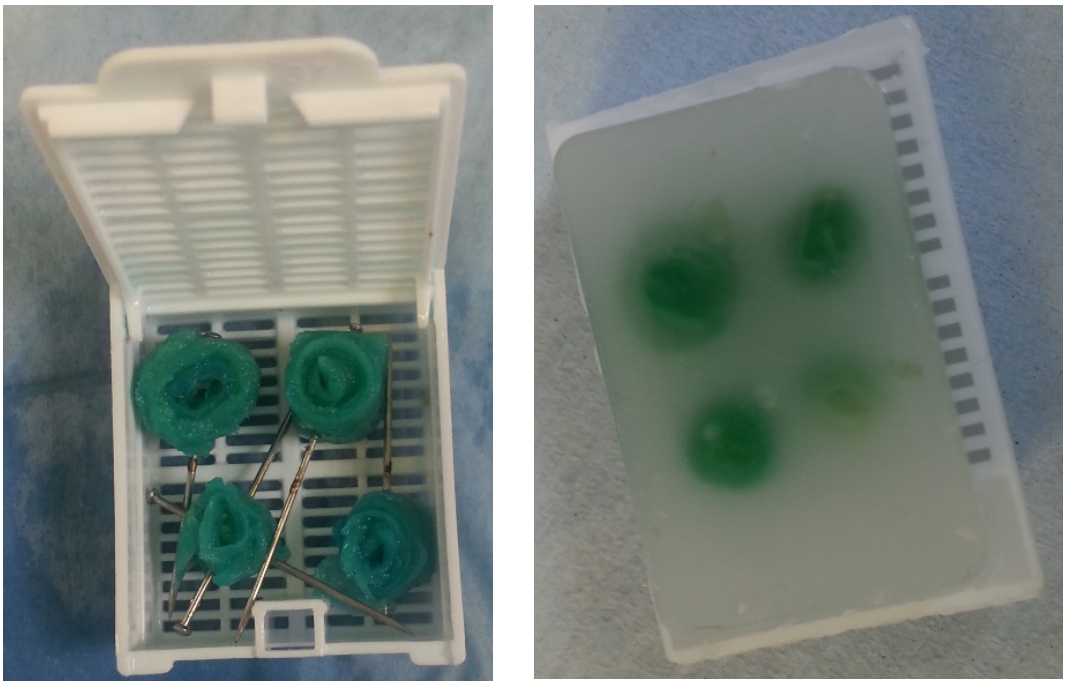

Figure 2.4. Gut rolls pinned and placed in a large cassette (left) and embedded in wax (right). SB1 top left, SB2 top right, SB3 bottom left and LB bottom right. SB, small bowel; LB, large bowel.

Table 2.5. Tissue processing and embedding details.

Step	Solution	Time (min)
1	70% ethanol	45
2	90% ethanol	30
3	95% ethanol	45
4	100% ethanol	30
5	100% ethanol	45
6	100% ethanol	45
7	Histoclear	30
8	Histoclear	30
9	Histoclear	30
10	Wax	60
11	Wax	60
12	Embed in wax	2

2.2.7 Scoring of immunohistochemistry

Using NDPview.2 software (Hamamatsu) 50 villi and 100 crypts of which the entire length was visible, were selected from each mouse, for each stain, and an image was taken of each. All counting was done by eye.

2.2.8 Metabolite analysis

Capillary electrophoresis time of flight mass spectrometry (CE-TOF/MS) analysis was used to determine metabolites levels (nmol/g). Samples were dissected and flash frozen on dry ice then shipped to the Institute for Advanced Biosciences in Japan for CE-TOF/MS as described previously[371,372].

2.2.9 Statistics

Ordinary one-way ANOVA and two-way ANOVA was performed, both with Bonferroni *post hoc* test statistics were performed using Prism 7 (GraphPad) analysis software. A P-value of <0.05 was considered statistically significant.

2.3 Materials and Methods for Chapter 5

2.3.1 Cell culture

Human CRC cell lines DLD1, HT55 and SW387 were a gift from Professor Ian Tomlinson, (who also validated the cell lines) Wellcome Institute for Human Genetics, Oxford University, and were maintained in Dulbecco's modified Eagle's Medium (DMEM) (Gibco, #11966), with 10% fetal bovine serum (FBS) (Labtech, #FB-1001T/500), 171µM penicillin (Sigma, #P4333), 172µM streptomycin (Sigma, #P4333), 2mM L-glutamine (GE Healthcare, #M11-006) and either 25mM, 5mM or 0mM glucose (Sigma, #G7021) as detailed below.

I decided to reduce [glucose] in the media slowly over a period of 3 months: first, from 25mM to 12.5mM; then in 12.5mM glucose until their doubling time was stable. The process was repeated with 10mM, 7.5mM and 5mM when the cells were banked by storage in liquid nitrogen. The glucose was reduced further to 2.5mM and finally 0mM in the same way; the cells which grew at 0mM glucose were banked. Once the desired [glucose] was established, which was 25mM, 5mM and 0mM, the cells were cultured for a further 8 passages before using the cells for experimentation to ensure continued stability of doubling time.

Fh1 WT and KO MEFs were a gift from Dr Julie Adam, Oxford Centre for Diabetes, Endocrinology and Metabolism and were maintained in DMEM containing 10% fetal bovine serum (FBS), 171µM penicillin, 172µM streptomycin, 2mM L-glutamine and 25mM glucose. All cell lines were kept at 37°C under a humidified atmosphere containing 5% CO_2, and 20.9% O_2. A 1% and 0.2% O_2 atmosphere was provided by an INVIVO2 1000 (Baker Ruskinn). Stable doubling time was calculated using the following formula [h(ln2/ln(e2/e1)] where e1 is cell number plated and e2 is the total cell number harvested and h is the hours between plating and harvesting.

2.3.2 Western blotting

Cells were rinsed once with PBS and lysed with the addition of RIPA buffer (Sigma). Protein concentration was determined by the Pierce™ BCA Protein Assay (ThermoFisher, #23225). Equal amounts of protein were added to 4-12% Bis-Tris polyacrylamide gels (Life

Technologies). Proteins were transferred to a PVDF membrane using the Pierce Power Blotter (Life Technologies). Membranes were blocked in 5% dry-milk in PBS containing 0.1% Tween-20 (Sigma) (PBS-T) for 1 hour at room temperature. After washing in PBS-T, membranes were incubated with the appropriate primary antibody (Table 2.6) at 4°C overnight. After washing with PBS-T, membranes were incubated with the appropriate horseradish peroxidase (HRP)-conjugated secondary antibody at room temperature for 1 hour (see Table 2.6). Proteins were detected using Pierce ECL Plus Western Blotting Substrate (Thermo, #32106).

2.3.3 Viability assay

Cells were plated in 6 well plates and kept at 37°C under a humidified atmosphere containing 5% CO_2 and 20.9% O_2. At 24 hours, the cells were placed at 37°C under a humidified atmosphere containing 5% CO_2, and either 20.9% or 0.2% O_2. At 72 hours, cells were washed with PBS and harvested with TrypLE Express (Invitrogen, #12605-010). Cells were suspended with media and 0.4% trypan blue (Invitrogen, #15250061). The number of cells were counted using a haemocytometer, blue cells represented dead cells.

2.3.4 Fumarate detection by mass spectrometry

Fumarate (fmol/cell) was determined by CE-TOF/MS analysis by Professor Tomoyoshi Soga (Keio University, Japan). DLD1, HT55 and SW837 cell lines were cultured with 25mM glucose DMEM and held under 20.9%, 1% or 0.2% O_2 for 48 hours. Cells were then washed two times in 5% Mannitol (Wako, Japan) and harvested in methanol containing 25mM methionine sulfone, 25mM 2-morpholinoethanesulfate and 25mM D-camphor-10-sulfonic acid. Samples were next flash frozen on dry ice and shipped to the Institute for Advanced Biosciences in Japan for CE-TOF/MS as described previously[371,372].

2.3.5 Fumarate detection using fluorometric assay

Cells were plated in flasks and kept at 37°C under a humidified atmosphere containing 5% CO_2 and 20.9% O_2. At 24 hours, the cells were placed at 37°C under a humidified atmosphere containing 5% CO_2, and either 20.9% or 0.2% O_2. At 72 hours, cells were washed with PBS and harvested with TrypLE™ Express (Invitrogen, #12605-010). $1x10^6$

cells were then used in a commercially available assay to detect fumarate (Sigma, MAK060).

Table 2.6. Western blotting antibody details.

Primary antibody	**Company and catalogue no.**	**Dilution used**	**Secondary antibody**	**Company and catalogue no.**	**Dilution used**
2-SC	Not commercially available. Gift from Norma Frizzell, University of South Carolina.	1:10,000	HRP-linked anti-rabbit	Dako, #P0448	1:2,000
HIF-1α	BD, #610959	1:500	HRP-linked anti-mouse	Dako, #P0447	1:2,000

2.3.6 Fumarate Hydratase activity

Cells were plated in flasks and kept at 37°C under a humidified atmosphere containing 5% CO_2 and 20.9% O_2. At 24 hours, the cells were placed at 37°C under a humidified atmosphere containing 5% CO_2, and either 20.9% or 0.2% O_2. At 72 hours, cells were washed with PBS and the flask was put immediately at -80°C for at least 24 hours. Cells were thawed on ice, harvested with Hepes-KOH pH7.6 with phosphatase inhibitors, sonicated and stored at -80°C. Samples were incubated with a reaction mix containing 10µM NAD^+ (Sigma, #N7004), 1M KH_2PO_4 (Sigma), 1M $MgCl_2$ (Sigma), 50mM Hepes-KOH pH7.6 (Sigma), 10mM glutamic acid (Sigma, #G8415), malate dehydrogenase (Sigma, #M1567) and glutamic oxaloacetate transaminase (Sigma, #10105554001) for 10 mins at 37°C. 30mM fumeric acid (Sigma, F8509) was then added to the mix. Fluorescence was measured every 40 seconds at excitation 340nm, emission 460nm for 15 minutes and corresponded to NADH produced. NADH standards were made up fresh (Sigma, #N8129).

2.3.7 Immunostaining

Cells were plated in 96-well plates and kept at 37°C under a humidified atmosphere containing 5% CO_2 and 20.9% O_2. At 24 hours, the cells were placed at 37°C under a humidified atmosphere containing 5% CO_2, and either 20.9% or 0.2% O_2. At 72 hours, cells were washed with PBS and fixed with 4% paraformaldehyde, followed by 0.1% Triton X permeabilisation and blocking with 0.25% bovine serum albumin (BSA), followed by antibody incubations (Table 2.7).

Images were collected at 10x using the IN cell 2200 microscope (GE) and the InCell Developer Analysis V1.9 software (GE) was used for image analysis.

Table 2.7. Immunostaining antibody details.

Primary antibody	**Company and catalogue no.**	**Dilution used**	**Secondary antibody**	**Company and catalogue no.**	**Dilution used**
HIF-1α	BD, #610959	1:500	HRP-linked anti-mouse	Dako, #P0447	1:2,000
FH	Autogen Bioclear, #NE054	1:2,000	HRP-linked anti-rabbit	Dako, #P0448	1:2,000
Mitochondrial protein	Abcam, #ab3298	1:2,000	HRP-linked anti-mouse	Dako, #P0447	1:2,000
Hoechst 33342	Invitrogen, #H3570	1:5000	-	-	-
Cell Mask Deep Red	Invitrogen, #C10046	1:100,000	-	-	-

2.3.8 RT-qPCR

Cells were plated in flasks and kept at 37°C under a humidified atmosphere containing 5% CO2 and 20.9%. At 24 hours, the cells were placed at 37°C under a humidified atmosphere containing 5% CO_2, and either 20.9% or 0.2% O_2. At 72 hours, cells were washed with PBS and RNA was extracted using miRNeasy kit (Qiagen) according to manufacturer's protocol. RNA concentrations were determined using a Nanodrop Technologies spectrophotometer. RNA samples were reverse-transcribed using a Reverse Transcriptase kit (ABI) and reverse transcription (RT) products were incubated with selected TaqMan assays (Table 2.8) and TaqMan Universal MasterMix (Applied Biosystems) on a 7500 Fast System RealTime PCR cycler (Applied Biosystems), according to the manufacturer's instructions. DLD1 results were normalised to a geomean of 18S and RPLPO; HT55 to actin; SW837 to B2M. Data was analysed by the ΔΔ^ct method[373].

2.3.9 Seahorse

Cells were plated in XF24 plates (Agilent) and incubated at 37°C overnight. The next day, medium was changed to XF assay medium (Agilent) containing 25mM, 5mM or 0mM glucose, 1mM pyruvate, 2mM glutamine, and the cells were incubated at 37°C for 1 hour. Steady-state (baseline) oxygen consumption rates and extracellular acidification rates were measured using a XF24 extracellular flux analyser (Agilent). Addition of 1μM oligomycin was used to evaluate the amount of ATP produced by the mitochondria of the cells by inhibiting ATP synthase (complex V); addition of 0.6μM FCCP was used to evaluate the maximal oxygen consumption rate by uncoupling oxygen consumption from ATP production; addition of 0.5μM rotenone and antimycin A was used to measure the spare respiratory capacity of the cell by inhibiting complex I and III of the electron transport chain respectively.

2.3.10 Statistics

Unpaired two-tailed t-test, ordinary one-way ANOVA and two-way ANOVA was performed, both with Bonferroni *post hoc* test statistics were performed using Prism 7 (GraphPad) analysis software. A P-value of <0.05 was considered statistically significant.

Table 2.8. TaqMan Assay Details (all from Life Tech).

Gene	Probe no.
BAX	Hs00180269_m1
CA9	Hs00154208_m1
CASP9	Hs00609647_m1
COX4I2	Hs00261747_m1
FH	Hs00264683_m1
GAPDH	Hs99999905_m1
GLUT1	Hs00892681_m1
GLUT4	Hs00168966_m1
GPX1	Hs00829989_gH
HIF-1α	Hs00153153_m1
HIF-1ß	Hs01121918_m1
HIF-2α	Hs01026149_m1
HK2	Hs00606086_m1
LDHA	Hs01378790_g1
LONP1	Hs00998404_m1
PDK1	Hs01561850_m1
SOD2	Hs00167309_m1
VEGF	Hs00900055_m1
VHL	Hs00184451_m1

2.4 Materials and Methods for Chapter 6

2.4.1 Xenograft model

The study design and implementation was overseen by Professor Kairbaan Hodivala-Dilke. The ethics project licence for this work is PPL70/7411 (Professor Kairbaan Hodivala-Dilke). Mice were housed in a pathogen-free environment and all procedures were conducted according to the requirements of the United Kingdom Home Office Animals (Scientific Procedures) Acts, 1986.

Eight-week old female nude mice (*nu/nu*) were implanted with $5x10^6$ human DLD1 CRC cells in 200uL saline on a single flank. Once tumours were between 200-300mm^3 the dosing schedule was initiated. Mice were randomised into four treatment arms; 1) oxaliplatin 8mg/kg alone, 2) cetuximab (30mg/kg), 3) oxaliplatin 8mg/kg + cetuximab 30mg/kg, 4) saline as an untreated group. Drugs were administered by intraperitoneal injection.

24 hours post-drug injection, mice were killed and xenografts were harvested. Professor Hodivala-Dilke's staff conducted this work and I collected the xenografts for subsequent analysis. One half of the xenograft tissue was submerged in AllProtect (Qiagen, #76405) and kept at 4°C. The other half of the tissue was submerged for 12 hours in 10% neutral buffered formalin (Sigma, #HT501128), then moved to 70% ethanol for 12-24 hours before embedding in paraffin wax. Serial sections (5 µm) were cut for ISH and IHC.

2.4.2 RT-qPCR

RNA was extracted using miRNeasy kit (Qiagen) according to manufacturer's protocol. RNA concentrations were determined using a Nanodrop Technologies spectrophotometer. A tissue ruptor instrument (Qiagen) was used to assist with homogenisation of tissue. RNA samples were reverse-transcribed using a Reverse Transcriptase kit (ABI) and reverse transcription (RT) products were incubated with selected TaqMan assays and TaqMan Universal MasterMix (Applied Biosystems) on a

7500 Fast System RealTime PCR cycler (Applied Biosystems), according to the manufacturer's instructions. Probes used were DUOX2 (Qiagen, #Hs01595312_g1) and DUOXA2 (Qiagen, #Hs01595312_g1). The housekeeping gene used was GAPDH (Qiagen, #Hs00204187_m1). Data was analysed by the ½^ct method[373].

2.4.3 Immunohistochemistry

IHC was performed according to standard protocols. Briefly, serial sections were dewaxed, rehydrated and immersed in 3% hydrogen peroxide for 10 minutes to quench endogenous peroxidase activity. Antigen retrieval was performed by microwaving for 15 minutes in sodium citrate buffer (pH6.0). After cooling, sections were incubated with blocking buffer (1:25 goat serum in PBS) for 15 mins at RT. Primary antibodies were applied for 45 minutes at room temperature - rabbit anti-human Ki67 at 1:1000 dilution (Abcam, #ab92742); rabbit anti-human cleaved caspase 3 at 1:400 (Cell Signaling #9664); DUOX2 at 1:50 dilution (Millipore, #MABN787). Sections were then incubated with a biotinylated secondary antibody at room temperature for 45 min, followed by incubation with streptavidin-biotin peroxidase solution at room temperature for 45 min. Visualization of antibody binding was carried out using DAB and sections were lightly counterstained using haematoxylin.

2.4.4 In situ hybridisation

For *in situ* hybridisation (ISH), hDUOX2 expression was determined using the RNAscope 2.0 High Definition assay (Brown, #310035) according to the manufacturer's instructions (Advanced Cell Diagnostics, Hayward, CA). Briefly, samples were heated at 60˚C for 1 hour, dewaxed and rehydrated in water then incubated with Pre-treatment 1 buffer for 10 minutes at room temperature. Next slides were boiled in Pre-treatment 2 buffer for 15 minutes, followed by incubation with Pre-treatment 3 buffer for 30 minutes at 40˚C. Then slides were incubated with the probe for 2 hours at 40˚C, followed by successive incubations with Amp1 to 6 reagents. Staining was visualized with 3,3-diaminobenzine (DAB) then lightly counterstained with haematoxylin before dehydrating and mounting with distyrene plasticiser xylene (DPX).

2.4.5 Scoring of immunohistochemistry and in situ hybridisation

Slides were scanned using a NanoZoomer 2.0 H-T, (Hamamatsu Photonics UK Limited, Welwyn Garden City, UK). Images were viewed using NDPview2 and each target under investigation was aligned across serial sections. Seven randomly selected areas were then examined at x20. Total cell numbers and the number of positively stained cells within a field were counted for IHC and expressed as percentage positive cells. For ISH a positive cell was scored if a minimum of 3 dots could be seen within the cell boundary.

Ki67 and caspase 3 IHC and DUOX2 ISH were done as percentage positive cells as these are nuclear stains and easy to determine which cell the staining belongs to. DUOX2 IHC was quantified by the scoring system outlined in Table 2.9. This method was used as the staining is cytoplasmic. Two independent individuals (myself and Rosemary Jeffery) blinded to the experimental group performed the counts and scores.

2.4.6 Statistics

Two-tailed student's t-test with Welch's correction was performed using Prism (GraphPad) analysis software. A P-value of <0.05 was considered statistically significant.

Table 2.9. Scoring method for DUOX2 IHC.

Score	Description
0	No positive staining
1	Less than 5% of the tissue had positive staining
2	Less than 10% but more than 5% of the tissue had positive staining
3	Less than 15% but more than 10% of the tissue had positive staining
4	Less than 20% but more than 15% of the tissue had positive staining
5	20% or more of the tissue had positive staining

Chapter 3 – Succination is elevated in CRC tissue from T2D patients

3.1 Introduction

Succination, a process where fumarate causes post-translational modification of cysteine residues in proteins to form 2-SC (Chapter 1, Section 8.5, Figure 10), has been described in adipose and skeletal muscle cells of diabetic animal models[341,346]. Its functional consequences include loss of activity of the mitochondrial Krebs cycle aconitase[345] and the glycolytic enzyme glyceraldehyde 3-phopshate dehydrogenase (GAPDH)[338].

To date, the only cancer in which protein succination has been described is HLRCC[374]. HLRCC patients have a loss of function mutation in FH that results in millimolar levels of fumarate, which leads to succination[330]. Fumarate is a member of the TCA cycle in mitochondria, where it is converted to malate by FH. Fumarate is also produced by the urea cycle and amino acid catabolism in the cytoplasm; excess fumarate here is mopped up by cytoplasmic FH. Other known roles for fumarate are promotion of cancer cell survival by stabilisation of HIF-1α by competitively inhibiting 2-OGDDs leading to activation of HIF-dependent pathways such as glucose metabolism[332]. Fumarate can also reduce DNA methylation by inhibiting TET 5-mC 2-OGDDs. Fumarate has since been described as an oncometabolite[375]. Fumarate is elevated in CRC tissue compared to matched normal[335] and the functional consequences of succination might explain why those with T2D who present with CRC have more invasive CRC, as well as a poorer outcome due to loss of activity of key proteins within the cell. Moreover, mutations in *KRAS* and *BRAF* are found in approximately 40% and 10% of CRC cases respectively[376,377], and these changes have recently been linked with alterations in cancer cell metabolism[376,377]. As fumarate is a metabolite, this could suggest a link between 2-SC and *KRAS/BRAF* mutation status.

3.1.1 Hypotheses

I hypothesised increased levels of 2-SC in normal, adenoma and CRC tissue from type 2 diabetic patients compared to non-diabetic patients due to a lack of or inactive FH in this population. I also hypothesised that 2-SC levels would be higher in *KRAS/BRAF* mutant CRC tissue compared to *KRAS/BRAF* WT CRC.

3.1.2 Aims

- To test a panel CRC, adenoma and normal tissue from non-diabetic and T2D individuals for the presence of 2-SC.
- To test a panel CRC, adenoma and normal tissue from non-diabetic and T2D individuals for the presence of FH.
- To examine whether *KRAS/BRAF* mutation in CRC is linked to 2-SC staining score.

In this chapter, statistical significance was determined by ordinary one-way ANOVA with Bonferroni *post-hoc* test unless otherwise stated. Statistically significant results are denoted with * in figures, exact p values can be found in the appendix (Chapter 9).

3.2 Succination is present in normal, adenoma and CRC tissue

IHC for 2-SC was performed on normal, adenoma and CRC tissue (Figure 3.1). Evidence of succination, by histology, was found in the majority of samples, including normal tissue (Table 3.1). This suggested that succination is a normal process which happens in the GI tract. The 2-SC staining was non-uniform across tumours, underlining metabolic heterogeneity of CRC.

Table 3.1. Percentage of tissue samples with evidence of succination.

	Tissue					
	Normal		Adenoma		CRC	
	ND	T2D	ND	T2D	ND	T2D
Total no. of samples	67	26	23	7	57	25
Percentage (%) of samples with succination evidence	85.29	76.92	100	100	98.25	100

3.3 Succination is elevated in CRC

IHC for 2-SC was performed on matched normal intestinal mucosa and CRC patient samples; 58 from non-diabetic patients and 25 from T2D patients (Table 3.1, Figure 3.1). I identified and sourced the patient blocks from The Royal London hospital pathology archive, collated and analysed the data. IHC was carried out by Julie Adam using a validated antibody that detects 2-SC motifs[342] that was gifted by Norma Frizzell (the antibody is not commercially available and Julie Adam holds the material transfer agreement) (Chapter 2, Section 2.1.2). The sections were scored by Roger Feakins (consultant pathologist) according to protocol given in Chapter 2, Section 2.1.3.

2-SC was significantly elevated in CRC tissue compared to matched normal tissue ($p<0.0001$, unpaired t-test, Figure 3.2.A, Table 3.2). In non-diabetic patients, 2-SC was significantly elevated in CRC tissue compared to matched normal tissue ($p<0.0001$, Figure 3.2.B, Table 3.2). Similarly, in T2D patients, 2-SC was significantly elevated in CRC tissue compared to matched normal tissue ($p<0.0001$, Figure 3.2.B, Table 3.2). Moreover, 2-SC was significantly higher in CRC tissue from T2D patients compared to non-diabetic patients ($p=0.001$).

The 2-SC score difference between the normal and CRC tissue is significantly different between non-diabetic and T2D patients ($p=0.0264$, Figure 3.2.C. Table A.3.1,2). There was a greater difference in T2D patients compared to non-diabetic patients. In non-diabetic patients, the 2-SC score was higher in the CRC compared to the matched normal in 85.96% and lower in 14.03%. In T2D patients the 2-SC score was higher in the CRC compared to the matched normal in in 96.15% of patients and lower in 3.85%.

These results highlight that increased succination is a feature of CRC and bring to light an interaction between succination and T2D in CRC tissue. The presence of T2D increases the amount of 2-SC. This association between cancer, T2D and succination has not been shown before.

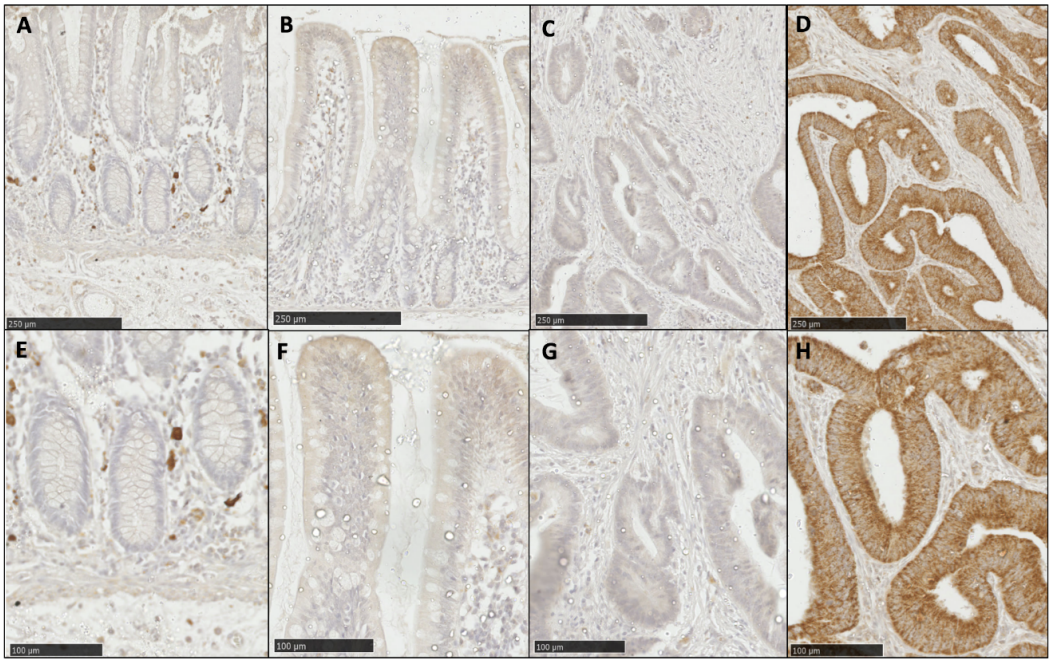

Figure 3.1. Representative images of 2-SC IHC in CRC tissue. IHC was performed on sections with a 2-SC antibody. (**A**) Normal tissue from showing weak or no 2-SC staining in the epithelium. (**B**) Normal tissue showing weak to medium 2-SC staining. (**C**) CRC tissue showing weak to medium 2-SC staining. (**D**) CRC tissue showing intense 2-SC staining. (**E**) Close up of (A), (**F**) close up of (B), (**G**) close up of (**C**), (**H**) close up of (**D**). (**A-D**) Scale bar 250µm, (**E-H**) scale bar 100µm).

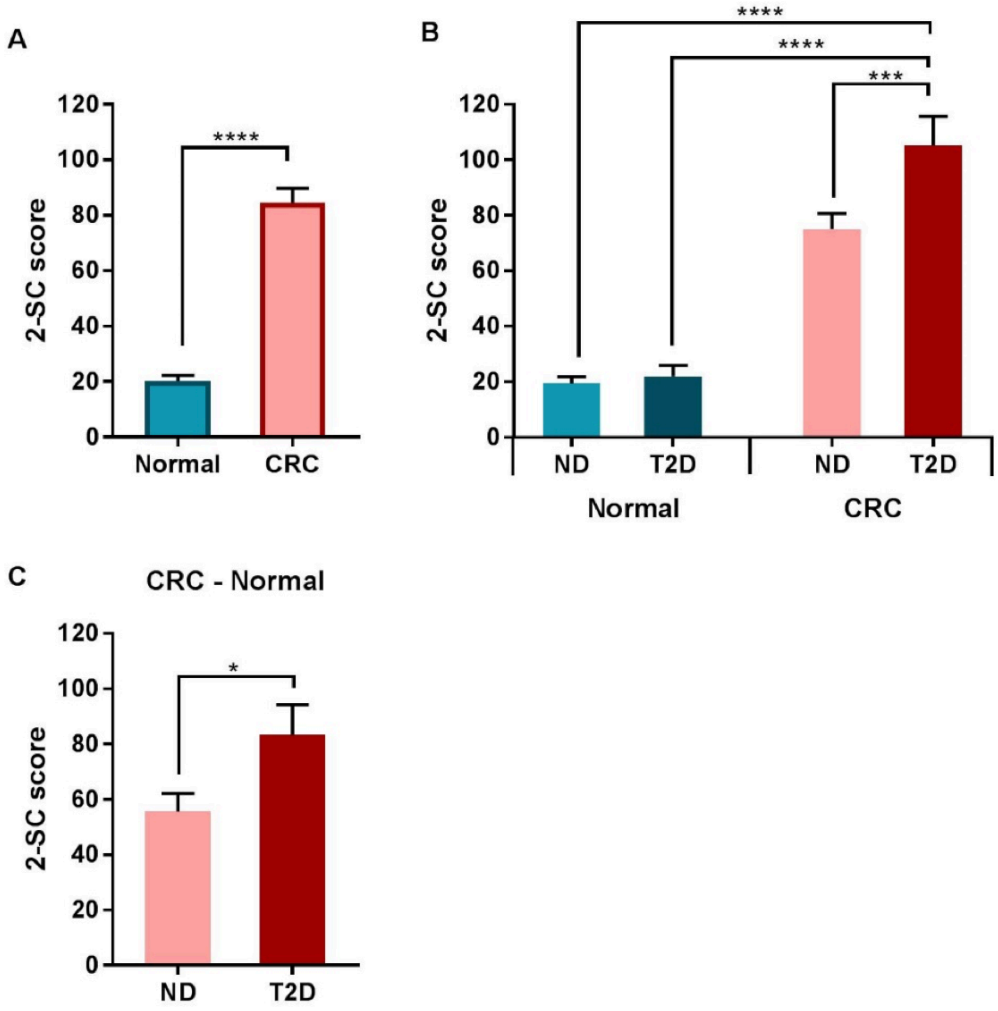

Figure 3.2. 2-SC score in matched normal and CRC tissue from non-diabetics and T2Ds. IHC was carried out on tissue sections with 2-SC antibody. Sections were then scored by Roger Feakins, a consultant pathologist. (**A**) 2-SC score of matched normal and CRC tissue (n=83), unpaired two-tailed t-test was performed. (**B**) 2-SC score of matched normal and CRC tissue, spilt into non-diabetic (ND) (n=57) and T2D (n=25) patients. (**C**) CRC minus normal 2-SC scores for matched normal and CRC tissue. All mean±SEM (Table 3.2). * $p<0.05$, ** $p<0.01$, **** $p<0.0001$. Statistics details in Table A.3.1,2.

Table 3.2. Summary of 2-SC scores for matched normal and CRC tissue. Data shown as mean ± SEM. See also Figure 3.2.

		2-SC score		
	Number	**Normal**	**CRC**	**CRC - Normal**
Total	83	20.23±2.06	84.49±5.22	64.27±5.81
Non-diabetic	57	19.45±2.39	75.05±5.55	55.61±6.55
T2D	25	21.94±4.14	105.19±10.66	83.25±11.25

3.4 Succination is elevated in adenomas

It was next hypothesised that succination occurs early in the progression of CRC. Adenomas are the precursor to CRC. In the same way as described in Section 3.1, IHC for succination was performed on matched normal intestinal mucosa and adenoma tissue resected from patients with CRCs; 23 from non-diabetic patients and 7 from T2D patients.

It was difficult to find adenomas from T2D patients for this study, due to lack of reporting diabetic status. The results must be interpreted with caution until this study can be repeated with larger numbers.

The amount of 2-SC was significantly elevated ($p<0.0001$, unpaired t-test) in adenoma tissue compared to matched normal tissue (Figure 3.3.A, Table 3.3, A.3.3,4). In non-diabetic patients, 2-SC is significantly elevated in adenoma tissue compared to matched normal tissue ($p<0.0001$, Figure 3.3.B, Table A.3.3,4). In T2D patients, 2-SC was elevated in adenoma tissue compared to matched normal tissue but was not significant. There was no significant difference in adenoma 2-SC score between T2D patients and non-diabetic patients.

When the 2-SC score of the normal tissue was taken away from the 2-SC score of the adenoma tissue, there was no significant difference between non-diabetic and T2D patients (Figure 3.3.C. Table A.3.3). There was a greater difference in the 2-SC score between adenoma and normal tissue in the non-diabetic patient group compared to T2D patients. In non-diabetic patients, the 2-SC score was higher in the adenoma compared to the matched normal in 91.30% and lower in 8.70%. In T2D patients the 2-SC score was higher in the adenoma compared to the matched normal in in 87.50% of patients and lower in 12.50%.

These results suggest that succination is present in elevated levels at the early stages of CRC, however, the presence of T2D leads to lower 2-SC scores. This suggests that T2D could be more influential on the level of 2-SC in more advanced stages of CRC.

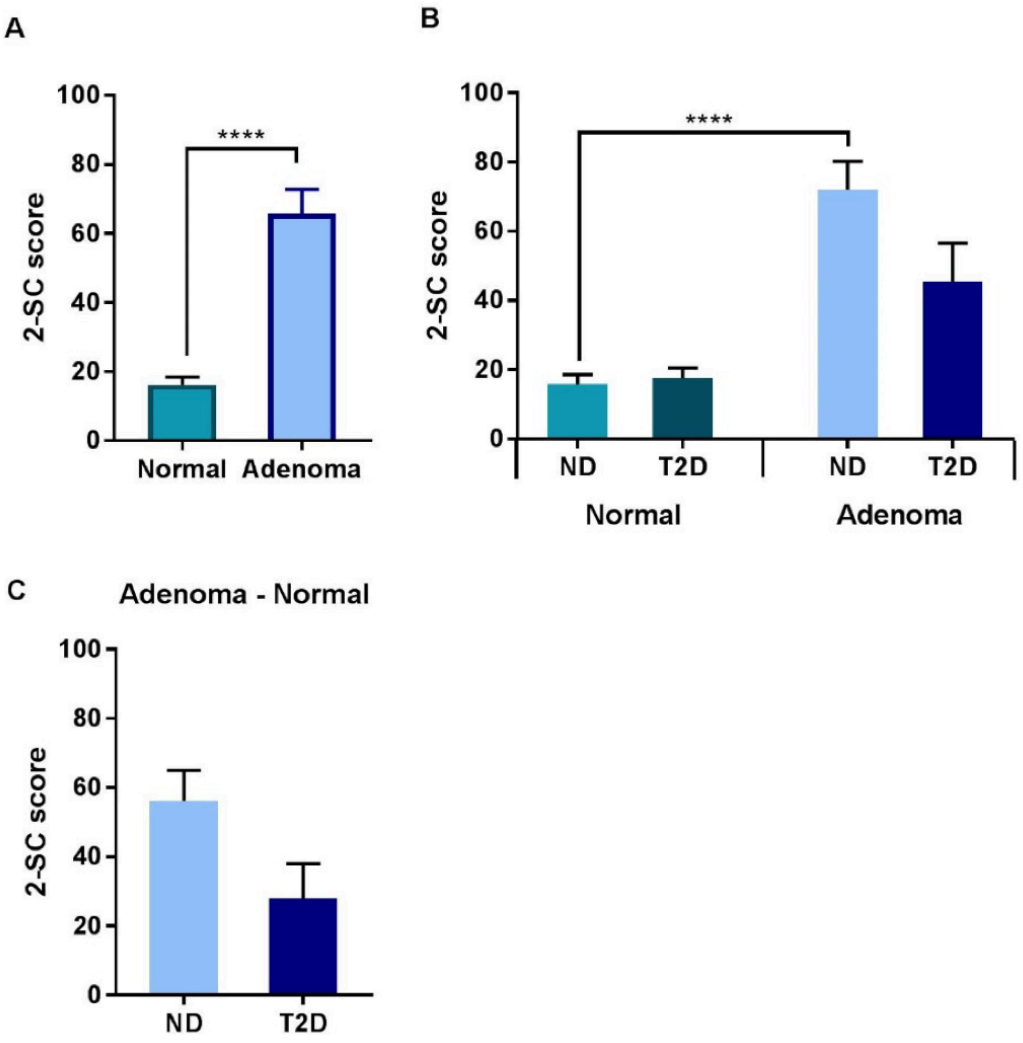

Figure 3.3. 2-SC score in matched normal and adenoma tissue from non-diabetics and T2Ds. IHC was carried out on tissue sections with 2-SC antibody. Sections were then scored by Roger Feakins a consultant pathologist. (**A**) 2-SC score of matched normal and adenoma tissue (n=26). Unpaired two-tailed t-test was performed. (**B**) 2-SC score of matched normal and adenoma tissue, spilt into non-diabetic (n=19) and diabetic (n=7) patients. (**C**) Adenoma minus normal 2-SC scores for matched tissue. All mean±SEM (Table 3.3). **** $p<0.0001$. Statistics details in Table A.3.3,4.

Table 3.3. Summary of 2-SC scores for matched normal and adenoma tissue. Data shown as mean ± SEM. See also Figure 3.3.

		2-SC score		
	Number	**Normal**	**Adenoma**	**Adenoma - Normal**
Total	30	16.17±2.27	65.80±7.02	46.63±7.41
ND	23	15.76±2.84	72.00±8.18	56.24±8.81
T2D	7	17.50±3.00	45.43±11.23	27.93±10.08

3.5 2-SC score is significantly different between adenoma and CRC

Overall, 2-SC score in normal tissue was significantly lower than the 2-SC score found in both adenoma and CRC tissue ($p<0.0001$, one-way ANOVA) (Figure 3.4.A, Table 3.4, A.3.5,6). There was also a small significant difference between adenoma and CRC 2-SC score ($p=0.0432$) (Table 3.4).

In non-diabetic patients, 2-SC was significantly lower in normal tissue when compared to adenoma tissue and CRC tissue ($p<0.0001$) (Figure 3.4.A, Table 3.4, A.3.7,8) and no significant difference was observed between adenoma and CRC tissue. In T2D patients, 2-SC was also significantly lower in normal tissue when compared to adenoma tissue ($p=0.001$) and CRC tissue ($p<0.0001$) (Figure 3.4.B, Table 3.4, A.3.7,8). There was a significant difference between adenoma and CRC tissue in T2Ds ($p=0.001$).

These data further confirm a role for succination in CRC progression as well as a role for T2D in increasing the presence of succination in CRC patient samples.

Nevertheless, 2-SC is consistently found at an elevated level compared to normal tissue within adenoma and CRC samples, again confirming a role for succination in CRC progression (Table 3.5).

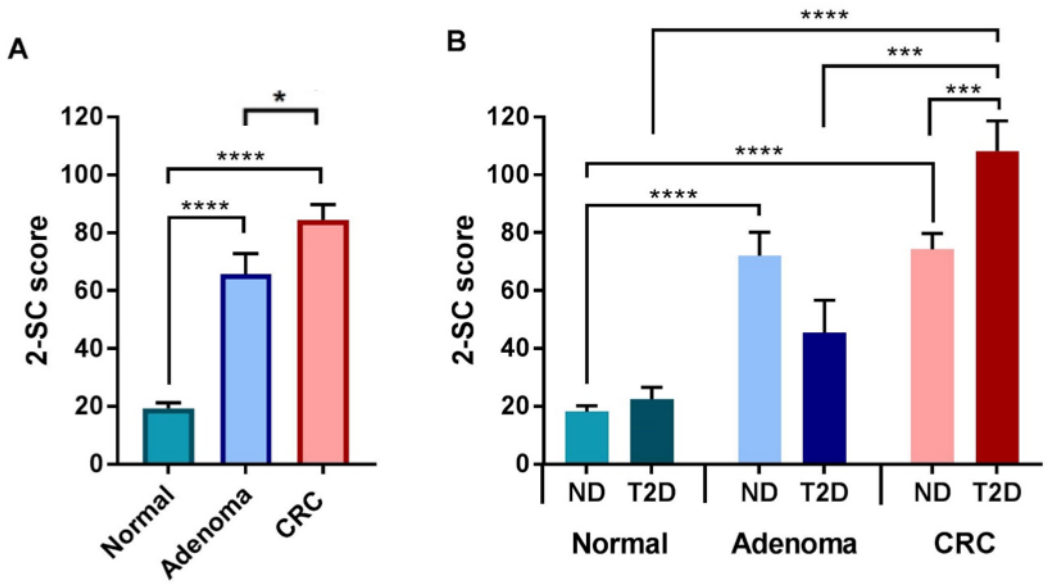

Figure 3.4. 2-SC score in total normal, adenoma and CRC tissue in non-diabetics and T2Ds. IHC was carried out on tissue sections with 2-SC antibody. Sections were then scored by a pathologist. (**A**) 2-SC score of normal (n=94), adenoma (n=30) and CRC tissue (n=83). One-way ANOVA was performed. (**B**) 2-SC score of normal, adenoma and CRC tissue, spilt into non-diabetic (normal n=67, adenoma n=23, CRC n=57) and diabetic (normal n=27, adenoma n=7, CRC n=26) patients. All mean±SEM in Table 3.4. **** p<0.0001, *** p<0.001, ** p<0.01, * p<0.05. Statistics details in Table A.3.5,6,7,8.

Table 3.4. Summary of 2-SC score in total normal, CRC adenoma and CRC tissue. Data shown as mean ± SEM. See also Figure 3.4.A.

	Number			**2-SC score**		
	Normal	Adenoma	CRC	Normal	Adenoma	CRC
Total	94	30	83	19.35±1.87	67.55±6.92	84.49±5.22
ND	67	23	57	18.37±2.11	72.00±8.18	75.05±5.55
T2D	27	7	26	21.76±3.91	50.50±10.98	105.19±10.46

Table 3.5. Percentage of 2-SC staining 20% above the mean of 2-SC score of normal tissue. T2D normal n=27, adenoma n=7, CRC n=26. ND normal n=67, adenoma n=23, CRC n=57.

	Samples with 2-SC staining 20% above the mean of 2-SC score of normal tissue		
Tissue	All	T2D	ND
Adenoma	86.67%	71.43%	91.30%
CRC	91.57%	96.15%	89.47%

3.6 FH is present at high levels in CRC tissue

Patients with HLRCC have loss of expression mutations in FH which results in fumarate accumulation and extremely elevated levels of 2-SC. No FH mutations have been identified in CRC patient samples to date. It was hypothesised that where 2-SC staining is high, FH staining would be low.

A small selection (4) of normal and CRC tissue serial sections were stained for 2-SC and FH by Julie Adam. Some representative images are shown in Figure 3.5. Interestingly, FH staining was consistently present in normal tissue and consistently elevated in CRC tissue, especially those with high 2-SC scores.

This observation suggests that FH is present in CRC tissue, but unable to control the level of fumarate, leading to elevated levels of succination. The role of FH in CRC tumorigenesis is further investigated in Chapter 4 and 5.

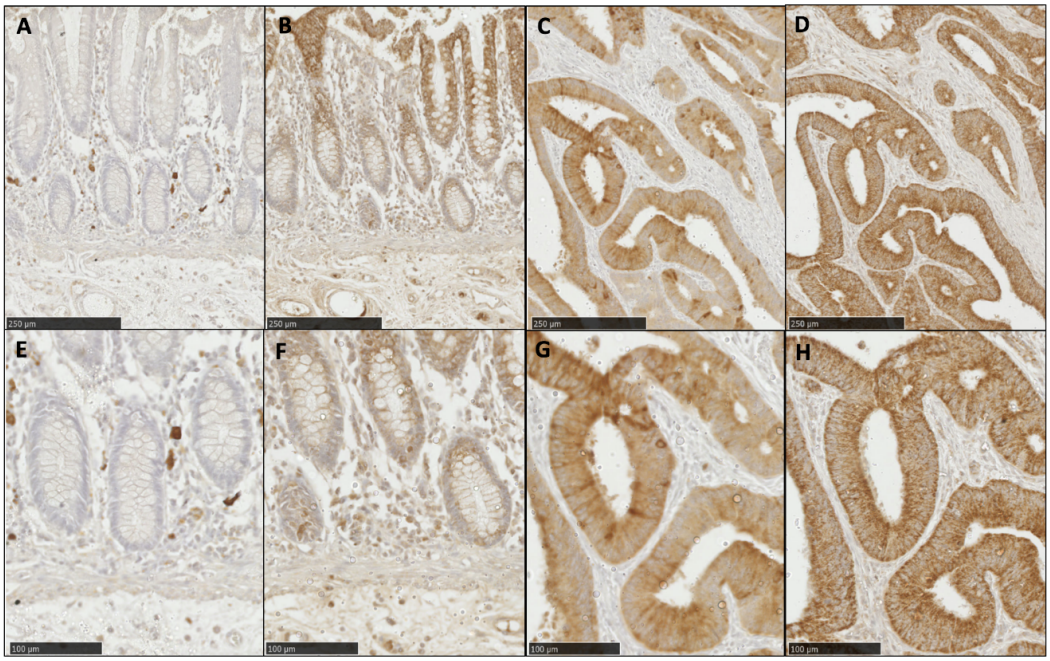

Figure 3.5. Representative images of 2-SC and FH IHC on serial sections. Serial normal and CRC tissue sections were stained for 2-SC and FH by Julie Adam. (**A**) Normal tissue stained for 2-SC, low score. (**B**) Serial normal tissue to (A) stained for FH. (**C**) CRC tissue stained for 2-SC, high score. (**D**) Serial CRC tissue to (C) stained for FH. (**E**) Close up of (A), (**F**) close up of (B), (**G**) close up of (C), (**H**) close up of (D). (**A-D**) Scale bar 250µm, (**E-H**) scale bar 100µm).

3.7 *KRAS*/*BRAF* mutation status influences succination in CRC patients.

Fumarate generates 2-SC, therefore, if there is an increased level of 2-SC, it could be assumed that fumarate is also elevated. Fumarate is a metabolite of the TCA and urea cycle. Mutations in *KRAS* and *BRAF* have recently been postulated to be linked with changes in cancer cell metabolism. *KRAS* and *BRAF* mutations are found in approximately 40% and 10% of CRC cases respectively. It was hypothesised that the presence of *KRAS* or *BRAF* mutation could promote succination by altering fumarate metabolism.

Thirty-eight CRC patient samples in the cohort examined above had already been *KRAS* and *BRAF* genotyped by the Royal London Hospital Core Pathology. For the remaining 40, DNA was extracted from CRC FFPE sections or frozen tissue. To ensure CRC tissue was used for genotyping it was first confirmed by Roger Feakins. PCR was completed for the most common mutations which are codons 12 and 13 of *KRAS*[378] and the V600E mutation of *BRAF*[379]. First, the PCR was optimised to give a 200bp product for *KRAS* and a 224bp product for *BRAF* (Figure 3.6.A,B). PCR product was cleaned and sent for Sanger sequencing (Chapter 2, Section 2.1.6). The single nucleotide polymorphism (SNP) mutations shown in Figure 3.6.C were identified from the traces. The mutations were then matched to the tissue's corresponding 2-SC score. Representative examples of WT and mutant Sanger sequence traces for *KRAS* and *BRAF* are shown in Figure 3.6.D,E.

It was found that 40.5% of CRC tissue samples had either a *KRAS* or *BRAF* mutation; 31.6% had a *KRAS* mutation and 8.9% a *BRAF* mutation. These results are in line with findings from previous studies[29,380–383].

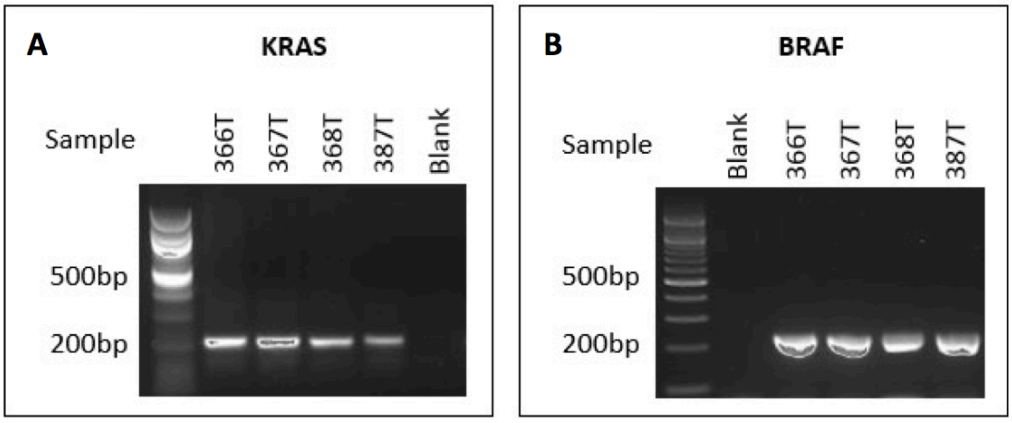

C. Common mutations found in *KRAS* and *BRAF* genes.

	KRAS		***BRAF***
Location	Codon 12	Codon 13	V600E
WT	GGT	GGC	GTT
Mutation	GGG, GGC, GGA GTT, GTC, GTA, GTG, GAT	GAT, GAC, GGT, GGG, GGA	GAA, GAG, GTC, GTA, GTG

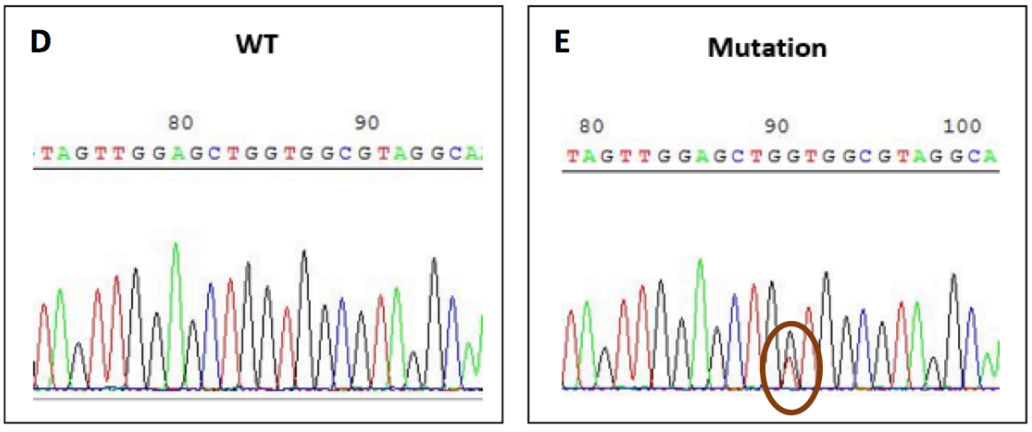

Figure 3.6. *KRAS/BRAF* PCR and Sanger sequencing. DNA was extracted from frozen tissue or paraffin sections. PCR was performed using Qiagen Master Mix then run on a 2% agarose gel and visualised using a Chemi Doc (Chapter 2, Section 2.1.5). PCR product was cleaned using ExoSAP-IT (Qiagen) and sent for Sanger sequencing (GATC biotech). (**A**) Product from *KRAS* PCR (200bp). (**B**) Product from *BRAF* PCR (200bp). (**C**) Common mutations for *KRAS* and *BRAF*. (**D**) WT KRAS sequence, (**E**) KRAS codon 12 sequence with a G→ T mutation (circled).

There was an elevated 2-SC score in CRC patient samples with mutant *KRAS*/*BRAF* compared to WT patient samples, but this was not significant when tested by unpaired t-test (p=0.2994) (Figure 3.7.A, Table 3.6). When *KRAS*/*BRAF* mutation status of CRC tissue was matched to 2-SC score as well as the patient's diabetic status it was found that the diabetic status had a significant effect on 2-SC score (p=0.0034) (Figure 3.7.B) (Table A.3.13,14). CRC tissue from non-diabetic WT *KRAS/BRAF* patients had the lowest 2-SC score which was increased with the presence of a *KRAS/BRAF* mutation. CRC tissue from T2D WT patients showed a further increase in 2-SC score which again increased with the presence of a *KRAS/BRAF* mutation. The difference between the 2-SC score of CRC tissue from patients with T2D and *KRAS/BRAF* mutation was significantly different to that from non-diabetic WT patients (p=0.05) (Figure 3.7.B, Table A.3.9,10). These data suggest that *KRAS/BRAF* mutation is complimentary to the effect of T2D on the process of succination, leading to a further increase in 2-SC score.

When the 2-SC score for the matched normal tissue is taken away from the CRC tissue 2-SC score, there is no significant difference between groups when tested by unpaired t-test, however, mutant *KRAS/BRAF* patient samples have a higher average 2-SC score compared to WT patient samples (Figure 3.7.C). When this data is split into non-diabetic and T2D patients (Figure 3.7.D), the same trend exists as in Figure 3.7.B. Non-diabetic WT *KRAS/BRAF* patients had the lowest 2-SC score difference of which was increased with the presence of a *KRAS/BRAF* mutation. T2D WT patients showed a further increase in 2-SC score difference which again increased with the presence of a *KRAS/BRAF* mutation (Figure 3.7.D, Table 3.6). This is explained by similar average normal tissue 2-SC score for each group.

Between normal and CRC tissue, the 2-SC score increased in 82.14% of non-diabetic WT patients and decreased in 17.86%. In T2D WT patients the 2-SC score increased in 94.44% or patients and decreased in 5.56%. The 2-SC score increased in 91.67% of non-diabetic mutant patient samples and decreased in 8.33%. In T2D mutant patient samples the 2-SC score increased in 100% and decreased in 0%. These data confirm that presence of a *KRAS/BRAF* mutation alongside T2D is more likely to lead to an elevation in 2-SC score.

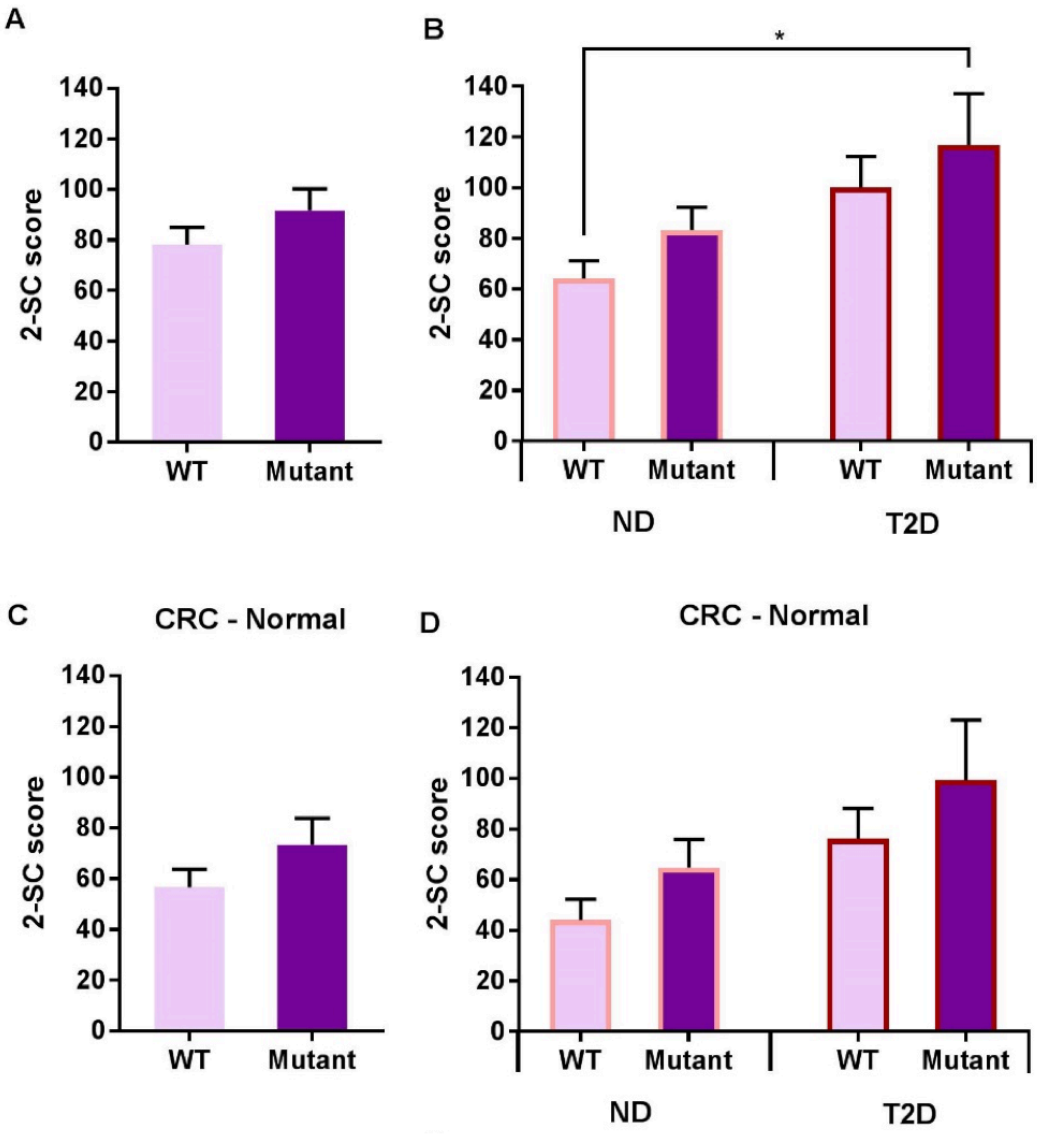

Figure 3.7. KRAS/BRAF mutation status, diabetic status and 2-SC score of CRC samples. CRC samples from non-diabetic and T2D patients underwent IHC for 2-SC, which was then scored by Roger Feakins (consultant pathologist). Alongside this DNA extracted from the samples and examined by PCR for *KRAS* and *BRAF* mutation status. PCR product was sent for Sanger sequencing and scored for mutations in *KRAS* and *BRAF*. (**A**) 2-SC score of CRC tissue from WT (n=46) and mutant (n=32) patients. (**B**) 2-SC score of CRC tissue from non-diabetic (ND) WT (n=28) and mutant (n=24) patients and T2D WT (n=18) and mutant (n=8) patients. (**C**) CRC minus normal 2-SC scores for matched tissue. (**D**) 2-SC score of matched normal and CRC tissue from WT and mutant patients. All mean±SEM in Table 3.6. * $p<0.05$. Statistics details in Table A.3.9,10,11.

Table 3.6. Summary of 2-SC score for WT and *KRAS*/*BRAF* mutant CRC samples from NDs and T2Ds. Data shown as mean ± SEM. See also Figure 3.7.

			2-SC score			
	Number		**CRC**		**CRC - Normal**	
	WT	**Mutant**	**WT**	**Mutant**	**WT**	**Mutant**
Total	46	32	78.18± 6.85	91.61± 8.69	56.60± 7.17	73.45± 10.36
ND	28	24	64.16± 6.96	81.15± 9.04	44.05± 8.18	64.83± 11.09
T2D	18	8	100.00± 12.32	116.88± 20.29	76.11± 12.08	99.31± 23.73

3.8 Discussion

Metabolites such as fumarate are not widely quantitated in tissue due to high cost of current methods as well as a lack of effective methodology. Metabolites are often highly polar, non-volatile and have poor detectability making analysis difficult. Chan et al. used high resolution magic angle spinning-nuclear magnetic resonance (NMR) and gas chromatography coupled to mass spectrometry (GC-MS) to compare the metabolic profile of biopsied CRC tumours and matched normal tissue from 31 patients[384]. They identified a reduction of fumarate in CRC compared to normal tissue. A similar result was found by Denkert et al. using GC time-of-flight MS (GC-TOFMS) for 15 paired CRC and normal tissue patient samples[385]. Both of these studies showed a reduction in TCA cycle metabolites which links well with Otto Warburg's theory of reduced mitochondrial metabolism[386].

Hirayama et al. used capillary electrophoresis TOFMS (CE-TOFMS), which they argue is more suited to metabolism analysis due to its high resolution and ability to simultaneously quantify charged low-molecular weight compounds[335]. They identified an increase in fumarate in 16 CRC tissue samples compared to matched normal.

My findings are in accord with Hirayama and colleagues finding of elevated fumarate in CRC tissue compared to matched normal[335]. In a cohort of 83 matched normal and CRC tissue, for the first time an elevation in succination, as measured by 2-SC staining, is shown (Figure 3.2.A). My work has also shown elevated succination in the early stage of the cancer, an adenoma, compared to matched normal tissue (Figure 3.3.A). These data suggest that elevated fumarate is an early event in CRC tumorigenesis and that protein succination could be a factor influencing tumour development.

Succination in CRC tissue is further elevated by the presence of T2D. This is another novel finding. The trend of succination in adenomas is still to be confirmed. In this study, the number of adenomas with known T2D status was limited. From the small cohort used, succination was lower in tissue from T2D patients compared to non-diabetic patients, however, this was not significant.

Interestingly, succination was not significantly elevated in normal tissue from T2D compared to non-diabetics, although it was raised in T2D compared to non-diabetic patients. This suggests that the elevated fumarate is a consequence of an oncogenic event that has led to a change in cellular metabolism, which is then exacerbated by the presence of T2D and could be one reason why T2D patients with CRC have a poorer outcome and more invasive cancer[124].

T2D is a metabolic disorder where succination has already been confirmed elevated in certain tissues. Adipocytes from db/db and ob/ob mice[342] which are mouse models of human diabetes, and skeletal muscle from streptozotocin-induced diabetic rats[333] were found to have elevated succination as well as adipocytes treated with 30mM glucose versus 5mM glucose[339] *in vitro*. Interestingly, undifferentiated fibroblasts cultured in the same high glucose media did not exhibit an increase in succination[339] whereas differentiated 3T3 fibroblasts do exhibit increased succination under 30mM glucose[310]. Frizzell et al. 2012 showed that 3T3 cells treated with 30mM glucose compared to 5mM also showed significant increases in cellular ATP/adenosine diphosphate (ADP), NADH/NAD+, mitochondrial membrane potential and cellular fumarate concentration. This was postulated to an increase in NADH/NAD+ ratio resulting in the inhibition of NAD+-dependent dehydrogenases. Cellular fumarate and succination was decreased upon addition of chemical uncouplers which reduce the NADH/NAD+ ratio and upon addition of metformin (an inhibitor of complex I in the ETC) to high glucose culture media. The conclusion of the study was that elevated succination in diabetic conditions was a result of glucotoxicity-driven mitochondrial stress[310,343].

Mitochondrial function is known to be deregulated in cancer[387] and that increased glycolysis is a feature of cancer. Therefore, it could be suggested that glucotoxicity-driven mitochondrial stress exists within CRC which leads to elevated fumarate and, therefore, elevated succination. In turn, the glucotoxicity-driven mitochondrial stress is further elevated in patients with T2D, leading to higher levels of succination. Unfortunately, I was unable to determine the diabetic treatment for the majority of the CRC patients, as hospital records are incomplete. Nevertheless, it would be interesting to study the succination levels in T2D CRC patients with and without metformin treatment; I would hypothesise that succination would be lower in patients on metformin.

Surprisingly, FH was elevated in CRC tissue compared to matched normal (Figure 3.5). This suggests that FH is upregulated in conjunction with, or as a consequence of elevated fumarate, but is unable to remove the excess fumarate. FH may be dysfunctional. However, somatic FH mutations are rare and restricted to HLRCC patients[388]; No FH mutations have been found in CRC patients[388]. More work to determine FH expression in this set of patients will be completed so that more concrete conclusions can be made.

FH is a tetrameric enzyme, composed of four identical subunits of 50kDa each[389]. There are 3 active sites (site A) and one lower affinity site (site B). A report by Mescam et al. suggests that at low fumarate concentrations (<1mM) the enzyme shows Michaelis-Menten kinetics; at 0.001-0.033M allosteric activation of the enzyme by binding to site B is observed; at 0.1M and above fumarate actually inhibits FH[390]. Therefore, it could be that fumarate itself is inhibiting the action of FH, leading to further increases in fumarate. Hirayama et al. showed that the fumarate concentration in colon tumour was around an average of 50nmol/g which is equivalent to 50mM and, therefore, close to allosteric inhibition. This is an average concentration and local concentrations maybe much higher leading to inhibition.

Approximately 35-40% of human CRCs have an activating missense mutation in *KRAS*[380–383]. These affect hotspots in codons 12 and 13 which lock KRAS in an active GTP-bound conformation, constitutively presenting a docking surface for RAF kinases[391]. *BRAF* mutations are found in 10% of CRCs, and are most likely to be a V600E amino acid substitution, although other mutations at codon 600 or neighbouring positions are documented[29]. The presence of these mutations in our cohort is in accord with these results and were selected for examination as they are amongst the most prevalent mutations found.

Although the use of *KRAS* and *BRAF* mutation status as a predictive biomarker of response to anti-EGFR therapy is well supported, there are inconsistencies within the literature regarding the association between *KRAS* and *BRAF* mutations and CRC survival. There are discrepancies related to specific mutations, age, stage at diagnosis and treatment. The largest study to date, included 4268 patients from 42 centres in 21 countries in a

collaborative database called RASCAL (The Kirsten ras in-colorectal-cancer collaborative group)[392]. They identified that only one mutation of codon 12, the *KRAS* p.G12V mutation, found in 8.6% of patients had a statistically significant impact on outcome, but only among patients with Dukes' C CRC[392]. *BRAF* mutation is associated with poorer survival of CRC patients[29,393]. Unfortunately, the specific *KRAS* or *BRAF* mutation is not reported in patient notes, therefore, it was not possible to distinguish the effect of specific *KRAS* and *BRAF* mutations on 2-SC score in this study.

In vitro data identified that HCT116 and DLD1 CRC cell lines with *KRAS* mutations increase GLUT1 expression after 4 days of culture in 0.5mM glucose, leading to increased glucose uptake and increased lactate production, although mitochondrial function and oxidative respiration were not affected[394]. It was also shown that the WT *KRAS* CRC cells which survived 4 days of culture with 0.5mM glucose increased their mutation rate of *KRAS* to increase GLUT1 expression and, therefore, glucose uptake[394]. Another study which involved 8 *KRAS* WT and 8 *KRAS* mutant human colon tumours identified an association between a 2-fold increase in expression of glycolytic and glutamine metabolic proteins and *KRAS* mutation status[376]. *KRAS* mutation in CRC has also been found to affect amino acid metabolism. Human CRC cell lines and clinical specimens with *KRAS* mutation were found to have an increase in asparagine synthetase (ASNS) which was induced via the PI3K-AKT-mTOR pathway[395]. Subsequent knock down of ASNS in *KRAS* mutant CRC cell lines led to growth suppression. It was also found that asparagine addition prevented cell death from glutamine depletion. Weinberg et al. reported that the pentose phosphate pathway (PPP), not glycolysis was essential for *KRAS* mutant CRC cell growth[396]. Miyo et al. reported that in *KRAS* mutant CRC cell lines resistance to glucose-deprived conditions is associated with increased levels of both GLUD1 and SLC25A13 (a mitochondrial aspartate-glutamate carrier)[397].

From the work detailed above it is clear that *KRAS* mutations influence cancer cell metabolism in a cell and tissue dependent manner. It has also been reported that *KRAS* driven NSCLC cells *in vitro* use nutrients differently compared to human lung tumours; *KRAS* mutant tumours were less dependent on glutaminase that NSCLC cells *in vitro*[398]. This highlights the importance of studying cancer metabolism in a physiological context. More work is needed to determine the exact role of *KRAS* in cancer.

Currently, there is no literature which link *KRAS* or *BRAF* mutation to an increase in succination. This study hypothesised that presence of *KRAS* or *BRAF* mutation would increase succination via increased use of the TCA cycle. The data show that there is no significant effect of *KRAS* or *BRAF* mutation status on 2-SC score. However, there is an increase in 2-SC score in samples from patients with T2D and *KRAS* or *BRAF* mutation combined compared to samples from non-diabetic *KRAS* or *BRAF* WT patients. This suggests an interaction between T2D and *KRAS* or *BRAF* mutation which could be attributed to greater glucose availability and increased ability to uptake glucose leading to more succination. I would, therefore, hypothesise that *KRAS* mutant CRC cells would channel glucose-derived metabolites into the TCA cycle to a greater extent than *KRAS* WT CRC cells and, therefore, lead to increased fumarate and increased succination.

This chapter presented evidence that fumarate is elevated in the early stage of CRC, an adenoma. There is increased succination in both adenoma and CRC tissue compared to match normal tissue. Succination in CRC is further increased in the presence of T2D. Additionally, the 2-SC staining was non-uniform across tumours, underlining the metabolic heterogeneity of CRC tissue. T2D patients with *KRAS*/*BRAF* mutation exhibit a further increase in succination compared to T2D patients with WT *KRAS*/*BRAF.* The possibility of a link between 2-SC score and patient prognosis requires further investigation and would be an interesting avenue to pursue. The functional effects of succination are likely to be wide-spread and would take more time to investigate through collaboration. Additionally, the role of FH in CRC patients should be further investigated (Chapter 8, Section 8.1). Here, I found FH is present in CRC tissue at an elevated level, although it remains to be determined if FH is fully active or inhibited by high levels of fumarate. Loss of function at the genetic levels is less likely, as there are no known mutations in FH in CRC patients.

Chapter 4 – Influence of diabetes on intestinal polyp numbers in mice

4.1 Introduction

The work described in Chapter 3 raises further questions about the role of diabetes in the development of CRC. As it is known that the presence of T2D in humans leads to more serious CRC features such as more advanced stage at presentation[124], it was hypothesised that diabetes in mice would also lead to enhanced tumour multiplicity and progression. Hence, a novel mouse model was generated by crossing a mouse commonly used to study polyps in the small intestine[15] (*Apc*^{1322T}) with a novel diabetic mouse model[268] (*Fh1*$^{flox/flox\ RipCre\ CAGFH}$); models were introduced in Chapter 1, Section 1.10 and Section 1.12, respectively. The breeding steps are outlined in Figure 4.1 and described below; for further details, refer to Chapter 2, Section 2.2.1. All animals used were backcrossed on a C57BL/6J background at least 3 times and littermate controls were used. Animal experiments were conducted in accordance with the UK Animals Scientific Procedures Act (1986) and University of Oxford local ethical guidelines under the direction of Dr J Adam.

The novel diabetic model (*Fh1*$^{flox/flox\ RipCre\ CAGFH}$ mice[268] (designated *Fh1βKO* mice for this thesis)) was originally generated by inter-crossing an *Fh1* conditional knockout mouse (*Fh1*$^{tm1Pjpfl/fl}$)[325] with mice expressing Cre recombinase driven by the rat insulin promoter (Tg(*Ins2-Cre*)^{23Herr}Cre recombinase, *Rip2-Cre*$^{+/-}$)[267]. Thus, a tissue-specific RipCre promoter was used to knock out *Fh1* in the β-cells of the pancreas by recombination (Chapter 2, Section 2.2.1). Mice lacking *Fh1* in pancreatic β-cells have elevated fumarate that leads to fumarate accumulation, which competitively inhibits PHDs which leads to stabilisation of HIF-1α, as well as a reduction in intracellular calcium levels. This leads to a reduction in glucose stimulated insulin secretion and blood glucose levels consistent with those seen in an uncontrolled T2D human[268]. The mice display progressive diabetes and are initially normoglycaemic.

Fh1βKO mice become very diabetic by approximately 16 weeks of age (with a blood glucose of >33.3mM)[268] so it is not possible to use female *Fh1βKO* for breeding purposes. Also, the pups of a diabetic mother become diabetic much faster To enable breeding, *Fh1βKO* mice were crossed with mice stably expressing the cytoplasmic form of human FH, under the CAG promoter (designated *FH*^{cyt} for this thesis)[330] to generate

Fh1^{tm1Pjp}*Gt(ROSA)26Sor*$^{tm1(CAG-FH*)Pjp}$*Tg(Cdh16-cre)91Igr* (designated *Fh1ßKO* FH^{cyt} for this thesis to designate that that the FH is human and added to the mouse). Introduction of *FH*^{cyt} as well as full length FH has been shown to fully reverse the glucose intolerance of *Fh1ßKO* mice, as tested in a glucose tolerance test, and maintains them with only a slightly elevated blood glucose compared to *WT* for >1 year[268]. Female *Fh1ßKO FH*^{cyt} mice were then intercrossed with male *Apc*^{1322T} mice (designated *1322* for this thesis). Female *Apc*^{1322T} mice cannot be used for breeding purposes because the mice become sick due to the polyp burden and anaemia.

The addition of cytoplasmic FH allowed the role of FH in tumourigenesis to be further scrutinised. Cytoplasmic FH has a role in the urea cycle, and it can also translocate to the nucleus to aid repair of double strand breaks in DNA[399]. It is unclear if the high levels of FH shown in the human CRC samples are cytoplasmic, nuclear and/or mitochondrial. Ideally, a mouse model with overexpression of mitochondrial Fh1 with and without overexpression of cytoplasmic Fh1 in the gut tissue would be used to determine the effect of FH position on polyposis in the mouse. However, these models were not available for use in this study.

4.1.1 Hypotheses

I hypothesised that mice with diabetes will have more and/or larger polyps compared to non-diabetic mice and mice with overexpression of FH will have fewer and/or smaller polyps. I also hypothesised that diabetes may alter the cellular profile of the gut.

4.1.2 Aims

- Create and a phenotype a mouse model predisposed to both diabetes and intestinal polyposis.
- Overexpress FH as a rescue of diabetes in the diabetic/polyposis mouse model.

In this chapter, statistical significance was determined by ordinary one-way ANOVA with Bonferroni *post-hoc* test unless otherwise stated. Statistically significant results are denoted with * in figures, exact p values can be found in the appendix (Chapter 9).

4.2 Genotyping of mice

The crossing of these two mouse lines generated eight genotypes that are summarised in Table 4.1 along with their denoted name, diabetic and polyp phenotype and purpose (Figure 4.1). All the genotypes were compared in the following investigations in this chapter. Of main interest was the *Fh1βKO 1322* genotype, which was genetically predisposed to polyps in the small intestine and to T2D.

Ear tissue biopsies were used to check the genotype of mice shortly after weaning, (three weeks of age), tail tissue was used to check recheck genotyping after culling and was done in all cases. Ear and tail tissue was digested, DNA extracted and PCR performed for four alleles by PCR: $Fh1^{flox/flox}$, *RipCre*, FH^{cyt} and Apc^{1322T}. PCR products were run on 2% agarose gels and the genotype of the mice determined Chapter 2, Section 2.2.2.

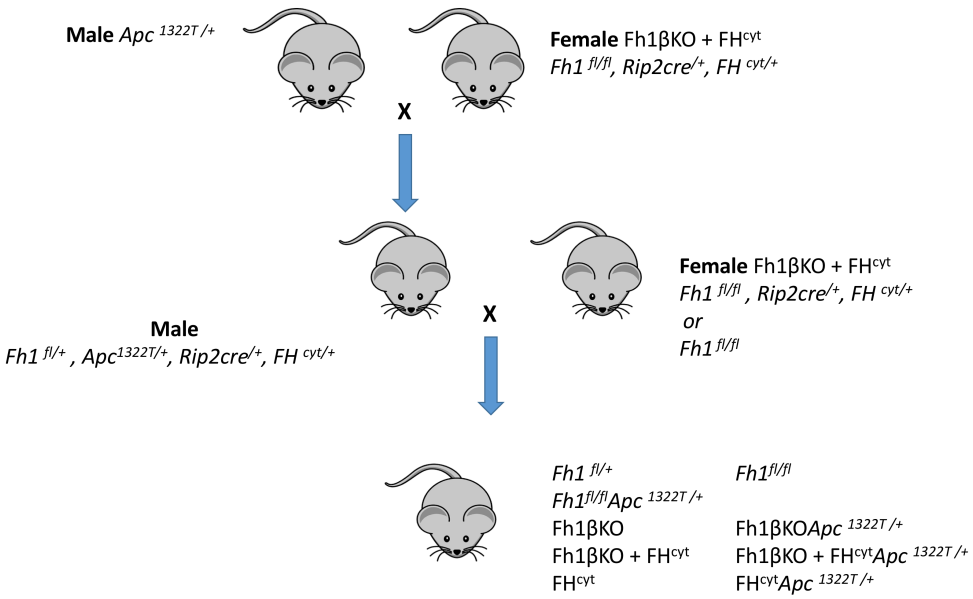

Figure 4.1. Breeding details of the *Fh1*$^{flox/flox}$ *Apc*$^{1322+/-}$ mice model. Schematic diagram to show the breeding steps taken to create the experimental mice used in this study.

Table 4.1. Description of the resultant phenotype and purpose for each mouse genotype. T2D status determined using parameters explained in Table 1.6.

Genotype name	Genotype explanation	Phenotype		Purpose
		T2D	Polyps	
WT	WT C57BL/6J mouse	No	No	No polyps; control for
1322	*Apc*^{1322T} allele	No	Yes	Polyp control
FH^{cyt}	FH overexpressed in the cytoplasm of all somatic cells	No	No	No polyp control for *FH^{cyt} 1322*
FH^{cyt} 1322	FH overexpressed in the cytoplasm of all somatic cells, *Apc*^{1322} allele	No	Yes	To study the effect of overexpression of FH in gut epithelial cells on polyp burden
Fh1βKO FH^{cyt}	No Fh1 in β-cells, FH overexpressed in the cytoplasm of all somatic cells	Pre-diabetes	No	No polyp control for *Fh1βKO FH^{cyt} 1322*
Fh1βKO FH^{cyt} 1322	No Fh1 in β-cells, FH overexpressed in the cytoplasm of all somatic cells, *Apc*^{1322} allele	Pre-diabetes	Yes	To study the effect of pre-diabetic blood glucose coupled with overexpression of FH in gut epithelial cells on polyp burden
Fh1βKO	No Fh1 in β-cells	Yes	No	No polyp control for *Fh1βKO 1322*
Fh1βKO 1322	No Fh1 in β-cells, *Apc*^{1322} allele	Yes	Yes	To study the effect of diabetes on polyp

4.3 Genotyping for *Mom-1* locus shows all mice are *Mom-1*^{S}

There are two forms of the *Mom-1* allele[367] which form different products when incubated with the restriction endonuclease BamH1. The *Mom-1*^{S} allele is not digested so retains a 500bp length, whereas the *Mom-1*^{R} allele forms 400bp and 100bp products[367,370] (Figure 4.2). Mice with *Mom-1*^{S} allele are susceptible to higher numbers of polyps. Mice with the *Mom-1*^{R} allele are resistant to polyp formation and mice present with fewer polyps[367,370].

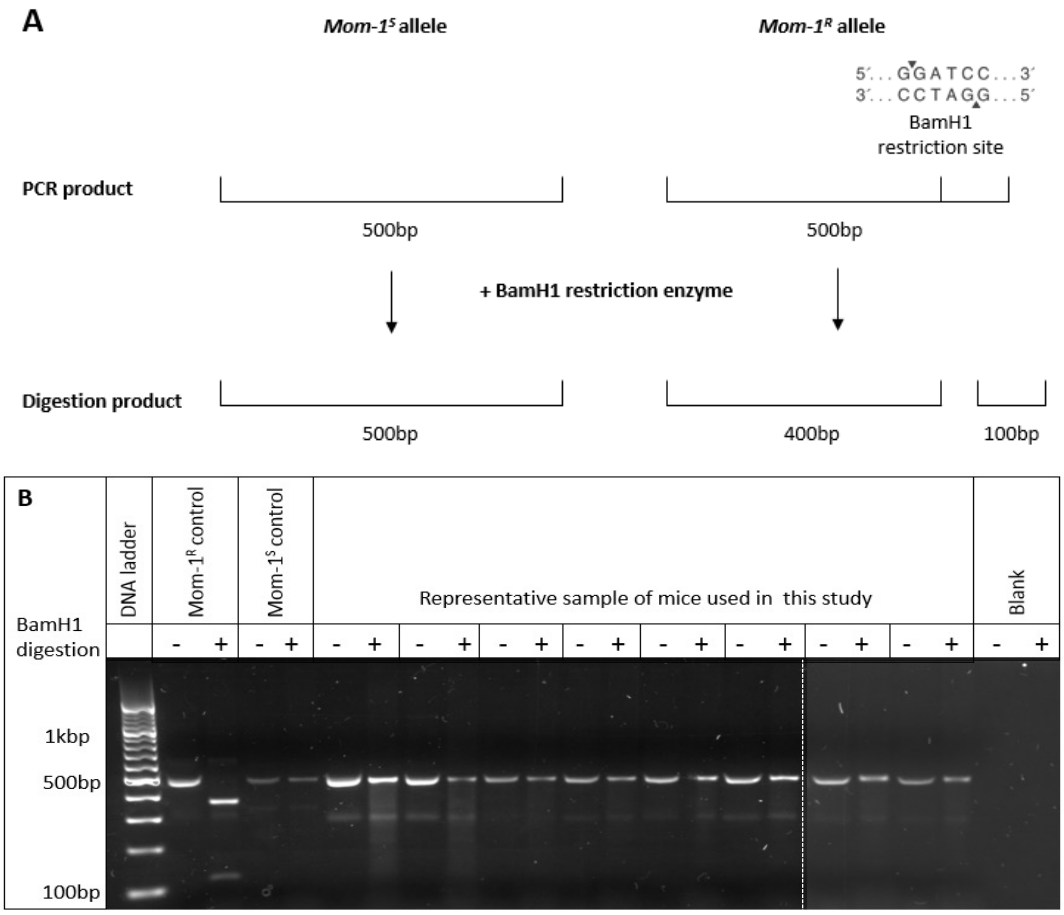

Figure 4.2. *Mom-1* genotyping. (**A**) Schematic representation of BamH1 digestion of *Mom-1* alleles. The *Mom-1*^{S} allele does not have a BamH1 restriction site and, therefore, the PCR product remains intact, whereas the *Mom-1*^{R} allele PCR product has a BamH1 restriction site, which is digested by BamH1 restriction enzyme to give a 400bp and 100bp fragment. (**B**) PCR for *Mom-1* was performed, product was incubated with BamH1 to determine if mice were resistant to polyps (*Mom-1*$^{R)}$ or susceptible to polyps (*Mom-1*^{S}). Two gels were run due to number of samples used.

4.4 Fh1βKO and Fh1βKO 1322 mice are diabetic

It was necessary to determine that the blood glucose of the mice generated by the crossing *Fh1βKO FH*^{cyt} mice with *Apc*^{1322T} mice was as predicted. It was unlikely that the *Apc*^{1322T} allele would interfere with the diabetic phenotype generated by the presence of the *Fh1βKO* and/or *FH*^{cyt} alleles. Before culling, an Accu-check monitor was used to measure blood glucose level from tail vein blood. This was done within the same 3-hour time window of the day to reduce variation due to day/night feeding. Table 4.1 details the diabetic status of the genotypes. This is expanded and explained below.

As expected, *Fh1βKO* and *Fh1βKO 1322* mice had significantly higher blood glucose compared to all other genotypes ($p<0.0001$) (Figure 4.3, Table A.4.2,3); *Fh1βKO* mice were strongly diabetic with the maximum read on the blood glucose monitor (33.3 mmol/L) reached for 71% (10 out of 14) of these mice. *Fh1βKO 1322* mice had a lower blood glucose reading compared to *Fh1βKO* mice, as well as a larger range of blood glucose values (Figure 4.3.A, Table 4.2). *Fh1βKO FH*^{cyt} and *Fh1βKO FH*^{cyt} *1322* mice had lower blood glucose levels compared to the *Fh1βKO* and *Fh1βKO 1322* mice respectively (Figure 4.3.A, Table A.4.1). All other genotypes had pre-diabetic levels of blood glucose (Figure 4.3.A, Table A.4.1). There was no difference in blood glucose levels between male and female mice of the same genotype (Figure 4.3.B).

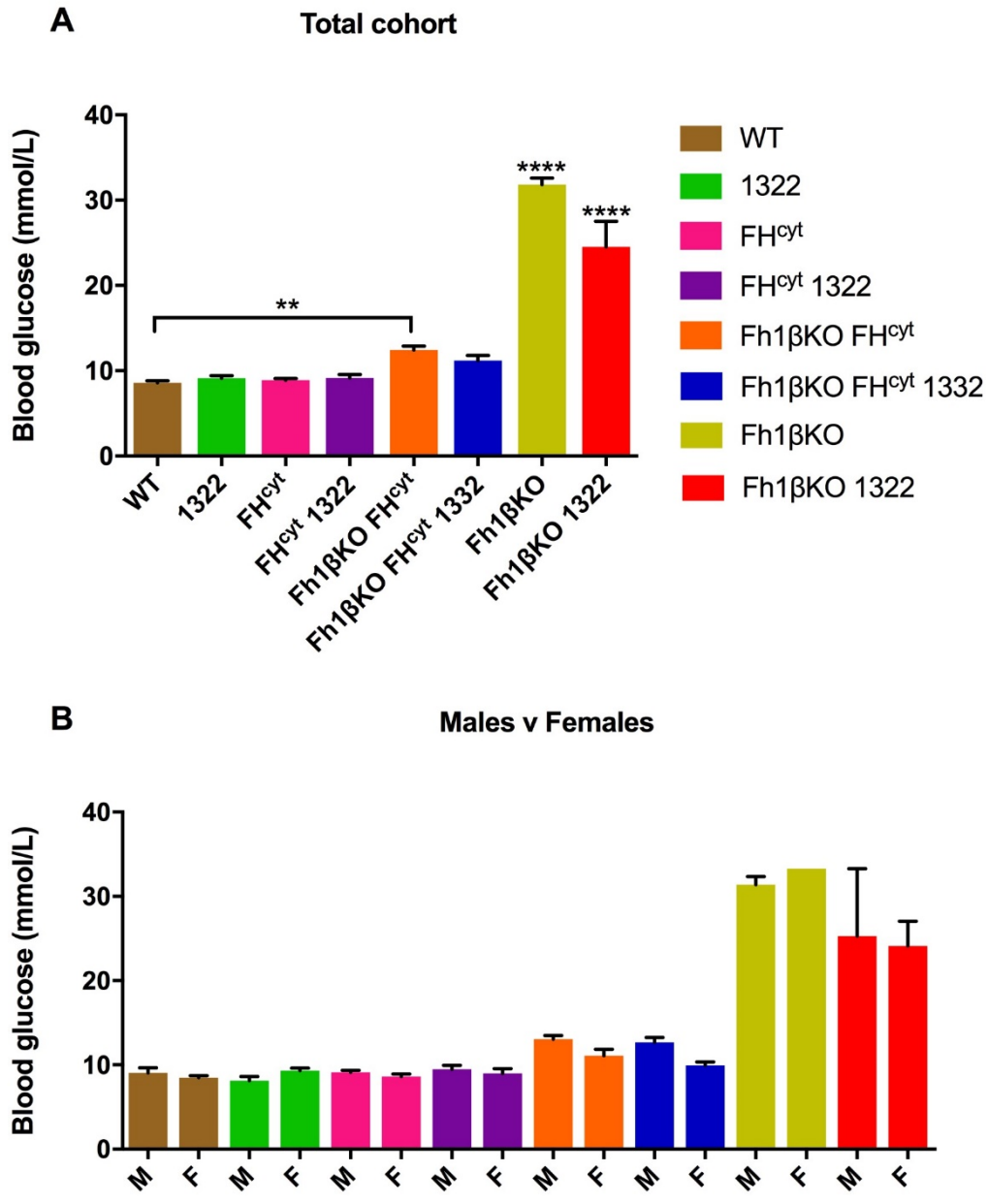

Figure 4.3. Blood glucose of mice. Blood glucose from the tail vein was measured with an Accu-Check monitor immediately before culling. Blood glucose (mean ± SEM, details in Table A.4.1) (**A**) in the total cohort and (**B**) in males (M) and females (F). *WT* n=25, *1322* n=12, *FH^{cyt}* n=9, *FH^{cyt} 1322* n=16, *Fh1βKO FH^{cyt}* n=16, *Fh1βKO FH^{cyt} 1322* n=9, *Fh1βKO* n=14 and *Fh1βKO 1322* n=9. * p<0.05, ** p<0.01, *** p<0.001. Statistics details in Table A.4.1,2.

Table 4.2. Summary of blood glucose for each mouse genotype. Normal <8.3, pre-diabetic 8.3-13.9, diabetic >13.9[266]. Data shown as mean ± SEM. Figure 4.3.

Genotype	Number	Blood glucose (mmol/L)
WT	25	8.6±0.2
1322	12	9.1±0.3
FH^{cyt}	9	8.9±0.2
FH^{cyt} 1322	16	9.2±0.4
Fh1βKO FH^{cyt}	16	12.4±0.4
Fh1βKO FH^{cyt} 1322	9	11.2±0.6
Fh1βKO	14	31.8±0.8
Fh1βKO 1322	9	24.5±3.0

4.5 Glucose metabolomics

Polyps and adjacent normal tissue samples from each mouse genotype with the *1322* allele were snap frozen by Dr Julie Adam and glucose concentration was measured by Tomoyoshi Soga (Keio University, Japan) (methods detailed in Chapter 2, Section 2.2.8). Data is presented here to provide additional clarity on the mouse model used (Figure 4.4, Table 4.3 for mean ± SEM).

Although no significant difference in gut tissue [glucose] was found between genotypes, it can be seen that on average the [glucose] was lower in the corresponding polyp tissue compared to the normal tissue from each genotype, suggesting that the polyp tissue was utilising the glucose more for metabolism (Figure 4.4).

Although not significantly different, [glucose] in the gut tissue was the highest in mice with the *Fh1ϐKO* allele. When the FH^{cyt} allele is present in mice it led to a reduction in gut tissue [glucose] by half when compared to gut tissue from mice with the *Fh1ϐKO* mice.

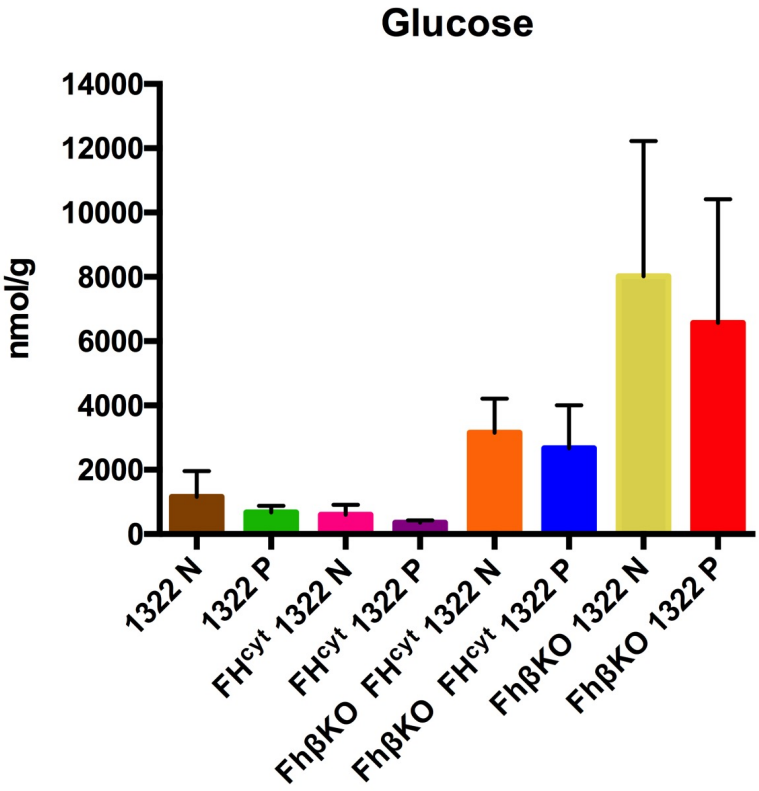

Figure 4.4. Glucose concentration in normal (N) and polyp (P) tissue from each genotype. Normal and polyp tissue was flash frozen and [glucose] was measured by CE-TOF/M. Mean ± SEM found in Table A.4.4.

Table 4.3. Summary of glucose (nmol/g) from normal and polyp samples from each genotype. Data shown as mean ± SEM. N=3 per genotype. See also Figure 4.4.

Genotype	Normal (N) or polyp (P) tissue	Glucose (nmol/g)
1322	N	1159.98±799.47
	P	661.53±204.61
FH^{cyt} 1322	N	599.19±313.55
	P	350.13±74.60
Fh1βKO FH^{cyt} 1322	N	3149.63±1062.75
	P	2671.35±1336.71
Fh1βKO 1322	N	8020.27±4208.49
	P	6564.43±3851.36

4.6 Total gut length but not width was increased in *Fhϐ1KO* mice

When removing the guts of the mice for further analysis it was noted that the length of the gut from the start of the intestine to the anus was longer in diabetic mice compared to non-diabetic animals. The gut is very delicate once removed from the body, so to preserve the architecture the tissue was fixed immediately as described in Chapter 2, Section 2.2.3. Guts were then split into four sections. The large bowel (LB) and then 3 roughly equal sections of the small bowel (SB1, SB2 and SB3). A ruler was used to measure the length and width of each gut section post-fixation. Length results are displayed as total length and then broken down into small and large bowel length (Figure 4.5.B,C, Table 4.5, A.4.3,4). Not all mice where used for dissection, therefore, numbers below differ from those for blood glucose measurement (Figure 4.3).

When comparing the length of the entire gut, the *Fh1ϐKO* mice was the longest, and significantly longer than the guts of the *Fh1ϐKO* FH^{cyt} (p=0.0449), the *Fh1ϐKO* FH^{cyt} *1322* (p=0.0391), the FH^{cyt} *1322* (p=0.0025) and the *1322* mice (p=0.0025) (Figure 4.4.A, Table 4.5). The gut length of the *Fh1ϐKO 1322* mice and the FH^{cyt} or *WT* mice was not significantly different to any other genotype.

The gut of the *Fh1ϐKO* mice was longer in both the SB and LB section compared to all other genotypes. The greatest difference is seen in the SB section where the gut of the *Fh1ϐKO* mice was significantly longer than the gut of the FH^{cyt} *1322* (p=0.0034) and *1322* mice (p=0.0020) which had the shortest SB section. The other genotypes had guts at least 5cm shorter than the *Fh1ϐKO* mice, but this did not reach significance. Similarly, the length of the LB of *Fh1ϐKO* mice was at least 1cm longer than all other genotypes, but this was not significant.

Even though, on average guts from very diabetic mice are longer, when gut length is plotted against blood glucose there is no trend overall or per genotype. Table 4.2 details the R^2 value overall and for each genotype. There are only two mice from the FH^{cyt} and *Fh1ϐKO* genotypes which had both blood glucose and length measured, therefore, the R^2 value is 1, so they are not shown in the table.

Table 4.4. R^2 value for length (cm) *vs* blood glucose (mmol/L) of mice. *FH^{cyt}* and *Fh1βKO* mice not shown due to n=2 in these groups.

Genotype	Number of mice	R^2 values
All	43	0.2748
WT	3	0.1152
1322	7	0.0545
FH^{cyt} 1322	12	0.0428
Fh1βKO FH^{cyt}	3	0.0229
Fh1βKO FH^{cyt} 1322	7	0.3198
Fh1βKO 1322	7	0.2056

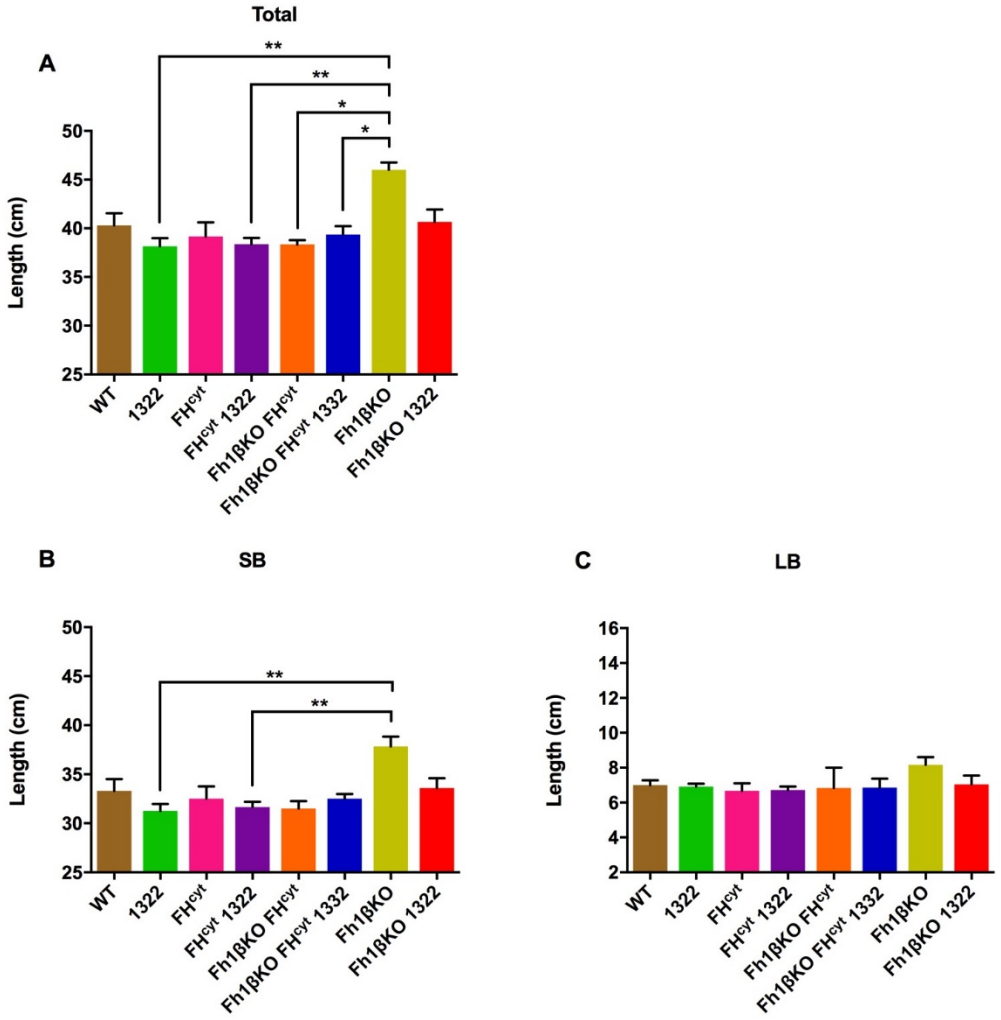

Figure 4.5. Small and large bowel length. Mouse gut was removed and fixed. Length was measured by ruler. (**A**) Length (mean ± SEM (Table 4.5)) of total intestine, (**B**) small bowel (SB) section, (**C**) large bowel (LB). *1322* n=12, *WT* n=5, *FH^{cyt} 1322* n=16, *FH^{cyt}* n=3, *Fh1βKO FH^{cyt} 1322* n=7, *Fh1βKO FH^{cyt}* n=3, *Fh1βKO 1322* n=10, *Fh1βKO* n=3. * p<0.05, ** p<0.01, *** p<0.001. Statistics details in Table A.4.3,4.

Table 4.5. Summary of total, SB, SB1, SB2, SB3 and LB gut length (cm) for each mouse genotype. Data shown as mean ± SEM. SB, small bowel; LB, large bowel. See also Figure 4.5.

Genotype	Number	Total	SB	LB
WT	5	40.3±1.3	33.3±1.2	7.0±0.3
1322	12	38.2±0.8	31.3±0.7	6.9±0.2
FH^{cyt}	3	39.2±1.5	32.5±1.3	6.7±0.4
FH^{cyt} 1322	16	38.4±0.6	31.7±0.5	6.7±0.2
Fh1βKO FH^{cyt}	3	38.3±0.4	31.5±0.8	6.8±1.2
Fh1βKO FH^{cyt} 1322	7	39.4±0.9	32.5±0.5	6.9±0.5
Fh1βKO	3	46.0±0.8	37.8±1.0	8.2±0.4
Fh1βKO 1322	10	40.7±1.3	33.6±1.0	7.1±0.5

4.7 Epithelial and goblet cell numbers remain constant across genotypes but paneth cell numbers change

To establish if there are any fundamental differences in the differentiated cells of the small bowel of mice used in this study, IHC was used to determine percentage of epithelial goblet and paneth cells in the crypt and villi.

Guts were embedded in paraffin wax, sectioned and used for IHC procedures (Figure 4.5). Next, the sections were imaged using the Nanozoomer scanner and visualised using NDP.2 software. To match previously published and similar studies[400], 50 villi and 100 crypts were selected from the small bowel of each mouse and an image was taken of each. The percentage of positive cells for each of cell type was then counted by eye.

H+E staining was completed and used to quantify the number of epithelial cells per crypt and villus. Representative example of an H+E stain of the entire section and a polyp is shown in Figure 4. There was no difference in the number of epithelial cells in the villi and crypts from the small bowel of each genotype (Figure 4.7, Table 4.6, A.5,6).

IHC was next carried out using alcian blue stain to detect goblet cells (Figure 4.10). The number of goblet cells was not different between the small bowel of each genotype (Figure 4.8, Table 4.6, A.5,6).

Anti-lysozyme antibody was used to detect paneth cells (Figure 4.9), which are not found in the villi of mice and, therefore, only crypt data is shown. The number of paneth cells was significantly lower (p=0.0108) in the crypts from *Fh1βKO FH^{cyt} 1322* mice compared to the *Fh1βKO FH^{cyt}* mice (Figure 4.9, Table 4.6, A.5,6). In general, there were fewer Paneth cells in all mice with the *1322* allele compared to their specific control, but this was not significant. This suggests an interaction of the *1322* allele and paneth cell development which has not been reported in any previous publication with mice with the *1322* allele.

Figure 4.6. Histological assessment of polyps. (**A**) An example H+E section showing the entire mouse gut. Top left SB1, top right SB2, bottom left SB3, bottom right LB. (**B**) A high power image of an H+E of a polyp. From a *Fh1ϐKO 1322* mouse.

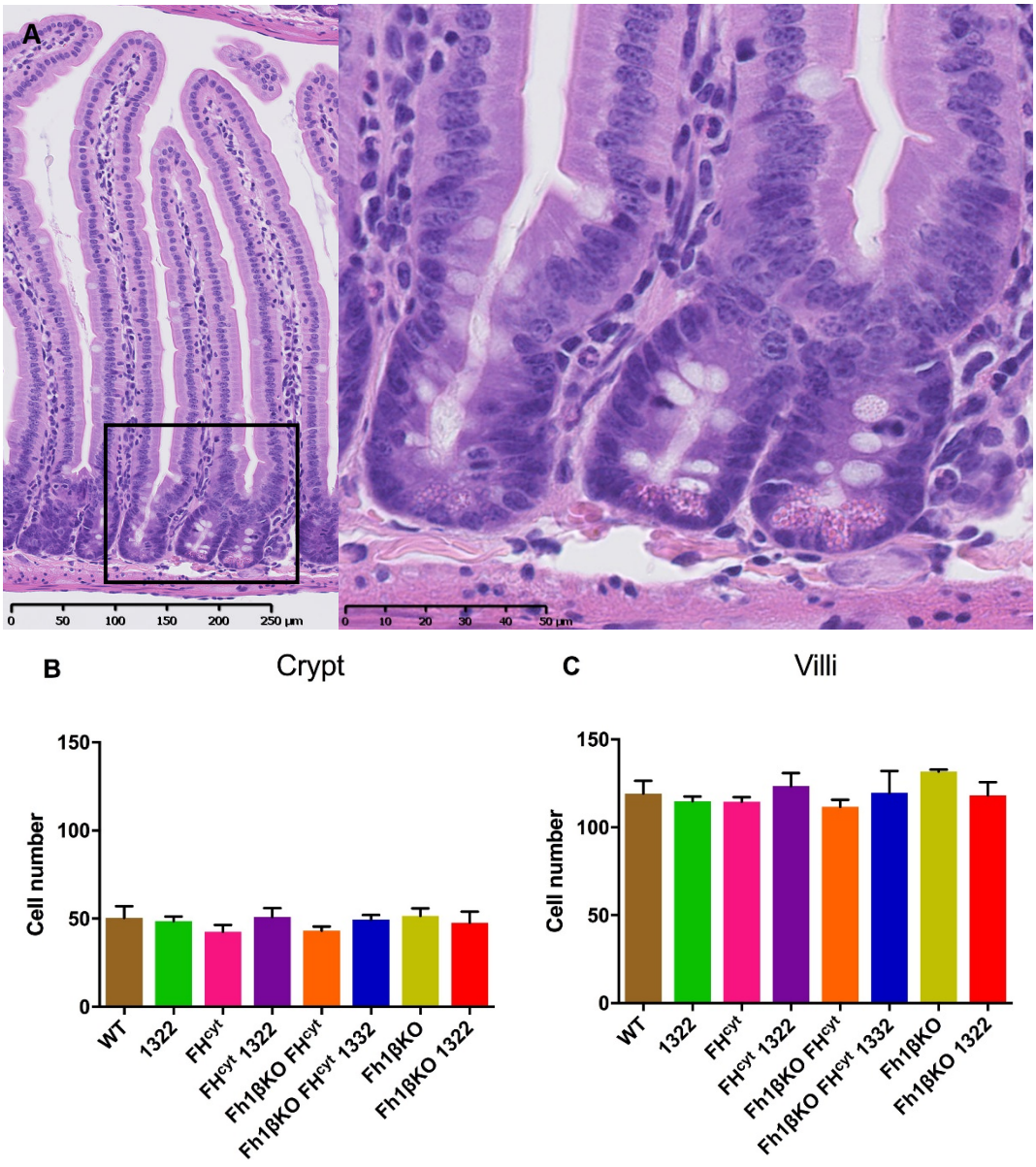

Figure 4.7. Epithelial cell number in crypt and villi of the small bowel. Sections were stained with H+E and scanned using a Nanozoomer Digital Pathology system to create high quality images which were used to calculate percentage positive cells (n=3 mice per group, n=50 villi and n=100 crypts per mouse). (**A**) Example H+E images. (**B**) Percentage positive cells in crypt and (**C**) villi (mean ± SEM (Table 4.6)). There were no significant differences; statistics details in Table A.4.5).

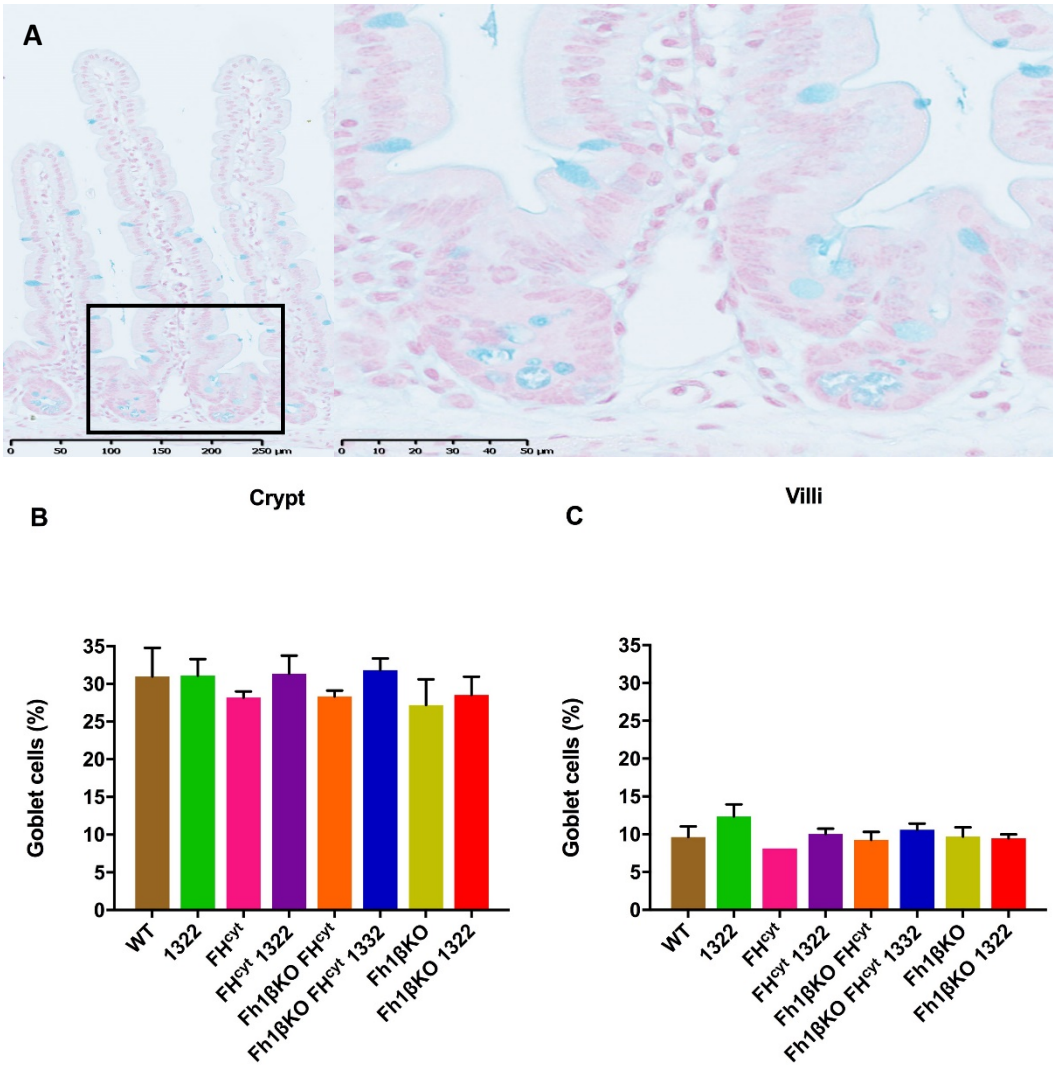

Figure 4.8. Percentage of goblet cells in crypt and villi of the small bowel. Sections were stained with alcian blue and scanned using a Nanozoomer Digital Pathology system to create high quality images which were used to calculate percentage positive cells (n=3 mice per group, n=50 villi and n=100 crypts per mouse) by Liliane El Eid a masters student. (**A**) Example alcian blue staining images. (**B**) Percentage positive cells in villi and (**C**) crypt (mean ± SEM (Table 4.6)). There were no significant differences; details in Table A.4.5.

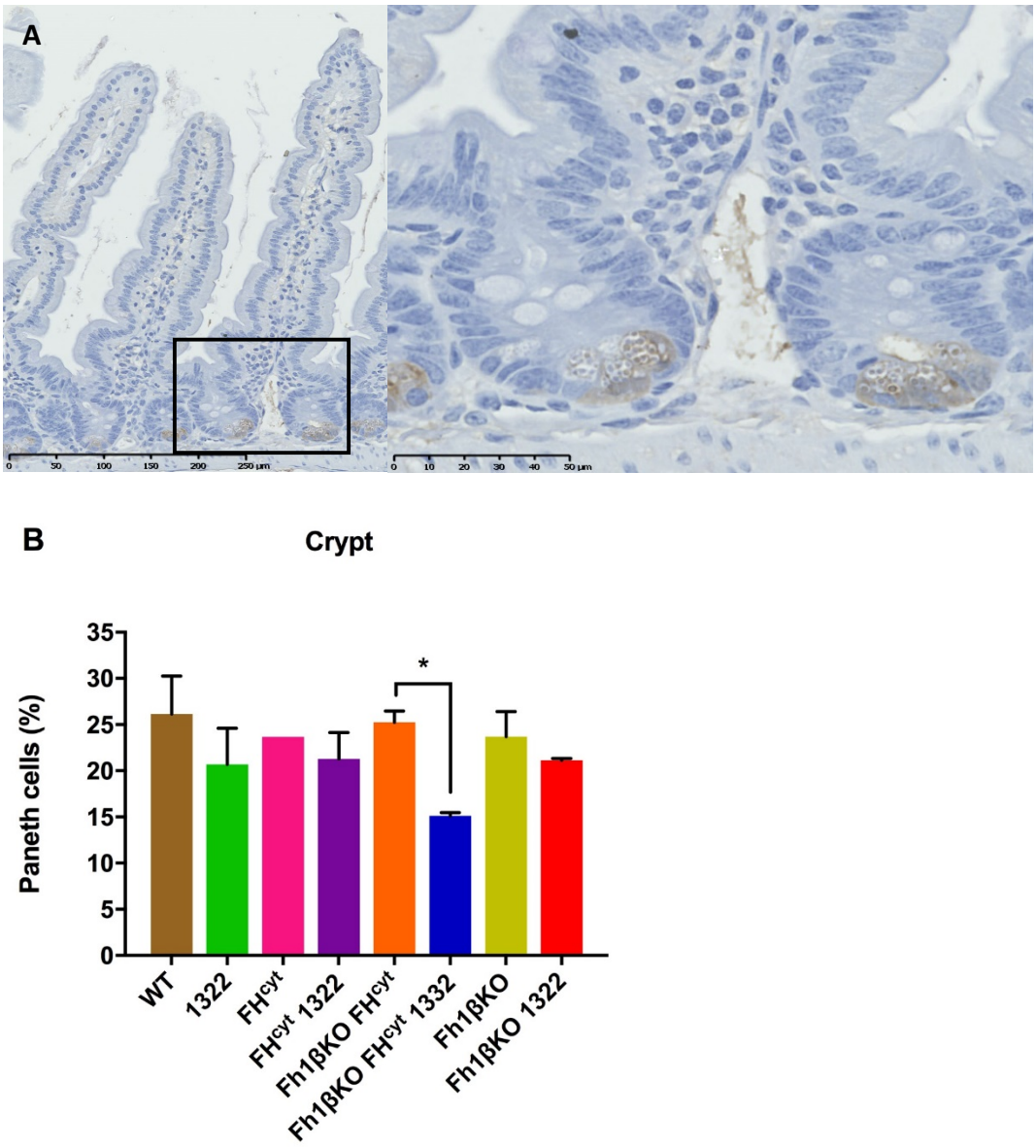

Figure 4.9. Percentage of paneth cells in crypt of the small bowel. Gut tissue was embedded in paraffin and IHC was performed for anti-lysozyme which is a paneth cell marker. Stained sections were scanned using a Nanozoomer Digital Pathology system to create high quality images which were used to calculate percentage positive cells (n=3 mice per group, n=50 villi and n=100 crypts per mouse). (**A**) Example IHC images. (**B**) Percentage positive cells in crypt (mean ± SEM (Table 4.6)). * $p<0.05$. Statistics details in Table A.4.5,6.

Table 4.6. Summary table of cell number of epithelial, percentage of goblet and paneth cells for crypt and villi for each mouse genotype. Data shown as mean ± SEM. N=3 per genotype. See also Figure 4.7,8,9.

	Epithelial cells (no.)		**Goblet cells (%)**		**Paneth cells (%)**
Genotype	**Crypt**	**Villi**	**Crypt**	**Villi**	**Crypt**
WT	50.5±6.7	119.2±7.2	31.0±3.8	9.6±1.4	26.2±4.1
1322	48.6±2.6	114.9±2.7	31.1±2.2	12.3±1.6	20.7±3.9
FH^{cyt}	42.6±3.9	114.5±2.7	28.2±0.8	8.1±0.3	23.7±0.0
FH^{cyt} 1322	51.0±4.9	123.4±7.4	31.4±2.4	10.1±0.7	21.3±2.9
Fh1βKO FH^{cyt}	43.1±2.4	111.7±4.1	28.3±0.8	9.2±1.1	25.2±1.2
Fh1βKO FH^{cyt} 1322	49.5±2.6	119.7±12.4	31.8±1.5	10.6±0.8	15.1±0.3
Fh1βKO	51.6±4.3	131.7±1.1	27.2±3.4	9.7±1.2	23.7±2.7
Fh1βKO 1322	47.7±6.2	118.2±7.4	28.5±2.4	9.5±0.5	21.1±0.2

4.8 Polyp count is not increased in mice with extremely elevated blood glucose

Next, the polyp count was determined for each genotype to allow assessment of the effect of diabetes on polyp burden. Post fixation, guts were stained with methylene blue to improve visualisation of polyps under a dissection microscope. Polyp counts for the three SB sections, the LB and the total gut were identified. Polyps were also categorised by size, based on diameter: <1mm, 1-2mm, 2-3mm and >3mm; an example image of each of these categories is shown in Chapter 2, Section 2.2.4 and Figure 2.3. Mice without the *Apc*^{1322T} allele (*WT, FH*^{cyt}*, Fh1ϐKO FH*^{cyt}*, Fh1ϐKO*, n=22) were checked for polyps and as expected none were found; these mice are not included in the data presented below.

FH^{cyt} *1322* mice had the highest total polyp count. The next highest total polyp count was the *1322* mice. *Fh1ϐKO FH*^{cyt} *1322* mice and *Fh1ϐKO 1322* mice had very similar total polyp counts which were much lower than *FH*^{cyt} *1322* and *1322*. However, these were not significantly different when analysed by (p=0.0645), although the p value approached significance (Figure 4.10.A, Table 4.7, A.4.7).

Polyp distribution in the gut was as expected. The majority of polyps were found in the SB1 and SB2 sections and the least number of polyps were found in the LB section (Figure 4.10.B+C, Table A.4.13). Ninety-eight percent of mice had one or more polyps in the SB1 and SB2 sections (47 out of 48). In the SB3 section, 81.25% (39 out of 48) of mice had one or more polyps. One or more polyps were found in the LB of 62.5% (30 out of 48) of mice with polyps.

In every section of the gut, generally, more polyps were found in *FH*^{cyt} *1322* or *1322* mice compared to *Fh1ϐKO 1322* and *Fh1ϐKO FH*^{cyt} *1322* mice (4.10.B). In the SB1 section there were significantly more polyps in *FH*^{cyt} *1322* mice compared to *Fh1ϐKO FH*^{cyt} *1322* and *Fh1ϐKO 1322* (p=0.0014, two-way ANOVA). *FH*^{cyt} *1322* also had more polyps than *1322* mice, although the difference was not significant (Figure 4.10.B, Table 4.8, A.4.8,9).

FH^{cyt} *1322* mice had the highest percentage of total polyps in the SB1 section compared to *Fh1ϐKO FH*^{cyt} *1322*, *Fh1ϐKO 1322* and *1322* mice (Figure 4.10.C). *1322* mice had the highest percentage of total polyps in the SB2 section compared to *Fh1ϐKO 1322*, *FH*^{cyt} *1322* and *Fh1ϐKO FH*^{cyt} *1322* mice. *Fh1ϐKO 1322* and *1322* mice had very similar percentages in the SB3 section, compared to *FH*^{cyt} *1322* and *Fh1ϐKO FH*^{cyt} *1322* mice. In

the LB section, *1322* mice had the highest percentage of total polyps compared to *Fh1ϐKO FH^{cyt} 1322*, *Fh1ϐKO 1322* and *FH^{cyt} 1322* mice (Figure 4.10.C, Table 4.8, A.4.8,9).

Overall, *FH^{cyt} 1322* and *1322* mice have a higher polyp burden in terms of total number of polyps compared to *Fh1ϐKO 1322* and *Fh1ϐKO FH^{cyt} 1322* mice.

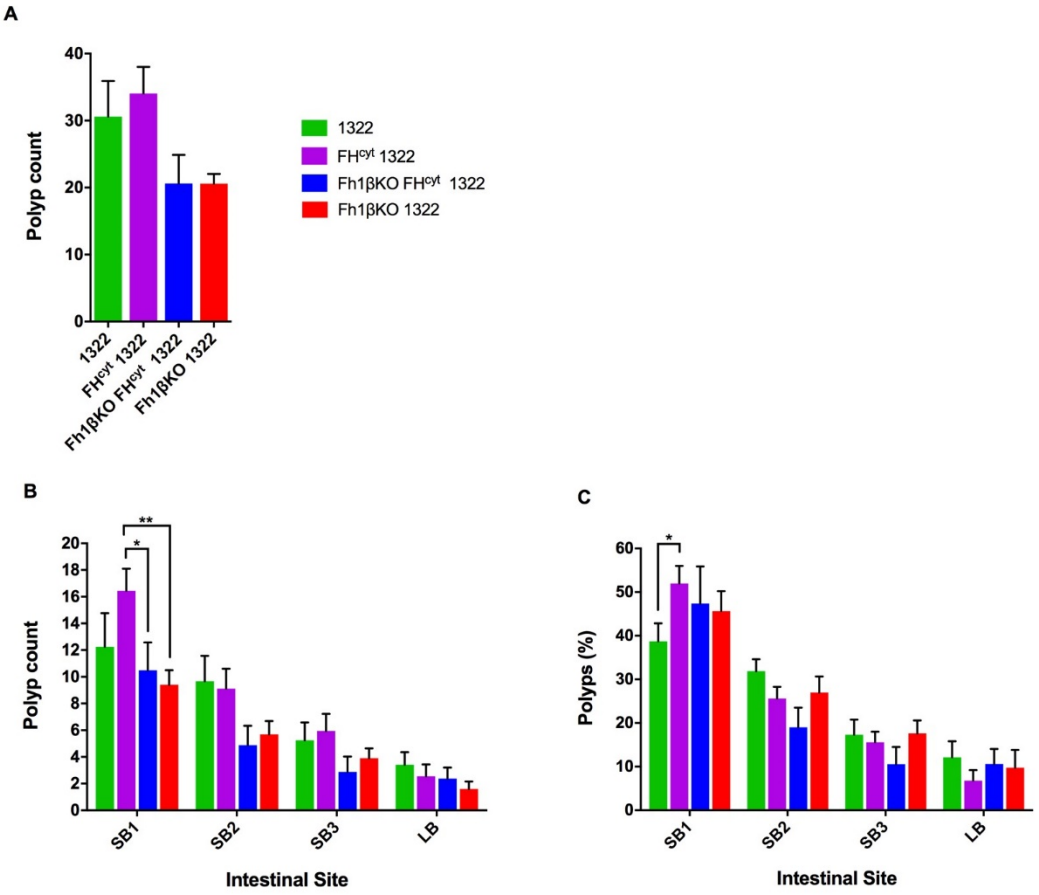

Figure 4.10. Polyp count by intestinal site. Guts were removed, fixed, stained with methylene blue and polyps were counted using a dissection microscope. Total polyp count (± SEM (Table 4.7)) by (**A**) genotype, (**B**) by site, (**C**) percentage polyps by site. Two-way ANOVA was performed, with Bonferroni *post hoc* test * $p<0.05$, ** $p<0.01$. Statistics details in Table A.4.8,9. SB, small bowel; LB, large bowel.

Table 4.7. Summary of total polyp count per genotype. See also Figure 4.10.A.

Genotype	Number	Total polyp count
1322	12	32.64±5.85
FH^{cyt} 1322	18	31.61±3.91
Fh1βKO FH^{cyt} 1322	8	20.61±4.24
Fh1βKO 1322	10	20.60±1.45

Table 4.8. Summary of total and percentage polyp count for each mouse genotype by bowel site. Data shown as mean ± SEM. SB, small bowel; LB, large bowel. See also Figure 4.10.B,C.

	Total count				
Genotype	**Total**	**SB1**	**SB2**	**SB3**	**LB**
1322	30.58±5.32	12.25±2.52	9.67±1.90	5.25±1.33	3.42±0.94
FH^{cyt} 1322	34.06±3.96	16.44±1.66	9.11±1.49	5.94±1.28	2.56±0.89
Fh1βKO FH^{cyt} 1322	20.63±4.24	10.50±2.08	4.88±1.46	2.88±1.16	2.38±0.82
Fh1βKO 1322	20.60±1.45	9.40±1.10	5.70±0.99	3.90±0.74	1.60±0.56
	Percentage				
Genotype		**SB1**	**SB2**	**SB3**	**LB**
1322		38.69±4.15	31.88±2.73	17.31±3.48	12.14±3.67
FH^{cyt} 1322		51.98±4.00	25.63±2.65	15.59±2.40	6.80±2.38
Fh1βKO FH^{cyt} 1322		47.38±8.48	19.00±4.51	10.54±3.94	10.57±3.46
Fh1βKO 1322		45.65±4.54	26.96±3.70	17.62±9.40	9.76±4.05

4.9 More >3mm polyps are found in *FH^{cyt} 1322* mice than in any other genotype

To determine if the presence of diabetes enhanced polyp growth, polyps were categorised by size. In previous studies using *Apc^{1322T}* mice, the majority or polyps are between 1 and 2mm and 37% polyps were >2mm in diameter[15]. In this study, over half of the polyps in *FH^{cyt} 1322* mice (53.6%) and *Fh1ϐKO FH^{cyt} 1322* mice (53.3%) were >2mm polyps; *1322* mice had 37.9% and *Fh1ϐKO 1322* mice had 35.0%. This suggests that *FH^{cyt}* presence leads to an increase in polyp size. Furthermore, this study found polyps of >3mm, which is unusual. The majority of mice had at least one polyp >3mm, (94.4% (17 out of 18) of *FH^{cyt} 1322* mice, 91.7% (11 out of 12) of *1322* mice, 90% (9 out of 10) of *Fh1ϐKO 1322* and 87.5% (7 out of 1) of *Fh1ϐKO FH^{cyt} 1322* mice) (Figure 4.10.A). On average *FH^{cyt} 1322* mice again had the highest percentage of total polyps that were >3mm (28.5%), followed by *Fh1ϐKO FH^{cyt} 1322* mice (20.5%), *Fh1ϐKO 1322* mice (15.3%) and finally *1322* mice (11.7%) (Figure 4.11.B).

Overall *FH^{cyt} 1322* mice had significantly more >3mm polyps ($p<0.0001$, two-way ANOVA) compared to *Fh1ϐKO FH^{cyt} 1322*, *1322* and *Fh1ϐKO 1322* mice. Specifically, *FH^{cyt} 1322* mice had significantly more 3mm+ polyps in the SB1 segment ($p=0.0063$, two-way ANOVA) compared to *Fh1ϐKO FH^{cyt} 1322*, *Fh1ϐKO 1322* and *1322* mice (Figure 4.11.C, Table 4.9, A.4.10,11). There were no significant differences in the number of 3+mm polyps in the other bowel sections (Figure 4.11.D.E.F) (Table 4.9, A.4.10,11).

There were a similar number of 2-3mm polyps in each genotype and SB sections of the bowel. In the LB section, there were significantly more 2-3mm polyps in *1322* mice compared to *FH^{cyt} 1322* mice ($p=0.05$), although the overall numbers here are very small compared to the SB (Table 4.9, A.4.10,11).

When looking at 1-2mm polyps, in total, there were more in the *1322* mice and *FH^{cyt} 1322* mice compared to *Fh1ϐKO 1322* mice and *Fh1ϐKO FH^{cyt} 1322* mice. Of note, there were significantly more in the SB3 section of *1322* mice (2.67±0.90) compared to the *Fh1ϐKO FH^{cyt} 1322* mice ($p=0.0424$, two-way ANOVA) (Table 4.9, A.4.10,11). In general, numbers in SB3 tended to be lower than in the other two SB segments.

Similarly, to 1-2mm polyps, for <1mm polyps, in total, there were more in the *1322* mice and *FH^{cyt} 1322* mice compared to *Fh1ϐKO 1322* mice and *Fh1ϐKO FH^{cyt} 1322* mice. Of note,

there were significantly more <1mm polyps in the SB2 section of *1322* mice compared to *Fh1βKO 1322* and *Fh1βKO* FH^{cyt} *1322* mice (p=0.0424, two-way ANOVA) (Table 4.9, A.4.10,11).

Overall, of the high polyp count genotypes, FH^{cyt} *1322* mice had more >3mm polyps, whereas *1322* mice had more <1-2mm polyps. The polyp burden of the FH^{cyt} *1322* mice can perhaps be classified as the highest suggesting that the presence of FH^{cyt} leads to increased polyp growth.

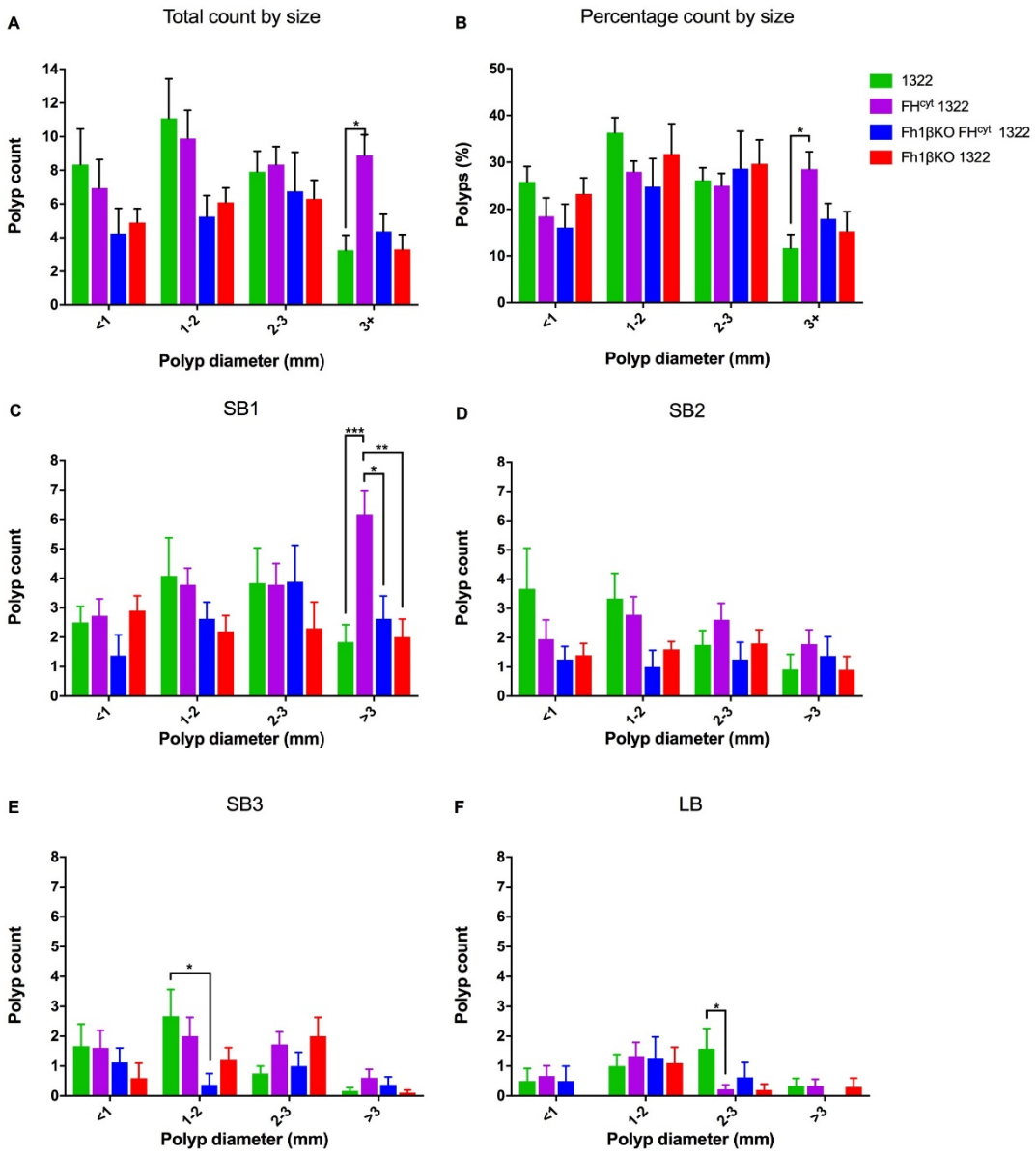

Figure 4.11. Polyp count by size. Guts were removed, fixed, stained with methylene blue and polyps were counted using a dissection microscope. Frequency of polyp sizes (mean ± SEM (Table 4.9 found in (**A**) SB1, (**B**) SB2, (**C**) SB3 and (**D**) LB. *1322* n=12, *FH^{cyt} 1322*, n=18, *Fh1βKO FH^{cyt} 1322*, n=8, *Fh1βKO 1322* n=10. Two-way ANOVA was performed, with Bonferroni *post hoc* test * p<0.05, ** p<0.01, *** p<0.001. Statistics details in Table A.4.10,11. SB, small bowel; LB, large bowel.

Table 4.9. Summary of frequencies of each polyp size in the bowel. Frequencies are given by size of polyp in SB1, SB2, SB3 and LB for each mouse genotype. Data given as mean ± SEM. SB small bowel; LB large bowel. See also Figure 4.11.

	SB1			
Genotype	**<1mm**	**1-2mm**	**2-3mm**	**3+mm**
1322	2.50±0.54	4.48±1.29	3.83±1.20	1.83±0.59
FH^{cyt} 1322	2.72±0.58	3.78±0.56	3.78±0.72	6.17±0.82
Fh1βKO FH^{cyt} 1322	1.38±0.71	2.63±0.56	3.88±1.25	2.63±0.78
Fh1βKO 1322	2.90±0.50	2.20±0.53	2.30±0.90	2.00±0.61
	SB2			
Genotype	**<1mm**	**1-2mm**	**2-3mm**	**3+mm**
1322	3.67±1.39	3.33±0.87	1.75±0.49	1.78±0.51
FH^{cyt} 1322	1.94±0.66	2.78±0.62	2.40±0.57	1.78±0.49
Fh1βKO FH^{cyt} 1322	1.25±0.45	1.00±0.57	1.25±2.61	1.38±0.65
Fh1βKO 1322	1.40±0.40	1.60±0.27	1.80±0.47	0.90±0.46
	SB3			
Genotype	**<1mm**	**1-2mm**	**2-3mm**	**3+mm**
1322	1.67±0.74	2.67±0.89	0.75±0.25	0.17±0.11
FH^{cyt} 1322	1.61±0.59	2.00±0.64	1.72±0.43	0.61±0.28
Fh1βKO FH^{cyt} 1322	1.13±0.48	0.38±0.38	1.00±0.46	0.38±0.26
Fh1βKO 1322	0.60±0.50	1.20±0.42	2.00±0.63	0.10±0.10
	LB			
Genotype	**<1mm**	**1-2mm**	**2-3mm**	**3+mm**
1322	0.50±0.42	1.00±0.39	1.59±0.68	0.33±0.26
FH^{cyt} 1322	0.67±0.34	1.33±0.46	0.22±0.15	0.33±0.23
Fh1βKO FH^{cyt} 1322	0.50±0.50	1.25±0.73	0.63±0.50	0.00±0.00
Fh1βKO 1322	0.00±0.00	1.10±0.53	0.20±0.20	0.30±0.30

4.10 Discussion

The eight genotypes generated by the breeding of female *Fh1ϐKO* FH^{cyt} mice and male Apc^{1322T} mice allowed the study of the effect of blood glucose, alone or combined with overexpression of FH on polyposis.

Mice with the *Fh1ϐKO* allele display greatly elevated blood glucose levels as matched by the original paper[268]. The Accu-Check blood glucose monitor used for the measurement of blood glucose levels had a maximum reading of 33.3, which 10 out of 14 (71.43%) of *Fh1ϐKO* and four out of nine (44.44%) of *Fh1ϐKO 1322* mice met indicating the very high nature of the blood glucose in this model system.

Metabolomics data for [glucose] (Figure 4.4) highlight that polyps from mice with elevated blood glucose due to the *Fh1ϐKO* allele do have additional [glucose] available in the tissue for polyp growth compared to all other genotypes. Nevertheless, the polyp size data suggests that elevated blood glucose alone, is not sufficient to generate the largest polyps in this model. Interestingly, the presence of the FH^{cyt} allele also leads to a slight reduction in [glucose] found in the tissue, further alluding to the role of glucose and therefore fumarate in polyposis in this model.

Presence of FH in the β-cells of the pancreas allows insulin secretion and glucose homeostasis[268], as discussed in Chapter 1, Section 1.12. As seen previously, addition of the FH^{cyt} allele increased blood glucose compared to WT mice and reduced the blood glucose of mice with the *Fh1ϐKO* allele to pre-diabetic levels[268].

The total gut length of *Fh1ϐKO* mice was longer than all other genotypes. This phenotype has been previously noted in other mouse models of obesity and diabetes such as *ob/ob* and *db/db* mice[401] as well as mice with over nutrition[402]. The average number of epithelial cells per villi and crypt were not different between genotypes. This suggests that the gut of the *Fh1ϐKO* mice is made up of more villi and crypts, not larger villi and crypts. The small intestine is a critical site for nutrient absorption and important for maintenance of normal blood glucose. There may be a link between elevated blood glucose and increased intestinal length, the causes of which have not thus far been investigated in the literature.

There was no difference in goblet cell number between genotypes. However, Paneth cell content was variable between genotypes. For example, the presence of *1322* allele led to a reduction in Paneth cells. There is no previous report in the literature on this observation. Presence of the *Fh1βKO* or FH^{cyt} allele alone did not lead to a reduction in Paneth cell number. Whereas, when both *Fh1βKO* and FH^{cyt} alleles are present a reduction in Paneth cell number is found. However, the *Fh1βKO* allele is not expressed in the gut but the FH^{cyt} allele is, therefore, there is no logical explanation for the reduction in Paneth cell numbers. At this time, there is no obvious phenotypic consequence or explanation as to why paneth cell numbers would change in this genotype.

Of the four genotypes with the *1322* allele, which led to polyps, in terms of polyp number, there was a distinct split between mice with and without the *Fh1βKO* allele, which leads to very high blood glucose. *Fh1βKO 1322* and *Fh1βKO* FH^{cyt} *1322* mice had lower polyp count compared to *1322* and FH^{cyt} *1322* mice. This is an opposite result to hypothesized, rather that diabetes in mice as a consequence of *Fh* loss does not increase total polyp count.

1322 mice have a high polyp count with most of their polyps <1-2mm in size found in the SB1 and SB2 sections of the gut. FH^{cyt} *1322* mice had the most polyps, established due to high numbers of polyps in the SB1 section of the gut compared to all other genotypes. Interestingly, the greatest percentage of polyps from FH^{cyt} *1322* mice were in the >3mm category. Furthermore, FH^{cyt} *1322* mice had the most >3mm polyps which were mainly found in the SB1 section of the gut where all the other genotypes had significantly fewer >3mm polyps. Together this suggests that over-expression of FH in the gut epithelial cells promotes polyposis, both in number and size of polyps. There is currently no literature on cytoplasmic FH promoting polyposis in the gut; cytoplasmic FH is seen as a tumour suppressor[399,403]. However, KO Fh1 MEFs proliferate much slower than their WT Fh1 MEFs counterparts (Chapter 5, Section 5.3, Figure 5.2). This could be due to the DNA damage reduction role of FH, leading to more healthy cells, which in turn proliferate.

However, this is not backed up results from *Fh1βKO* FH^{cyt} *1322* mice, who had a much lower polyp count than FH^{cyt} *1322* mice, and a similar number of >3mm polyps to *1322* and *Fh1βKO 1322* mice, which is much lower than FH^{cyt} *1322* again. This maybe a

consequence of high blood glucose levels inhibiting the potential polyposis promotion by FH in the gut.

Different again is the size distribution of polyps in *Fh1βKO FH^{cyt} 1322* and *Fh1βKO 1322* mice. The majority of their polyps are between 1 and 3mm. In fact, more 2-3mm polyps are found when the *Fh1βKO* allele is present. Equally there are slightly more >3mm polyps in *Fh1βKO FH^{cyt} 1322* and *Fh1βKO 1322* mice than found in *1322* mice. This could suggest that elevated blood glucose promotes polyposis growth, but not as much as *FH^{cyt}* alone.

This data suggests a role for cytoplasmic FH in tumourigenesis. This is in conflict to previous *in vivo* studies which have shown that overexpression of cytoplasmic FH in renal cells ameliorates signs of renal cysts which can lead to the development of HLRCC suggesting that FH is a tumour suppressor[330]. However, it could suggest that the role of FH is cell dependent. The main known role of mitochondrial FH is to convert fumarate into malate in the TCA cycle, and the main known role of cytosolic FH is to aid DNA damage repair, perhaps in this case, this allows polyp cells to survive and grow. Further investigations *in vitro* are necessary to fully understand the role of cytoplasmic FH in CRC (Chapter 8, Section 8.2).

Chapter 5 - Investigating the link between T2D and CRC *in vitro*

5.1. Introduction

My investigations into the link between T2D and CRC *in vivo* (Chapter 3 and 4) have led to further questions surrounding the role of fumarate and FH in CRC patients with T2D. There are a number of questions that still need answering, such as, does FH contribute to tumorigenesis in CRC? What is the role of fumarate and succination in CRC?

FH is the enzyme which breaks down fumarate into malate in the TCA cycle. It has previously been shown that lack of FH and subsequent increase in [fumarate] leads to decreased mitochondrial respiration, alteration of the TCA cycle functionality and reversal of the urea[321,322,332,404,405] (Chapter 1, Figure 1.8 and 1.10). Fumarate can also inhibit 2-OGDDs, alter gene expression and generate 2-SC by a process named succination[332,406] (Figure 1.11). The interplay between loss of FH, high [fumarate] and different aspects of metabolism is still unclear.

In vivo, CRC can be extremely nutrient poor and oxygen low at the tumour core[335,407]. Therefore, it is important to understand the molecular events involved in tumour adaptation to these conditions; the effect of different glucose concentrations on CRC cells in hypoxia requires investigation. Most *in vitro* studies use oxygen tensions in the region of 0.8–1.0%. However, there is a marked lack of data from experiments that consider conditions of more severe hypoxia[408]. Large gradients of oxygen tension do occur in both tumours and spheroid models, including very low oxygen tension (0.1% O_2) and almost total anoxia[154,409–412]. Additionally, preliminary data in our lab from a collaboration with Tomoyoshi Soga (Keio University, Japan) highlighted a possible relationship between fumarate and oxygen tension (at 0.2%) (further explained in Section 5.2) which warranted further investigation with respect to this project.

To recapitulate the conditions of variable nutrient levels and very low oxygen caused by inadequate vascularisation, *in vitro* CRC cells were cultured in different glucose concentrations and held in 0.2% O_2 to simulate hypoxia. To aid investigations into the possible relationship between fumarate and oxygen tension, mouse embryonic fibroblasts (MEFs) with Fh1 (murine FH) completely deleted, named KO Fh1 MEFs and WT Fh1 MEFs were used in some experiments. KO Fh1 MEFs have previously been used in

studies to understand the role of fumarate and FH further in HLRCC[316,334,345]. KO Fh1 MEFs are known to have a different cellular metabolism, previously shown by Frezza et al. 2011 and Zheng et al. 2013[321,405]. Fh1 deficient cells use accumulated TCA cycle metabolites to generate haem, which is then degraded to bilirubin. This process creates mitochondrial NADH which can be used to generate ATP by OXPHOS. It has also been shown that Fh1 deficient cells can generate citrate and malate from glutamine by revering parts of the TCA cycle to perform reductive carboxylation of α-ketoglutarate to isocitrate. This process then provides the anabolic building blocks allowing cell proliferation[320]. Additionally, Fh1 deficient mice and media from FH-deficient cell lines excrete increased amounts of fumarate and arginosuccinate compared to their WT counterparts[321]. This was found to be a result of the reversed activity of the urea cycle enzyme arginosucinnate lyase (Chapter 1, Figure 1.10). These alterations in cellular metabolism must be considered throughout the analysis of the results of this chapter.

5.1.1 Hypotheses

- Fumarate concentration will be highest in CRC cells held in hypoxia compared to normoxia and cultured in glucose compared to no glucose.
- FH concentration will be highest in CRC cells held in normoxia compared to hypoxia and cultured in no glucose compared to glucose.
- FH activity will be highest in CRC cells held in hypoxia compared to normoxia and cultured in glucose compared to no glucose.
- Expression of genes involved in glycolysis will be highest in CRC cells held in hypoxia compared to normoxia and cultured in glucose compared to no glucose.
- Expression of genes involved in mitochondrial metabolism will be highest in CRC cells held in normoxia compared to hypoxia and cultured in no glucose compared to glucose.
- Mitochondria concentration will be highest in CRC cells held in normoxia compared to hypoxia and cultured in no glucose compared to glucose.
- Mitochondrial oxygen consumption rate will be highest in CRC cells held in normoxia compared to hypoxia and cultured in no glucose compared to glucose.

5.1.2 Aims

To generate an *in vitro* model of CRC and T2D and characterise:

- Concentration of fumarate.
- Amount and activity of FH.
- Changes in gene expression.
- Amount and activity of mitochondria.

Statistics were performed with two-way ANOVA with Bonferroni *post-hoc* test unless otherwise stated.

5.2 Preliminary data

Previously, our lab collaborated with Professor Tomoyoshi Soga (Keio University, Japan) to quantify changes in the levels of metabolites in the cell lines DLD1, HT55 and SW837 by CETOF-MS after 48 hours of treatment with 20.9%, 1% or 0.2% O_2[408]. Experiments were performed on cells which were cultured in media with 25mM glucose. The findings by Nijhuis et al. concluded that the CRC cell lines used have many differences in metabolites. Of particular relevance to this study was the intracellular fumarate concentration, which responded differently to a change in O_2 tension in the DLD1, HT55 and SW837 cell lines (Figure 5.1; Table 5.1.). From now on [fumarate] will be used to denote 'the fumarate concentration'.

In DLD1 cells [fumarate] was significantly higher at 0.2% O_2 compared to 20.9% O_2 (p=0.0011, one-way ordinary ANOVA; 4.5-fold increase) (Figure 5.1; Table A.5.1,2). [Fumarate] was also higher at 1% O_2 compared to 20.9% O_2 but the difference was not significant (p=0.0897, one-way ordinary ANOVA; 2.4-fold increase). The increase in [fumarate] between 1% O_2 and 0.2% O_2 was significant (p=0.0138, one-way ordinary ANOVA; 1.9-fold increase).

The HT55 cell line followed the same pattern to the DLD1 cell line. [Fumarate] was significantly higher at 0.2% O_2 compared to 20.9% O_2 (p<0.0001, one-way ordinary ANOVA; 8.75-fold increase) (Figure 5.1; Table A.5.2 and A.5.3). [Fumarate] was also significantly higher at 1% O_2 compared to 20.9% O_2 (p<0.0001, one-way ordinary ANOVA; 6.75-fold increase). The increase in [fumarate] between 1% O_2 and 0.2% O_2 was significant (p=0.0248, one-way ordinary ANOVA; 1.3-fold increase).

The trend for the SW837 cell line was in direct contrast to the trend for the DLD1 and HT55 cell lines. [Fumarate] was significantly decreased at 0.2% O_2 compared to 20.9% O_2 (p=0.0036, one-way ordinary ANOVA; 2.3-fold decrease) (Figure 5.1; Table A.5.1,2). [Fumarate] was also significantly decreased at 1% O_2 compared to 20.9% (p=0.0035, one-way ordinary ANOVA; 2.4-fold decrease). Furthermore, there was minimal difference between [fumarate] at 1% and 0.2% O_2.

Interestingly, [fumarate] differs the most at 20.9% O_2 between the three cell lines. At 20.9% O_2, SW837 cells have a significantly higher [fumarate] compared to DLD1 and HT55

cells, p=0.0004 and p=0.0002 respectively (one-way ordinary ANOVA) (Figure 5.1; Table A.5.1.). [Fumarate] is very similar between the three cell lines at 1% O_2. Whereas there are differences at 0.2% O_2, although non-significant (Figure 5.1). Overall, these data show that DLD1 and HT55 cells increased [fumarate] as O_2% was reduced, whereas SW837 cells had the opposite response and decreased [fumarate] in response to reduced O_2%.

It is possible that differences in gene expression and metabolism between these cells lines are responsible for the differences in [fumarate]. The DLD1 and HT55 cell lines originate from a colon cancer and the SW837 cell line originates from a rectal cancer. It is possible cell lines from these separate intestinal regions have different metabolisms, however, the TCGA study found no significant differences in the genetic progression of colon and rectal cancers[413]. HT55 cells were found to be WT *KRAS* whereas DLD1 and SW837 cells were mutant *KRAS,* results confirmed in our laboratory as part of cell line verification. It is also important to note that extensive mutation analysis by Moudarov and colleagues has failed to identify any FH mutations in a significant number of CRC cell lines and CRC[50].

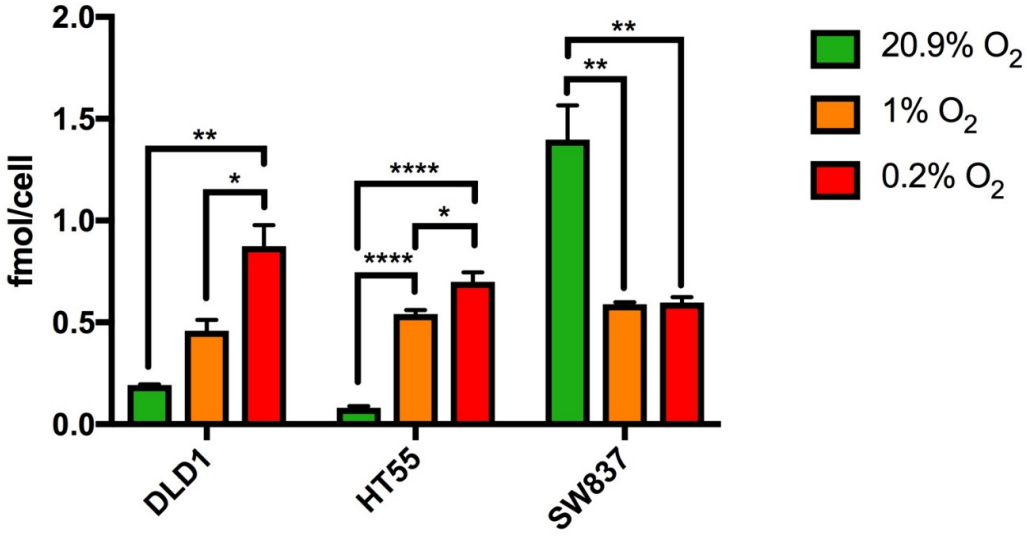

Figure 5.1. Fumarate concentration in CRC cell lines determined by mass spectrometry. DLD1, HT55 and SW837 cells were grown in media with 25mM glucose, then all lines cultured for 48 hours under normoxia (20.9% O_2) or hypoxia at 1% or 0.2% O_2 conditions. Cell lysates were harvested and analysed by capillary electrophoresis time of flight mass spectrometry and the concentration of fumarate (fmol/cell) determined. Mean ± SEM in Table 5.1. One-way ordinary ANOVA was used. ** p<0.01, *** p<0.001, **** p<0.0001 (Table A.5.1 and A.5.2).

Table 5.1. Summary table of fumarate concentration in DLD1, HT55 and SW837 CRC cell lines maintained in 20.9%, 1% or 0.2% O_2 for 48 hours. Identified by mass spectrometry. Concentrations are given in fmol/cell and shown as mean ± SEM. N=3. See also Figure 5.1.

Cell line and treatment	Fumarate (fmol/cell)
DLD1 20.9% O_2	0.19±0.00
DLD1 1% O_2	0.46±0.05
DLD1 0.2% O_2	0.87±0.10
HT55 20.9% O_2	0.08±0.01
HT55 1% O_2	0.54±0.20
HT55 0.2% O_2	0.70±0.05
SW837 20.9% O_2	1.40±0.17
SW837 1% O_2	0.59±0.00
SW837 0.2% O_2	0.60±0.03

For the further *in vitro* experiments described in this chapter, I wanted the conditions used to be similar to *in vivo* T2D CRC conditions. Hypoxia is a common feature of solid tumours like CRC[154]. To study the effect of hypoxia on FH, fumarate, succination and T2D in CRC cells I chose to hold the cells in 0.2% O_2 to reflect the very low oxygen tensions that occur in both tumours and spheroid models; such low oxygen tension remains significantly understudied[409–412,414]. Moreover, there were differences in [fumarate] in CRC cells recorded by mass spectrometry at 0.2% O_2 and these observations warrant further investigation (Figure 5.1). The blood glucose of the patient may influence how much glucose is available to a tumour *via* its vasculature. The centre of a CRC is known to receive fewer nutrients such as glucose, compared to the outer most margin of the tumour[335]. Also, in Chapter 4 it was shown the intestinal mucosa and polyps of mice with diabetes had a higher glucose content than non-diabetic mice. Therefore, to mirror this situation *in vitro*, it was necessary to culture CRC cells in non-diabetic and diabetic concentration of glucose (further described in section 5.2). However, another feature of T2D is hyperinsulinemia which was not modelled in this work. Therefore, the findings must be considered in light of this.

I continued to use DLD1, HT55 and SW837 cell lines for the *in vitro* investigations described in this chapter as this also allowed me to investigate the influence of cell line origin and mutation profile on FH, fumarate, succination and T2D in CRC cells.

5.3 Creating CRC cell populations grown in media with 25mM, 5mM or 0mM glucose

To model non-diabetic and T2D conditions *in vitro* I decided upon three final concentrations of glucose in the media of the cells: 25mM which represents the very high blood glucose experienced by a T2D patient; 5mM reflecting a non-diabetic patient blood glucose or a very well controlled T2D patient[415,416]; and 0mM as a hypoglycaemic condition and because nutrient concentration in a solid tumour like CRC can be extremely low at the core[335]. From here on [glucose] will be used to denote 'the glucose concentration'.

Glutamate is another nutrient found in excess concentration in cell culture media. Glutamate can be used to generate energy by a cell through the TCA cycle by entry via α-ketoglutarate (Chapter 1, Figure 1.8). Glutamine is the preferred anaplerotic precursor of many cancer cells[417]. It is known that intestinal cells are particularly dependent on glutamine and depletion leads to rapid necrosis[418]. Glutamine remained in the media of all cells used in this study, to isolate the effect of reduction of glucose and to ensure cells remained alive.

DLD1, HT55 and SW837 cells are usually cultured with 25mM glucose in their media. To create cells comfortable with being cultured in 5mM and 0mM glucose and to reduce the stress and possible death of the cells, I decided to reduce [glucose] in the media slowly over a period of 2 months (Chapter 2, Section 2.3.1). This method led to creation of unique cell lines, which I could use for experimental work.

It is interesting to note here that CRC cells cultured in higher [glucose] acidified the media more rapidly than those cultured in no glucose. Rapid acidification of the media is also a feature of WT Fh1 MEFs.

It should be noted that the HT55 cells were used by Anthony Xi Tan, an undergraduate student under my supervision and were only used for some experiments and, therefore, do not appear in all figure panels.

5.4 Doubling time of DLD1, HT55 and SW837 cells grown increased as [glucose] was reduced in their media

It is generally accepted that doubling time is a simple and quick health check of cell populations. I measured the doubling time of cells to determine stability at each reduction of media [glucose] (Figure 5.2) (Table 5.2). The equation (hrs*log(2))/(log(final cell number)-log(initial cell number)) was used to calculate doubling time.

[Glucose] had a significant effect on the doubling time of DLD1 cells ($p<0.0001$, one-way ANOVA) (Figure 5.2.A). There was a significant increase in the doubling time of cells grown in 0mM compared to those grown in 5mM and 25mM ($p<0.0001$ in both cases). There was also a significant increase in the doubling time of cells grown in 5mM compared to 25mM glucose ($p=0.0002$, one-way ANOVA) (Table A.5.3).

[Glucose] concentration also had a significant effect on the doubling time of HT55 cells ($p=0.0365$, one-way ANOVA) but *post-hoc* analysis revealed no significant difference between the groups (Table A.5.3,4). The doubling time of HT55 cells at 25mM glucose was longer than DLD1 and SW837 cells. However, the doubling time of HT55 cells remained relatively stable as [glucose] decreased (Figure 5.2.B).

Again, [glucose] had a significant effect on the doubling time of SW837 cells ($p<0.0001$, one-way ANOVA) (Figure 5.2.C) (Table A.5.3). There was a significant increase in the doubling time of cells grown in 0mM compared to those grown in 5mM and 25mM ($p<0.0001$ in both cases, one-way ANOVA). There was also a significant increase in the doubling time from cells grown in 5mM compared to 25mM glucose ($p<0.0001$, one-way ANOVA) (Table A.5.3).

Overall, the doubling time of all the CRC cells increased as [glucose] decreased. Glucose is the fuel for glycolysis, and increased glycolysis leads to increased ATP for the proliferation of cells.

The doubling time of the KO Fh1 MEFs was significantly longer than the doubling time of the WT Fh1 MEFs ($p<0.0001$ paired t-test; Figure 5.2.D). The presence of Fh1 increased doubling time two-fold in WT Fh1 MEFs compared to KO Fh1 MEFs. This suggests that presence of Fh1 has an increased proliferation effect on cells, likely due to the use of

different metabolism pathways used by KO Fh1 MEFs compared to the full TCA cycle of the WT Fh1 MEFs.

As all CRC cells have a higher doubling time compared to KO Fh1 MEFs this suggests that they have functional FH, which is allowing generation of maximum NADH *via* the TCA cycle for use in ATP generation *via* OXPHOS.

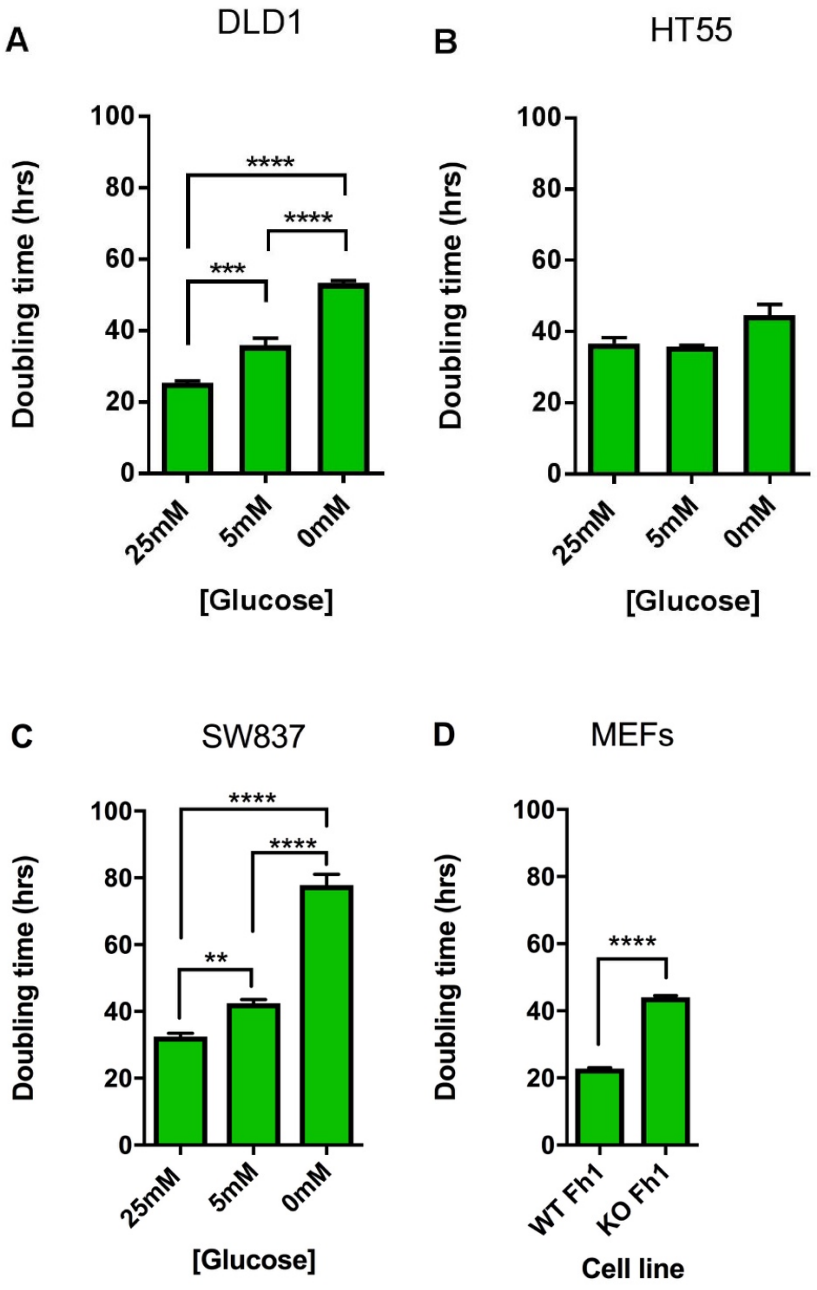

Figure 5.2. Doubling time of CRC and MEFs cell lines. Doubling time was calculated using the formula (hrs*log(2))/(log(final cell number) – log(initial cell number)). (**A**) DLD1 cells**,** (**B**) HT55 cells**,** (**C**) SW837 cells were cultured in 25mM, 5mM or 0mM glucose. Ordinary one-way ANOVA was performed with Bonferroni *post hoc* test (**D**) MEFs were cultured in 25mM glucose. Unpaired two-tailed t-test was performed. ** $p<0.01$, *** $p<0.001$. A summary of the mean ± SEM is given in Table 5.2 and statistics in Table A.5.3,4.

Table 5.2. Summary of doubling time (hrs). Data shown as mean ± SEM. N=3. See also Figure 5.2.

Cell line	Doubling time (hrs)
DLD1 25mM	25.23±0.54
DLD1 5mM	35.90±1.95
DLD1 0mM	53.29±0.72
HT55 25mM	36.68±1.68
HT55 5mM	35.85±0.40
HT55 0mM	44.66±2.96
SW837 25mM	28.06±0.34
SW837 5mM	41.98±0.24
SW837 0mM	90.43±1.06
WT Fh1 MEFs	22.77±0.25
KO Fh1 MEFs	44.02±0.54

5.5 HIF-1α is upregulated in CRC cells when held under 0.2% O_2

For the following experiments in this chapter 0.2% O_2 was used as a model of extreme hypoxia. Confirmation of a hypoxic environment is typically proven with presence of HIF-1α protein. Therefore, it was necessary to determine if HIF-1α was upregulated when the CRC cell lines were held under 0.2% O_2.

This was done *via* western blot. Protein lysates were taken from the CRC cell lines after 48 hours in 0.2% O_2. HIF-1α is an unstable protein, therefore, lysates were taken as quickly as possible and ice was used to prevent protein degradation. Protein quantification was always completed prior to western blot, and the same ng of protein were loaded for each sample (Chapter 2, Section 2.3.2). To confirm the loading is correct, it is best practice to blot for a protein which is highly expressed and stable within the cell such as cytoskeletal proteins. Alteration of glucose concentration in media and / or oxygen tension influences most cytoskeletal proteins, therefore, the standard protein controls for western blot such as actin could not be used in this investigation[419–422].

It was decided that a Ponceau red blot was the quickest way to control for protein transfer to membrane, as the Coomasie blue method does not take into account the transfer step. This was not a perfect solution, however, as my samples consistently show a difference in protein loading at different kDa. So, it was decided not to quantify the blots but use the Ponceau blot to determine that some protein was present.

DLD1 cells have been previously shown to produce HIF-1α in hypoxia[163,423,424]. The HIF-1α protein is 120kDa, however, the HIF-1α antibody (BD #610959) used for the Western blot unfortunately gave multiple bands between 100 – 150kDa. It is possible that the other bands seen on the Western blot are HIF-1α conjugated to other proteins involved in the hypoxic response such as HIF-1ß or VHL for example. A protein detected at 120kDa by the HIF-1α antibody, which is assumed to be HIF-1α was found to be elevated in both DLD1 and SW837 cell lines cultured with 25mM, 5mM and 0mM glucose held in 0.2% O_2 compared to 20.9% O_2 (Figure 5.3), if it is assumed that all the samples do have equal loading. The upregulation is not as strong when cells are cultured with 0mM glucose.

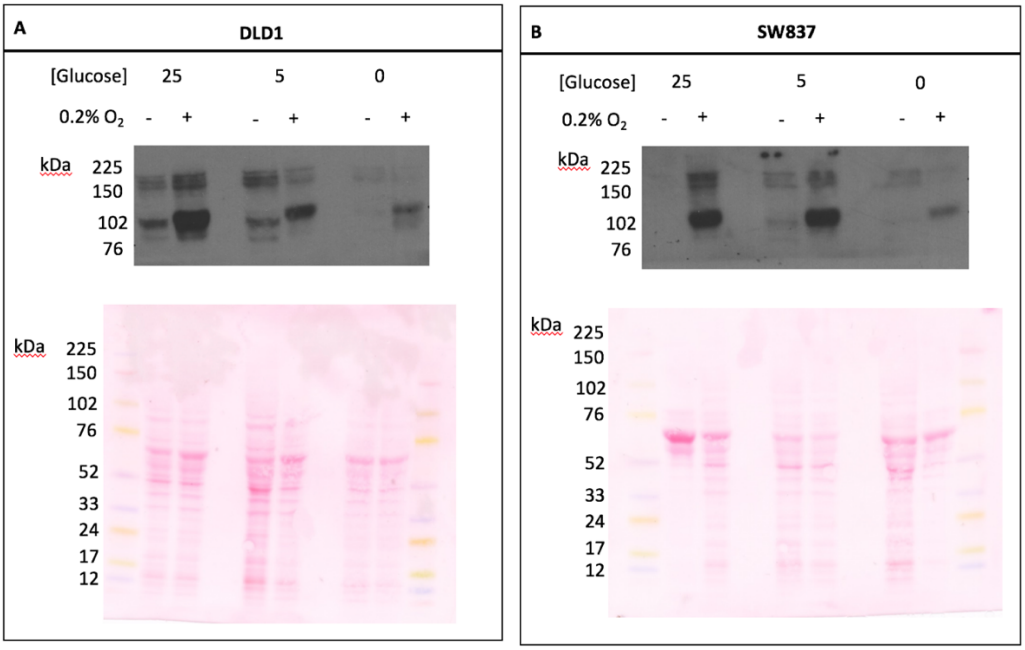

Figure 5.3. Western blot for HIF-1α. Cells were held in 20.9% or 0.2% O_2 for 48 hours, then harvested on ice. Protein was quantified and equal volumes of protein were loaded per sample onto an SDS-PAGE gel. Membranes were blotted for HIF-1α. (**A**) DLD1 cells and (**B**) SW837 cells.

5.6 Viability of DLD1 and SW837 cells cultured with 25mM, 5MM or 0mM glucose

A viability assay was performed to determine if the [glucose] in the media affected cell survival after the CRC cells were maintained in 20.9% or 0.2% O_2 for 48 hours. The viability of the cell lines was tested using trypan blue exclusion assay. The percentage of viable cells was calculated by taking away the dead cell count from the total cell count and expressing that number as a percentage of total cells (Table 5.3).

There was a significant effect of [glucose] on the viability of DLD1 cells ($p<0.0001$) (Figure 5.4.A) (Table A.5.5,6). The viability of DLD1 cells in 20.9% O_2 did not change with [glucose]. However, when DLD1 cells were maintained in 0.2% O_2, compared to DLD1 cells cultured in 25mM glucose, the viability significantly decreased as [glucose] in media decreased. There was also a significant effect of oxygen on the viability of DLD1 cells ($p<0.0001$) and a significant decrease in viability when DLD1 cells were cultured in 5mM glucose and maintained in 0.2% O_2 compared to those in 20.9% O_2 ($p<0.0001$). Similarly, there was a significant decrease in viability when DLD1 cells cultured in 0mM glucose were held at 0.2% O_2 compared to 20.9% O_2 ($p<0.0001$). There was no significant difference in viability when DLD1 cells cultured in 25mM glucose at 0.2% O_2 compared to 20.9% O_2. There was a significant interaction between [glucose] and oxygen on the viability of DLD1 cells ($p<0.0001$).

[Glucose] had a significant effect on the viability of SW837 cells ($p=0.0009$) (Figure 5.4.B) (Table A.5.5,6). The viability of SW837 cells in 20.9% O_2 did not change with [glucose]. However, when SW837 cells were maintained in 0.2% O_2, compared to SW837 cells cultured in 25mM glucose (99.74±0.14%), the viability significantly decreased as [glucose] in media decreased. There was also a significant effect of oxygen on the viability of SW837 cells ($p<0.0001$) and a significant decrease in viability when SW837 cells were cultured in 5mM glucose and held at 0.2% O_2 compared to 20.9% O_2 ($p<0.05$). Similarly, there was a significant decrease in viability when SW837 cells were cultured in 0mM glucose and maintained at 0.2% O_2 compared to 20.9% O_2 ($p<0.0001$). There was no significant difference in viability when SW837 cells cultured in 25mM glucose were held in 0.2% O_2 compared to 20.9% O_2. There was a significant interaction between glucose and oxygen on the viability of SW837 cells ($p=0.0011$).

Overall, these data highlight an interaction with oxygen tension, glucose availability and cell viability independent of the differences in fumarate concentration between DLD1 cells and SW837. Perhaps not surprisingly, the less glucose available in combination with lower oxygen, the lower the viability of both DLD1 and SW837 CRC cells.

The viability of WT and KO Fh1 MEFs was not affected by reducing O_2 to 0.2% compared to 20.9% O_2 (Figure 5.4) (Table 5.3, A.5.5,6). This highlights that Fh1 presence is not necessary for cell viability at 0.2% O_2 when 25mM glucose is present in media, suggesting elevated fumarate could be protective in hypoxia.

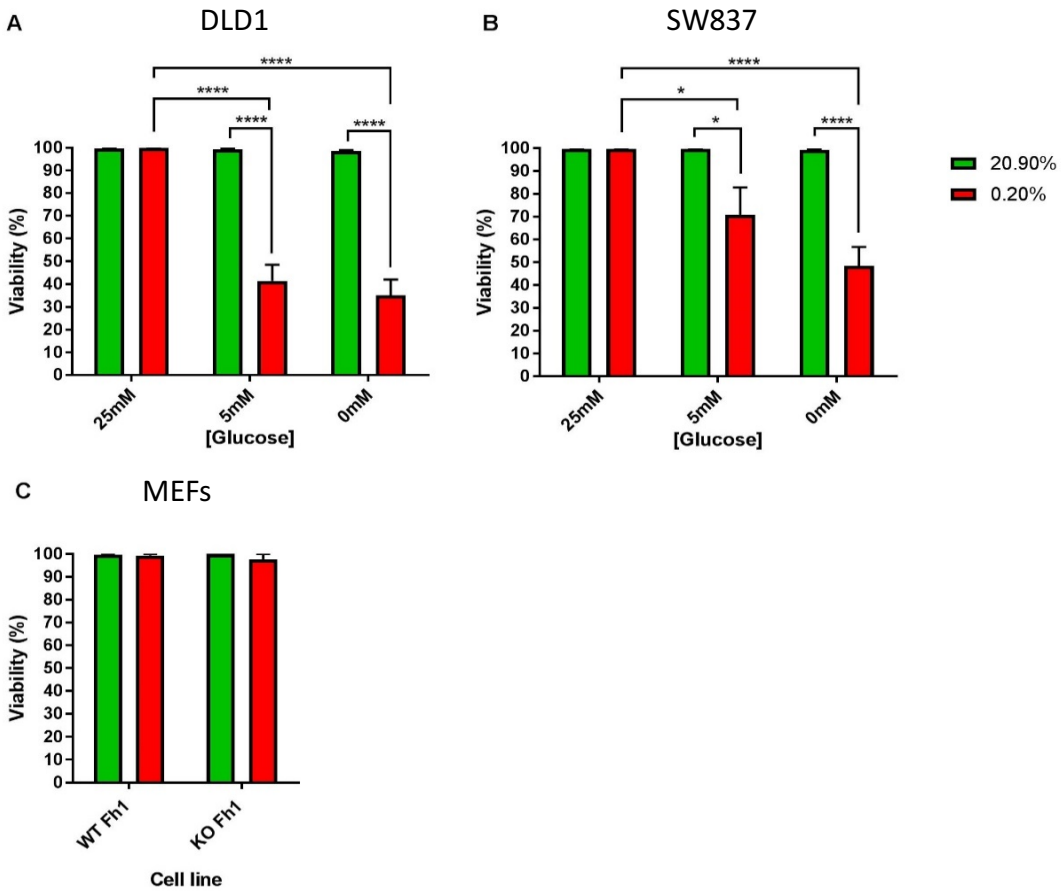

Figure 5.4. Viability of DLD1, SW837 and MEFs cells. Viability was determined by trypan blue assay for (**A**) DLD1 cells, (**B**) SW837 cells cultured in 25mM, 5mM or 0mM glucose for 48 hours with 20.9% or 0.2% oxygen. (**C**) MEFS cultured in 25mM glucose. Mean ± SEM in Table 5.3. * p<0.1, ** p<0.01, *** p<0.001 (Table A.5.5,6).

Table 5.3. Summary of viability. Viability is given as a percentage of live cells. Data shown as mean ± SEM. N=3. See also Figure 5.4.

Cell line and treatment	**Viability (%)**
DLD1 25mM glucose; 20.9% O_2	99.70±0.17
DLD1 25mM glucose; 0.2% O_2	99.97±0.03
DLD1 5mM glucose; 20.9% O_2	99.27±0.52
DLD1 5mM glucose; 0.2% O_2	41.46±7.08
DLD1 0mM glucose; 20.9% O_2	98.56±0.48
DLD1 0mM glucose; 0.2% O_2	35.16±6.77
SW837 25mM glucose; 20.9% O_2	99.77±0.12
SW837 25mM glucose; 0.2% O_2	99.74±0.14
SW837 5mM glucose; 20.9% O_2	99.76±0.15
SW837 5mM glucose; 0.2% O_2	70.91±12.00
SW837 0mM glucose; 20.9% O_2	99.31±0.36
SW837 0mM glucose; 0.2% O_2	48.46±11.07
WT Fh1 MEFs; 20.9% O_2	99.74±0.25
WT Fh1 MEFs; 0.2% O_2	99.36±0.64
KO Fh1 MEFs; 20.9% O_2	100±0.00
KO Fh1 MEFs; 0.2% O_2	97.67±2.33

5.7 Fumarate concentration in CRC cells was glucose and oxygen responsive

Preliminary [fumarate] data identified by mass spectrometry (Figure 5.1) was only completed on CRC cells grown in 25mM glucose. It was necessary to identify the effect on [fumarate] of growing CRC cells cultured in 25mM, 5mM and 0mM glucose at 20.9% or 0.2% O_2 for 48 hours. To keep costs low for this work, [fumarate] of the CRC cell lines measured using a fluorometric kit (Chapter 2, Section 2.3.5) where the final readout would not be influenced by altered metabolism. Cells were harvested and assayed three times with DLD1 and SW837 cells, but only once with HT55 cells by Anthony Xi Tan under my supervision due to reagent and time availability. The assay gave a readout of fumarate in ng/μL; the same number of viable cells and final volume were used for each sample (n=3) (Figure 5.5) (Table 5.4).

There was a significant effect of [glucose] on [fumarate] in DLD1 cells (p=0.0019, two-way ANOVA; Figure 5.5.A) (Table A.5.7,8). [Fumarate] in DLD1 cells maintained at 20.9% O_2 increased when cells were cultured with 5mM glucose compared to cells cultured with 25mM and 0mM glucose. When DLD1 cells were held in 0.2% O_2, compared to DLD1 cells cultured in 25mM glucose, [fumarate] significantly decreased as [glucose] in media decreased. There was also a significant effect of oxygen on [fumarate] in DLD1 cells (p=0.0148; Figure 5.5.A). A significant increase in [fumarate] between DLD1 cells cultured in 25mM glucose and those maintained at 0.2% O_2 compared to 20.9% O_2 was identified (p<0.0001). However, there was no difference in [fumarate] between DLD1 cells cultured in 5mM or 0mM glucose at 20.9% O_2 compared to 0.2% O2. A significant interaction between glucose and oxygen concentration on [fumarate] in DLD1 cells was identified (p=0.0006).

A possible trend can only be described for HT55 due to n being only 1. [Fumarate] in HT55 cells at 20.9% O_2 increased when cells were cultured with 5mM glucose compared to cells cultured with 25mM and 0mM glucose (Figure 5.5.B). When HT55 cells were maintained at 0.2% O_2, compared to HT55 cells cultured in 25mM glucose, the concentration of fumarate decreased as glucose concentration in media decreased. There was an increased [fumarate] between HT55 cells cultured in 25mM glucose at 0.2% O_2 compared to 20.9%

O_2. However, there was no difference in [fumarate] between HT55 cells cultured in 5mM or 0mM glucose at 20.9% O_2 compared to 0.2% O2.

[Glucose] had a significant effect on [fumarate] in SW837 cells ($p<0.0001$, two-way ANOVA; Figure 5.5.C) (Table A.5.7,8). SW837 cells at 20.9% O_2 and 25mM glucose media had a significantly higher [fumarate] compared to SW837 cells with 20.9% O_2 and 5mM glucose ($p<0.05$), and a higher [fumarate] compared to SW837 cells maintained at 20.9% O_2 and 0mM glucose. SW837 cells at 0.2% O_2, compared to SW837 cells cultured in 25mM glucose, showed a significant decrease in [fumarate] as [glucose] in media decreased ($p<0.0001$ with two-way ANOVA). There was, therefore, a significant effect of oxygen on [fumarate] in SW837 cells ($p=0.0010$) (Figure 5.5.C). At 0mM glucose, there was also a significant increase in [fumarate] between SW837 cells cultured at 0.2% O_2 compared to 20.9% O_2 ($p<0.05$). However, there was no difference in [fumarate] between SW837 cells cultured in 25mM or 5mM glucose at 20.9% O_2 compared to 0.2% O_2. A significant interaction between [glucose] and oxygen concentration on [fumarate] in SW837 cells was not found ($p=0.1106$).

These data showed that DLD1 and HT55 had a similar pattern of [fumarate] in response to culture in 25mM, 5mM or 0mM glucose at 20.9% or 0.2% O_2 for 48 hours. SW837 cells showed a slightly different pattern to DLD1 and HT55 cells. The main difference is the higher concentration of fumarate found in SW837 cells when they were cultured with 25mM glucose and treated with 20.9% O_2 compared to DLD1 and HT55 cells under the same conditions.

The fact that fumarate can be detected in DLD1, HT55 and SW837 cells cultured in 0mM glucose suggests that alternative substrates, such as glutamine, feed into the TCA cycle.

There was a significant effect of Fh1 presence in MEFs on [fumarate] ($p=0.0034$) (Figure 5.5.D) (Table A.5.7,8). When MEFs were cultured at 20.9% O_2 and with 25mM glucose in the media KO Fh1 MEFs had a significantly higher [fumarate] compared to WT Fh1 MEFs treated with 0.2% O_2 and 25mM glucose ($p<0.001$). When MEFs placed in 0.2% O_2 and 25mM glucose media there was no difference between WT Fh1 MEFs and KO Fh1 MEFs. There was not a significant effect of O_2 on [fumarate] in MEFs ($p=0.0613$) (Figure 5.5.D).

However, when the interaction of [glucose] and oxygen concentration was considered there was a significant effect on [fumarate] ($p=0.0002$, two-way ANOVA, Table A.5.7,8).

It is difficult to compare between techniques due to the different methods, the different amount of input and the different units used to measure [fumarate]. Mass spectrometry is a much more sensitive method compared to the fluorometric assay. Using mass spectrometry, the ratio of fumarate between DLD1, HT55 and SW837 cells treated with 0.2% O_2 compared to 20.9% O_2 is 4.58, 6.75 and 0.43 respectively. Whereas, when using the fluorometric assay, the ratio of fumarate between DLD1, HT55 and SW837 cells treated with 0.2% O_2 compared to 20.9% O_2 is 3.3, 2.56 and 1.23 respectively. These results could suggest an influence of passage number on CRC cell concentration of fumarate. The cells used for mass spectrometry were earlier in passage than those used for the fluorometric assay.

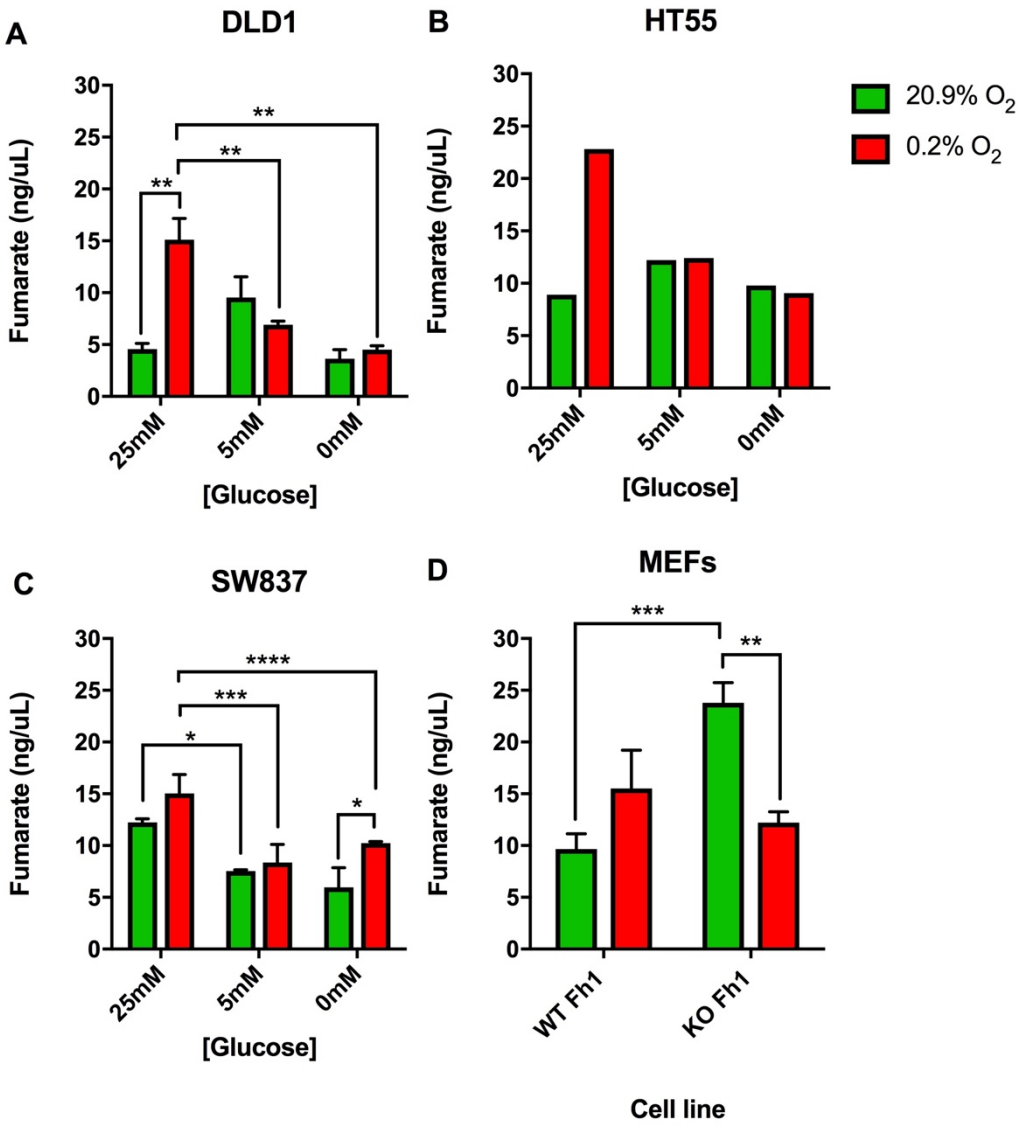

Figure 5.5. Fumarate concentration in determined by fluorometric assay. (**A**) DLD1, (**B**) HT55, (**C**) SW837 and (**D**) MEFs after 48 hours 20.9% or 0.2% oxygen. Concentration is given as ng/µL and a summary of mean ± SEM shown in Table 5.4. * p<0.05, ** p<0.01, *** p<0.001, **** p<0.0001. Statistics in Table A.5.7,8.

Table 5.4. Summary table of fumarate concentration from fluorometric assay after 48 hours treatment with 20.9% or 0.2% O_2. Concentration is given as ng/µL and data shown as mean ± SEM. N=3. See also Figure 5.5.

Cell line and 48-hour treatment	Fumarate concentration (ng/µL)
DLD1 25mM glucose; 20.9% O_2	4.57±0.54
DLD1 25mM glucose; 0.2% O_2	15.11±2.07
DLD1 5mM glucose; 20.9% O_2	9.53±2.00
DLD1 5mM glucose; 0.2% O_2	6.92±0.33
DLD1 0mM glucose; 20.9% O_2	3.65±0.86
DLD1 0mM glucose; 0.2% O_2	4.51±0.38
HT55 25mM glucose; 20.9% O_2	8.91±0.00
HT55 25mM glucose; 0.2% O_2	22.81±0.00
HT55 5mM glucose; 20.9% O_2	12.21±0.00
HT55 5mM glucose; 0.2% O_2	12.42±0.00
HT55 0mM glucose; 20.9% O_2	9.79±0.00
HT55 0mM glucose; 0.2% O_2	9.07±0.00
SW837 25mM glucose; 20.9% O_2	12.23±0.20
SW837 25mM glucose; 0.2% O_2	15.05±1.04
SW837 5mM glucose; 20.9% O_2	7.53±0.08
SW837 5mM glucose; 0.2% O_2	8.36±1.02
SW837 0mM glucose; 20.9% O_2	5.96±1.10
SW837 0mM glucose; 0.2% O_2	10.25±0.09
WT Fh1 MEFs; 20.9% O_2	9.66±0.85
WT Fh1 MEFs; 0.2% O_2	15.50±2.15
KO Fh1 MEFs; 20.9% O_2	23.80±1.12
KO Fh1 MEFs; 0.2% O_2	12.21±0.60

5.8 Succination is present in CRC cell lines

Succination is one action of fumarate (Chapter 1, Figure 1.11). As it was found that it was possible to detect fumarate in all cell lines, the next step was to ascertain if succination was present in the cell lines. This was done by Western blot. Norma Frizzell (University of South Carolina) create an antibody, which was made available to me, that detects succination (2-SC motifs). An equal amount of protein was loaded per cell line according to a protein quantification assay.

However, this does not provide an adequate means of quantifying the levels of succination. This method does not allow determination of which proteins undergo succination in each sample and to what extent, therefore, the blots were primarily used to assess if any succination was present *in vitro.*

KO Fh1 MEFs were a positive control as they have no Fh1 (murine FH), therefore, fumarate is not controlled and succination is elevated[330] (Figure 5.6.D).

All the cell lines have succination present (Figure 5.6). It appears that generally there is more succination in samples from cells held in 20.9% O_2 compared to their equivalent held in 0.2% O_2. However, it is not possible to say this for sure as it is difficult to quantify the blot. This result would be opposite to predicted based on fumarate being generally elevated at 0.2% O_2 compared to equivalent samples held at 20.9% O_2.

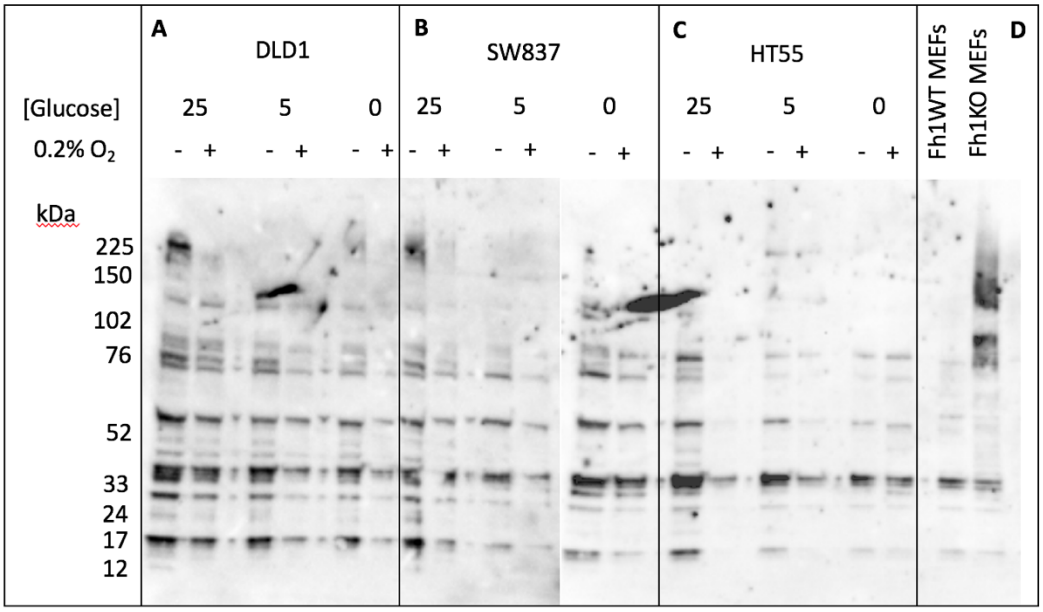

Figure 5.6. Western blot for succination. CRC cells were held in 20.9% or 0.2% O_2 for 48 hours. An equal amount of protein was loaded per sample according to a protein quantification assay. The resultant blot was probed for 2-SC. (**A**) DLD1, (**B**) SW837, (**C**) HT55 and (**D**) MEFs as controls.

5.9 Fumarate hydratase activity

After detecting differences in [fumarate] between CRC cells held in 20.9% O_2 compared to 0.2% O_2 it was necessary to determine if the activity of FH was responsible. It was considered that when [fumarate] is elevated, the activity of FH is compromised. Also, in Chapter 3 I identified that FH was present at an unexpected high level in CRC samples, even though fumarate was also high. This generated questions, such as, is FH functional in CRC?

I was able to detect FH activity in CRC cells using an assay created by Jakob Knudsen (OCDEM, University of Oxford) where the output measurement was the fluorescence of NADH generated by FH (Table 5.5). DLD1 and SW837 cell lines were cultured in 25mM, 5mM and 0mM glucose and MEFs were cultured in 25mM glucose at 20.9% or 0.2% O_2 for 48 hours, the cells were then harvested and assayed (Chapter 2, Section 2.3.6). The experiment was done three times for each condition.

There was a significant effect of [glucose] on the activity of FH in DLD1 cells (p=0.0007, two-way ANOVA; Figure 5.7.A) (Table A.5.9,10). When DLD1 cells were maintained at 20.9% O_2, compared to DLD1 cells cultured in 25mM glucose, the activity of FH decreased when [glucose] in media was 5mM and was significantly decreased when DLD1 cells were cultured without glucose. When DLD1 cells were maintained at 0.2% O_2 the activity of FH remained stable whatever [glucose] of the media. There was a significant effect of oxygen on the activity of FH in DLD1 cells (<0.0001) (Figure 5.7.A). There was a significant decrease in FH activity between DLD1 cells cultured in 25mM glucose at 20.9% O_2 compared to 0.2% O_2 ($p<0.001$) and between DLD1 cells cultured in 5mM glucose and treated with 20.9% O_2 compared to 0.2% O_2 ($p<0.01$). However, there was no difference in [fumarate] between DLD1 cells cultured in 0mM glucose treated with 20.9% O_2 compared to 0.2% O2. A significant interaction between [glucose] and oxygen tension on the activity of fumarate hydratase in DLD1 cells (p=0.0131).

There was a significant effect of [glucose] on FH activity in SW837 cells (p=0.0185) (Figure 5.7.B) (Table A.5.9,10). When SW837 cells were treated with 20.9% O_2, there was no significant difference between the different [glucose]. A slight drop in activity was seen with SW837 cells cultured in 0mM glucose. Similarly, when SW837 cells at 0.2% O_2, there

was no significant difference between the different glucose concentrations, although there was a small drop in activity in SW837 cells cultured in 0mM glucose. A significant effect of oxygen on SW837 FH activity in SW837 cells was identified (p=0.0297) (Figure 5.7.B). However, on *post-hoc* analyse for multiple correction there was no significant differences between cells cultured in 25mM, 5mM or 0mM at 20.9% O_2 and 0.2% O_2. A significant interaction between [glucose] and oxygen tension on FH activity in SW837 cells was not found (p=0.8121).

As expected, there was a significant effect of Fh1 presence in MEFs on the activity of FH (p=0.0044) (Figure 5.7.C) (Table A.5.9,10). When MEFs were maintained at 20.9% O_2 and 25mM glucose media WT Fh1 MEFs had a significantly higher FH activity compared to KO Fh1 MEFs at 0.2% O_2 and 25mM glucose (p<0.0001). When MEFs were held at 0.2% O_2 in 25mM glucose media there was no difference between the enzyme activity of WT Fh1 MEFs and KO Fh1 MEFs. There was not a significant effect of O_2 (p=0.2980) or the interaction of cell line and oxygen (p=0.1983) on the activity of FH in MEFs (Figure 5.7.C).

This work identifies that FH is active in the CRC cell lines used in this study. There are, however, differences between the cell lines. DLD1 cells held in 20.9% O_2 and cultured with 25mM or 5mM glucose in their media have a much higher FH activity when compared to their SW837 counterparts. SW837 cells are not as flexible with their FH activity. Importantly, the FH activity data (Chapter 5, Section 5.11) corresponds well with [fumarate] data (Chapter 5, Section 5.10). When [fumarate] is high, fumarate hydratase activity is lower.

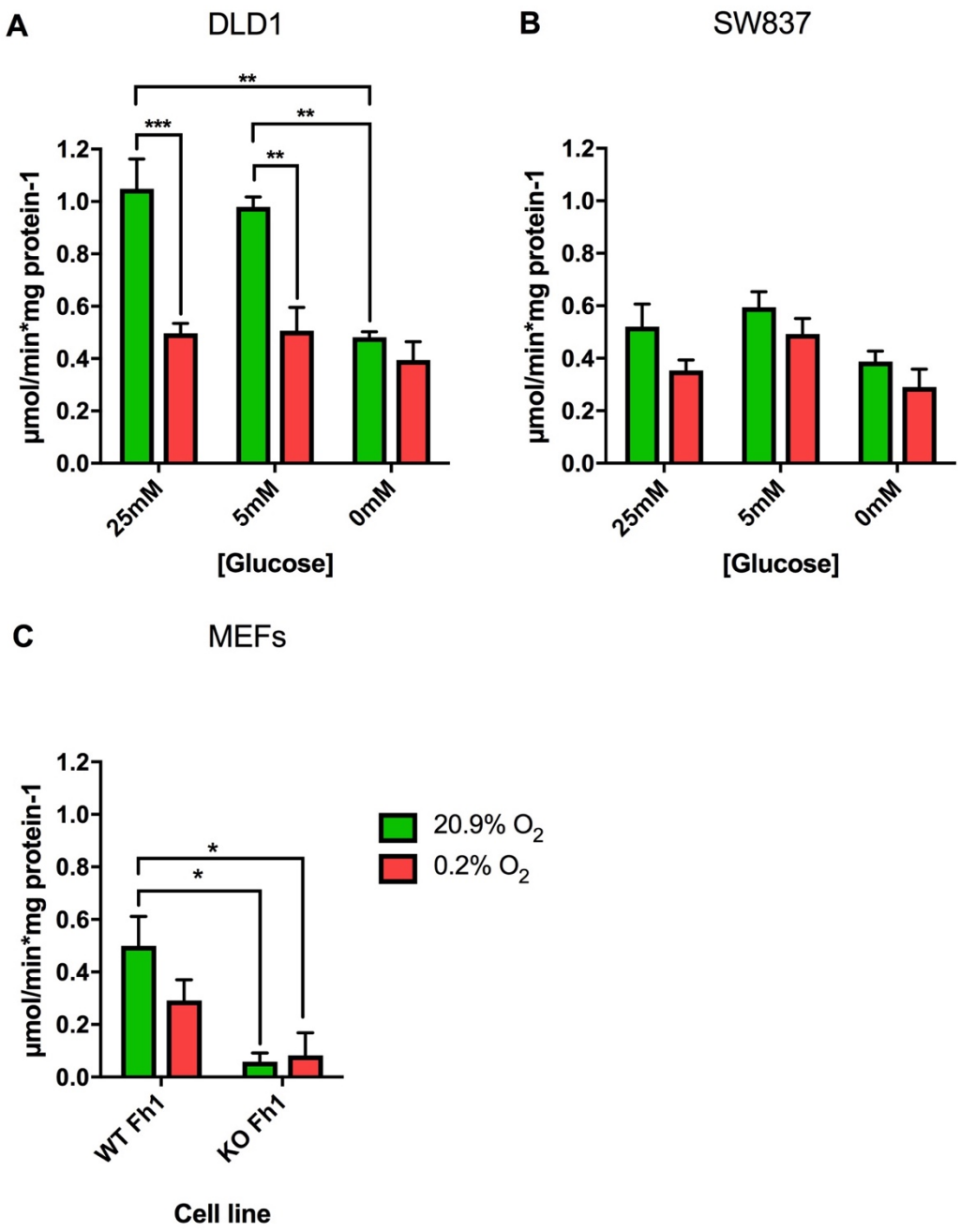

Figure 5.7. Fumarate hydratase activity. Determined by fluorometric assay in (**A**) DLD1 (**B**) SW837 cells and (**C**) MEFs after 48 hours 20.9% or 0.2% oxygen. Activity is given as µmol/min*mg protein-1. See Table 5.5 for a summary of mean ± SEM. * p<0.1, ** p<0.01, *** p<0.001 (Table A.5.9,10).

Table 5.5. Summary table of fumarate hydratase activity from fluorometric assay after 48 hours treatment with 20.9% or 0.2% O_2. Activity is given as µmol/min*mg protein-1 and data shown as mean ± SEM. N=3. See also Figure 5.7.

Cell line and 48-hour treatment	**Fumarate hydratase activity µmol/min*mg protein-1**
DLD1 25mM glucose; 20.9% O_2	1.05±0.11
DLD1 25mM glucose; 0.2% O_2	0.50±0.04
DLD1 5mM glucose; 20.9% O_2	0.98±0.04
DLD1 5mM glucose; 0.2% O_2	0.51±0.09
DLD1 0mM glucose; 20.9% O_2	0.48±0.02
DLD1 0mM glucose; 0.2% O_2	0.39±0.07
SW837 25mM glucose; 20.9% O_2	0.52±0.09
SW837 25mM glucose; 0.2% O_2	0.35±0.04
SW837 5mM glucose; 20.9% O_2	0.59±0.06
SW837 5mM glucose; 0.2% O_2	0.49±0.06
SW837 0mM glucose; 20.9% O_2	0.39±0.04
SW837 0mM glucose; 0.2% O_2	0.29±0.07
WT Fh1 MEFs 20.9% O_2	0.50±0.11
WT Fh1 MEFs 0.2% O_2	0.29±0.08
KO Fh1 MEFs 20.9% O_2	0.06±0.03
KO Fh1 MEFs 0.2% O_2	0.08±0.08

5.10 Fumarate hydratase foci and area in cells cultured in 0mM glucose is cell line and oxygen dependent

To further quantify the effect of different [glucose] in cell culture media on FH, it was necessary to quantify the amount of FH. Cells were held in 20.9% or 0.2% O_2 for 48 hours, then fixed and stained with DAPI, plasma membrane stain and an antibody validated against FH. The staining was imaged using an InCell 2200 microscope. The resultant images were analysed by InCell Developer V1.9. For further information on the method please refer to Chapter 2, Section 2.3.7). This allowed the quantification of FH as foci per cell as well as the area covered by all the FH foci for each cell (Figure 5.8) (Table 5.6).

For the purpose of this work one focus is defined as a discrete area of staining. It cannot be assumed that each focus is equal to one FH protein. Therefore, area covered by foci is likely to be a more accurate measurement of FH quantity. Nevertheless, area and foci correlate well.

[Glucose] has a significant effect on the number of FH foci per cell in DLD1 cells ($p<0.0001$) (Figure 5.9.A) (Table A.5.11,12). When DLD1 cells maintained at 20.9% O_2, the number of FH foci per cell in DLD1 cells cultured in 0mM glucose was significantly increased compared to DLD1 cells cultured in 25mM glucose ($p<0.0001$) as well as DLD1 cells cultured in 5mM glucose ($p<0.0001$). When DLD1 cells were at 0.2% O_2, the number of FH foci per cell in DLD1 cells cultured in 0mM glucose was significantly increased compared to DLD1 cells cultured in 25mM glucose ($p<0.0001$) and compared to DLD1 cells cultured in 5mM glucose ($p<0.01$). Oxygen had a significant effect on the number of FH foci per cell in DLD1 cells ($p=0.0124$) (Figure 5.9.A). There was a significant increase in the number of FH foci per cell between DLD1 cells cultured in 0mM glucose and at 0.2% O_2 compared to 20.9% O_2 ($p<0.05$). However, there was no difference in the number of FH foci per cell between DLD1 cells cultured in 25mM or 5mM glucose held at 20.9% O_2 compared to 0.2% O2. A significant interaction between [glucose] and oxygen tension on the number of FH foci per cell in DLD1 cells was not found, although this approach significance ($p=0.0746$).

[Glucose] concentration had a significant effect on the area of FH per cell in DLD1 cells ($p<0.0001$) (Figure 5.9.B) (Table A.5.11,12). When DLD1 cells were maintained at 20.9%

O_2, the area of FH per cell in DLD1 cells cultured in 0mM glucose was significantly increased compared to DLD1 cells cultured in 25mM glucose ($p<0.0001$) as well as DLD1 cells cultured in 5mM glucose ($p<0.0001$). When DLD1 cells were held at 0.2% O_2, the area of FH per cell cultured in 0mM glucose was significantly increased compared to DLD1 cells cultured in 25mM glucose ($p<0.0001$) as well as DLD1 cells cultured in 5mM glucose ($p=0.001$). In addition, there was no significant effect of oxygen tension on the area of FH per cell in DLD1 cells ($p=0.9407$) (Figure 5.9.B). There was no difference in the area of FH per cell between DLD1 cells cultured in 25mM, 5mM or 0mM glucose and maintained at 20.9% O_2 compared to 0.2% O2. In line with these findings, a significant interaction between [glucose] and oxygen tension on the area of FH per cell in DLD1 cells was not identified ($p=0.$ 0.6619).

[Glucose] had a significant effect on the number of FH foci per cell in SW837 cells ($p<0.0001$) (Figure 5.9.C) (Table A.5.11,12). When SW837 cells were at 20.9% O_2, the number of FH foci per cell in SW837 cells cultured in 0mM glucose was significantly increased compared to SW837 cells cultured in 25mM glucose ($p<0.05$) and increased compared to SW837 cells cultured in 5mM glucose. When SW837 cells were held at 0.2% O_2, the number of FH foci per cell in SW837 cells cultured in 0mM glucose was significantly increased compared to SW837 cells cultured in 25mM glucose ($p<0.001$) and compared to SW837 cells cultured in 5mM glucose ($p<0.001$). Oxygen did not have a significant effect on the number of FH foci per cell in SW837 cells ($p=0.1296$) (Figure 5.9.C). No significant difference in the number of FH foci per cell between SW837 cells cultured in 0mM, 5mM or 25mM glucose and treated with 20.9% O_2 compared to 0.2% O_2 was found. However, a significant interaction between [glucose] and oxygen tension on the number of FH foci per cell in SW837 cells was found ($p=0.0423$).

[Glucose] had a significant effect on the area of FH per cell in SW837 cells ($p<0.0001$) (Figure 5.9.D) (Table A.5.11,12). When SW837 cells were held at 20.9% O_2, the area of FH per cell in SW837 cells cultured in 0mM glucose was not significantly different compared to SW837 cells cultured in 25mM glucose or in 5mM glucose. When SW837 cells were maintained at 0.2% O_2, the area of FH per cell in SW837 cells cultured in 0mM glucose was significantly increased compared to SW837 cells cultured in 25mM glucose ($p<0.0001$) as well as SW837 cells cultured in 5mM glucose ($p<0.0001$). Oxygen had a significant effect

on the area of FH per cell in SW837 cells (p=0.0132) (Figure 5.9.D). There was a significant increase in the area of FH per cell between SW837 cells cultured in 0mM glucose and at 0.2% O_2 compared to 20.9% O_2 (p<0.01). There was no difference in the area of FH per cell between SW837cells cultured in 25mM or 5mM glucose and held at 20.9% O_2 compared to 0.2% O_2. A significant interaction between [glucose] and oxygen tension on the area of FH per cell in SW837 cells was not identified (p=0.0019).

In summary, FH foci number and area increased when DLD1 and SW837 cells are cultured in 0mM glucose compared to 5mM and 25mM glucose. However, FH in cells cultured in 0mM glucose is cell line and oxygen dependent. When DLD1 cells are cultured in 0mM glucose their FH foci number is 1.23 fold higher in 20.9% O_2 compared to 0.2% O_2. However, when this is converted to area there is no difference between the two oxygen tensions. When SW837 cells are cultured in 0mM glucose their FH foci number is 1.51 fold higher when maintained at 0.2% O_2 compared to 20.9% O_2. When this is converted to area, cells treated with 0.2% O_2 have 1.97 fold more FH area compared to cell treated with 20.9% O_2.

This data suggests that hypoxia does not influence FH production dramatically. There are minimal non-significant differences between cells held in 20.9% and 0.2% O_2 in all [glucose]. There was a 2-fold increase in amount of area of FH protein in cells cultured with 0mM glucose, compared to cells cultured with 25mM and 5mM glucose at both 20.9% and 0.2% O_2. However, there was at least a 2-fold decrease in FH activity in cells cultured with 0mM glucose compared to cells cultured in 25mM and 5mM glucose at 20.9% O_2. The FH activity in DLD1 cells was not different at 0.2% O_2. This suggests that at 0mM glucose FH is abundant but not active. This may be due to a lack of substrate (fumarate) for FH, due to no glucose. Even when fumarate is present at high concentrations, such as in the FH activity assay, the FH in DLD1 cells cultured with 0mM is unable to work as it does in cells cultured with 25mM or 5mM glucose.

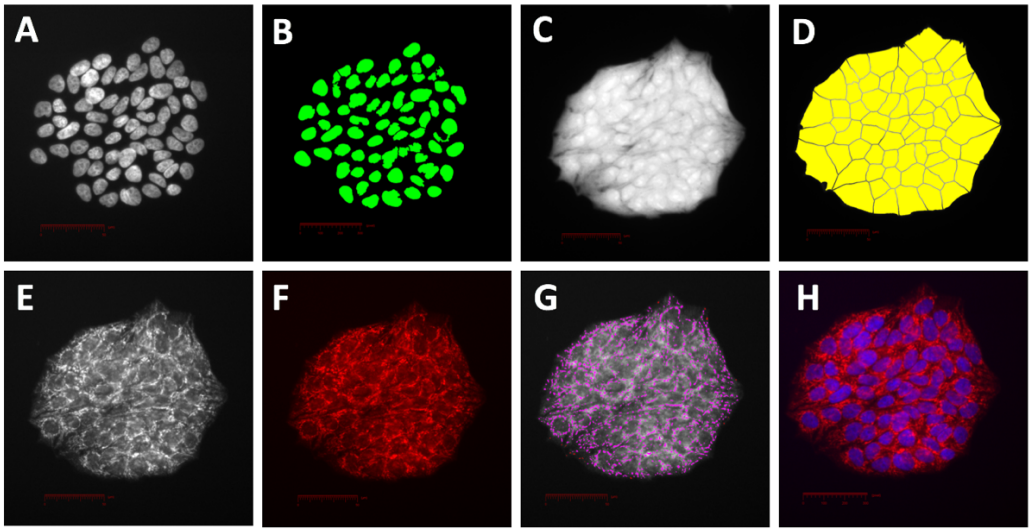

Figure 5.8. Fumarate hydratase staining analysis process. Cells were held in 20.9% or 0.2% O_2 for 48 hours, then fixed and stained with DAPI, cell mask and FH antibody. The staining was imaged using an InCell 2200 microscope. And the images were then analysed by InCell Developer V1.9. (**A**) Briefly, cells are located via DAPI nuclear stain. (**B**) The programme was set to identify single nuclei and separate multiple nuclei which are close together. (**C**) Alongside this, the programme was set to identify whole cells by using the cell mask stain. (**D**) Single cells are then defined as a nucleus (DAPI) with a cell body (cell mask). (**E, F**) FH staining was generally collected in foci. (**G**) Therefore, a FH foci analysis was completed. (**H**) The analysis programme was then able to determine how many FH foci there were per cell. From these images it was possible to determine the area covered by all the FH foci for each cell. Scale bar 50µm.

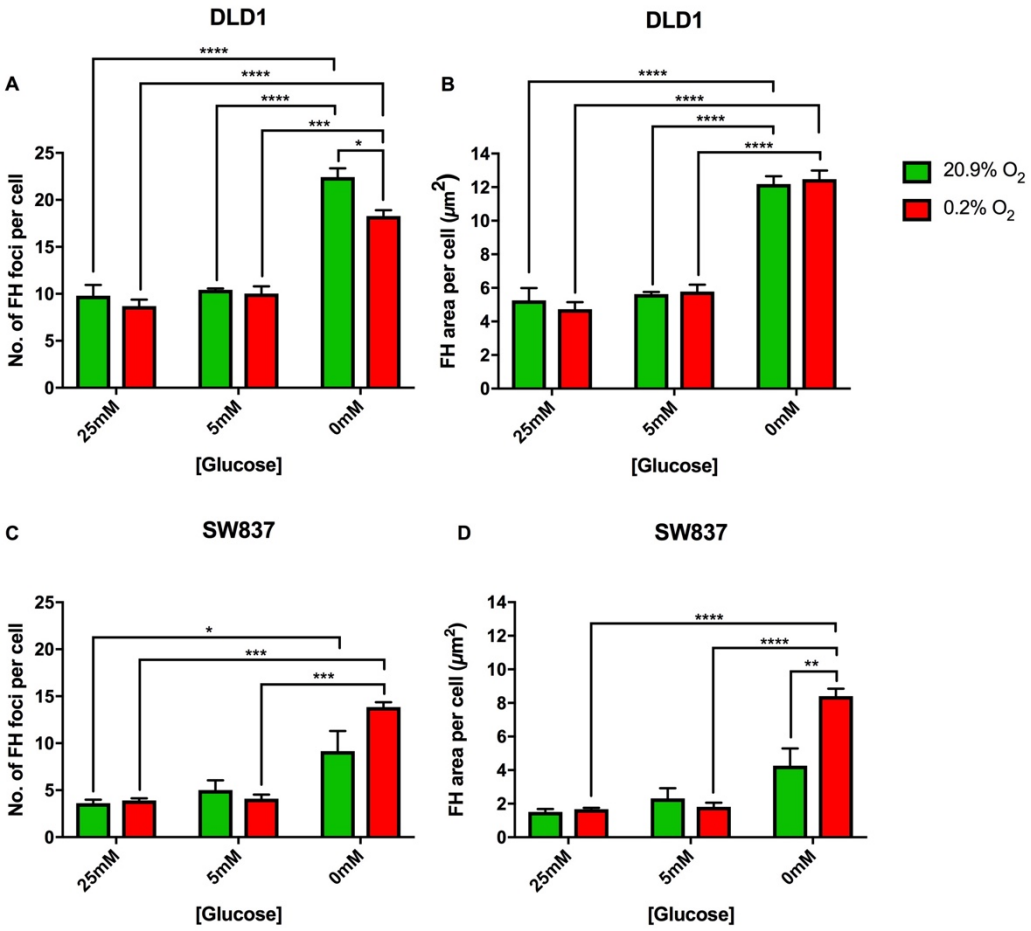

Figure 5.9. Fumarate hydratase foci and area per cell. DLD1 and SW837 cells were maintained at 20.9% or 0.2% O_2 for 48 hours. Immunofluorescence was performed to detect FH protein. Images were captured on INCA 2200 microscope and analysed using InCell Developer v1.9 software to determine the number and area of foci for FH per cell. (**A**) Number of FH foci per DLD1 cell. (**B**) Area of FH per DLD1 cell. (**C**) Number of FH foci per SW837 cell. (**D**) Area of FH per SW837 cell. Mean ± SEM in Table 5.6. * p<0.5, ** p<0.01, *** p<0.001 (Table A.5.11,12).

Table 5.6. Summary of fumarate hydratase foci and area per cell. Data shown as mean ± SEM. N=3. See also Figure 5.9.

Cell line and 48-hour treatment	**Number of FH foci per cell**	**FH area per cell (μm^2)**
DLD1 25mM glucose; 20.9% O_2	9.80±1.15	5.26±0.73
DLD1 25mM glucose; 0.2% O_2	8.71±0.68	4.73±0.42
DLD1 5mM glucose; 20.9% O_2	10.43±0.15	5.63±0.12
DLD1 5mM glucose; 0.2% O_2	10.03±0.78	5.78±0.41
DLD1 0mM glucose; 20.9% O_2	22.43±0.94	12.19±0.46
DLD1 0mM glucose; 0.2% O_2	18.28±0.63	12.48±0.51
SW837 25mM glucose; 20.9% O_2	3.61±0.38	1.51±0.18
SW837 25mM glucose; 0.2% O_2	3.91±0.22	1.67±0.09
SW837 5mM glucose; 20.9% O_2	5.02±1.03	2.31±0.61
SW837 5mM glucose; 0.2% O_2	4.10±0.43	1.81±0.25
SW837 0mM glucose; 20.9% O_2	9.16±2.14	4.26±1.03
SW837 0mM glucose; 0.2% O_2	13.85±0.50	8.41±0.44

5.11. Changing the glucose and oxygen tension significantly changes the expression of *BAX, CA9, PDk1, LDHA, HK2, HIF-2α* and *GLUT1*

To determine differences in DLD1, HT55, SW837 gene expression induced by culture in 25mM, 5mM or 0mM glucose then held in 20.9% or 0.2% O_2 for 48 hours, a panel of 19 genes was selected based on their involvement with glycolysis (Table 5.1), mitochondrial function (Table 5.2), hypoxic response (Table 5.3) and apoptosis (Table 5.4).

Unfortunately, it was difficult to identify a housekeeping gene which was stable for all three cell lines under the changes in glucose and oxygen tension used (Figure 5.10). It was decided to select different housekeeping genes for each CRC cell line: DLD1 results were normalised to a geomean of 18S and RPLPO; HT55 to actin; SW837 to B2M. Data was analysed by the ½^ct method[373].

Normalised RT-PCR data of the 19 genes across the three cell lines was subjected to multivariate analysis to uncover the relationship between the expression of each gene and the [glucose] and oxygen tension conditions that the cells were held in. A linear regression model was used to determine a p-value for each gene in relation to [glucose], oxygen tension and interaction of [glucose] and oxygen tension. The 19 genes were ranked according to the p-value for [glucose]. Next the normalised RT-PCR data was expressed as fold change from cells cultured in 25mM glucose at 20.9% O_2. This data is shown in Figure 5.11 as a heat map.

The p-values for oxygen tension and interaction of [glucose] and oxygen tension are shown in Table A.5.19. The normalised RT-PCR data is shown in Table A.5.20-28. The normalised RT-PCR data expressed as fold change from cells cultured in 25mM glucose at 20.9% O_2 for each gene is shown in Figures A.5.1-6, with mean ± SEM and statistical data in Table A.5.30-37.

Table 5.7. Details of genes involved in glycolysis for expression analysis in DLD1, HT55 and SW837 cell lines.

Gene	Expanded gene name	Brief description of role
GLUT1	Glucose transporter 1	Transports glucose into all cells[425].
GLUT4	Glucose transporter 4	Insulin-responsive glucose transporter[426].
GAPDH	Glyceraldehyde 3-phosphate dehydrogenase	Enzyme that catalyses the sixth step of glycolysis. Emerging evidence suggests GAPDH is deregulated in cancer cells[427]. In diabetes it is known that GAPDH activity is reduced and this has been linked to high levels of fumarate[338].
LDHA	Lactate dehydrogenase	Catalyses the conversion of pyruvate to lactate. Transcriptionally regulated by HIF-1α. Elevated in many cancers and linked to tumour growth and invasion[428].
HK2	Hexokinase 2	Catalyses the first step of glucose metabolism (glucose to glucose 6-phosphate). Upregulated in many tumours. Potentially facilitates autophagy in response to glucose deprivation[429].
PDK1	Pyruvate dehydrogenase kinase 1	Multi-enzyme complex in the mitochondria that catalyses the oxidative decarboxylation of pyruvate. Can contribute to cancer by facilitating invasion[430].

Table 5.8. Details of genes involved in mitochondrial function for expression analysis in DLD1, HT55 and SW837 cell lines.

Gene	Expanded gene name	Brief description of role
BAX	BCL2 associated X	Cell death regulator whose activation induces mitochondrial membrane permeabilisation leading to the release of apoptotic factor cytochrome c and consequently cell death[431].
FH	Fumarate hydratase	Enzyme that catalyses the conversion of fumarate to malate. There are two forms, mitochondrial and cytosolic[209] (both detected by the probe used in this study).
LONP1	Mitochondrial protease	Mitochondrial matrix protein which mediates the selective degradation of misfolded, unassembled or oxidatively damaged polypeptides[432].
SOD2	Mitochondrial manganese superoxide dismutase	Mitochondria antioxidant enzyme. Many human cancers have reduced SOD2 activity[433].
COX4I2	Cytochrome c oxidase subunit 4 isoform 2	The terminal enzyme of the mitochondrial respiratory chain. Subunit 4 is the largest nuclear encoded subunit which plays a pivotal role in COX regulation[165434].

Table 5.9. Details of genes involved in hypoxia for expression analysis in DLD1, HT55 and SW837 cell lines.

Gene	Expanded gene name	Brief description of role
HIF-1α	Hypoxia inducible factor 1 alpha	A transcription factor that has a major role in tumour response to hypoxia[407]. Leads to upregulation of glycolysis and survival genes (Chapter 1, Section 1.8). HIF-1 is stabilised by hypoxia and fumarate[435].
HIF-1ß	Hypoxia inducible factor 1 ß	Also known as aryl hydrocarbon receptor nuclear translocator (ARNT). Forms a transcription factor when bound to HIF-1α[436].
HIF-2α	Hypoxia inducible factor 2 alpha	Also known as endothelial PAS domain protein 1 (EPAS1). A transcription factor involved in the induction of genes when oxygen concentration falls[437].
VHL	Von Hippel-Lindau	Key role in oxygen sensing within the cell. Targets hypoxia-inducible factors for ubiquitination and proteasomal degradation[438].
CA9	Carbonic anhydrase 9	Catalyses carbon dioxide hydration to bicarbonate and proton[439]. Role in pH maintenance of the cell.
VEGF	Vascular endothelial growth factor	Key regulator of blood vessel development and network patterning. Upregulated in hypoxia[440].

Table 5.10. Details of genes involved in apoptosis for expression analysis in DLD1, HT55 and SW837 cell lines.

Gene	Expanded gene name	Brief description of role
BAX	BCL2 associated X	Cell death regulator whose activation induces mitochondrial membrane permeabilisation leading to the release of apoptotic factor cytochrome c and consequently cell death[431].
CASP9	Caspase-9	Initiates the mitochondrial apoptotic pathway[441].
GPX1	Glutathione peroxidase	Protects cells from oxidative stress. This isoform exists in the cytoplasm[442].

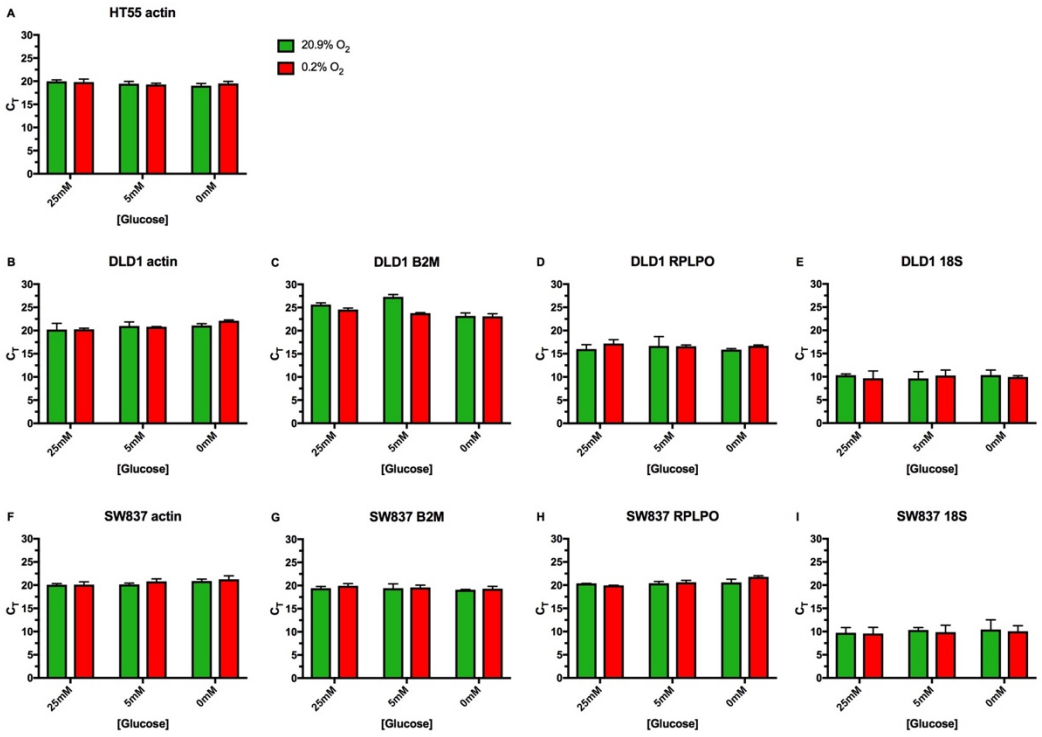

Figure 5.10. House-keeping gene choice for qPCR panel. DLD1, HT55, SW837 cells were cultured in 25mM, 5mM or 0mM glucose then held in 20.9% or 0.2% O_2 for 48 hours. RNA was extracted and analysed via qPCR. DLD1 results were normalised to a geomean of 18S and RPLPO; HT55 to actin; SW837 to B2M.

When all cell lines are considered in analysis [glucose] at which the cells were cultured significantly altered the expression of *BAX* (p=0.01370), *CA9* (p=0.01723), *PDK1* (p=0.01900) and *LDHA* (p=0.02906). The oxygen tension significantly altered the expression of *CA9* (p=0.00958), *PDK1* (p=0.00864), *LDHA* (p=0.00836), *HK2* (p=0.00221), *HIF-2α* (p=0.03318) and *GLUT1* (p=0.00125). When oxygen tension and [glucose] are both taken into account in analysis, only *CA9* gene expression is significantly changed (p=0.0172).

BAX is involved in the process of apoptosis as well as mitochondrial function. This analysis proves there is a relationship between [glucose], apoptosis and mitochondrial function. *BAX* mRNA expression is reduced when oxygen tension is lowered to 0.2% O_2 and when [glucose] is lowered. This suggests that apoptosis is triggered less *via* mitochondria in these conditions to allow generation of ATP when [glucose] is lower or when oxygen tension is reduced. However, it would be necessary to study the mitochondrial membrane potential and the structure of the mitochondria to determine if the mitochondria are fully functional (Chapter 8, Section 8.3).

Interestingly, BAX protein has been shown to be prognostic in human CRC, with higher amounts linked to more severe disease[443]. It is necessary to study the level of BAX protein in the CRC cell line studied in this thesis to determine if BAX protein levels are altered by [glucose] and O_2 tension.

CA9 and *HIF-2α* are involved in the cells response to hypoxia suggesting there is a relationship between hypoxia and [glucose], as already widely reported in literature[444,445]. *PDK1, LDHA, HK2* and *GLUT-1* are all involved in glycolysis (Chapter 1, Figure 1.7), suggesting that glycolysis is affected by both [glucose] and oxygen tension, as already corroborated by the literature[446].

One surprising result was the very low quantities of *COX4I2* in most samples. *COX4I2* is the terminal enzyme of the mitochondrial respiratory chain. *COX4I2* has been shown to have a HRE, and, therefore, be upregulated in hypoxia[165]. However, this was not seen in my results. Further analysis of this mRNA and protein is necessary.

To validate these results, it would be necessary to do a western blot for all the protein products of the genes analysed by qPCR as mRNA and protein results can be different. Unfortunately, there was not enough time to do this as part of this study.

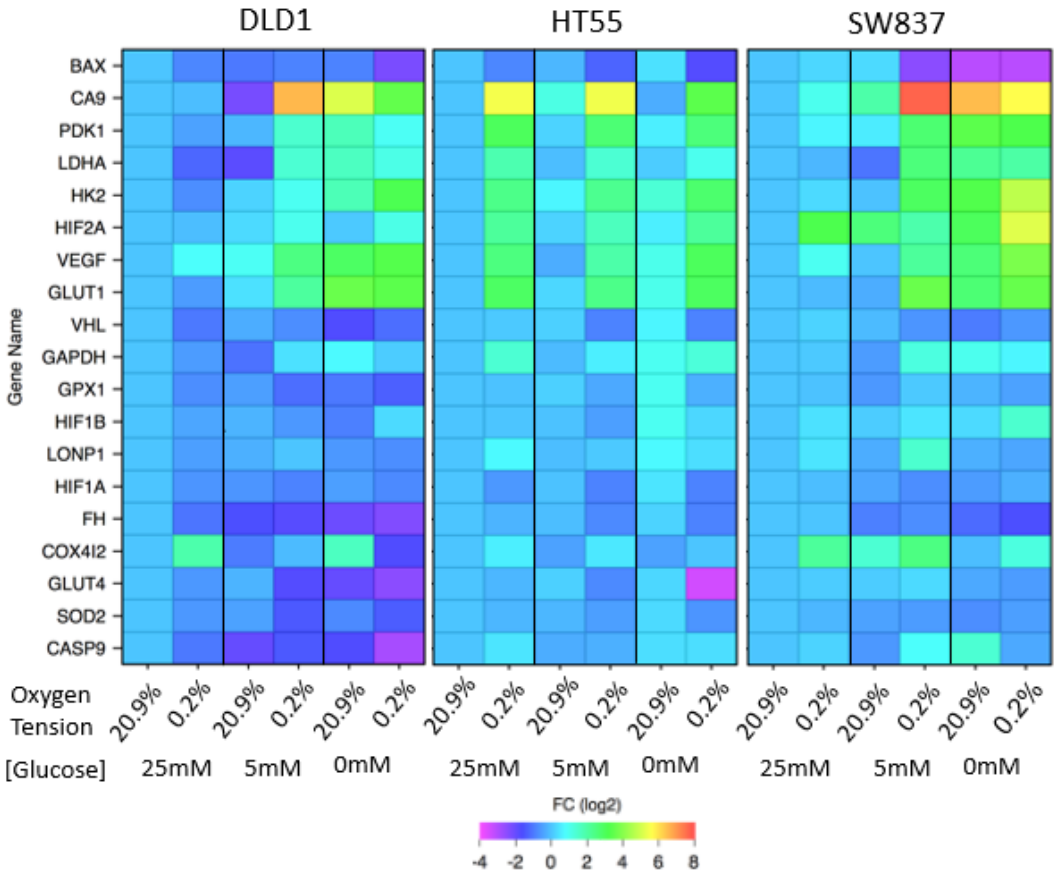

Figure 5.11. Altered CRC cell gene expression profile after 48 hours treatment with 20.9% or 0.2% oxygen. A heat map of log transformed fold changes between the different oxygen tensions normalised to 25mM and 20.9% treatment is shown. Genes are ranked by significance of glucose concentration identified by linear regression multivariate analysis.

5.12 Mitochondrial foci number and area are increased in cells cultured in 0mM glucose

FH protein can be found throughout the cell, however, it is mainly found within the mitochondria where it participates in the TCA cycle. To understand if changes in the amount of FH protein and, therefore, in [fumarate] and FH activity are linked to the number of mitochondria within the CRC cells it was necessary to quantify mitochondria (Figure 5.13, Table 5.11).

Cells were treated to 20.9% or 0.2% O_2 for 48 hours, then fixed and stained with DAPI for nucleus identification, plasma membrane stain and with an antibody validated against a non-disclosed protein found in mitochondria (Chapter 2, Section 2.3.7, Table 2.7). From this mitochondria foci and area could be determined. Staining was imaged by InCell 2200 microscope and the resultant images were analysed by InCell Developer V1.9 as described in Figure 5.12.

It cannot be assumed that each focus is equal to one mitochondria. Therefore, area covered by focus is likely to be a more accurate measurement of mitochondria quantity. Nevertheless, area and foci correlate well.

[Glucose] had a significant effect on the number of mitochondrial foci per cell in DLD1 cells ($p<0.0001$) (Figure 5.13.A). When DLD1 cells were at 20.9% O_2, the number of mitochondrial foci per cell in DLD1 cells cultured in 0mM glucose was significantly increased compared to DLD1 cells cultured in 25mM glucose ($p<0.0001$) as well as DLD1 cells cultured in 5mM glucose ($p<0.0001$). When DLD1 cells maintained at 0.2% O_2, the number of mitochondrial foci per cell in DLD1 cells cultured in 0mM glucose was significantly increased compared to DLD1 cells cultured in 25mM glucose ($p<0.01$) and increased compared to DLD1 cells cultured in 5mM glucose. Oxygen had a significant effect on the number of mitochondrial foci per cell in DLD1 cells ($p=0.0140$) (Figure 5.13.A). There was a significant increase in the number of mitochondrial foci per cell between DLD1 cells cultured in 0mM glucose held at 0.2% O_2 compared to 20.9% O_2 ($p<0.001$). However, there was no difference in the number of mitochondrial foci per cell between DLD1 cells cultured in 25mM or 5mM glucose maintained at 20.9% O_2 compared

to those at 0.2% O2. A significant interaction between [glucose] and oxygen tension on the number of mitochondrial foci per cell in DLD1 cells was identified (p=0.0002).

[Glucose] had a significant effect on the area of mitochondria per cell in DLD1 cells (p<0.0001) (Figure 5.13.B). When DLD1 cells were held at 20.9% O_2, the area of mitochondria per cell in DLD1 cells cultured in 0mM glucose was significantly increased compared to DLD1 cells cultured in 25mM glucose (p<0.0001) as well as DLD1 cells cultured in 5mM glucose (p<0.0001). When DLD1 cells were at 0.2% O_2, the area of mitochondria per cell in DLD1 cells cultured in 0mM glucose was significantly increased compared to DLD1 cells cultured in 25mM glucose (p<0.05) as well as DLD1 cells cultured in 5mM glucose (p<0.01). There was no significant effect of oxygen on the area of mitochondria per cell in DLD1 cells (p=0.0564) (Figure 5.13.B). However, there was a significant increase in the area of mitochondria per cell between DLD1 cells cultured in 0mM glucose held at 0.2% O_2 compared to those cells at 20.9% O_2 (p<0.05). However, there was no difference in the area of mitochondria per cell between DLD1 cells cultured in 25mM or 5mM glucose at 20.9% O_2 compared to 0.2% O_2. A significant interaction between [glucose] and oxygen tension on the area of mitochondria per cell in DLD1 cells was found (p=0.0082).

[Glucose] had a significant effect on the number of mitochondrial foci per cell in SW837 cells (p=0.0003) (Figure 5.13.C). When SW837 cells were maintained at 20.9% O_2, the number of mitochondrial foci per cell in SW837 cells cultured in 0mM glucose was increased compared to SW837 cells cultured in 25mM glucose as well as SW837 cells cultured in 5mM glucose. When SW837 cells at 0.2% O_2, the number of mitochondrial foci per cell in SW837 cells cultured in 0mM glucose was increased compared to SW837 cells cultured in 25mM glucose and was significantly increased compared to SW837 cells cultured in 5mM glucose (p<0.001). Oxygen had a significant effect of on the number of mitochondrial foci per cell in SW837 cells (p=0.9646) (Figure 5.13.C). There was a no difference in the number of mitochondrial foci per cell between SW837 cells cultured in 0mM, 5mM or 25mM glucose and at 20.9% O_2 compared to 0.2% O_2. A significant interaction between [glucose] and oxygen tension on the number of mitochondrial foci per cell in SW837 cells (p=0.6084).

[Glucose] had a significant effect on the area of mitochondria per cell in SW837 cells ($p<0.0001$) (Figure 5.13.D). When SW837 cells were maintained at 20.9% O_2, the area of mitochondria per cell in SW837 cells cultured in 0mM glucose was not significantly different compared to SW837 cells cultured in 25mM glucose or in 5mM glucose. When SW837 cells were held at 0.2% O_2, the area of mitochondria per cell in SW837 cells cultured in 0mM glucose was significantly increased compared to SW837 cells cultured in 25mM glucose ($p<0.01$) as well as SW837 cells cultured in 5mM glucose ($p<0.001$). Oxygen tension did not have a significant effect on the area of mitochondria per cell in SW837 cells ($p=0.2712$) (Figure 5.13.D). There was no difference in the area of mitochondria per cell between SW837cells cultured in 25mM, 5mM or 0MM glucose and maintained at 20.9% O_2 compared to 0.2% O_2. A significant interaction between [glucose] and oxygen tension on the area of mitochondria per cell in SW837 cells was not found ($p=0.0706$).

The readings for both mitochondrial foci number and area per cell are similar when DLD1 and SW837 cells were cultured in 25mM and 5mM at both 20.9% and 0.2% O_2. When DLD1 cells were cultured in 0mM glucose their mitochondrial foci number and area increase, more so when held at 20.9% O_2 compared to 0.2% O_2. When SW837 cells were cultured in 0mM glucose their mitochondrial foci number and area increase, more so when treated with 0.2% O_2 compared to 20.9% O_2, but not as much as DLD1 cells.

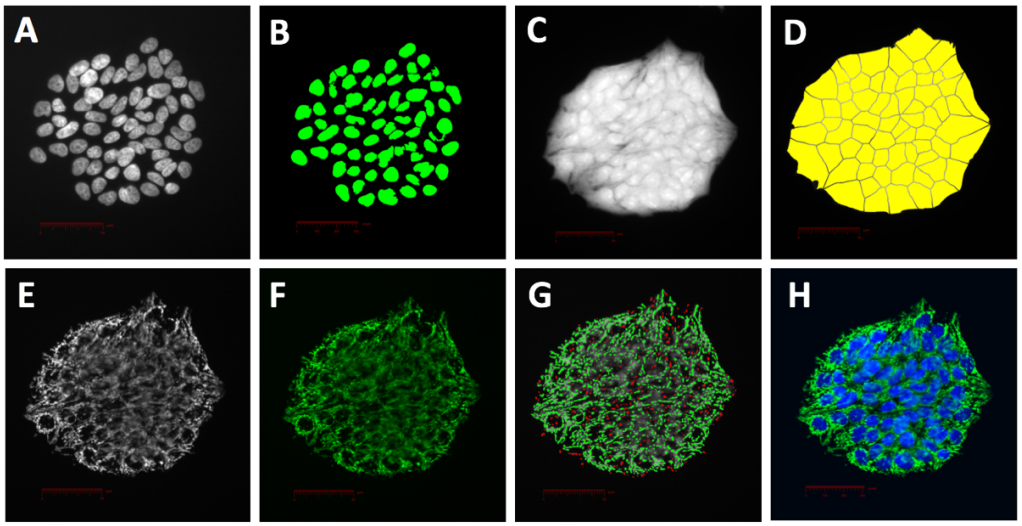

Figure 5.12. Mitochondrial staining analysis process. Cells were held in 20.9% or 0.2% O_2 for 48 hours, then fixed and stained with DAPI, cell mask and mitochondrial antibody. The staining was imaged using an InCell 2200 microscope. And the images were then analysed by InCell Developer V1.9. Briefly, (**A**) cells are located via DAPI nuclear stain. (**B**) The programme was set to identify single nuclei and separate multiple nuclei which are close together. (**C**) Alongside this, the programme was set to identify whole cells by using the cell mask stain. (**D**) Single cells are then defined as a nucleus (DAPI) with a cell body (cell mask). (**E, F**) Mitochondrial staining was generally collected in foci. (**G**) Therefore, a mitochondrial foci analysis was completed. (**H**) The analysis programme was then able to determine how many mitochondrial foci there were per cell. From these images it was possible to determine the area covered by all the mitochondrial foci for each cell. Scale bar 50µm.

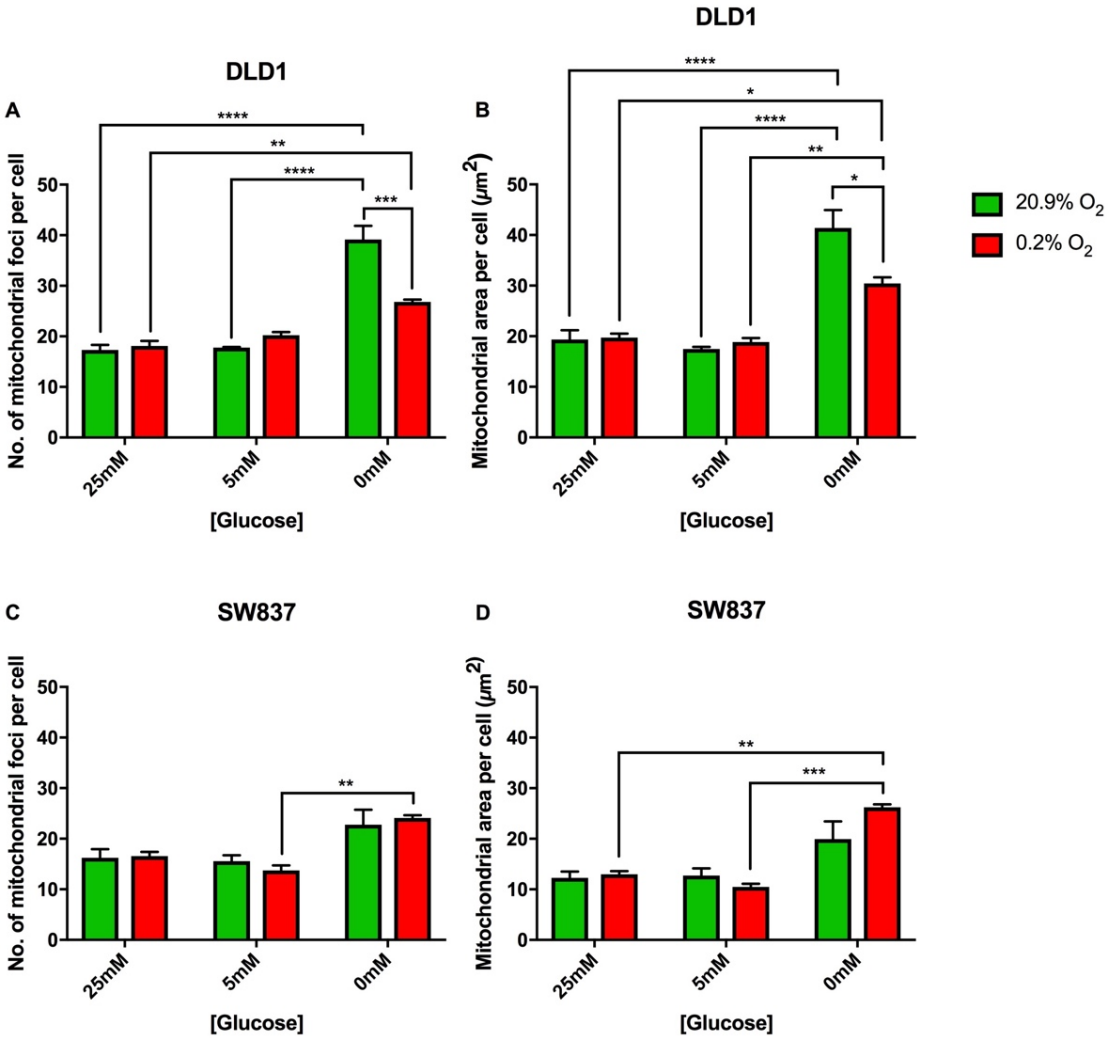

Figure 5.13. Mitochondrial foci and area per cell. DLD1 and SW837 cells were maintained at 20.9% or 0.2% O_2 for 48 hours. Immunofluorescence was performed to detect mitochondrial. Images were captured on INCA 2200 microscope and analysed using InCell Developer v1.9 software to determine the number and area of foci for mitochondria per cell. (**A**) Number of mitochondrial foci per DLD1 cell. (**B**) Area of mitochondria per DLD1 cell. (**C**) Number of mitochondrial foci per SW837 cell. (**D**) Area of mitochondria per SW837 cell. Mean ± SEM in Table 5.11. * p<0.1, ** p<0.01, *** p<0.001 (Table A.5.32,33).

Table 5.11. Summary table of mitochondrial foci and area per cell. Data shown as mean ± SEM. N=3. See also Figure 5.14.

Cell line and 48-hour treatment	**Number of mitochondrial foci per cell**	**Mitochondrial area per cell (μm^2)**
DLD1 25mM glucose; 20.9% O_2	17.31±0.99	19.36±1.85
DLD1 25mM glucose; 0.2% O_2	18.09±1.02	19.74±0.78
DLD1 5mM glucose; 20.9% O_2	17.76±0.13	17.49±0.41
DLD1 5mM glucose; 0.2% O_2	20.22±0.64	18.84±0.82
DLD1 0mM glucose; 20.9% O_2	39.15±2.71	41.38±3.56
DLD1 0mM glucose; 0.2% O_2	26.83±0.46	30.44±1.21
SW837 25mM glucose; 20.9% O_2	16.23±1.70	12.25±1.25
SW837 25mM glucose; 0.2% O_2	16.55±0.84	13.00±0.60
SW837 5mM glucose; 20.9% O_2	15.56±1.17	12.74±1.41
SW837 5mM glucose; 0.2% O_2	13.74±0.98	10.46±0.66
SW837 0mM glucose; 20.9% O_2	22.77±2.96	19.94±3.51
SW837 0mM glucose; 0.2% O_2	24.10±0.56	26.23±0.58

5.13 FH is mainly found in mitochondria

FH is largely present in mitochondria, but can also be found in the cytoplasm, where it participates in the urea cycle (Chapter 1, Figure 1.10). To determine the distribution of FH in the cell when cultured in 25mM, 5mM or 0mM glucose and held in 20.9% or 0.2% O_2, the amount of coinciding staining for mitochondria and FH was quantified. Data shown in Figure 5.9 for FH staining and Figure 5.13 for mitochondrial staining was analysed again to identify FH staining which was present in the same area as mitochondrial staining (Figure 15, Table 5.12). The remaining FH staining was then classified as cytoplasmic or nuclear (abbreviated to cytoplasmic in explanation and figures for ease). Figure 5.14 displays some fusion images from each condition.

[Glucose] had a significant effect on the mitochondrial vs. cytoplasmic ratio of FH in DLD1 cells ($p=0.0002$) (Figure 5.15.A). When DLD1 cells were held at 20.9% O_2 the location of FH was significantly different at 25mM glucose compared to DLD1 cells cultured in 5mM glucose ($p<0.005$). DLD1 cells cultured in 0mM glucose had a ratio of. When DLD1 cells were held at 0.2% O_2 the location of FH was significantly different at 5mM glucose compared to cells cultured in 25mM glucose ($p<0.001$) and 0mM glucose ($p<0.001$). There was a significant effect of oxygen on the location of FH in DLD1 cells ($p=0.0254$), but no significant interaction between [glucose] and oxygen was found ($p=0.253$).

There was no significant effect of [glucose] on the location of FH in SW837 cells ($p=0.2218$) or oxygen ($p=0.1029$) (Figure 5.15.B). There was very little change in the distribution of FH. The amount of FH was between 83 and 90% in the mitochondria and 10 and 17% in the cytoplasm.

In all [glucose] and oxygen tensions the cells were cultured in, FH was overwhelmingly present in the mitochondria, with less than a quarter in the cytoplasm and nucleus (Figure 5.15) (Table 5.12). Unfortunately, no non-cancerous cells were used in this experiment.

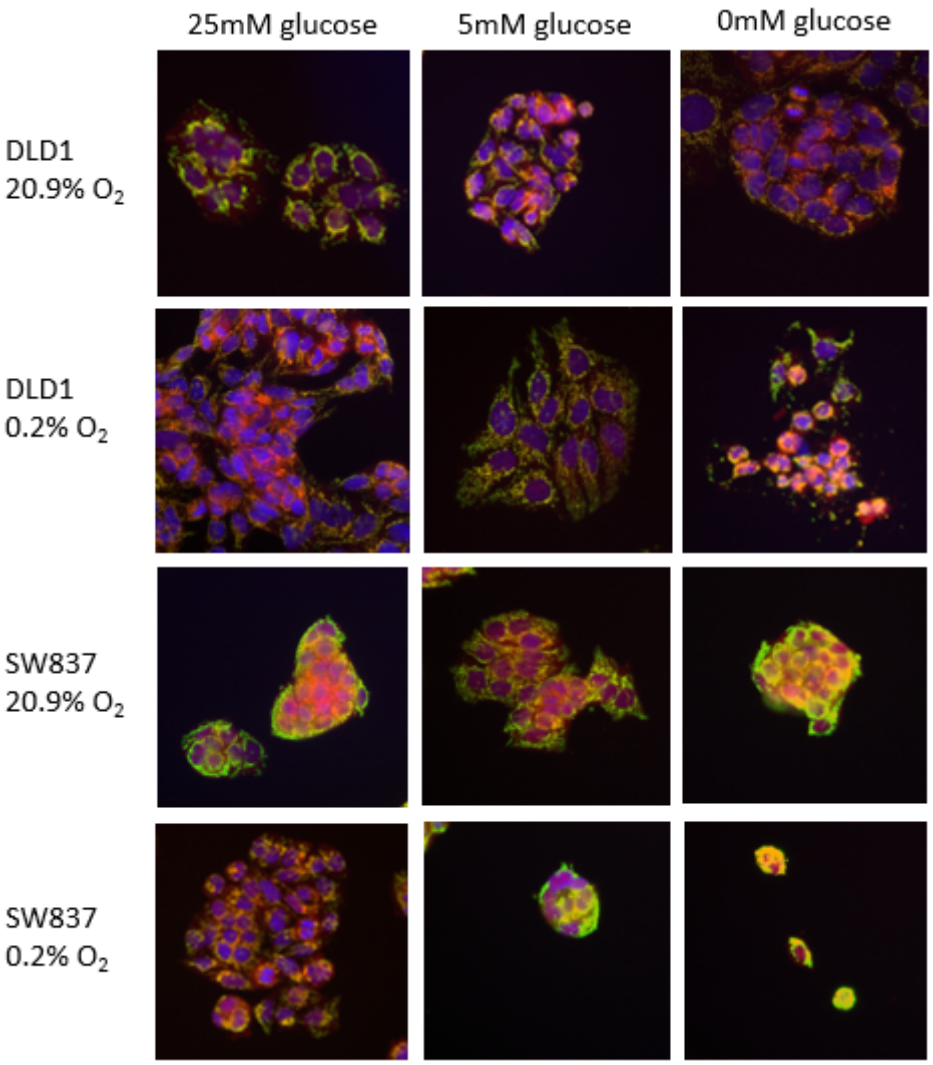

Figure 5.14. Representative fusion images of FH and mitochondria staining. Cells were treated to 20.9% or 0.2% O_2 for 48 hours, then fixed and stained for mitochondria (green) and FH (orange), nucleus is blue.

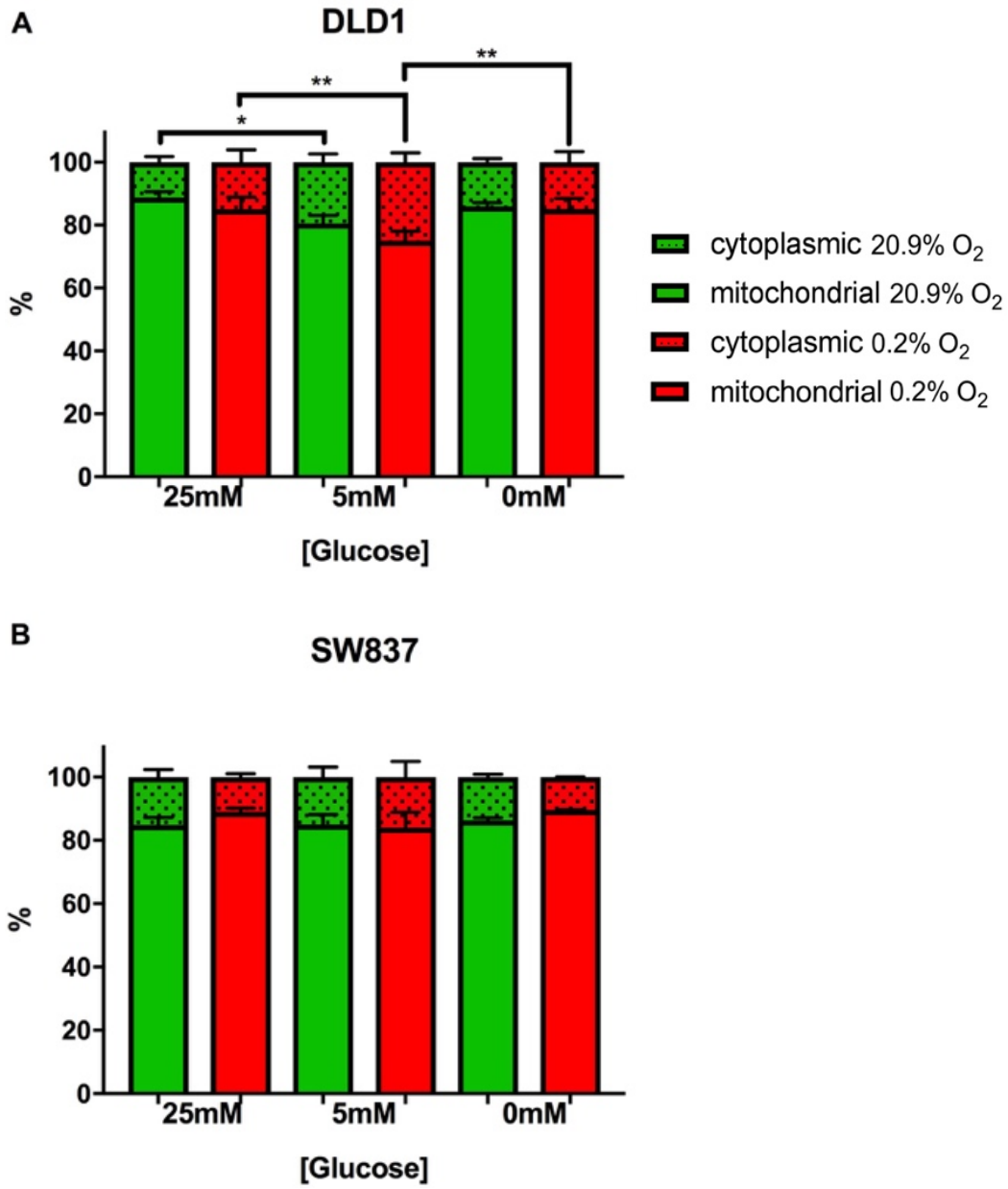

Figure 5.15. Distribution of FH within CRC cells. (**A**) DLD1 and (**B**) SW837 cells were maintained at 20.9% or 0.2% O_2 for 48 hours. Immunofluorescence was performed to detect a FH and a mitochondrial protein. Images were captured on INCA 2200 microscope and analysed using InCell Developer v1.9 software to determine the location of FH. Mean ± SEM in Table 5.12. * p<0.1, ** p<0.01, *** p<0.001 (Table A.5.34,35).

Table 5.12. Summary table of percentage of total FH in mitochondria and cytoplasm.

Data shown as mean ± SEM. N=3. See also Figure 5.16.

Cell line and 48-hour treatment	% FH in mitochondria	% FH in cytoplasm
DLD1 25mM glucose; 20.9% O_2	88.76±0.88	11.24±0.88
DLD1 25mM glucose; 0.2% O_2	85.02±4.90	14.98±4.90
DLD1 5mM glucose; 20.9% O_2	80.50±2.54	19.50±2.54
DLD1 5mM glucose; 0.2% O_2	75.06±3.41	24.94±3.41
DLD1 0mM glucose; 20.9% O_2	85.97±1.94	14.03±1.95
DLD1 0mM glucose; 0.2% O_2	85.10±0.78	14.90±0.78
SW837 25mM glucose; 20.9% O_2	84.86±2.17	15.15±2.17
SW837 25mM glucose; 0.2% O_2	89.09±0.78	10.91±0.78
SW837 5mM glucose; 20.9% O_2	84.98±1.46	15.01±1.46
SW837 5mM glucose; 0.2% O_2	83.97±5.22	16.03±5.22
SW837 0mM glucose; 20.9% O_2	86.30±1.60	13.70±1.60
SW837 0mM glucose; 0.2% O_2	89.64±0.70	10.36±0.70

5.14 Mitochondria are less functional when cells are cultured in 25mM glucose

As it has been found previously that there was more mitochondrial staining in cells cultured in 0mM glucose compared to 25mM and 5mM glucose (Chapter 5, Section 5.9), the next step was to determine if these mitochondria were functional. A functional mitochondrion will provide energy to the cell via the TCA cycle, which involves fumarate and FH.

To determine differences in mitochondrion function the Seahorse XF Cell Mito Stress Test[447] was used (Chapter 2, Section 2.3.9). The test uses compounds which target components of the electron transport chain (ETC) of the mitochondria. The Seahorse XF machine can determine key parameters of mitochondria metabolic function interpreted from the oxygen consumption rate (OCR) and extracellular acidification rate (ECAR) of the cells. The compounds oligomycin, carbonyl cyanide-4 (trifluoromethoxy) phenylhydrazone (FCCP), rotenone and antimycin A (described in Table 5.5) are serially injected to measure ATP production, maximal respiration, non-mitochondrial respiration, proton leak and spare capacity (defined in Table 5.6). A model OCR output from the Seahorse Mito Stress test is shown in Figure 5.16.

DLD1 and SW837 cells cultured in 25mM, 5mM or 0mM glucose were used in this assay. Cell response to different oxygen tensions could not be determined as the Seahorse XF machine was not in the hypoxic chamber. The experiment was done in two ways. First, the compounds were dissolved in media with the same concentration of glucose as the cells were cultured in. Second, all cells were pre-treated with 25mM glucose media for 1 hour and all compounds were dissolved in 25mM glucose media. Data was normalised to the numbers of cells (100,000 cells). Figure 5.17 and 5.18 show the same data with a different layout: Figure 5.17 illustrates the data as a real time OCR trace whereas Figure 5.18 shows the data separated into the parameters that can be measured from the Mito Stress test. MEFs were also used, but only in the first way, where they were used with 25mM glucose in their media.

Table 5.13. Summary of mode of action of compounds used in Seahorse Mito Stress test.

Oxygen Consumption Rate (OCR).

Compound	**Mode of action**	**Effect on OCR**
Oligomycin	ATP synthase (complex V) inhibitor	Decrease
Carbonyl cyanide-4 (trifluoromehtoxy) phenylhydrazone (FCCP)	Disrupts the mitochondrial membrane potential. An uncoupling agent that collapses the proton gradient resulting in an uninhibited flow of electrons through the electron transport chain (ETC) and maximal oxygen consumption by complex IV.	Increase
Rotenone	Complex I inhibitor	Decrease
Antimycin A	Complex III inhibitor	Decrease

Table 5.14. Description of metabolic parameters measured by Seahorse Mito Stress test.

Term	Explanation
Basal respiration	Oxygen consumption used to meet energetic demand of the cell in baseline conditions; as a result of cellular ATP demand and natural mitochondrial proton leak.
ATP production	ATP produced by the mitochondria. The decrease in OCR upon oligomycin administration represents the proportion of basal respiration that was being used for ATP production.
Proton leak	Basal respiration which is not coupled to ATP production. Can be a sign of mitochondrial damage or a mechanism to regulate the mitochondrial ATP production.
Maximal respiration	The maximum rate of respiration. Administration of FCCP mimics a physiological energy demand. This stimulates the respiratory chain to operate at maximum capacity leading to the rapid oxidation of substrates such as sugars, fats and amino acids.
Spare capacity	The capability of the cell to respond to an energetic demand. Also, a measurement of how close a cell is to respiring to its theoretical maximum. An indicator of cell fitness and flexibility.
Non-mitochondrial respiration	Measurement of OCR created by a subset of cellular enzymes produce oxygen.

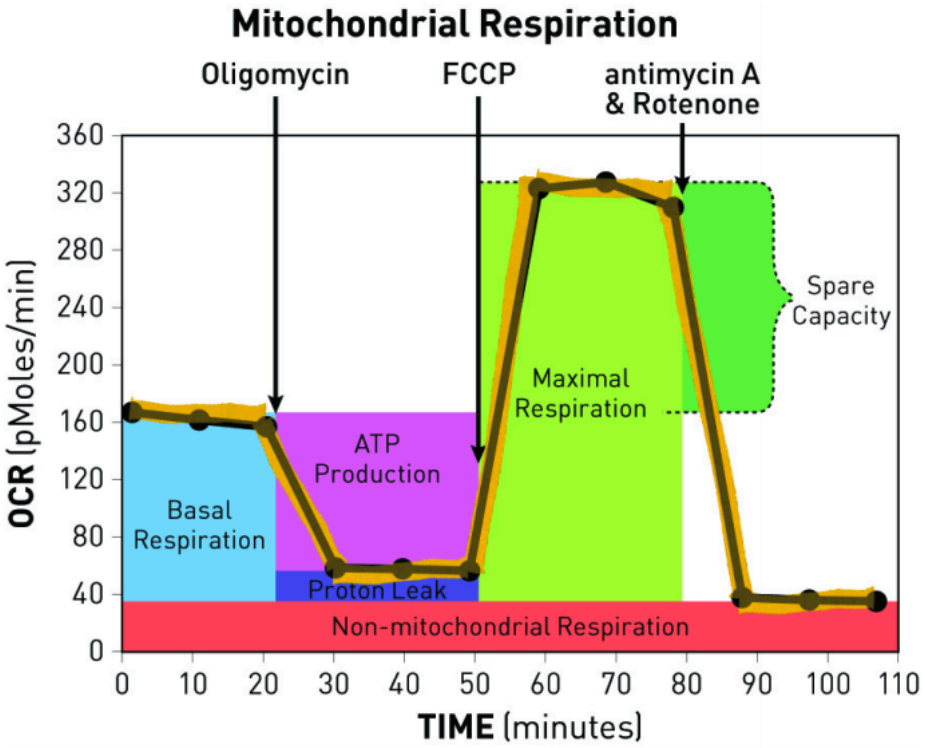

Figure 5.16. Representation of the Seahorse XF Cell Mito Stress Test which measures mitochondrial function by directly measuring the oxygen consumption rate of cells. Sequential injections of oligomycin, FCCP, and a mix of rotenone and antimycin A enable measurement of ATP production, maximal respiration and non-mitochondrial respiration. Proton leak and spare capacity can then be calculated from these measurements[447]. Image from Agilent[447].

There was an effect of [glucose] on mitochondrial metabolic parameters measured by OCR using the Seahorse machine (Figure 5.17 and 5.18). In general, the lower [glucose] of the media in which the cells were cultured, the higher the OCR measurement of the mitochondrial metabolic parameter. DLD1 cells had lower OCR measurements of all parameters when compared to SW837 cells cultured in equivalent/identical conditions (see Table 5.15 for mean ± SEM).

Within the cell lines, the metabolic parameter most often significantly different between [glucose] is the spare capacity. Interestingly, this is often reduced when cells have more glucose available suggesting that cells rely on the continuous glucose supply, instead of storing energy in other ways.

When CRC cells cultured in 0mM glucose were treated with 25mM glucose for 1 hour prior to the Mito Stress Test this reduced the OCR measurements for all parameters suggesting that cells had not lost the ability to utilise glucose. This may be aided by the increased expression of glycolysis related mRNA such as GLUT-1, HK2 and PDK1 in cells cultured in 0mM glucose. This suggests that the cells are still flexible in their energy creating pathways.

Overall it was found that cells cultured with 0mM glucose have the highest basal mitochondrial respiration rate, produce the most ATP via mitochondria, have the highest maximal capacity in their mitochondria as well as the greatest spare capacity. When cells cultured in 0mM glucose are treated with 25mM glucose for one hour, all of these measurements are reduced and significance is lost when compared to 5mM and 25mM glucose cells. They have potentially upregulated glycolysis within 1 hour.

KO Fh1 MEFs have reduced mitochondrial function compared to WT Fh1 MEFs on all parameters confirming that FH has a critical role in mitochondrial metabolism. It can be concluded from this data that glucose presence prevents cells from using their mitochondria to full capacity.

Measuring other mitochondrial parameters such as membrane permeability, fusion and fission would allow further insight into the functionality in the cells used in this study (Chapter 8, Section 8.3).

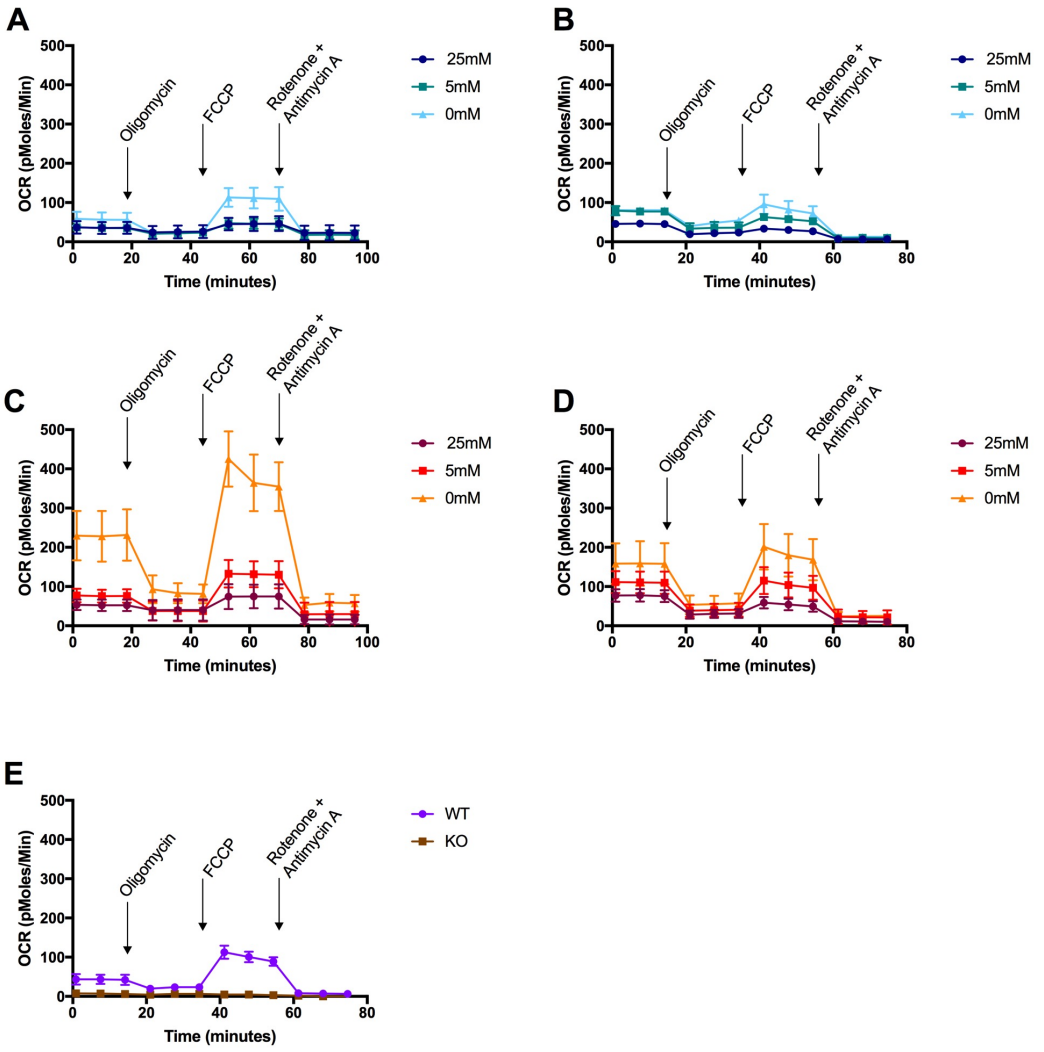

Figure 5.17. Seahorse Mito Stress test output. Cells were incubated within a Seahorse machine which injected the denoted drugs (arrowed) at the time points indicated to test the mitochondrial metabolism of (**A**) DLD1 cells in media at their denoted glucose concentration, (**B**) DLD1 cells all treated with 25mM glucose for 1 hour prior to the assay, (**C**) SW837 cells in media at their denoted glucose concentration, (**D**) SW837 cells all treated with 25mM glucose for 1 hour prior to the assay, (**E**) MEFs in 25mM glucose media. Oxygen consumption rate (OCR).

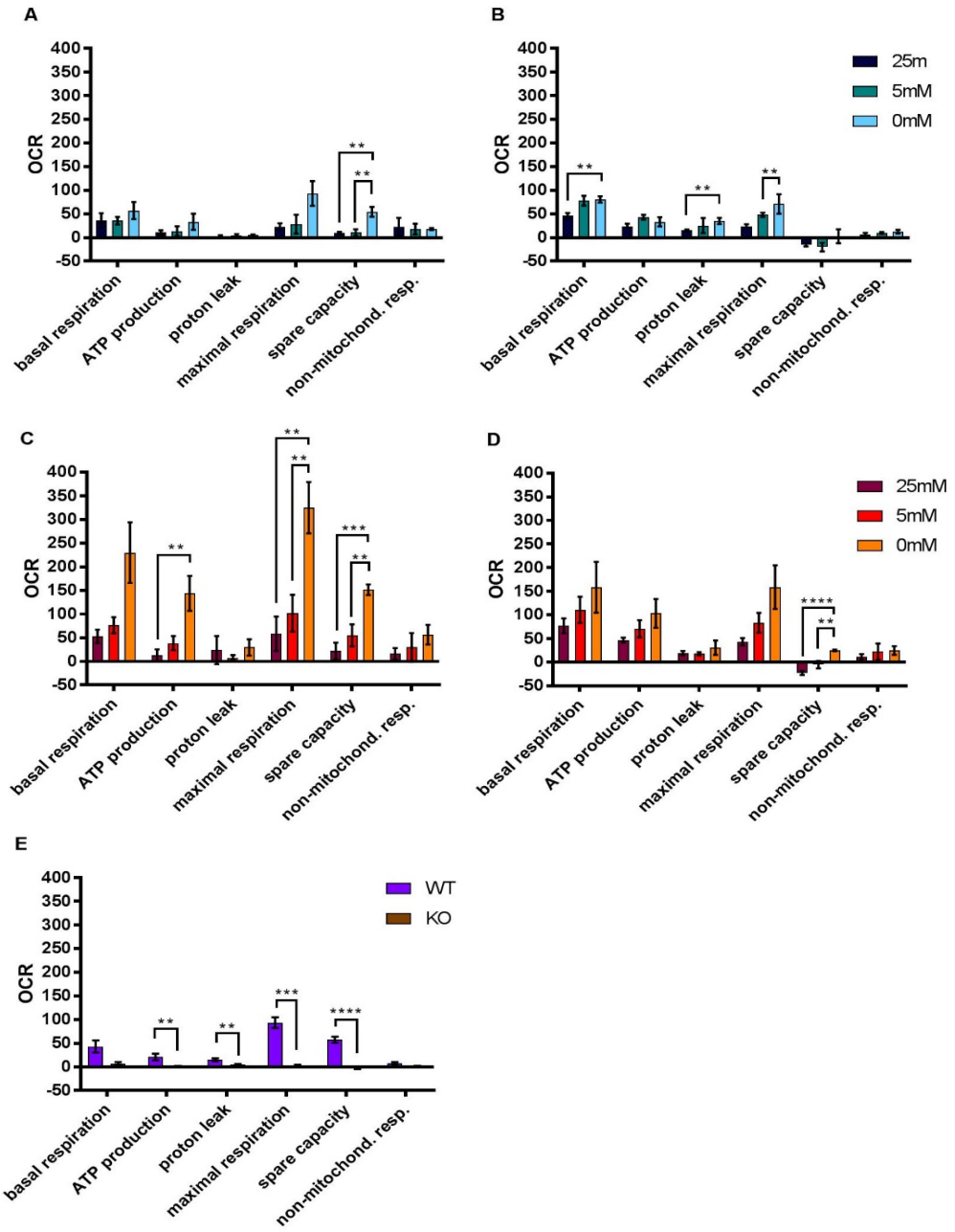

Figure 5.18. Mitochondrial respiration parameters. (**A**) DLD1 cells in media at their denoted glucose concentration, (**B**) DLD1 cells all treated with 25mM glucose for 1 hour prior to the assay, (**C**) SW837 cells in media at their denoted glucose concentration, (**D**) SW837 cells all treated with 25mM glucose for 1 hour prior to the assay, (**E**) MEFs in 25mM glucose media. Oxygen consumption rate (OCR). Mean ± SEM (Table 5.15). Un-paired t-test was performed * p<0.5, ** p<0.01, *** p<0.001, **** p<0.0001 (Table A.5.36).

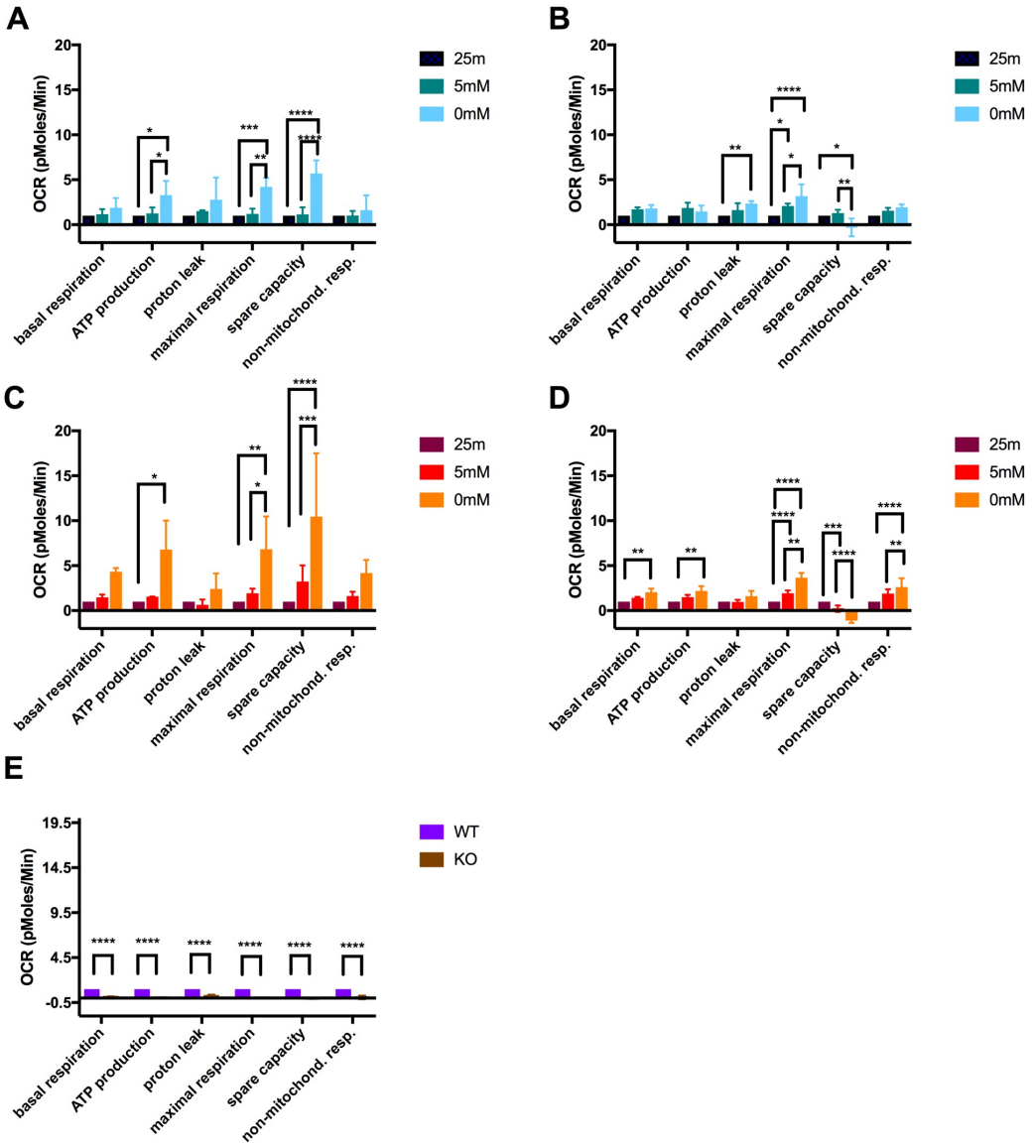

Figure 5.18b. Mitochondrial respiration parameters, A-D fold change from cells cultured in 25mM glucose, E fold change from WT MEFs. (**A**) DLD1 cells in media at their denoted glucose concentration, (**B**) DLD1 cells all treated with 25mM glucose for 1 hour prior to the assay, (**C**) SW837 cells in media at their denoted glucose concentration, (**D**) SW837 cells all treated with 25mM glucose for 1 hour prior to the assay, (**E**) MEFs in 25mM glucose media. Oxygen consumption rate (OCR). Mean ± SEM (Table 5.15). Two-way ANOVA with Bonferroni *post hoc*, * p<0.5, ** p<0.01, *** p<0.001, **** p<0.0001 (Table A.5.36b).

Table 5.15. Oxygen consumption rate for CRC cell lines determined by Seahorse Mito Stress test. Oxygen consumption rate (OCR) was obtained when cells were assayed with the glucose concentration they were cultured in (25mM, 5mM or 0mM glucose; un-shaded rows) or after they were incubated with 25mM glucose for 1 hour prior to the assay (shaded rows). Data shown as mean ± SEM. N=3. See also Figure 5.18.

Cell line	Basal resp.	ATP production	Proton leak	Maximal resp.	Spare capacity	Non-mito. resp.
DLD1 25mM	35.88± 8.94	10.82± 2.77	2.26± 1.59	22.90± 4.23	9.82± 1.27	22.80± 10.89
DLD1 5mM	35.57± 4.70	13.49± 5.96	4.25± 1.75	28.33± 11.55	10.50± 3.93	17.83± 6.61
DLD1 0mM	57.06± 10.48	33.18± 9.90	5.86± 0.37	93.33± 15.04	54.29± 5.93	18.01± 1.16
DLD1 25mM	45.74± 3.61	24.10± 3.00	14.92± 1.24	23.45± 2.70	-15.57± 1.89	6.72± 1.80
DLD1 5mM	77.96± 5.99	42.88± 3.03	25.37± 9.18	47.99± 2.55	-20.25± 5.15	9.71± 1.24
DLD1 0mM	80.62± 3.96	33.13± 5.73	35.13± 3.82	70.96± 11.93	2.70± 8.50	12.36± 2.16
SW837 25mM	52.86± 8.25	12.88± 7.22	23.90± 17.29	58.67± 21.02	21.89± 10.32	16.08± 7.04
SW837 5mM	76.39± 9.78	38.62± 8.62	8.09± 2.87	101.79± 22.44	55.09± 13.51	29.69± 17.60
SW837 0mM	229.85± 37.07	143.80± 21.36	29.59± 9.99	325.00± 31.19	151.61± 6.54	56.46± 11.97
SW837 25mM	76.93± 9.01	46.84± 2.95	19.14± 2.62	43.15± 4.67	-22.82± 2.46	10.96± 3.75
SW837 5mM	110.57± 16.08	70.80± 10.45	17.69± 1.95	83.26± 12.01	-5.24± 4.56	22.08± 10.06
SW837 0mM	158.55± 31.05	103.21± 17.47	30.67± 8.70	158.73± 26.70	24.85± 1.02	24.66± 5.36

When baseline values for OCR and ECAR are plotted it is possible to determine the metabolic phenotype of the cells (Figure 5.19). Both DLD1 and SW837 cells cultured in 5mM and 25mM glucose are similar. In comparison with MEFs the CRC cells are much less glycolytic. It is difficult to directly compare murine and human cells. Plus, KO Fh1 MEFs use different metabolic pathways as described in Chapter 5, Section 5.1. DLD1 cells cultured in 0mM glucose are much more quiescent than DLD1 cells cultured in 5mM and 25mM glucose, suggesting that they do not generate as much energy. In contrast, SW837 cells cultured in 0mM glucose are much more aerobic than SW837 cells cultured in 5mM and 25mM glucose, suggesting that they are able to generate energy well. Post incubation with 25mM glucose cells are grouped together suggesting that their glycolysis and mitochondrial metabolism pathways are functioning in a similar way. Cells cultured in 5mM and 25mM glucose do not change their metabolic phenotype on incubation with 25mM glucose.

However, this data is hard to interpret. The results are relative to samples tested at the same time. Each graph represents an experiment. Unfortunately, the Agilent Seahorse machine available only took 24-well plates so it was not possible to test every condition on the same plate.

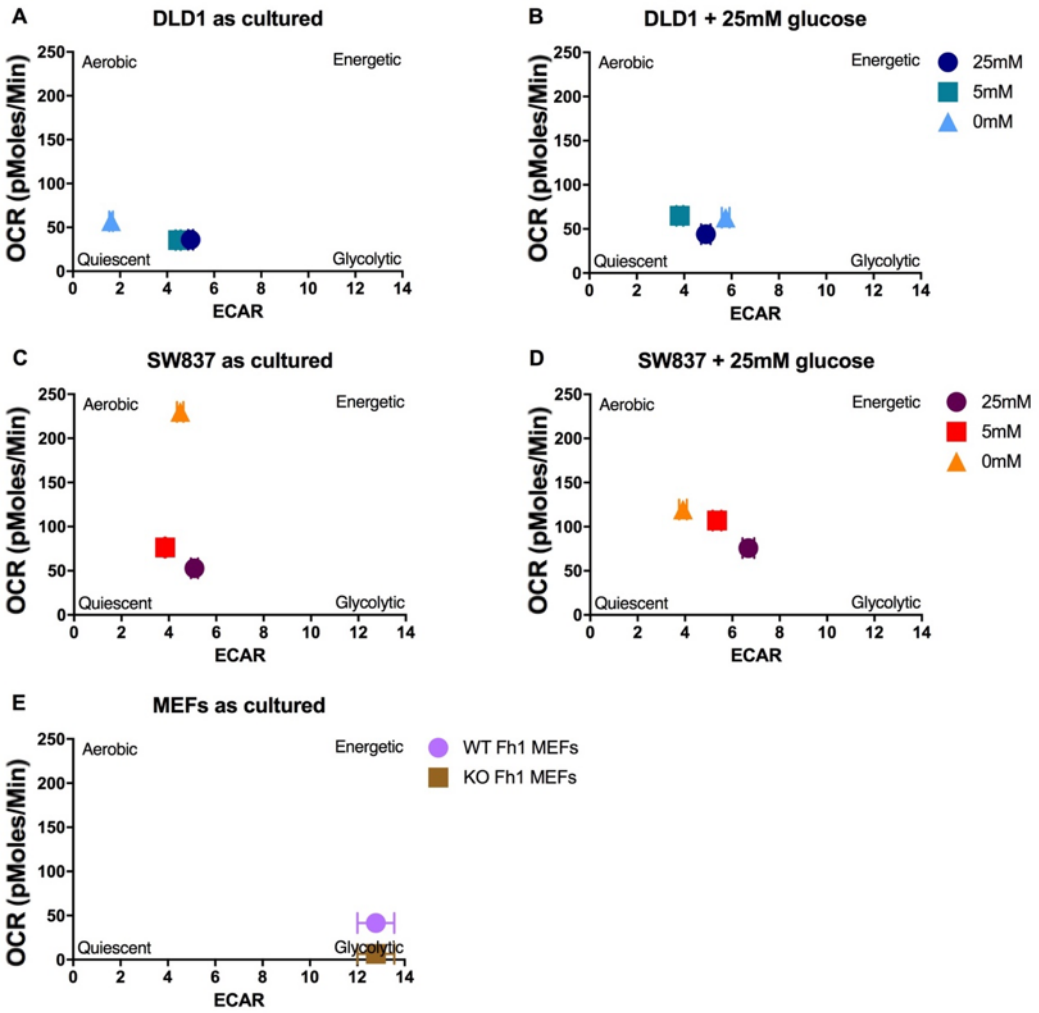

Figure 5.19. Metabolic phenotype of CRC cells. The metabolic phenotype of cells can be determined from baseline oxygen consumption rate (OCR) and extracellular acidification rate (ECAR). Cells with high OCR and ECAR are determined energetic, those with low OCR and ECAR are quiescent. Cells with high OCR and low ECAR are aerobic, whereas cells with low OCR and high ECAR are glycolytic. (**A**) DLD1 cells in media at their denoted glucose concentration, (**B**) DLD1 cells all treated with 25mM glucose for 1 hour prior to the assay, (**C**) SW837 cells in media at their denoted glucose concentration, (**D**) SW837 cells all treated with 25mM glucose for 1 hour prior to the assay, (**E**) MEFs in 25mM glucose media. OCR, Oxygen consumption rate; ECAR, extracellular acidification rate.

5.15 Discussion

The physiology of normal and tumour tissues is different in many aspects, the majority of which are as a result of differences in vasculature. Solid tumours, such as CRC, have deficient vascular systems due to excessive and unregulated cancer cell growth alongside insufficient angiogenesis. As a result, perfusion within solid tumours is inadequate, leading to tumour regions which are transiently and chronically exposed to nutrient and oxygen starvation[448]. Cancer cells respond to these conditions by adapting their metabolism to enable survival and proliferation. Several reports have indicated that changes in cancer cell metabolism are induced by oncogenes and mutations in tumour suppressor genes. Some examples relating to CRC are *MYC, HIF1α* and *p53* which lead to increased expression of genes with a role in glycolysis such as *GLUT-1, HK2, LDHA* and *PDK1*[195,413,449–452]. It has also been found that glucose deprivation promotes development of *KRAS* mutations in cancer cells[453]. Overall these genetic changes lead to high rates of glucose consumption and lactate production in cancer cells, despite low availability of oxygen for complete oxidation of glucose, known as the Warburg effect[446].

The interruption of glycolysis by inhibition of GLUT-1, HK2 and LDH for example, is an attractive method for cancer treatment[454–456]. However, targeting glycolysis has not yet translated into the clinic. The precise effects of oncogenes and mutations in tumour suppressor genes on CRC cell metabolism are still disputed. Tumours are known to be heterogeneous so, it is likely that cancer cells in different tumour regions have different adaptions according to their microenvironment pressures[457]. Cells further from blood vessels will have selection pressure for those that survive low oxygen and nutrient conditions. This heterogeneity contributes to therapy resistance and poses a major challenge for personalised therapy.

In vitro studies to determine effect of oxygen deprivation or hypoxia on cancer cells predominantly use oxygen concentrations below 2%[144]. Healthy tissues experience between 2 and 9% oxygen[144]. Experimentally such oxygen tensions are achieved through use of a heated humidified chamber where the oxygen concentration can be controlled. Cells are plated in atmospheric oxygen (20.9%) and then transferred to the hypoxic treatment for 24-72 hours. A concentration of 0.2% O_2 for 48 hours was used as the hypoxic treatment for this thesis. CO_2 content remained at 5% to maintain the pH of the

media. These conditions were chosen based on previous work in the lab which identified stronger changes in microRNAs in CRC cell lines when treated with 0.2% O_2 compared to 1% O_2[408–412,414].

Traditionally, most cancer cell lines are cultured in media with 25mM glucose. However, normal blood glucose in humans is equivalent to 5mM glucose[415,416]. And the glucose concentration that solid tissues experience is lower than 5mM[335]. Culturing of cancer cells *in vitro* with 25mM glucose does not accurately represent physiological conditions and could be one reason why glycolysis inhibitors developed *in vitro* do not translate to the clinic. And, *in vitro* studies to determine effect of glucose deprivation on cancer cells typically remove glucose from the media for 24-72 hours and then test for observations. The removal of glucose from the media in this short time frame often leads to cancer cell death *via* caspase activation and ROS[458–460]. In my opinion, this is not an accurate representation of tumours *in vivo*. The time-frame over which tumours grow and adapt to low glucose concentrations *in vivo* is much longer than 72 hours. To enable me to study the effect of glucose concentration on CRC cells in a way that represents *in vivo* conditions I gradually reduced the concentration of glucose in CRC cell media over a period of 3 months instead of dropping the glucose concentration dramatically. Over this prolonged time period, glucose would not be totally removed from the cells, so those cultured in 0mM glucose were truly glucose free. This approach has not been taken before to my knowledge. Originally, I was interested in 25mM and 5mM glucose to simulate blood glucose concentrations of an uncontrolled diabetic and a normal individual, respectively. However, CRC cells were able to survive without any glucose in their media which I found interesting and, therefore, decided to include this condition in my study.

The first part of work I did was to phenotype the CRC cells that I had created to understand baseline differences. As expected, reducing the glucose concentration increased the doubling time of all CRC cell lines (Figure 5.1). Glycolysis is a major producer of ATP for the cancer cell, therefore, if less glucose is entering the pathway then less ATP will be made for processes like proliferation. However, there is more than one metabolic pathway that can generate ATP. It is known that glutamine is metabolised more abundantly than other non-essential amino acids in cancer cells[461,462]. Glutamine remained in the CRC cell media at 2mM regardless of glucose concentration. This allowed

for only the effects of changing glucose concentration to be studied. Glutamine is, therefore, likely to be contributing to cell survival under glucose free conditions. DLD1 cells have previously been shown to have increased levels of glutamate dehydrogenase 1 (GLUD1) which metabolises glutamine and feeds it into the TCA cycle via α-ketoglutarate to generate ATP[397]. And knock-down of GLUT1 in DLD1 cells in glucose-deprived conditions (removal of glucose for 72 hours) led to decreased growth[397].

Doubling time of KO Fh1 MEFs was higher than WT Fh1 MEFs (Figure 5.2). This is likely due to the alteration in the TCA cycle of KO Fh1 MEFs, leading to lower generation of energy for cell proliferation. Tyrakis et al. 2017 recently reported that Fh1 deficient cells are unable to grow in glucose-free medium[322]. It was reported that cells were unable to further increase the function of their mitochondria to meet energy demands. However, it was not reported in the methods how the reduction of glucose was accomplished. This evidence suggests that the CRC cells have functional FH as they are able to cope without glucose.

It was also necessary to confirm HIF-1α upregulation during the 0.2% O_2 treatment (Figure 5.6). Upregulation of HIF-1α was identified strongly in cells cultured in 25mM and 5mM glucose. The presence of HIF-1α is not as strong in CRC cells cultured with 0mM glucose. The dependence of HIF-1α stability on glucose has previously been described in human pancreatic cancer cells[463], human prostate cancer cells[463], human pharyngeal cancer cells[464] and human glioma cells[185]. It is suggested that pyruvate, the end product of glycolysis, has a role in preventing the degradation of HIF-1α protein[185]. Despite this fact, gene expression data in Figure 5.11 shows that in CRC cells cultured with 0mM glucose there was upregulation of genes controlled by HIF-1α, which implies there must be some stabilisation of HIF-1α. Alternatively, the genes could be upregulated via a different mechanism.

Cancer cells are known to survive in a hypoxic environment by increasing their glucose uptake facilitated by increased expression of HIF-1α[465]. However, when both glucose and oxygen are in low supply and cell energy demand is high, cell survival can be compromised. The *in vitro* cell viability results (Figure 5.5) corroborate this observation: viability was decreased at 0.2% O_2 in CRC cells cultured with 5mM and 0mM glucose compared to those cultured with 25mM glucose. Viability of MEFs (Figure 5.5) with both

WT and KO Fh1 was equal in hypoxia and normoxia likely due to their culture in 25mM glucose. This suggests that CRCs in T2D patients may be able to survive hypoxia better if blood [glucose] is increased.

Next, it was important to understand the changes in fumarate and how they relate to [glucose] and oxygen tension. It has previously been shown that [fumarate] can be elevated 200-300 times in HLRCC samples compared to normal fibroblast cell samples[324]. Stomach and colon cancer samples have also been shown to have elevated fumarate compared to normal tissue, which is attributed the oncogenic changes within the cell leading to increased demand for ATP leading to an increase in metabolism and, therefore, more fumarate and other metabolites[335]. Fumarate impairs HIF-1 prolyl hydroxylation leading to stabilisation of HIF-1α[316]. High levels of intrinsic fumarate in a cell can, therefore, promote pseudohypoxia and the Warburg effect, both survival mechanisms for cancer cells. Fumarate is also generated during a DNA damage repair carried out by FH[330]. FH travels to sites of DNA damage, which are more likely in hypoxia[466], to promote repair of double strand breaks in DNA; fumarate is generated in this process[467].

In line with the above evidence, [fumarate] was found to generally increase in CRC cells held in 0.2% O_2. Recently, treatment with increasing [fumarate] has been shown to reduce the viability of HepG2 cells, due to extensive DNA damage and activation of an apoptotic pathway[468]. A [fumarate] of 2.5mM reduced HepG2 cell viability to around 20%. Although, viability of cells in this study is reduced at 0.2% O_2, it appears that the intrinsic [fumarate] in this study is not sufficient to affect cell viability. The highest [fumarate] found in this study was in KO Fh1 MEFs of around 23 ng/uL which equates to 198µM and is, therefore, not high enough to potentially effect cell viability. Interestingly, DLD1 cells held in 0.2% O_2 more FH was found in the nucleus or the cytoplasm (Figure 5.9) suggesting that the increase in [fumarate] could be due to the role of FH in DNA repair, which protects cells from DNA damage. Increasing [fumarate] and measuring cell viability would be an interesting experiment to complete with the CRC cells generated for this work (Chapter 8, Section 8.3).

Although, fumarate concentration was dependent on cell type, oxygen and [glucose]. The effect of [glucose] on [fumarate] was more closely related to cell line. In SW837 cells [fumarate] was highest in cells cultured with 25mM glucose, but in DLD1 and HT55 cells, [fumarate] was highest when cells were cultured in 5mM glucose, and this was comparable to the [fumarate] of SW837 cells cultured in 25mM glucose. DLD1 and HT55 cell lines are both derived from colon cancer patients whereas SW837 cell line is derived from a rectal cancer patient. It is interesting that the DLD1 and HT55 cell lines have similar [fumarate] under the same treatment and that these are different to the SW837 cell line. The same grouping of cell lines occurred in the [fumarate] mass spectrometry results (Figure 5.1). I can find no literature which suggests that cells from the colon and rectum have intrinsically different fumarate or glucose levels. However, it is known that there is less blood supply to the rectum. This work highlights a potential novel finding in the relationship between [fumarate] and [glucose] in cells from different tissue origins, and should be followed up (Chapter 8, Section 8.3).

KO Fh1 MEFs had the highest [fumarate], as expected due to no Fh1 converting fumarate into malate. However, this decreased upon treatment with 0.2% O_2, which was the opposite result to all other cell lines. This is an interesting result, which suggests that when Fh1 is not present another mechanism could be operating which is regulating fumarate concentration under hypoxia. The [fumarate] found in KO Fh1 MEFs was almost matched by HT55 cells cultured in 25mM glucose and held at 0.2% O_2 which suggests that FH could be inhibited by lack of oxygen alongside high [glucose] in HT55 cells.

The NADH-fumarate reductase system is an anaerobic form of respiration that exists in anaerobic organisms. This system results in the formation of succinate from the reverse reaction of complex II in the mitochondria but has not been widely studied in human cells. Paddenburg et al. describe the use of this system in hypoxic pulmonary vasculature where they suggest that complex II switches its catalytic activity from succinate dehydrogenase to fumarate reductase at reduced oxygen tension[469]. It could be speculated that this is a mechanism to generate extra energy under hypoxic conditions in CRC cells, where fumarate levels rise.

As I had been able to detect fumarate it was next necessary to determine if it was possible to identify succination in the CRC cell lines. This was crudely done by western blot. Succination was present in all cell lines. However, it would be better to identify 2-SC motifs on proteins by mass spectrometry, which would enable identification of exact proteins that have been succinated.

Differences in [fumarate] in CRC lines found by fluorometric assay can be explained by FH activity. As predicted, when [fumarate] is high, FH activity is low. Differences in FH activity are more pronounced in the DLD1 cell line, with activity much higher in cells cultured in 25mM and 5mM glucose and/or treated with 20.9% O_2 compared to cells cultured in 0mM glucose and/or 0.2% O_2. This suggests that in the DLD1 cell line, FH activity is more dependent on [glucose] and oxygen availability relative to the SW837 cell line where FH activity is only slightly increased at each glucose concentration when cells were maintained in 20.9% O_2 over 0.2% O_2. FH activity has been linked to cell growth rate and carbon source utilisation independently by a study done in *Escherichia coli*[470]. The researchers found that FH activity increased under aerobic conditions and when acetate was used instead of glucose as the sole carbon source. It has also been shown that inhibition of FH activity at low glucose concentrations is cytotoxic[471], therefore, there must be a relatively precise window of FH activity that is advantageous to the cell.

As expected in WT Fh1 MEFs FH activity is higher in 20.9% O_2 compared to 0.2% O_2. Some minimal activity is observed in KO Fh1 MEFs which suggests that the assay is not perfect, as there should be no read out if Fh1 is not present. However, the readout is cellular NADH which is made elsewhere in the cell. Therefore, the value for KO Fh1 MEFs was used as a background value, and substituted from all final readouts. As CRC cell lines produce a readout from this assay, this suggests that FH activity is not fully compromised in CRC like HLRCC. Further critical work needs to be completed to ascertain the full potential and changes in FH activity relating to [glucose] and O_2 tension in CRC.

As detailed in the Chapter 3 discussion, at concentrations above 0.1M fumarate can inhibit FH and at 0.001-0.033M allosteric activation of the enzyme by binding to site B is observed [390]. Both the mass spectrometry and fluorometric assay readouts for CRC cell [fumarate] were lower than 0.001M so FH was not inhibited by fumarate in the cell conditions used for this study.

It was thought that FH activity could be linked to amount of FH protein in the cells. Therefore, it was necessary to determine the area of FH in the cell. DLD1 cells had more FH than SW837 cells at each [glucose]. For both cell lines, the area of FH did not change in cells cultured in 25mM and 5mM glucose when held in 0.2% O_2. As the FH activity data suggest that FH is more active in DLD1 cells held in 20.9% O_2 this suggests that FH area does not correlate with FH activity.

FH staining did not correlate with [fumarate], suggesting that presence of FH is not influenced by fumarate. Furthermore, in both DLD1 and SW837 cells the area of FH was greater upon culture in 0mM glucose compared to culture in 25mM and 5mM (Figure 5.9). This suggests that the cell is able to up-regulate FH when glucose is not present. However, *FH* mRNA expression was not increased in 0mM glucose, suggesting a post-translational control over FH. Rossignol et al., studied HeLa cells grown in no glucose for 3 weeks[472]. They identified that in HeLa cells grown in glucose, 80% of glucose is metabolised by glycolysis and only 4-5% of glucose carbon entered the TCA cycle. Whereas, when HeLa cells are grown in galactose medium, glutamine provided 98% of the ATP used for growth via the TCA cycle. They also found by Western blot that cells synthesis more respiratory chain protein when grown without glucose which matches with the upregulation of FH shown in cells grown in 0mM glucose in this study. I could find no similar studies in tumour cells. Even though more FH is present in cells cultured in 0mM glucose, the activity of FH is lowest in this condition which suggests that FH is inhibited in some way by culture in 0mM glucose.

One other point of note is that the number of FH foci in DLD1 cells is lower in 0.2% O_2 compared to 20.9% O_2, however, the FH area is similar. This could suggest that the hypoxic stress generates a clumping of FH protein. Because the majority of FH is within the mitochondria (Figure 5.16) this could suggest that mitochondrial fission is occurring. The opposite is true for SW837 cells; there are more foci and a greater area in SW837 cells cultured in 0mM glucose when they are treated with 0.2% O_2 compared to 20.9% O_2 which suggests a stimulus in production of FH. To determine these ideas, further experiments with higher resolution imagery should be completed, such as confocal and/or electron microscopy (Chapter 8, Section 8.3).

Gene expression between DLD1, HT55, SW837 cells after culture in 25mM, 5mM or 0mM glucose and treatment with 20.9% O_2 or 0.2% O_2 is different. No similar gene expression studies have been published that I can find. When multivariate linear regression is completed with the data for all three cell lines, glucose concentration significantly influenced *BAX, CA9, PDK1* and *LDHA* which, have all been previously implicated as having a role in metabolism[428,430,473,474]. Oxygen concentration significantly influenced *CA9*, *PDK1*, *LDHA*, *HK2* and *GLUT1* gene expression which, are known to be regulated by HIF and have been reported upregulated in hypoxia previously[475]. This suggests that in this study HIF is activated with 0.2% O_2 treatment. Interestingly, the mRNA for HIF and FH genes is not increased suggesting post-translational effects on protein abundance. To validate these results, it would be necessary to do a western blot for all the protein products of the genes analysed by qPCR as mRNA and protein results can be different. Unfortunately, there was not enough time to do this as part of this study.

There was less *BAX* when [glucose] is reduced and oxygen tension is 0.2% O_2. *BAX* deletion or inactivation is rare in cancers, but has been reported in CRC[476]. Interestingly, BAX protein has also been shown to be prognostic in human CRC, with higher amounts linked to more severe disease[443]. A paper studying the effect of loss of *BAX* in HCT116 cells, suggests that loss of *BAX* expression leads to a defect in mitochondrial oxidative capacity and favouring of the glycolysis pathway by the cell[473]. In my work, a reduction in mitochondrial oxidative capacity is not seen when [glucose] and *BAX* expression is reduced. In healthy cells BAX has been shown to be required for normal mitochondria fusion[477]. To investigate if CRC cells used in this study had differences in mitochondria, it would be necessary to use confocal or electron microscopy to get high power images of mitochondria (Chapter 8, Section 8.3).

CA9 and *HIF-2α* are involved in the cells response to hypoxia suggesting there is a relationship between hypoxia and [glucose], as already widely reported in literature[444,445]. *PDK1, LDHA, HK2* and *GLUT-1* are all involved in glycolysis, suggesting that glycolysis is affected by both [glucose] and oxygen tension, as already corroborated by the literature[446].

One surprising result was the very low quantities of *COX4I2* in most samples. *COX4I2* is the terminal enzyme of the mitochondrial respiratory chain. *COX4I2* has been shown to have a HRE, and can thereby be upregulated in hypoxia[165]. However, this wasn't seen in my results. Further analysis of this mRNA and protein is necessary.

To further understand if [glucose], [fumarate] and FH levels and activity are in any way linked to mitochondria, it was necessary to determine the number of mitochondria within the cells. Mitochondria are important organelles within the cell, hosting the TCA cycle and OXPHOS.

Area of mitochondria was stable in DLD1 and SW837 cells cultured in 25mM and 5mM glucose, with no difference between oxygen tension treatment. When cells are cultured in 0mM glucose the area of mitochondria increases. This could be explained by mitochondrial fusion and fission, processes which respond to changes in metabolism[478]. Fusion is a result of energy demand and stress. New mitochondria are generated by fission which is essential for growing cells. When cells have to rely on OXPHOS due to withdrawal of glucose, mitochondria become more fused[479]. This suggests that the larger area of mitochondria found in cells cultured in 0mM glucose is due to mitochondrial fusion. However, the number of mitochondrial foci is not reduced when DLD1 and SW837 cells are cultured in 0mM glucose, suggesting there is a similar number of mitochondria which are larger. Further work using confocal and electron microscopy would confirm differences in area as well as determining mitochondria morphology in the CRC cells used in this study. This also correlates with the increased OCR in cells cultured in 0mM glucose shown by the Seahorse Mito Stress Test (Figure 5.18). Suggesting that larger mitochondria are able to generate a higher OCR.

There is a correlation between FH and mitochondria area per cell, the greater the mitochondrial area, the greater the FH area. As FH has a role within the mitochondria, this was expected. FH also has a cytoplasmic role in the urea cycle and in the nucleus in the DNA damage response[399]. It was possible to calculate the percentage of total FH within the mitochondria and outside the mitochondria. FH was overwhelmingly found in the mitochondria in the DLD1 and SW837 cells in all conditions. In SW837 cells the ratio of FH

in the mitochondria to FH in the cytoplasm and nucleus was very similar in all conditions. Whereas, in DLD1 cells, more FH was found in the cytoplasm and the nucleus when cells were held in 0.2% O_2, which could be due to the participation of FH in DNA damage response as suggested earlier.

Fibroblast cell lines have previously been shown to have an equal or more balanced distribution of FH between mitochondria and cytoplasm *via* Western blot[314], when these are compared to samples from HLRCC patient the amount cytoplasmic FH in greatly reduced, similar to the distribution of FH seen in the CRC cell lines in this study[314]. The difference between HLRCC patients and CRC cells lines is that HLRCC patient samples have a mutation in FH which renders FH inactive, whereas CRC cell lines have no mutation[211,480]. This suggests that the FH in CRC cell lines is dysfunctional in some way. It would be interesting to do this experiment with matched normal and CRC tissue samples (Chapter 8, Section 8.3).

To test the influence of [glucose] on the function of mitochondria I chose to do a Seahorse Mito Stress Test. The data identified that CRC cells cultured in 0mM and 5mM glucose have enhanced basal OCR compared to cells cultured in 25mM glucose and have, therefore, adapted their metabolism to use more mitochondrial metabolism. Almost all measurements were highest in cells cultured in 0mM glucose, including proton leak. This suggests that although cells are able to adapt and use their mitochondria more, they could be damaged too. To confirm damaged mitochondria mitochondrial membrane potential should be measured (Chapter 8, Section 8.3).

Cancer cells are known to generate the majority of their energy through glycolysis and preferring to use the end product of glycolysis pyruvate to make lactate instead of acetyl-CoA for the TCA cycle[481]. This data suggests that CRC cells are able to function without glucose, so aerobic glycolysis is not necessary for their survival.

In both cell lines spare capacity is significantly lower in cells cultured in 25mM and 5mM glucose compared to 0mM glucose. This correlates with the area of mitochondria results. When more mitochondria are present, the cell has a greater spare capacity. For other measurements, there was no significant difference in DLD1 cells. In SW837 cells ATP production and maximal respiration is significantly higher in cells cultured in 0mM glucose

compared to 25mM glucose. Even though it is known that mitochondrial respiration generates more ATP than glycolysis I was still surprised by the huge difference seen. This may again be due to the increase in number of mitochondria in SW837 cells cultured with 0mM glucose. To confirm the change in mitochondria area and number, further work measuring mitochondrial DNA would add to the evidence (Chapter 8, Section 8.3).

There was a great difference between OCR for DLD1 and SW837 cells. As SW837 cells had a lower mitochondrial area when cultured in 0mM glucose, I predicted that their OCR would be lower than DLD1 cells. However, the exact opposite was found. SW837 cells had higher values than DLD1 cells for all conditions and measurements. DLD1 cell readouts were similar to WT Fh1 MEFs. Whereas KO Fh1 MEFs had almost no hint of mitochondrial respiration. This suggests that SW837 cells have more active or efficient mitochondria, which could potentially be fuelled by greater input into the TCA cycle, but this was not measured in this study. Perhaps DLD1 cells are using an alternative form of energy generation. SW837 cells cultured in 0mM glucose also have a longer doubling time than DLD1 cells cultured in 0mM glucose, which suggests that the energy generation from mitochondria isn't being used for proliferation.

The mitochondrial metabolism of DLD1 cells was not affected by the addition of 25mM glucose, suggesting that their metabolism is not as flexible as SW837 cells. Perhaps the long period of culture in 25mM, 5mM or 0mM glucose has permanently altered their make-up. To test this, cells would be incubated with 25mM glucose for longer periods of time before testing again.

In SW837, addition of 25mM glucose for one hour before the Seahorse Mito Stress Test led to a reduction in OCR for cells cultured in 0mM glucose for all mitochondrial metabolic parameters. This suggests that these cells are not permanently changed from being cultured in 0mM glucose; they still have plasticity to up-regulate glycolysis again. Interestingly, the cells with the least spare capacity are those cultured in 25mM glucose which suggests that the cells are used to a continuous supply of glucose and do not hold much reserve for stress situations.

These results are further highlighted with the metabolic phenotype plot. SW837 cells cultured in 0mM glucose are much more energetic than any other cell type tested.

Unfortunately, the Seahorse Mito Stress Test could not be done with cells held in 0.2% O_2 as the Seahorse machine is not within the INVIVO chamber I used for reducing oxygen tension. I would, however, expect mitochondrial respiration to be reduced in 0.2% O_2 compared to 20.9% O_2.

There are no similar Seahorse studies on cancer cell lines where the glucose has been reduced over a prolonged period of time. However, it is widely known that a glycolytic phenotype is linked to cancer progression and aggressiveness. There was not much difference in OCR measured by Seahorse of cells cultured in 25mM and 5mM glucose at 20.9% O_2, which suggests that cancer cells can generate energy well via glycolysis and mitochondrial metabolism with a wide range of [glucose]. Nevertheless, I was surprised to see SW837 cells cultured with 0mM glucose generating such high OCR reads. This suggests that as expected tumour cells are able to adapt to different tumour microenvironments by using different substrates for metabolism. It would be useful to repeat the Seahorse Mito Stress Test with cells held in 0.2% O_2 which is more similar to an *in vivo* tumour microenvironment.

Unfortunately, the Seahorse Mito Stress Test could not be done with cells held in 0.2% O_2 as the Seahorse machine is not within the INVIVO chamber I used for reducing oxygen tension. I would, however, expect mitochondrial respiration to be reduced in 0.2% O_2 compared to 20.9% O_2. It is known that hypoxia impairs mitochondrial fusion which leads to mitochondrial depolarisation, loss of mtDNA and impaired distribution of mitochondria within the cells can be accompanied by altered respiration rate[482].

The work in this chapter has confirmed that CRC cell lines are very different, which matches the findings of Nijhuis et al. 2017[408]. These differences should be considered in the implications of this work as well as across the wider scientific field. Overall the work has shown that [fumarate] in CRC cells is responsive to [glucose] and O_2 tension. It was identified that 2-SC is present *in vitro* in CRC cells. The work has additionally confirmed that FH in CRC cells is active to some extent *in vitro*, although, the amount of FH and FH activity do not correlate. CRC cells were also found to have functional mitochondria and are plastic in their use of glycolysis and OXPHOS. Further questions have been raised about the control of FH and its activity in different compartments of the cell.

These data suggest that T2D patients with CRC, which is likely to be hypoxic at the core, could experience elevated fumarate in their tumour compared to non-diabetic patients, leading to changes in succination, metabolism and gene expression.

Chapter 6 – DUOX2 activity is increased by cetuximab

6.1 Introduction

This work is focused on examining DUOX expression in xenografts of DLD1 cells in response to exposure to the oxaliplatin and cetuximab. The motivation for this work was the surprising results from the New Eloxatin Peri-Operative Chemotherapy (EPOC) study[132]. Patients who received oxaliplatin and 5-FU combined with cetuximab demonstrated reduced progression-free survival than those who received oxaliplatin or 5-FU alone[132]. In collaboration with Prof. Daniel Hochhauser's group at University College London, the presented data within this chapter formed part of a publication in the JNCI journal that describes the role of ROS as generated by DUOX in the abrogation of oxaliplatin activity by cetuximab in CRC cells[133].

Oxaliplatin is a chemotherapy for CRC patients given in combination with 5-FU (FOLFOX) or capecitabine (CAPOX). Unfortunately, this therapy does not work for every patient and cancer cell populations that are resistant to oxaliplatin can develop, leading to treatment failure[129–131]. Newer biologic treatments, such as cetuximab, are being developed and trialled in combination with drugs like oxaliplatin to try to prevent resistant cell populations from developing and thereby improving patient outcome[483,484].

Cetuximab is a monoclonal antibody to EGFR that benefits CRC patients without a *KRAS* mutation[485]. Promising *in vitro* studies showed positive effects of combining oxaliplatin and cetuximab[486,487]. Phase II data showed promise for combination of cetuximab with oxaliplatin as a first line therapy for patients with metastatic CRC[488]. The addition of EGFR targeted antibodies cetuximab or panitumumab to chemotherapy was further tested and found to show benefit, especially when patients had a cancer without a *KRAS* mutation[489–493]. However, the COIN trial, which investigated addition of cetuximab to oxaliplatin and 5-FU chemotherapy in first-line treatment of advanced CRC, did not confirm the synergistic benefit of cetuximab[494]. The NORDIC trial was another study including 566 patients which also investigated addition of cetuximab to oxaliplatin and 5-FU/folinic acid

chemotherapy in previously untreated advanced CRC[495], but again showed no benefit to patients. The New EPOC trial was carried out as an extension to the COIN and EPOC[496] studies and used very similar investigational strategies to assess any improvement of patient outcome with the addition of cetuximab to oxaliplatin and 5-FU therapy[132].

Antagonism between platinum drugs and cetuximab has been reported previously in KRAS wild-type CRCs[497]. ROS have been shown to mediate resistance to chemotherapy. For example, preclinical studies have shown that treatment with platinum drugs and cetuximab in combination with gefitinib in colon and lung cancer cells resulted in antagonistic effects because of inhibition of chemotherapy-induced ROS by EGFR-targeted agents[497,498]. By contrast, others have shown that EGFR inhibition by erlotinib resulted in ROS production via NOX4 overexpression[499].

ROS includes superoxide and hydrogen peroxide. In the cell, ROS are produced by the membrane bound enzymatic family of NADPH oxidases (NOX 1-5 and dual oxidases DUOX1/2)[500], the mitochondrial electron transport chain, xanthine oxidase as well as other systems[501–503]. ROS formation can lead to tumour initiation and / or progression (Chapter 1, Section 1.8). Therefore, ROS is an important signalling molecule which controls the balance between proliferation and anti-proliferative signalling pathways *in vivo,* especially in tumours and their microenvironment[504]. Inflammatory cells in the tumour microenvironment stimulate NOX-mediated ROS production by tumour cells leading to enhanced angiogenesis and altered DNA integrity promoting genomic instability[505].

The work in this chapter specifically involves DUOX2 and its obligate maturation factor DUOXA2 (Chapter 1, Section 1.15). In summary, DUOX2 was initially described as a H_2O_2-producing enzyme in the thyroid and does indeed have an important role in thyroid hormone biosynthesis[135]. DUOX2 has since been identified as an important part of the host defence system in the airway epithelium and our lab. has shown recently that DUOX2 and DUOXA2 form the predominant H_2O_2-producing enzyme system in the mucosa of the human gastrointestinal tract[136–139]. As a consequence of this work our lab has developed and used *DUOX2/DUOXA2* qPCR and *in situ* hybridisation (ISH) to identify and locate mRNA in the intestinal mucosa of patients with UC and CRC[139]. High levels of DUOX2 have

been observed in the colonic epithelium of IBD patients and in colonic and pancreatic cancers[141]. Recently, DUOX2 has been shown to be regulated by a STAT-dependent JAK-independent pathway[142].

In vitro lab. work by Daniel Hochhauser and colleagues found that cetuximab inhibited STAT1 activation and DUOX2-mediated ROS generation which opposed p38-dependent apoptosis by oxaliplatin[133], an observation which required additional supportive *in vivo* data. However, patient biopsies before and after treatment were not available from the New EPOC study and, therefore, a xenograft model was deemed necessary.

6.1.1 Hypotheses

- Cetuximab reduces the efficacy of oxaliplatin.
- *DUOX2* and *DUOXA2* expression is increased with oxaliplatin treatment, and reduced with cetuximab treatment.
- DUOX2 expression is increased with oxaliplatin treatment, and reduced with cetuximab treatment.
- Xenografts treated with cetuximab and oxaliplatin have more proliferating cells.

6.1.2 Aims

- Generate a xenograft mouse model using DLD1 cells. Treat with oxaliplatin and/or cetuximab.
- Analyse *DUOX2* and *DUOXA2* gene expression by RT-PCR, and DUOX2 protein expression by IHC.
- Assess the proliferation and apoptotic status of cells within xenograft tumours using Ki67 and caspase 3 staining.

6.2 Effect of cetuximab on ROS production by oxaliplatin

A mouse xenograft model was available via collaboration with Professor Kairbaan Hodivala-Dilke at the Barts Cancer Institute, QMUL. This involved nude (nu/nu) mice and their injection with DLD1 CRC cells in one flank and subsequent treatment with oxaliplatin and cetuximab alone and in combination. This portion of the work was performed within the animal unit at the St George's Hospital unit by Valeria Santoro and Ruochen Jia from Daniel Hochhauser's lab and Bruce Williams at the animal unit. At the endpoint of the study, I collected the xenograft tissue, split the xenograft tissue into two sections and fixed one piece of tissue with neutral buffered formalin, which was then embedded in paraffin wax by Rebecca Carroll from the pathology service at The Royal London Hospital. The second piece of tissue was submerged in Tissue Protect solution and then RNA extracted from these samples.

Proven techniques were used to determine levels of DUOX2 mRNA in the embedded xenograft tissue[139]. Gene expression of DUOX2 and DUOXA2 in the xenografts was measured by RT-PCR and expressed relative to control (GAPDH) (Figure 6.1.A and B) (Table A.6.1). DUOX2 mRNA expression was also confirmed using ISH (Figure 6.1.C). The RT-PCR data showed that dosing with oxaliplatin alone increased DUOX2 mRNA levels (p=0.11), whereas combination with cetuximab greatly attenuated this response to 5.3-fold (p=0.16) (Figure 6.1A and B). Analysis of DUOXA2 mRNA revealed a similar pattern to DUOX2 results; oxaliplatin alone significantly upregulated expression of DUOXA2 mRNA (p=0.02), while combination with cetuximab only increased DUOXA2 mRNA by 4.77-fold (p=0.02). DUOX2 gene expression determined by ISH (Figure 1C), identified the same pattern, however, fold changes were not as striking.

Results from DUOX2 IHC were in agreement with mRNA expression findings (Figure 6.2). Treatment with oxaliplatin alone increased DUOX2 protein expression of DUOX2 more than treatment with cetuximab or treatment with a combination of oxaliplatin and cetuximab, although differences between treatments were not statistically significant. DUOX2 mRNA and protein expression was shown to co-localise (Figure 6.3). Serial sections were used for ISH and IHC and positive staining was found in similar areas in each section.

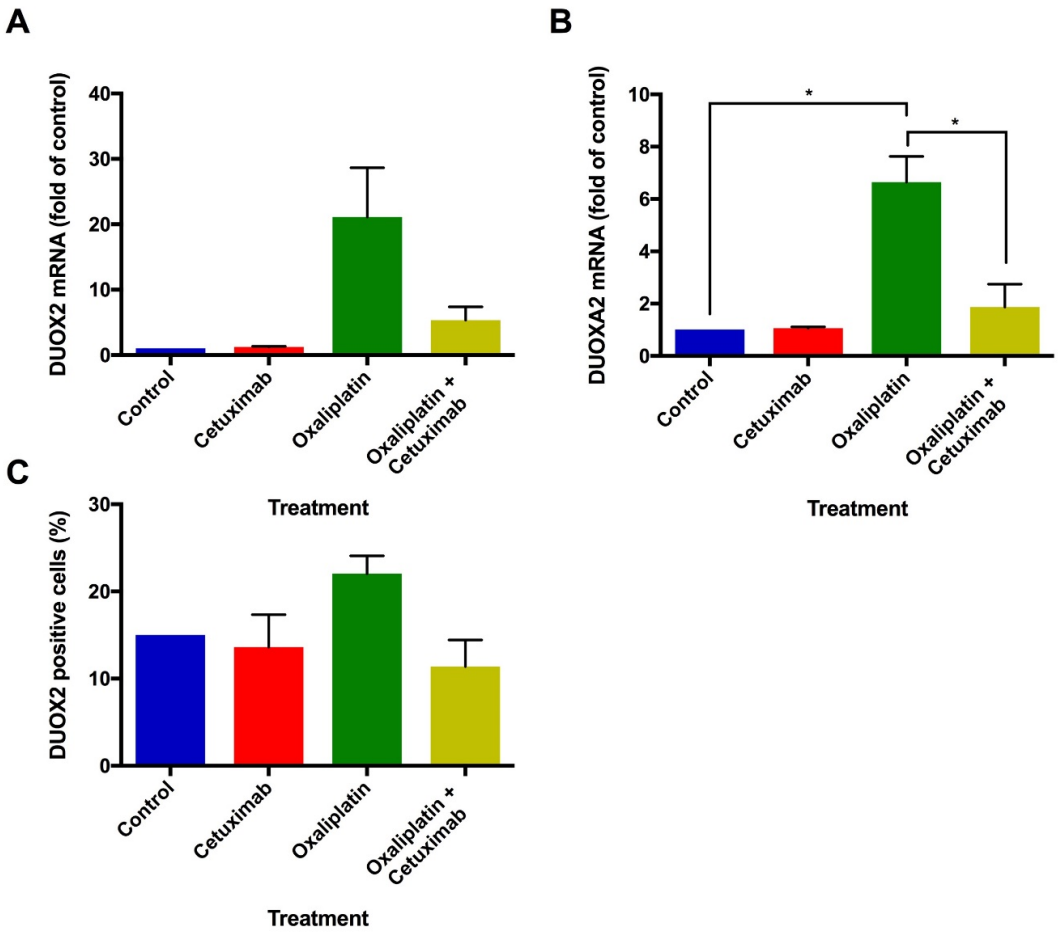

Figure 6.1. Effect of oxaliplatin and cetuximab treatment of DLD1 xenografts on DUOX2 and DUOXA2 mRNA. (A) Relative gene expression for mRNA for DUOX2 and **(B)** DUOXA2 determined by RT-PCR**, (C)** DUOX2 mRNA determined by ISH using xenograft sections (5µM); all results expressed as a fold-change (mean ± SEM) (Table 6.1) normalised to untreated control. N=3. Statistics was performed using two-tailed Student's *t* test with Welch's correction *p<0.05.

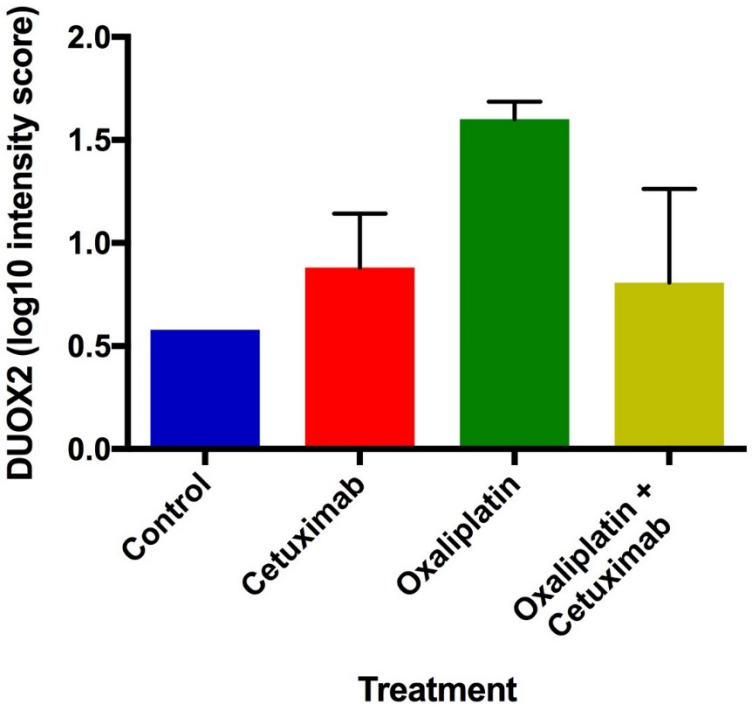

Figure 6.2. Effect of oxaliplatin and cetuximab treatment of DLD1 xenografts on DUOX2 protein expression. Xenograft sections (5 µM) were prepared and DUOX2 immunohistochemistry (IHC) was conducted and scored (mean ± SEM) (Table 6.1). No statistically significant observations were made. N=3.

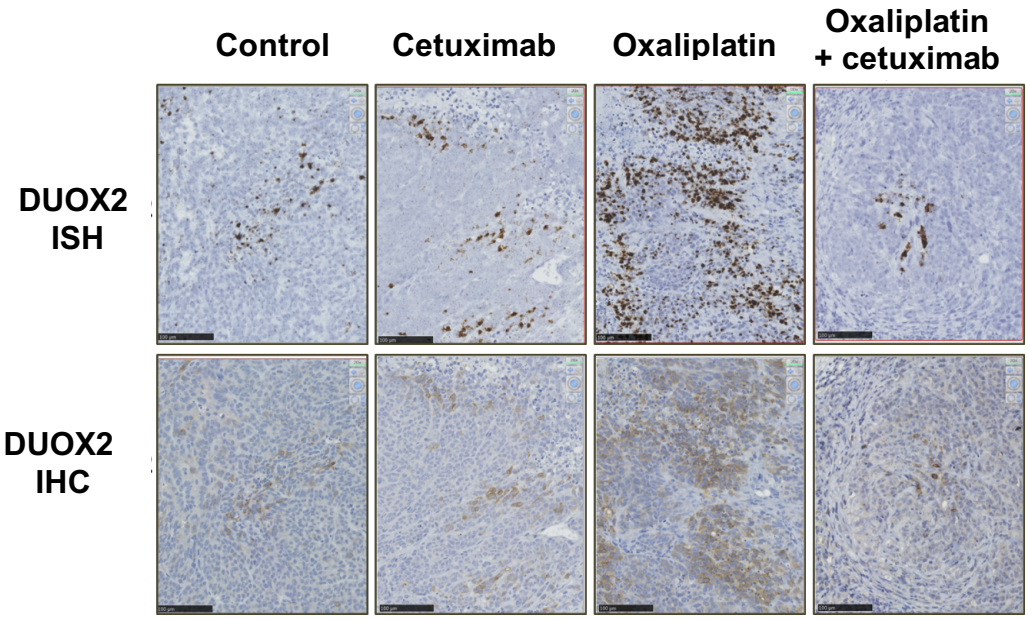

Figure 6.3. Effect of oxaliplatin and cetuximab treatment of DLD1 xenografts on DUOX2 mRNA and protein expression on serial xenograft sections. Representative images (40x magnification) of serial sections of xenograft, stained for DUOX2 mRNA by ISH and DUOX2 protein expression by IHC is presented for each treatment arm (scale bars = 100µm).

Table 6.1. Summary of DUOX2 mRNA fold change from control, DUOXA2 mRNA fold change from control, DUOX2 ISH and DUOX2 IHC. Data shown as mean ± SEM. See Figure 6.1,2,3.

Treatment	DUOX2 mRNA fold change from control	DUOXA2 mRNA from change from control	DUOX2 ISH score	DUOX2 IHC log 10 score
Control	1.00±0.00	1.00±0.00	15.02±0.00	0.58±0.00
Cetuximab	1.25±0.10	1.06±0.05	13.61±3.73	0.88±0.26
Oxaliplatin	21.11±7.53	6.64±0.99	22.03±2.07	1.60±0.09
Oxaliplatin + cetuximab	5.35±2.03	1.87±0.88	11.40±3.04	0.81±0.46

Ki67 IHC was used to determine proliferating cells within the xenografts (Figure 6.4.A, Figure 6.5) (Table 6.2). There were more Ki67 positive cells in xenografts treated with a combination of oxaliplatin and cetuximab compared to those treated with oxaliplatin alone. Caspase 3 IHC was used to determine apoptotic cells within the xenografts (Figure 6.4.B, Figure 6.6). The most apoptotic cells were found in mice treated with oxaliplatin alone, whereas the least apoptotic cells were found in the xenografts from mice treated with oxaliplatin and cetuximab, however, there was no significant difference.

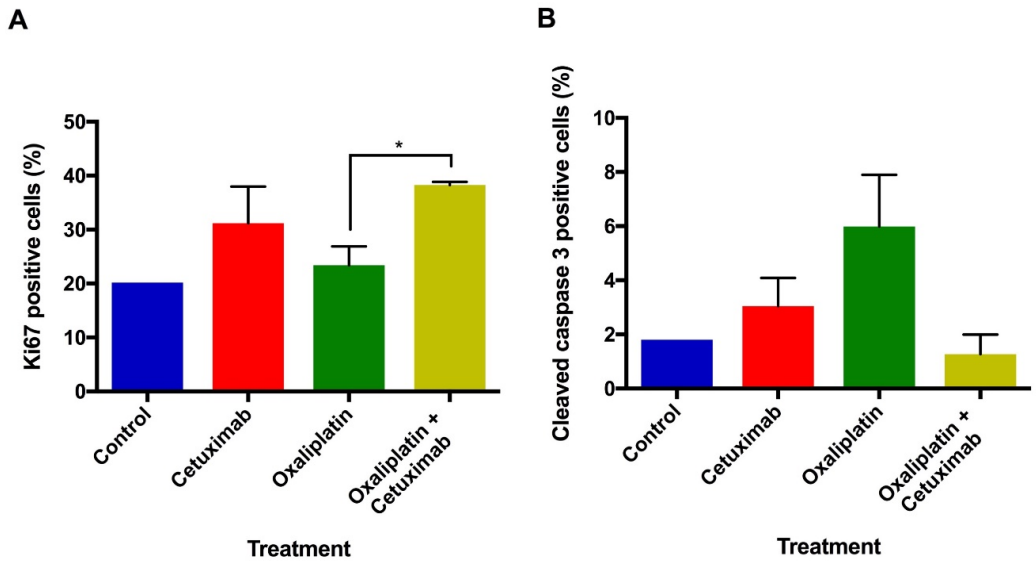

Figure 6.4. Effect of oxaliplatin and cetuximab treatment of DLD1 xenografts on proliferation and apoptosis. Proliferation and apoptosis of DLD-1 xenografts (n=3) treated with cetuximab, oxaliplatin alone or in combination were assessed using Ki67 (**A**) and cleaved caspase 3 (**B**) with results expressed as percentage positive cells (mean ± SEM) (Table 6.2). Statistics was performed using two-tailed, Student's *t*-test with Welch's correction *p<0.05.

Table 6.2. Summary of Ki67 and caspase 3 IHC. Data shown as mean ± SEM. Figure 6.4.

Treatment	**Ki67 IHC score**	**Caspase 3 IHC score**
Control	20.18±0.00	1.80±0.00
Cetuximab	31.20±6.77	3.05±1.04
Oxaliplatin	23.34±3.52	5.99±1.91
Oxaliplatin + cetuximab	38.28±0.57	1.27±0.72

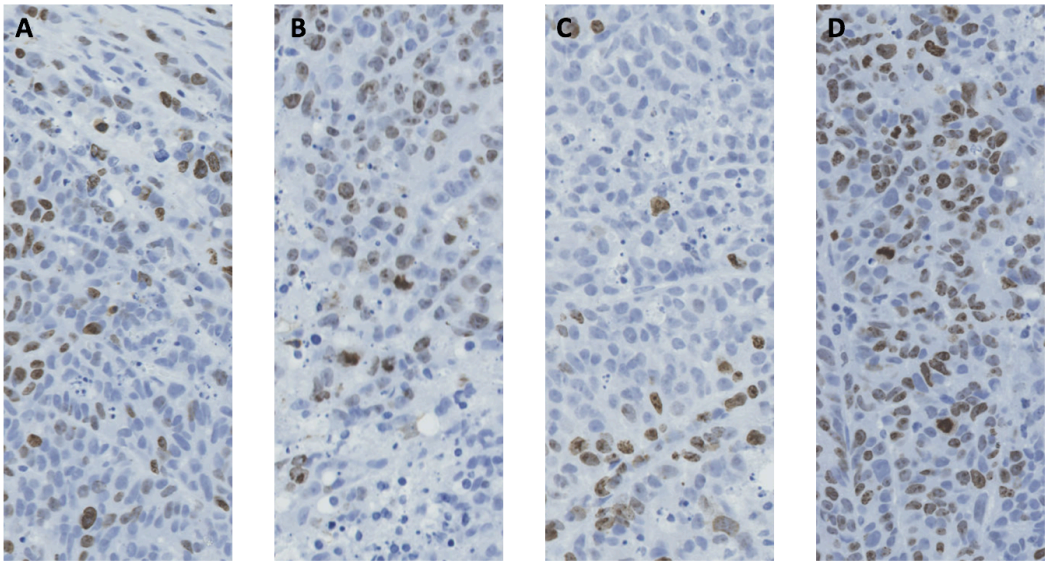

Figure 6.5. Representative images from Ki67 IHC. (A) Control, **(B)** Cetuximab treated, **(C)** Oxaliplatin treated and **(D)** Oxaliplatin and Cetuximab combined treated. Images taken at 20x from Nanozoomer scanner files.

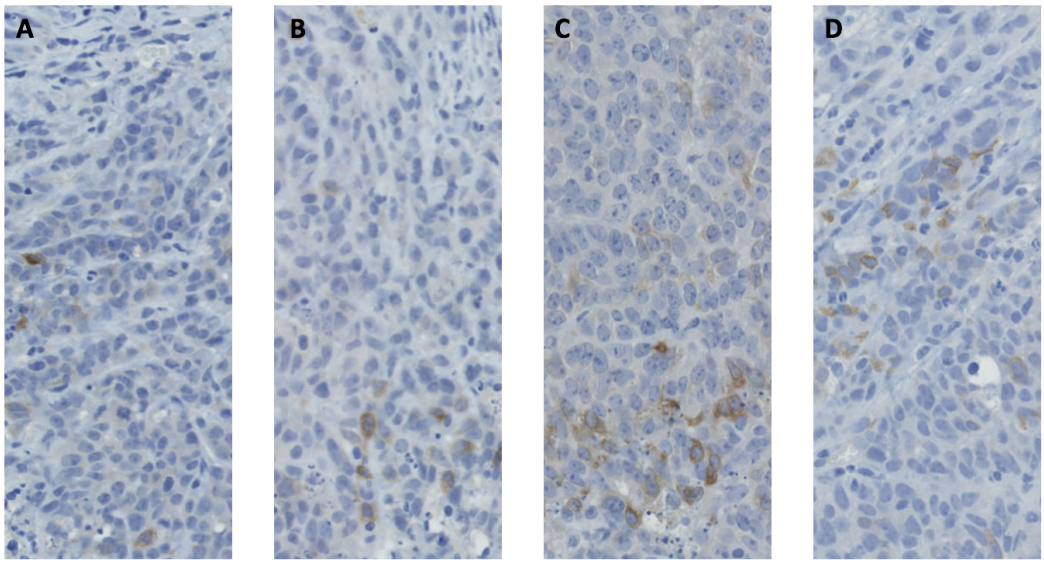

Figure 6.6. Representative images from Caspase 3 IHC. (A) Control, **(B)** Cetuximab treated, **(C)** Oxaliplatin treated and **(D)** Oxaliplatin and Cetuximab combined treated. Images taken at 20x from Nanozoomer scanner files.

6.3. Discussion

Both the *in vitro* data from Professor Hochhauser's group and my *ex vivo* data indicated that DUOX2/DUOXA2 induction by oxaliplatin is a dynamic process which occurs within 24 hours. In support of the *in vitro* data, treatment of xenograft animals with a combination of cetuximab and oxaliplatin showed higher tumour proliferation compared with oxaliplatin alone as highlighted by elevated Ki67 staining and reduced cleaved caspase 3 staining. *DUOX2*/*DUOXA2* mRNA expression was also in accordance with the *in vitro* findings: expression was increased by oxaliplatin treatment alone and reduced by combination with cetuximab, although statistical significance was only reached by *DUOXA2*. The same pattern was observed with DUOX2 protein levels[133].

In response to oxaliplatin therapy alone, the increase in *DUOX2* mRNA and protein led to subsequent elevation in ROS. Elevated ROS induced by oxaliplatin therapy resulted in activation of p38 and subsequent cell death. Cetuximab has inhibitory effects on EGFR as well as ROS production. Combination of cetuximab with oxaliplatin results in impaired activation of ROS-dependent cell death mechanisms induced by oxaliplatin via phosphorylation of p38. ROS is known to modulate response to chemotherapy and other studies have shown involvement of different NADPH oxidases (NOX) in producing ROS following chemotherapy[497,506].

The combined work identified that STAT1 mediates *DUOX2* transcription by direct promoter binding following treatment with oxaliplatin whereas cetuximab inhibits STAT1 activation, oxaliplatin-induced DUOX2 upregulation, and ROS generation[133].

It is likely that regulation of DUOX2/DUOXA2 expression in mouse xenografts and human tumours in response to oxaliplatin and cetuximab treatment is complex. For example, modulation of DUOX2 expression could be a direct effect of drugs, mouse/human immune response to the tumour cells influenced directly or indirectly by drug exposure, and / or a response to tumour cell death caused by the drugs.

It is important to note that our study has limitations. In the future, the effects described need to be examined in clinical samples from patients receiving oxaliplatin alone or in combination with cetuximab; unfortunately, these specimens were not available[133]. The effects of combination treatment on ROS production demonstrated here needs to be

balanced against the contribution made by EGFR inhibition of DNA repair and immune response, which would potentially favour this combination[507,508]. This could explain why the interaction of EGFR-inhibitory antibodies and chemotherapy is beneficial in some studies[491,509]. It is, therefore, critical to assess the effects of combining drugs for therapy by additional approaches, including patient-derived xenografts and analysis of circulating tumour cells. However, we have described an important mechanism of undesirable interaction between oxaliplatin and cetuximab that might explain why a subset of CRC patients does not respond to this combination. The study also provides a novel explanation for unexpected trial results and could be used for optimisation of studies for future combination therapies.

Chapter 7 – Conclusion

Fumarate has been identified previously as a oncometabolite[332,510]. It is known that fumarate is a competitive inhibitor of 2-OGDDs which includes the HIF hydroxylases and TET dioxygenases, leading to activation of oncogenic pathways[403]. Another mechanism of fumarate action is the non-enzymatic alteration of cysteine residues by succination which can disrupt protein function and, therefore, lead to dysfunctional cell signalling and metabolism[406]. Previous studies of succination have shown it is increased in diabetic tissue[343] and in HLRCC where one copy of FH is not mutated[374].

The literature has previously identified an increase in [fumarate] in CRC tissue compared to normal tissue[335]. The mechanism for the increase in [fumarate] in CRC is not clear, however, it is likely due to an increased use of glycolysis and the TCA cycle which helps the cancerous tissue to proliferate. In Chapter 3, this study provided the first report of increased succination in adenomatous and CRC tissue and significantly higher amounts of succination in tumour tissue compared to the normal bowel. There is an additional increase in succination if the CRC sample is from a T2D compared to a non-diabetic patient. The 2-SC staining was non-uniform across tumour tissue, underlining the metabolic heterogeneity of CRC. This is reinforced by evidence from *in vitro* work in Chapter 5 which identified [fumarate] was dependent on cell line, but was generally higher when cells are cultured with 25mM glucose and held in 0.2% O_2. Suggesting that increased [fumarate] in cell lines could be a result of external stress in the form of hypoxia or high glucose.

Upon further study, in Chapter 3, it was noted that T2D patients with *KRAS*/*BRAF* mutations in cancers had more succination compared to T2D patients with WT *KRAS*/*BRAF.* This is a further novel link; the influence of *KRAS*/*BRAF* mutation on succination should be pursued. It could be speculated that succination is one reason why CRC in T2D individuals is more invasive and more likely to relapse.

Succination was not studied in the *Fh1βKO* mouse model in Chapter 4, but is planned for future work (Chapter 8, Section 8.2). Based on our findings to date, of a small difference in succination in a small number of human adenomas, I would hypothesise that all polyps would show some evidence of succination, but that there would be no significant

difference in 2-SC staining intensity in polyps from diabetic and non-diabetic mice. Evidence of succination was found in DLD1 and SW837 cell lines, however, it could not be linked to [glucose] at this point. I would hypothesise that CRC cells cultured in hypoxia and high glucose would have increased succination compared to CRC cells cultured in normoxia and low glucose. Unfortunately, the identify of proteins that are succinated in CRC remains unknown at this point of writing and will require further investigation using, for example, micro-dissection of succinated areas and mass spectroscopy.

Interestingly, despite high levels of succination in CRC tissue, there was also an increase in FH in CRC tissue compared to adjacent normal tissue, which was opposite to what was predicted. In Chapter 3, FH staining in CRC samples was overwhelmingly cytoplasmic, but it was unclear if FH staining was also high in mitochondria. Evidence from the Human Protein Atlas suggests that FH staining is intense for a large number of cancers including CRC, breast, prostate, liver and lung[511]. It is possible that as fumarate levels rise, due to increased glycolysis and TCA cycle metabolism use, so do FH levels, then as levels of fumarate increase further FH can be inhibited, as shown by Mescam *et al*.[390]. Additionally, in Chapter 4, when FH was overexpressed in the cytoplasm of all cells in a mouse model of intestinal polyposis and diabetes, larger polyps were found. This suggests a potential role for cytoplasmic FH in tumourigenesis. Coupled with the fact that there are no indications of FH mutation in human CRC, this suggests that FH remains active but cannot control levels of fumarate. Studies involving measurement of both [fumarate] and FH activity in CRC tissue would bring evidence to support or disprove this theory.

In Chapter 5 the abundance of FH *in vitro* did not correlate with levels of fumarate in CRC cells. It is necessary to quantify the level of FH in normal epithelial bowel cells to determine the difference between normal and cancer cells. However, FH activity was lower where [fumarate] was increased, suggesting that FH activity is influenced by [fumarate] or *vice versa*. However, [fumarate] recorded in CRC cells in this study was not high enough to inhibit FH according to Mescam *et al*.[390]. Nevertheless, this warrants further study. Additionally, the readings for FH activity were established using whole cell extract. The majority of FH was found in the mitochondria and not in the cytoplasm or nucleus of CRC cells. This mimics what is seen in HLRCC patients which suggests some sort

of default in FH^{325}. It would be interesting to see if there are differences in FH activity between the cytoplasm and the mitochondria.

In Chapter 3 it was found that the addition of FH^{cyt} reduced the available glucose found in the gut tissue, suggesting that more glucose was used in metabolism and potentially polyposis. Perhaps the increase in FH in human CRC tissue is to increase the use of glucose and fumarate through the glycolysis and TCA cycle pathways, to generate more energy for tumorigenesis.

The finding in Chapter 5, that all CRC cells in this study have quantifiable OCR suggests that CRC cells are using the TCA cycle to generate NADH for ATP production via OXPHOS. Notably it was also found that OCR decreased when glucose was added to the media of cells cultured in 0mM glucose. This suggests that CRC cells are flexible with regards metabolism pathways, which is, of course, a desirable trait for cancer cells. Further study into the functionality of mitochondria would allow further links to [glucose] and [fumarate] to be made.

Overall, there remains a lot to be identified about the specific role of FH, fumarate and succination in CRC and T2D. An initial mechanism can be suggested. Once CRC starts to progress, fumarate increases and more succination occurs. This means that more of the proteins in the cell are unable to work properly, which can promote the cancer. On top of this, there is a further increase in succination in CRC samples from T2D patients suggesting that additional glucose can further promote succination. This could be one reason why CRC in T2D patients is more aggressive and had a poorer outcome.

The additional finding that overexpression of *FH* in intestinal cells in a mouse model of CRC leads to larger polyps was also novel. It is yet to be shown if more intense FH staining in CRC leads to a poorer outcome or the opposite.

It is important to highlight this work to clinicians working with T2D and CRC patients. Clinicians could encourage T2D patients to control their blood glucose by emphasising the possible risk of cancer associated with uncontrolled blood glucose.

It is important to educate the wider population so they fully understand the risks of T2D, which would hopefully lead to a reduction in T2D and CRC cases. My public engagement

work, listed below, has attempted to highlight the risks of T2D and CRC to the general public.

- Pint of Science, 2016

- QMUL Festival of Ideas, 2017

- Science Showoff, 2017-2018

- FameLab London Finals 2017, FameLab Cambridge Finals 2018

In a separate piece of work, in Chapter 6, I was able to help identify that following treatment with oxaliplatin, *DUOX2* transcription is mediated by STAT1, whereas cetuximab treatment inhibits STAT1 activation, oxaliplatin-induced DUOX2 upregulation, and ROS generation[133]. This mechanism may explain why CRC patients on oxaliplatin alone have a better prognosis than those treated with a combination of oxaliplatin and cetuximab.

Chapter 8 – Future Work

The work in this thesis on the link between T2D and CRC leads to the future research questions. These are given below along with potential experimental procedures.

8.1 Future work based on findings presented in Chapter 3

Findings presented in Chapter 3 indicate that a large patient study, possibly as a multi-centre trial, would be appropriate. The main questions would be:

1) Can the management of T2D and / or CRC be improved using a 2-SC score? Experiments would aim to answer the following:
    a. In CRC, is succination higher the longer the patient has been diagnosed as a T2D?
    b. Is a high 2-SC score indicative of poor prognosis?
    c. Can succination levels be measured meaningfully in blood as well as the tumour and can the output score be used as a prognostic biomarker?
    d. Is there a CRC preventative or pre-operative therapy that will lower 2-SC, reduce risk and improving outcome, respectively? Is metformin useful in this regard[512,513]?
    e. If T2D is well controlled, is 2-SC lower and does this reduce the risk of CRC?
2) What is the role of FH in human CRC?
    a. Which cellular compartment(s) is FH increased in CRC compared to normal tissue?
    b. Is FH active in human CRC?
    c. Does FH expression correlate with the presence of 2-SC?
    d. Is FH expression determined by fumarate levels in the tumours and is the ability of FH to reduce succination by fumarate limited, e.g. by compartmentalisation, such that 2-SC still occurs at high levels?
    e. Can FH act as an oncogene in particular context in CRC?
3) Which proteins are succinated in patients with T2D and CRC and how does this chemical process alter the activity of key proteins?

4) Do pre-adenoma dysplastic regions in the gut show 2-SC and, if so, which proteins are altered?

To answer these questions, the following would be necessary to support experimental protocols:

The study would have two independent cohorts and include the following types of patients:

- *Patients ± T2D and ± CRC; and*
- *Patients ± T2D and ± CRC adenoma and / or dysplasia.*

The following information would be recorded from the appropriate patients:

- *Age;*
- *Sex;*
- *Ethnicity;*
- *Stage of CRC;*
- *Type of T2D therapy;*
- *Type of CRC therapy;*
- *Any other medications, particularly metformin;*
- *Time diagnosed with T2D;*
- *Time diagnosed with CRC; and*
- *Control of T2D – preferably monitor blood glucose levels daily / weekly.*

A biopsy of normal and CRC tissue would be taken to determine:

- *Mutation profile of CRC determined by array or PCR;*
- *2-SC IHC of normal and CRC/adenoma/dysplastic tissue, scored by a trained pathologist;*
- *FH IHC of normal and CRC/adenoma/dysplastic tissue, scored by a trained pathologist;*
- *Detection of succinated proteins by mass spectrometry; and*
- *FH activity.*

A blood sample would also be taken to attempt to detect succinated proteins in blood; if this correlates with 2-SC in tumours and could be used to monitor CRC in patients more easily as a non-invasive biomarker.

8.2 Future work based on findings presented in Chapter 4

To complement the human work, it is necessary to further investigate the relationship between T2D and CRC in a whole animal system, of which the mouse remains the best model currently available for the earlier polyp stage.

Some questions remain regarding the mouse model developed in Chapter 4 of this thesis. These are:

1) Does knocking out FH in the cytoplasm of bowel epithelial cells lead to smaller or fewer polyps?
   Create 1322 mice with genetic conditional KO of Fh1 in bowel epithelial cells with mice and breed with mice with KO Fh1 in the ß-cells of the pancreas. Count and size the resultant polyps.
2) What is the mRNA expression profile of the polyps from different genotypes?
   Extract RNA from frozen polyps, send for array, analyse the data. Test any key findings in cell models to validate their tumorigenic potential.
3) What is the 2-SC, FH, HIF-1α, Ki67, caspase 3 score of the polyps and normal tissue from the different genotypes?
   Perform immunohistochemistry to identify differences in levels of the markers.
4) Do succination targets differ across the different genotypes?
   Use frozen polyps for mass spectrometry analysis to identify succinated proteins. Link differences to genotypes or blood glucose. Cross reference finding with mass spectrometry findings from Chapter 8, Section 8.2.
5) What is the effect of metformin therapy in the model?
   Re-measure all the parameters in this thesis and mentioned above.

The Fh1βKO mouse is a valuable new model for T2DM where glucose intolerance develops progressively and the mice are not obese and the model does not require alterations in diet. However, there are many challenges in developing the ideal model of T2D and CRC in the mouse. Currently, the mouse models for T2D and CRC have limitations (Chapter 1, Section 1.14). Ideally, the 'perfect' model would have features similar to the human tumour pathologies, such as polyps which progress to adenomas, cancers in the large

bowel and development of T2D as part of the ageing process through insulin resistance and hyperinsulinemia. Any new CRC model could then be used to repeat many of the measurements taken in this thesis.

8.3 Future work based on findings presented in Chapter 5

To further complement the mouse and human work it is important to do further mechanistic work *in vitro*. Following on from the work in Chapter 5, the possible questions and experimental work are outlined below:

1) Continue investigating the differences of DLD1 and SW837 cells grown in 25mM, 5mM or 0mM after treatment with 20.9% and 0.2% oxygen. Culture cells with insulin to make a model closer to physiological diabetic conditions *in vivo.* Measure the following:

- *FH activity in mitochondria, cytoplasm and nuclear fractions of cells;*
- *Glucose uptake by colourimetric / fluorometric assay pre- and post-treatment with glucose over a time course;*
- *Determine ratio of cells in cell cycle phases by flow cytometry;*
- *NAD/NADH ratio by colourimetric / fluorometric assay;*
- *ROS by immunofluorescence;*
- *Survival after drugs – cell count post drug treatment;*
- *Western blots to parallel the qPCR panel;*
- *Measure the mitochondrial membrane potential;*
- *Image mitochondria using electron microscopy to analyse structure changes;*
- *Cell migration by scratch assay;*
- *Overexpress and knock out FH and see if there is an effect on all the parameters measured in this thesis;*
- *Identify succinated proteins by mass spectrometry; and*
- *Attempt to build a spheroid and/or 3D organotypic model from intestinal epithelial cells. Which cells, CRC lines or primary cells from surgical resection, can create the most useful spheroids and organotypics? What influence does hypoxia play in proliferation and survival?*

2) Artificially alter fumarate levels in the cell model to test what happens to cell viability, gene expression and succination.

3) Culture intestinal organoids in different concentrations of glucose and measure the parameters used in this thesis to identify any changes.

4) What are the functional consequences of succination? Does it affect protein half-life? Is a succinated protein targeted for degradation?

   It may eventually be possible to identify an appropriate cell where the known succinated protein is present. Then, over-express said protein, dose with fumarate to increase succination and measure the effects (proliferation, protein turnover, protein localisation and drug-resistance).

8.4 Future work based on findings presented in Chapter 6

Additional further work questions based on the findings of the DUOX2 chapter are outlined below:

1) What is the optimum level of DUOX2 and production of hydrogen peroxide for CRC tumorigenesis? Is increased hydrogen peroxide production over a prolonged period of time sufficient to transform cells.
   Overexpress DUOX2 in CRC cells and measure:
   - *Proliferation rate;*
   - *Viability;*
   - *Response to drug challenge; and*
   - *Ability to form xenograft tumours.*
2) Would cyclic therapy of cetuximab and oxaliplatin be beneficial?
   Test a cyclic regime of cetuximab and then oxaliplatin therapy in an animal model of CRC. Measure tumour size and survival of animals.
3) Do all EGFR inhibitors reduce phosphorylation of STAT1? And, therefore, should be avoided in combination with oxaliplatin?
   Test if STAT1 phosphorylation is inhibited in response to EGFR inhibitor therapy in CRC cells. Determine if DUOX2 mRNA and protein levels are reduced after EGFR therapy in CRC cells.

4) Conditionally overexpress DUOX2/DUOXA2 in the mouse intestinal epithelium and assess resultant pathology.

Taken together this work would uncover more details surrounding the role of fumarate, FH and succination in the progression of CRC, as well as the link to T2D. It is also important to use the same approach as outlined in this thesis to look at other cancers, such as breast cancer, which are also linked to T2D[281,514].

Additionally, the role of DUOX2 in CRC progression would also be clearer, particularly in the context of IBD. And the optimum therapy for combined drug regimen where DUOX2 expression is important can be investigated. The mouse model of increased DUOX2/DUOXA2 will be important here.

Chapter 9 - Appendix

9.1 Chapter 3

Table A.3.1. Summary of two-way ANOVA of 2-SC score for matched normal and CRC tissue. See also Figure 3.2.

	F (DFn, DFd)	p value	p value summary
Interaction	F (1, 162) = 5.983	0.0194	*
Non-diabetic vs T2D	F (1, 162) = 75.33	0.0059	**
Normal vs CRC	F (1, 1620) = 6.074	<0.0001	****

Table A.3.2. Summary of Bonferroni *post hoc* test of 2-SC score for matched normal and CRC tissue. Only significant values shown. See also Figure 3.2.

	Summary
ND:Normal vs ND:CRC	****
ND:Normal vs T2D:CRC	****
ND:CRC vs T2D:Normal	****
ND:CRC vs T2D:CRC	**
T2D:Normal vs T2D:CRC	****

Table A.3.3. Summary of two-way ANOVA of 2-SC scores for matched normal and adenoma tissue. See also Figure 3.3.

	F (DFn, DFd)	p value	p value summary
Interaction	F (1, 56) = 2.762	0.1021	ns
ND vs T2D	F (1, 56) = 2.125	0.1505	ns
Normal vs CRC	F (1, 56) = 24.41	<0.0001	****

Table A.3.4. Summary of Bonferroni *post hoc* test of 2-SC scores for matched normal and adenoma tissue. See also Figure 3.3.

	Summary
ND:Normal vs ND:Adenoma	****
ND:Adenoma vs T2D:Normal	***

Table A.3.5. Summary of one-way ANOVA of 2-SC score in total normal, CRC adenoma and CRC tissue. See also Figure 3.4.A.

p value	Summary
<0.0001	****

Table A.3.6. Summary of Bonferroni *post hoc* test of 2-SC score in total normal, CRC adenoma and CRC tissue. See also Figure 3.4.A.

	Adjusted p value	p value summary
Normal vs. Adenoma	<0.0001	****
Normal vs. CRC	<0.0001	****
Adenoma vs. CRC	0.0432	*

Table A.3.7. Summary of two-way ANOVA of 2-SC score in total normal, CRC adenoma and CRC tissue. See also Figure 3.4.B.

	F (DFn, DFd)	p value	p value summary
Interaction	F (2, 291) = 7.454	0.0008	***
ND vs T2D	F (1, 201) = 0.4049	0.5253	ns
Normal vs CRC	F (2, 201) = 78.08	<0.0001	****

Table A.3.8. Summary of Bonferroni *post hoc* test of 2-SC score in total normal, CRC adenoma and CRC tissue. Only significant values shown. See also Figure 3.4.B.

	Summary
ND:Normal vs ND:Adenoma	****
ND:Normal vs ND:CRC	****
ND:Normal vs TD2:CRC	****
ND:Adenoma vs T2D:Normal	****
ND:Adenoma vs T2D:CRC	**
ND:CRC vs T2D:Normal	****
ND:CRC vs T2D:CRC	***
T2D:Normal vs T2D:CRC	****
T2D:Adenoma vs T2D:CRC	***

Table A.3.9. Summary of two-way ANOVA of 2-SC score for WT and *KRAS*/*BRAF* mutant CRC samples from NDs and T2Ds. See also Figure 3.7.B.

	F (DFn, DFd)	**p value**	**p value summary**
Interaction	F (1, 74) = 0.008782	0.9256	ns
WT vs Mutant	F (1, 74) = 2.445	0.01222	ns
Non-diabetic vs T2D	F (1, 74) = 9.169	0.0034	**

Table A.3.10. Summary of Bonferroni *post hoc* test of 2-SC score for WT and *KRAS*/*BRAF* mutant CRC samples from NDs and T2Ds. See also Figure 3.7.B.

	Summary
WT:NB vs. Mutant:T2D	*

Table A.3.11. Summary of two-way ANOVA of 2-SC score for WT and *KRAS*/*BRAF* mutant CRC samples from NDs and T2Ds. See also Figure 3.7.D.

	F (DFn, DFd)	**p value**	**p value summary**
Interaction	F (1, 74) = 0.008642	0.9262	ns
WT vs Mutant	F (1, 74) = 2.851	0.0956	ns
Non-diabetic vs T2D	F (1, 74) = 6.524	0.0127	*

9.2 Chapter 4

Table A.4.1. Summary of one-way ordinary ANOVA for blood glucose. See also Figure 4.3.

	F (DFn, DFd)	p value	p value summary
Blood glucose	F (7, 102) = 114.9	P<0.0001	****

Table A.4.2. Summary of one-way ordinary ANOVA Bonferroni *post hoc* test for blood glucose. See also Figure 4.3, Table A.4.1. Only significant values shown.

	p value	p value summary
WT vs. *Fh1ΔKO* FH^{cyt}	0.0032	**
WT vs. *Fh1ΔKO*	<0.0001	****
WT vs. *Fh1ΔKO 1322*	<0.0001	****
1322 vs. *Fh1ΔKO*	<0.0001	****
1322 vs. *Fh1ΔKO 1322*	<0.0001	****
FH^{cyt} vs. *Fh1ΔKO*	<0.0001	****
FH^{cyt} vs. *Fh1ΔKO 1322*	<0.0001	****
FH^{cyt} *1322* vs. *Fh1ΔKO*	<0.0001	****
FH^{cyt} *1322* vs. *Fh1ΔKO 1322*	<0.0001	****
Fh1ΔKO FH^{cyt} vs. *Fh1ΔKO*	<0.0001	****
Fh1ΔKO FH^{cyt} vs. *Fh1ΔKO 1322*	<0.0001	****
Fh1ΔKO FH^{cyt} *1332* vs. *Fh1ΔKO*	<0.0001	****
Fh1ΔKO FH^{cyt} *1332* vs. *Fh1ΔKO 1322*	<0.0001	****
Fh1ΔKO vs. *Fh1ΔKO 1322*	<0.0001	****

Table A.4.3. Summary of one-way ordinary ANOVA of gut length. See also Figure 4.5.

	F (DFn, DFd)	p value	p value summary
Total	F (7, 51) = 3.332	0.0053	**
SB	F (7, 51) = 3.432	0.0044	**
LB	F (7, 51) = 0.7037	0.6687	ns

Table A.4.4. Summary of one-way ordinary ANOVA Bonferroni *post hoc* test of gut length. See also Figure 4.5, Table A.4.6. Only significant values shown.

		p value	p value summary
Total	*1322* vs. *Fh1ΔKO*	0.0025	**
	FH^{cyt} 1322 vs. *Fh1ΔKO*	0.0025	**
	Fh1ΔKO FH^{cyt} vs. *Fh1ΔKO*	0.0499	*
	Fh1ΔKO FH^{cyt} 1332 vs. *Fh1ΔKO*	0.0391	*
SB	*1322* vs. *Fh1ΔKO*	0.0020	**
	FH^{cyt} 1322 vs. *Fh1ΔKO*	0.0034	**

Table A.4.5. Summary of one-way ordinary ANOVA of cell type count. See also Figure 4.11,12,13.

Cell type	Location	F (DFn, DFd)	p value	p value summary
Epithelial	**Crypt**	F (7, 16) = 0.5894	0.7553	ns
	Villi	F (7, 16) = 0.8975	0.5315	ns
Goblet	**Crypt**	F (7, 16) = 0.5574	0.7792	ns
	Villi	F (7, 16) = 1.338	0.2957	ns
Paneth	**Crypt**	F (7, 16) = 1.941	0.1289	ns

Table A.4.6. Summary of one-way ordinary ANOVA Bonferroni *post hoc* test of paneth cell counts. See also Figure 4.13.

Stain	Cell	Condition	**p value**	**p value summary**
Paneth	**Crypt**	*Fh1βKO FH^{cyt}* vs. *Fh1βKO FH^{cyt} 1322*	0.0108	*

Table A.4.7. Summary of one-way ordinary ANOVA for polyp count by genotype. See also Figure 4.8.A.

	F (DFn, DFd)	**p value**	**p value summary**
Genotype	F (3, 44) = 2.593	0.0645	ns

Table A.4.8. Summary of two-way ANOVA for polyps by site. See also Figure 4.10.B, C.

		F (DFn, DFd)	**p value**	**p value summary**
Site	Interaction	F (9, 176) = 0.9883	0.4514	ns
	Polyp site	F (3, 176) = 29.05	<0.0001	****
	Genotype	F (3, 176) = 5.397	0.0014	**
Site (%)	Interaction	F (9, 176) = 1.565	0.1290	ns
	Polyp site	F (3, 176) = 67.14	<0.0001	****
	Genotype	F (3, 176) = 0.5222	0.6676	ns

Table A.4.9. Summary of two-way ANOVA Bonferroni *post hoc* test for polyps by site. See also Figure 4.9.B, C, Table A.4.12. Only significant values shown.

	Condition	**p value summary**
Site	**SB1** *Fh1βKO 1322* vs. *FH^{cyt} 1322*	**
	SB1 *Fh1βKO FH^{cyt} 1322* vs. *FH^{cyt} 1322*	*
Site (%)	**SB1** *FH^{cyt} 1322* vs. 1322	*

Table A.4.10. Summary of two-way ANOVA for polyps by size results. See also Figure 4.9.

		F (DFn, DFd)	p value	p value summary
Size	Interaction	F (9, 176) = 1.135	0.3402	ns
	Polyp size	F (3, 176) = 2.883	0.0373	*
	Genotype	F (3, 176) = 4.977	0.0024	**
Size (%)	Interaction	F (9, 176) = 2.169	0.0263	*
	Polyp size	F (3, 176) = 6.98	0.0002	***
	Genotype	F (3, 176) = 0.4521	0.7161	Ns
SB1	Interaction	F (9, 176) = 2.089	0.0328	*
	Polyp site	F (3, 176) = 1.196	0.3128	ns
	Genotype	F (3, 176) = 4.252	0.0063	**
SB2	Interaction	F (9, 176) = 0.9839	0.4550	ns
	Polyp site	F (3, 176) = 1.38	0.2506	ns
	Genotype	F (3, 176) = 2.783	0.0424	*
SB3	Interaction	F (9, 176) = 1.15	0.3303	ns
	Polyp size	F (3, 176) = 3.899	0.0099	**
	Genotype	F (3, 176) = 1.529	0.2086	ns
LB	Interaction	F (9, 176) = 0.9324	0.4984	ns
	Polyp size	F (3, 176) = 3.829	0.0109	*
	Genotype	F (3, 176) = 0.8133	0.4881	ns

Table A.4.11. Summary of two-way ANOVA Bonferroni *post hoc* test for polyps by size.

See also Figure 4.9.A, B, Table A.4.14. Only significant values shown.

	Condition	**p value summary**
Size	**3+** *FH^{cyt} 1322* vs. *1322*	*
Size (%)	**3+** *FH^{cyt} 1322* vs. *1322*	**
SB1	**3+mm** *Fh1βKO 1322* vs. *FH^{cyt} 1322*	**
	3+mm *Fh1βKO FH^{cyt} 1322* vs. *FH^{cyt} 1322*	*
	3+mm *FH^{cyt} 1322* vs. *1322*	***
SB3	**1-2mm** *Fh1βKO FH^{cyt} 1322* vs. *1322*	*
LB	**2-3mm** *FH^{cyt} 1322* vs. *1322*	*

9.3 Chapter 5

Table A.5.1. Summary of one-way ANOVA statistics for fumarate concentration in CRC cell lines determined by mass spectrometry. See also Figure 5.1.

Cell line	F (DFn, DFd)	p value	p value summary
DLD1 (Figure 5.1.A)	F (2,6) = 26.49	0.0011	**
HT55 (Figure 5.1.B)	F (2,6) = 121.3	<0.0001	****
SW837 (Figure 5.1.C)	F (2,6) = 22.21	0.0017	**

Table A.5.2. Summary of Bonferroni *post hoc* test values for fumarate concentrations in CRC cell lines determined by mass spectroscopy. See also Figure 5.1.

	Condition	p value	p value summary
DLD1 (Figure 5.1)	20.9% O_2 vs. 1% O_2	0.0897	ns
	20.9% O_2 vs. 0.2% O_2	0.0011	**
	1% O_2vs. 0.2% O_2	0.0138	*
HT55 (Figure 5.1)	20.9% O_2 vs. 1% O_2	<0.0001	****
	20.9% O_2 vs. 0.2% O_2	<0.0001	****
	1% O_2vs. 0.2% O_2	0.0248	*
SW837 (Figure 5.1)	20.9% O_2 vs. 1% O_2	0.0035	**
	20.9% O_2 vs. 0.2% O_2	0.0036	**
	1% O_2vs. 0.2% O_2	>0.9999	ns

Table A.5.3. Summary of one-way ANOVA statistics for doubling time. See also Figure 5.2.

Cell line	F (DFn, DFd)	p value	p value
DLD1 (Figure 5.2.A)	F (2,6) = 128.9	<0.0001	****
HT55 (Figure 5.2.B)	F (2,6) = 6.043	0.0365	*
SW837 (Figure	F (2,6) = 2469	<0.0001	****

Table A.5.4. Summary of Bonferroni *post hoc* test values for doubling time. See also Figure 5.2.

	Conditions	p value	p value
DLD1 (Figure 5.2.A)	25mM vs. 5mM	0.0002	***
	25mM vs. 0mM	<0.0001	****
	5mM vs. 0mM	<0.0001	****
HT55 (Figure 5.2.B)	25mM vs. 5mM	<0.999	ns
	25mM vs. 0mM	0.0874	ns
	5mM vs. 0mM	0.0596	ns
SW837 (Figure 5.2.C)	25mM vs. 5mM	<0.0001	****
	25mM vs. 0mM	<0.0001	****
	5mM vs. 0mM	<0.0001	****

Table A.5.5. Summary of two-way ANOVA statistics for viability. See also Figure 5.4.

	ANOVA table	F (DFn, DFd)	p value	p value summary
DLD1 (Figure 5.4.A)	Interaction	F (2, 24) = 37.86	<0.0001	****
	Glucose	F (2, 24) = 39.95	<0.0001	****
	Oxygen	F (1, 24) = 148.4	<0.0001	****
SW837 (Figure 5.4.B)	Interaction	F (2, 24) = 9.151	0.0011	**
	Glucose	F (2, 24) = 9.467	0.0009	***
	Oxygen	F (1, 24) = 29.85	<0.0001	****
MEFs (Figure 5.4.C)	Interaction	F (1, 8) = 0.6403	0.4467	ns
	Cell line	F (1, 8) = 0.3504	0.5702	ns
	Oxygen	F (1, 8) = 1.25	0.2960	ns

Table A.5.6. Summary of Bonferroni *post hoc* test values for viability. See also Figure 5.4. Only significant values shown.

	Condition	**Bonferroni *post hoc* test value summary**
DLD1 (Figure 5.4.A)	25mM 20.90% vs. 5mM 0.20%	****
	25mM 20.90% vs. 0mM 0.20%	****
	25mM 0.20% vs. 5mM 0.20%	****
	25mM 0.20% vs. 0mM 0.20%	****
	5mM 20.90% vs. 5mM 0.20%	****
	5mM 20.90% vs. 0mM 0.20%	****
	5mM 0.20% vs. 0mM 20.90%	****
	0mM 20.90% vs. 0mM 0.20%	****
SW837 (Figure 5.5.B)	25mM 20.90% vs. 5mM 0.20%	*
	25mM 20.90% vs. 0mM 0.20%	****
	25mM 0.20% vs. 5mM 0.20%	*
	25mM 0.20% vs. 0mM 0.20%	****
	5mM 20.90% vs. 5mM 0.20%	*
	5mM 20.90% vs. 0mM 0.20%	****
	5mM 0.20% vs. 0mM 20.90%	*
	0mM 20.90% vs. 0mM 0.20%	****

Table A.5.7. Summary of two-way ANOVA statistics for fumarate concentration. See also Figure 5.5.

	ANOVA table	F (DFn, DFd)	p value	p value summary
DLD1 (Figure 5.5.A)	Interaction	F (2, 12) = 14.56	0.0006	***
	Glucose	F (2, 12) = 11.08	0.0019	**
	Oxygen	F (1, 12) = 8.090	0.0148	*
SW837 (Figure 5.5.C)	Interaction	F (2, 12) = 2.660	0.1106	ns
	Glucose	F (2, 12) = 37.15	0.0001	****
	Oxygen	F (1, 12) = 18.47	0.0010	**
MEFs (Figure 5.5.D)	Interaction	F (1, 8) = 43.66	0.0002	***
	Cell line	F (1, 8) = 16.91	0.0034	**
	Oxygen	F (1, 8) = 4.733	0.0613	ns

Table A.5.8. Summary of Bonferroni *post hoc* test values for fumarate concentration. See also Figure 5.5. Only significant values shown.

	Conditions	**Bonferroni *post hoc* test values summary**
DLD1 (Figure 5.5.A)	25mM 20.9% O_2 vs. 25mM 0.2% O_2	**
	25mM 0.2% O_2 vs. 5mM 0.2% O_2	**
	25mM 0.2% O_2 vs. 0mM 20.9% O_2	***
	25mM 0.2% O_2 vs. 0mM 0.2% O_2	**
SW837 (Figure 5.5.C)	25mM 20.9% O_2 vs. 5mM 20.9% O_2	*
	25mM 20.9% O_2 vs. 0mM 20.9% O_2	**
	25mM 0.2% O_2 vs. 5mM 20.9% O_2	***
	25mM 0.2% O_2 vs. 5mM 0.2% O_2	***
	25mM 0.2% O_2 vs. 0mM 20.9% O_2	****
	25mM 0.2% O_2 vs. 0mM 0.2% O_2	*
	0mM 20.9% O_2 vs. 0mM 0.2% O_2	*
MEFs (Figure 5.5.D)	WT Fh1 20.9% O_2 vs. KO Fh1 20.9% O_2	***
	WT Fh1 0.2% O_2 vs. KO Fh1 20.9% O_2	*
	KO Fh1 20.9% O_2 vs. KO Fh1 0.2% O_2	**

Table A.5.9. Summary of two-way ANOVA statistics for fumarate hydratase activity. See also Figure 5.7.

	ANOVA table	F (DFn, DFd)	p value	p value summary
DLD1 (Figure 5.7.A)	Interaction	F (2, 12) = 6.366	0.0131	*
	Glucose	F (2, 12) = 14.06	0.0007	***
	Oxygen	F (1, 12) = 42.30	< 0.0001	****
SW837 (Figure 5.7.B)	Interaction	F (2, 12) = 0.2118	0.8121	ns
	Glucose	F (2, 12) = 5.672	0.0185	*
	Oxygen	F (1, 12) = 6.084	0.0297	*
MEFs (Figure 5.7.C)	Interaction	F (1, 8) = 1.968	0.1983	ns
	Cell line	F (1, 8) = 15.34	0.0044	**
	Oxygen	F (1, 8) = 1.239	0.2980	ns

Table A.5.10. Summary of Bonferroni *post hoc* test values for fumarate hydratase activity. Only significant values shown. See also Figure 5.7.

	Conditions	Bonferroni *post hoc* test values summary
DLD1 (Figure 5.7.A)	25mM 20.9% O_2 vs. 25mM 0.2% O_2	**
	25mM 20.9% O_2 vs. 5mM 0.2% O_2	**
	25mM 20.9% O_2 vs. 0mM 20.9% O_2	**
	25mM 20.9% O_2 vs. 0mM 0.2% O_2	***
	25mM 0.2% O_2 vs. 5mM 20.9% O_2	**
	5mM 20.9% O_2 vs. 5mM 0.2% O_2	**
	5mM 20.9% O_2 vs. 0mM 20.9% O_2	**
	5mM 20.9% O_2 vs. 0mM 0.2% O_2	**
MEFs (Figure	WT Fh1 20.9% O_2 vs. KO Fh1 20.9%	*
	WT Fh1 20.9% O_2 vs. KO Fh1 0.2% O_2	*

Table A.5.11. Summary of two-way ANOVA data for fumarate hydratase foci and area per cell. See also Figure 5.9.

Measurement	ANOVA table	F (DFn, DFd)	p value	p value summary
DLD1 FH foci per cell (Figure 5.9.A)	Interaction	F (2, 12) = 3.248	0.0746	ns
	Glucose	F (2, 12) = 123.1	<0.0001	****
	Oxygen	F (1, 12) = 8.643	0.0124	*
DLD1 FH area per cell (Figure 5.9.B)	Interaction	F (2, 12) = 0.4272	0.6619	ns
	Glucose	F (2, 12) = 144.7	<0.0001	****
	Oxygen	F (1, 12) = 0.005771	0.9407	ns
SW837 FH foci per cell (Figure 5.9.C)	Interaction	F (2, 12) = 4.164	0.0423	*
	Glucose	F (2, 12) = 34.76	<0.0001	****
	Oxygen	F (1, 12) = 2.649	0.1296	ns
SW837 FH area per cell (Figure 5.9.D)	Interaction	F (2, 12) = 11	0.0019	**
	Glucose	F (2, 12) = 47.57	<0.0001	****
	Oxygen	F (1, 12) = 8.436	0.0132	*

Table A.5.12. Summary of Bonferroni *post hoc* test values for FH foci and area per cell after 48 hours treatment with 20.9% or 0.2% O_2. Only significant values shown. See also Figure 5.9.

Measurement	Conditions	Bonferroni *post hoc* value summary
DLD1 FH foci per cell (Figure 5.9.A)	25mM 20.9% O_2 vs. 0mM 20.9%	****
	25mM 20.9% O_2 vs. 0mM 0.2% O_2	****
	25mM 0.2% O_2 vs. 0mM 20.9% O_2	****
	25mM 0.2% O_2 vs. 0mM 0.2% O_2	****
	5mM 20.9% O_2 vs. 0mM 20.9% O_2	****
	5mM 20.9% O_2 vs. 0mM 0.2% O_2	***
	5mM 0.2% O_2 vs. 0mM 20.9% O_2	****
	5mM 0.2% O_2 vs. 0mM 0.2% O_2	***
	0mM 20.9% O_2 vs. 0mM 0.2% O_2	*
DLD1 FH area per cell (Figure 5.9.B)	25mM 20.9% O_2 vs. 0mM 20.9%	****
	25mM 20.9% O_2 vs. 0mM 0.2% O_2	****
	25mM 0.2% O_2 vs. 0mM 20.9% O_2	****
	25mM 0.2% O_2 vs. 0mM 0.2% O_2	****
	5mM 20.9% O_2 vs. 0mM 20.9% O_2	****
	5mM 20.9% O_2 vs. 0mM 0.2% O_2	****
	5mM 0.2% O_2 vs. 0mM 20.9% O_2	****
	5mM 0.2% O_2 vs. 0mM 0.2% O_2	****
SW837 FH foci per cell (Figure 5.9.C)	25mM 20.9% O_2 vs. 0mM 20.9%	*
	25mM 20.9% O_2 vs. 0mM 0.2% O_2	***
	25mM 0.2% O_2 vs. 0mM 0.2% O_2	***
	5mM 20.9% O_2 vs. 0mM 0.2% O_2	***
	5mM 0.2% O_2 vs. 0mM 0.2% O_2	***
SW837 FH area per cell (Figure 5.9.D)	25mM 20.9% O_2 vs. 0mM 0.2% O_2	****
	25mM 0.2% O_2 vs. 0mM 0.2% O_2	****
	5mM 20.9% O_2 vs. 0mM 0.2% O_2	****
	5mM 0.2% O_2 vs. 0mM 0.2% O_2	****
	0mM 20.9% O_2 vs. 0mM 0.2% O_2	**

Table A.5.13. Summary of p values from linear regression multivariate analysis. See also Figure 5.11.

	p value			
Gene ranked by glucose p value	**Glucose**	**Oxygen**	**Glucose * Oxygen**	**R Squared value**
BAX	0.01370	0.19994	0.11366	0.608292
CA9	0.01723	0.00958	0.01723	0.468597
PDK1	0.01900	0.00864	0.66805	0.503016
LDHA	0.02906	0.00836	0.08518	0.560577
HK2	0.05156	0.00221	0.35933	0.487454
HIF12a	0.07798	0.03318	0.13318	0.404661
VEGF	0.08164	0.11080	0.57847	0.3938
GLUT1	0.14398	0.00125	0.35915	0.489338
VHL	0.19989	0.08781	0.19838	0.708561
GAPDH	0.22010	0.22010	0.13628	0.741091
GPX1	0.22787	0.21652	0.22787	0.70272
HIF1b	0.23631	0.22897	0.23631	0.713115
LONP1	0.33639	0.18453	0.27880	0.535988
HIF-1α	0.46743	0.06651	0.58087	0.659095
FH	0.50686	0.03717	0.50686	0.817944
COX4I2	0.55882	0.02499	0.55882	0.494927
GLUT4	0.73180	0.05227	0.45613	0.636521
SOD2	0.73899	0.73899	0.74647	0.552914
CASP9	0.89299	0.89299	0.89299	0.221554

Table A.5.14. Summary of normalised values for RT-PCR data for DLD1 cells cultured in 25mM glucose. See also Figure 5.11.

	20.9% O_2			0.2% O_2		
	n=1	n=2	n=3	n=1	n=2	n=3
GLUT1	5.63E-06	5.55E-06	1.03E-05	4.32E-06	3.84E-06	6.66E-06
GLUT4	7.14E-09	3.51E-08	4.08E-08	1.56E-08	5.91E-05	2.22E-08
GAPDH	5.43E-04	1.22E-03	1.19E-03	3.69E-04	8.50E-04	8.13E-04
LDHA	1.67E-05	1.00E-04	7.98E-05	9.30E-06	7.64E-06	4.73E-05
HK2	2.89E-07	1.82E-06	1.17E-06	2.19E-07	1.07E-06	7.07E-07
FH	1.14E-06	3.20E-06	3.21E-06	5.77E-07	1.10E-06	1.99E-06
PDK1	4.03E-07	2.21E-06	7.67E-07	2.51E-07	1.72E-06	5.08E-07
LONP1	9.60E-06	2.07E-05	2.20E-05	4.14E-06	2.14E-05	1.20E-05
SOD2	1.46E-06	1.10E-05	4.78E-06	7.87E-07	6.84E-06	4.04E-06
COX4I2	2.03E-09	5.34E-09	9.33E-10	4.80E-09	2.11E-08	5.60E-09
HIF-1A	9.49E-07	4.92E-06	2.77E-06	6.52E-07	3.25E-06	1.76E-06
HIF1B	6.90E-07	5.68E-06	2.62E-06	3.84E-07	2.67E-05	1.69E-06
HIF-2A	4.30E-07	1.78E-06	1.19E-06	3.31E-07	1.84E-06	1.09E-06
VHL	1.52E-06	3.89E-06	3.35E-06	5.32E-07	1.89E-06	1.96E-06
CA9	4.42E-08	1.25E-07	6.15E-08	1.92E-08	1.60E-07	3.72E-08
VEGF	7.50E-07	4.56E-06	3.22E-06	8.52E-07	1.06E-05	3.78E-06
BAX	3.27E-06	1.54E-05	1.08E-05	2.78E-06	3.49E-07	6.49E-06
CASP9	1.81E-07	1.21E-04	5.88E-07	1.05E-07	8.50E-04	4.05E-07
GPX1	2.06E-05	6.30E-07	5.30E-05	1.23E-05	1.65E-08	3.29E-05

Table A.5.15. Summary of normalised values for RT-PCR data for DLD1 cells cultured in 5mM glucose. See also Figure 5.11.

	20.9% O_2			0.2% O_2		
	n=1	n=2	n=3	n=1	n=2	n=3
GLUT1	8.02E-06	7.74E-06	1.23E-05	3.08E-05	2.05E-05	4.14E-05
GLUT4	6.38E-09	3.78E-08	2.70E-08	1.15E-08	8.26E-09	5.83E-09
GAPDH	3.54E-04	5.06E-04	5.22E-04	1.10E-03	1.51E-03	1.30E-03
LDHA	1.25E-05	2.16E-05	2.25E-05	1.24E-04	1.96E-04	1.97E-04
HK2	4.13E-07	1.92E-06	1.51E-06	2.08E-06	2.14E-06	2.23E-06
PDK1	5.80E-07	1.74E-06	7.34E-07	2.70E-06	4.24E-06	2.23E-06
FH	5.17E-07	8.60E-07	1.17E-06	8.74E-07	5.74E-07	7.57E-07
LONP1	1.24E-05	1.11E-05	2.04E-05	1.36E-05	1.56E-05	2.40E-05
SOD2	1.81E-06	7.39E-06	3.30E-06	1.62E-06	2.99E-06	1.74E-06
COX4I2	1.15E-09	1.43E-09	1.74E-09	1.66E-09	4.57E-09	1.42E-09
HIF-1A	1.37E-06	1.71E-06	2.57E-06	1.60E-06	1.07E-06	2.00E-06
HIF1B	1.30E-06	3.59E-06	2.89E-06	1.04E-06	2.98E-06	2.04E-06
HIF-2A	1.08E-06	1.85E-06	1.22E-06	1.52E-06	2.63E-06	2.62E-06
VHL	1.15E-06	2.97E-06	2.92E-06	2.49E-06	9.86E-07	1.81E-06
CA9	1.64E-08	2.42E-08	9.81E-09	4.62E-06	1.23E-05	4.92E-06
VEGF	1.62E-06	6.15E-06	8.45E-06	6.53E-06	1.75E-05	2.38E-05
BAX	3.54E-06	6.96E-06	4.09E-06	5.02E-06	6.83E-06	4.25E-06
CASP9	1.62E-07	3.05E-05	3.47E-07	2.60E-07	4.46E-05	4.01E-07
GPX1	3.28E-05	4.14E-07	2.04E-05	1.74E-05	3.47E-07	1.60E-05

Table A.5.16. Summary of normalised values for RT-PCR data for DLD1 cells cultured in 0mM glucose. See also Figure 5.11.

	20.9% O_2			0.2% O_2		
	n=1	n=2	n=3	n=1	n=2	n=3
GLUT1	6.55E-05	5.27E-05	1.42E-04	9.03E-05	4.43E-05	9.11E-05
GLUT4	1.02E-08	9.51E-09	1.71E-09	3.20E-09	5.21E-09	6.54E-09
GAPDH	1.50E-03	1.62E-03	1.82E-03	1.05E-03	1.13E-03	1.06E-03
GPX1	2.32E-05	3.09E-07	1.33E-05	1.49E-05	3.33E-07	1.42E-05
LDHA	1.61E-04	2.23E-04	2.21E-04	9.58E-05	1.24E-04	2.09E-04
PDK1	2.87E-06	4.95E-06	3.45E-06	2.08E-06	0	2.21E-06
HK2	1.64E-06	4.97E-06	4.59E-06	6.64E-06	1.28E-05	9.25E-06
FH	6.56E-07	6.22E-07	5.53E-07	5.60E-07	3.20E-07	6.29E-07
LONP1	8.73E-06	5.03E-06	2.08E-05	1.55E-05	4.55E-06	1.15E-05
SOD2	1.81E-06	6.62E-06	1.50E-06	1.84E-06	1.37E-06	3.28E-06
COX4I2	1.41E-08	8.94E-09	2.52E-09	6.84E-10	6.14E-10	1.30E-09
HIF-1A	2.18E-06	1.74E-06	2.25E-06	2.52E-06	3.81E-07	2.13E-06
HIF1B	1.10E-06	2.01E-06	1.67E-06	3.21E-06	2.13E-06	5.85E-06
HIF-2A	9.70E-07	9.92E-07	1.63E-06	5.01E-06	3.31E-07	1.92E-06
VHL	1.06E-06	6.18E-07	1.05E-06	2.34E-06	7.72E-07	8.20E-07
CA9	1.94E-06	2.80E-06	3.41E-06	1.20E-06	2.23E-07	1.17E-06
VEGF	6.16E-06	1.55E-05	4.22E-05	2.23E-05	1.73E-05	4.50E-05
CASP9	2.05E-07	3.72E-05	3.68E-07	3.08E-07	1.61E-05	4.12E-07
BAX	4.97E-06	7.99E-06	3.17E-06	2.59E-06	1.98E-06	1.73E-06

Table A.5.17. Summary of normalised values for RT-PCR data for HT55 cells cultured in 25mM glucose. See also Figure 5.11.

	20.9% O_2			0.2% O_2		
	n=1	n=2	n=3	n=1	n=2	n=3
GLUT1	1.61E-01	2.61E-01	2.76E-01	7.25E-01	6.74E-01	1.12E+00
GLUT4	2.09E-04	2.83E-04	4.75E-04	9.98E-06	2.46E-05	4.33E-05
GAPDH	4.75E-01	2.39E-02	7.14E-01	5.44E-01	1.33E-01	9.76E-01
GPX1	2.86E-01	2.24E-01	2.46E-01	1.10E-01	9.39E-02	1.23E-01
LDHA	1.67E-01	7.22E-02	2.64E-01	2.65E-01	1.44E-01	5.45E-01
PDK1	3.00E-03	3.34E-03	4.60E-03	1.56E-02	1.15E-02	1.58E-02
HK2	7.04E-03	9.15E-03	1.28E-02	2.66E-02	1.46E-02	3.69E-02
FH	3.14E-02	3.30E-02	4.89E-02	2.07E-02	1.28E-02	1.85E-02
LONP1	4.54E-02	2.68E-02	3.13E-02	2.76E-02	2.78E-02	2.31E-02
SOD2	4.05E-02	3.25E-02	3.74E-02	2.13E-02	1.93E-02	1.84E-02
COX4I2	8.21E-06	1.10E-05	1.52E-06	1.49E-05	8.93E-06	1.67E-05
HIF-1A	1.07E-02	1.40E-02	3.36E-02	7.77E-03	5.86E-03	1.02E-02
HIF1B	4.80E-03	2.35E-03	4.55E-03	2.21E-03	1.93E-03	2.94E-03
HIF-2A	6.25E-03	7.91E-03	6.24E-03	1.79E-02	2.35E-02	1.99E-02
VHL	1.35E-02	1.26E-02	1.86E-02	4.70E-03	4.77E-03	5.89E-03
CA9	4.97E-04	4.19E-04	4.64E-04	7.86E-03	4.99E-03	5.18E-03
VEGF	1.38E-02	7.20E-03	1.96E-02	3.65E-02	4.28E-02	7.53E-02
CASP9	7.92E-04	5.38E-04	9.44E-04	5.70E-04	5.81E-04	1.08E-03
BAX	1.13E-02	6.22E-03	1.29E-02	2.67E-03	1.81E-03	2.39E-03

Table A.5.18. Summary of normalised values for RT-PCR data for HT55 cells cultured in 5mM glucose. See also Figure 5.11.

	20.9% O_2			0.2% O_2		
	n=1	n=2	n=3	n=1	n=2	n=3
GLUT1	1.24E-01	1.28E-01	1.40E-01	3.68E-01	5.93E-01	7.26E-01
GLUT4	2.69E-04	3.71E-04	2.73E-04	1.21E-04	1.58E-04	1.97E-04
GAPDH	2.88E-01	6.18E-02	2.83E-01	3.73E-01	2.53E-01	5.54E-01
GPX1	1.94E-01	1.11E-01	1.29E-01	1.25E-01	6.02E-02	1.14E-01
LDHA	1.79E-01	8.22E-02	1.77E-01	5.25E-01	2.15E-01	4.91E-01
PDK1	2.20E-03	3.95E-03	2.25E-03	1.83E-02	1.07E-02	1.71E-02
HK2	6.28E-03	3.60E-03	8.86E-03	9.65E-03	1.94E-02	2.82E-02
FH	2.94E-02	2.98E-02	3.35E-02	2.32E-02	1.35E-02	2.03E-02
LONP1	2.39E-02	1.95E-02	1.52E-02	2.95E-02	1.53E-02	2.07E-02
SOD2	2.72E-02	2.82E-02	2.51E-02	2.75E-02	1.88E-02	1.84E-02
COX4I2	1.70E-05	5.25E-06	6.18E-06	1.96E-05	2.22E-05	1.40E-05
HIF-1A	1.48E-02	1.11E-02	1.70E-02	8.99E-03	5.78E-03	9.06E-03
HIF1B	2.38E-03	1.55E-03	1.94E-03	1.82E-03	9.74E-04	1.49E-03
HIF-2A	4.90E-03	7.54E-03	3.67E-03	1.56E-02	1.61E-02	1.20E-02
VHL	1.01E-02	9.41E-03	1.14E-02	6.99E-03	3.01E-03	5.38E-03
CA9	1.47E-03	1.45E-03	8.79E-04	2.69E-02	2.79E-02	1.85E-02
VEGF	4.85E-03	5.76E-03	5.00E-03	2.39E-02	2.71E-02	2.43E-02
CASP9	5.13E-04	5.20E-04	4.18E-04	5.34E-04	4.18E-04	5.46E-04
BAX	7.71E-03	5.61E-03	7.01E-03	4.00E-03	2.11E-03	3.15E-03

Table A.5.19. Summary of normalised values for RT-PCR data for HT55 cells cultured in 0mM glucose. See also Figure 5.11.

	20.9% O_2			0.2% O_2		
	n=1	n=2	n=3	n=1	n=2	n=3
GLUT1	7.38E-02	1.02E-01	1.54E-01	5.85E-01	5.19E-01	1.32E+00
GLUT4	1.23E-04	3.34E-04	3.63E-04	1.42E-04	1.59E-04	4.27E-04
GAPDH	2.86E-01	8.80E-02	3.33E-01	9.12E-01	2.26E-01	7.02E-01
GPX1	1.44E-01	9.80E-02	1.44E-01	1.24E-01	8.18E-02	1.70E-01
LDHA	1.77E-01	8.41E-02	2.05E-01	7.47E-01	1.88E-01	7.75E-01
PDK1	2.21E-03	2.24E-03	2.85E-03	2.06E-02	1.03E-02	2.70E-02
HK2	3.32E-03	3.00E-03	5.29E-03	1.71E-02	8.35E-03	3.50E-02
FH	2.64E-02	2.80E-02	4.20E-02	2.45E-02	1.55E-02	4.42E-02
LONP1	2.34E-02	1.67E-02	2.18E-02	4.19E-02	2.48E-02	3.73E-02
SOD2	2.92E-02	2.94E-02	3.16E-02	3.12E-02	1.80E-02	3.00E-02
COX4I2	1.61E-05	5.28E-06	1.79E-05	1.53E-05	1.42E-05	2.93E-05
HIF-1A	1.25E-02	1.23E-02	1.86E-02	9.57E-03	4.48E-03	1.47E-02
HIF1B	2.05E-03	1.44E-03	2.47E-03	2.46E-03	1.08E-03	2.50E-03
HIF-2A	3.89E-03	4.88E-03	4.94E-03	2.08E-02	1.81E-02	2.18E-02
VHL	7.30E-03	8.20E-03	1.22E-02	6.82E-03	5.31E-03	1.71E-02
CA9	4.88E-04	5.51E-04	6.49E-04	2.11E-02	1.61E-02	3.85E-02
VEGF	6.42E-03	5.28E-03	7.90E-03	4.92E-02	2.57E-02	3.80E-02
CASP9	4.76E-04	5.71E-04	7.24E-04	7.62E-04	5.41E-04	1.11E-03
BAX	7.42E-03	5.68E-03	9.67E-03	5.21E-03	2.27E-03	5.38E-03

Table A.5.20. Summary of normalised values for RT-PCR data for SW837 cells cultured in 25mM glucose. See also Figure 5.11.

	20.9% O_2			0.2% O_2		
	n=1	n=2	n=3	n=1	n=2	n=3
GLUT1	1.21E-01	1.61E-01	8.08E-02	1.08E-01	1.40E-01	8.53E-02
GLUT4	7.23E-05	7.37E-05	5.99E-05	5.78E-05	1.35E-04	3.24E-05
GAPDH	2.83E+00	3.86E+00	2.36E+00	2.74E+00	4.75E+00	2.12E+00
GPX1	1.23E-01	9.82E-04	9.75E-02	1.30E-01	1.81E-03	8.43E-02
LDHA	1.26E-01	1.53E-01	1.15E-01	1.31E-01	1.17E-01	1.04E-01
PDK1	4.42E-03	8.80E-04	1.43E-03	5.09E-03	3.69E-03	1.91E-03
HK2	1.69E-03	1.89E-03	1.50E-03	2.20E-03	2.77E-03	1.32E-03
FH	8.85E-03	1.43E-02	7.82E-03	7.83E-03	1.69E-02	7.04E-03
LONP1	1.07E-01	1.75E-02	4.74E-02	1.11E-01	7.03E-02	5.53E-02
SOD2	5.13E-02	8.01E-02	7.44E-03	4.92E-02	7.08E-02	4.54E-03
COX4I2	5.60E-06	0.00E+00	1.71E-07	0.00E+00	2.50E-05	9.26E-07
HIF-1A	1.41E-02	1.33E-02	9.93E-03	1.37E-02	1.09E-02	1.06E-02
HIF1B	1.12E-02	4.24E-03	4.34E-03	1.12E-02	1.15E-02	3.65E-03
HIF-2A	2.37E-03	3.54E-03	1.24E-03	6.17E-03	5.51E-02	2.43E-03
VHL	9.65E-03	7.40E-03	4.79E-03	9.89E-03	1.05E-02	5.28E-03
CA9	6.07E-04	1.46E-05	2.28E-04	1.34E-03	1.98E-05	3.33E-04
VEGF	3.44E-02	5.11E-02	8.71E-03	2.63E-02	1.53E-01	5.72E-03
CASP9	1.06E-03	7.40E-02	9.43E-04	9.50E-04	8.59E-02	7.74E-04
BAX	1.65E-01	1.66E-01	1.56E-01	1.43E-01	3.15E-01	1.32E-01

Table A.5.21. Summary of normalised values for RT-PCR data for SW837 cells cultured in 5mM glucose. See also Figure 5.11.

	20.9% O_2			0.2% O_2		
	n=1	n=2	n=3	n=1	n=2	n=3
GLUT1	8.74E-02	1.46E-01	5.65E-02	1.05E+00	2.67E+00	6.27E-01
GLUT4	5.50E-05	1.06E-04	6.56E-05	9.50E-05	9.56E-05	6.28E-05
GAPDH	1.62E+00	2.80E+00	1.81E+00	5.37E+00	9.22E+00	5.94E+00
GPX1	7.51E-02	1.30E-03	7.13E-02	1.10E-01	1.66E-03	1.20E-01
LDHA	6.50E-02	7.09E-02	5.06E-02	6.08E-01	1.22E+00	5.21E-01
PDK1	5.96E-03	1.93E-03	1.90E-03	2.82E-02	4.74E-06	1.60E-02
HK2	1.94E-03	1.72E-03	1.37E-03	1.48E-02	1.51E-02	9.14E-03
FH	5.54E-03	6.58E-03	4.48E-03	4.16E-03	9.59E-03	5.02E-03
LONP1	7.34E-02	3.05E-02	3.29E-02	1.29E-01	2.51E-01	8.90E-02
SOD2	4.66E-02	5.19E-02	3.69E-03	3.28E-02	5.73E-02	5.14E-03
COX4I2	0.00E+00	7.45E-06	0.00E+00	8.34E-06	3.81E-05	9.57E-07
HIF-1A	1.15E-02	5.33E-03	1.11E-02	1.38E-02	2.41E-04	8.42E-03
HIF1B	9.69E-03	7.52E-03	4.31E-03	1.16E-02	1.07E-02	4.31E-03
HIF-2A	5.58E-03	2.83E-02	8.26E-03	1.02E-02	4.06E-03	1.24E-02
VHL	8.17E-03	6.16E-03	5.62E-03	4.84E-03	2.09E-03	7.15E-03
CA9	2.13E-03	3.91E-04	7.64E-04	9.44E-02	2.88E-02	5.02E-02
VEGF	3.09E-02	5.77E-02	7.80E-03	1.52E-01	1.96E-01	6.08E-02
CASP9	4.89E-04	4.88E-02	1.05E-03	7.96E-04	1.34E-01	1.16E-03
BAX	1.55E-01	2.28E-01	2.28E-01	3.03E-02	2.51E-02	3.24E-02

Table A.5.22. Summary of normalised values for RT-PCR data for SW837 cells cultured in 0mM glucose. See also Figure 5.11.

	20.9% O_2			0.2% O_2		
	n=1	n=2	n=3	n=1	n=2	n=3
GLUT1	8.17E-01	7.84E-01	7.05E-01	9.28E-01	1.82E+00	1.47E+00
GLUT4	2.77E-05	9.45E-05	3.91E-05	5.83E-05	3.27E-05	5.07E-05
GAPDH	4.77E+00	1.03E+01	3.49E+00	5.17E+00	5.39E+00	3.81E+00
GPX1	1.03E-01	1.39E-03	8.37E-02	1.07E-01	1.25E-03	5.58E-02
LDHA	4.66E-01	8.61E-01	5.06E-01	5.24E-01	4.78E-01	5.54E-01
PDK1	3.04E-02	2.00E-02	1.73E-02	3.45E-02	1.23E-02	1.57E-02
HK2	1.25E-02	2.55E-02	1.19E-02	2.95E-02	4.87E-02	5.72E-02
FH	2.80E-03	6.81E-03	4.06E-03	4.16E-03	2.49E-03	3.59E-03
LONP1	6.76E-02	3.23E-03	7.12E-02	9.17E-02	1.51E-02	2.45E-02
SOD2	3.36E-02	4.22E-02	8.23E-03	2.46E-02	6.07E-02	1.29E-02
COX4I2	2.79E-06	0.00E+00	0.00E+00	0.00E+00	6.53E-06	0.00E+00
HIF-1A	9.14E-03	2.08E-03	1.46E-02	1.17E-02	6.40E-03	1.32E-02
HIF1B	1.14E-02	7.99E-03	4.87E-03	1.21E-02	1.79E-02	2.30E-02
HIF-2A	2.82E-02	1.24E-02	1.57E-02	2.62E-02	1.44E-01	9.28E-02
VHL	4.33E-03	9.60E-04	5.82E-03	5.61E-03	3.74E-03	5.17E-03
CA9	3.30E-02	4.29E-03	4.08E-02	2.39E-02	5.85E-03	1.16E-02
VEGF	2.29E-01	2.55E-01	8.48E-02	1.59E-01	8.79E-01	3.23E-01
CASP9	3.16E-04	1.97E-01	7.12E-04	7.13E-04	5.71E-02	1.28E-03
BAX	1.51E-02	2.18E-02	2.00E-02	1.98E-02	1.81E-02	2.02E-02

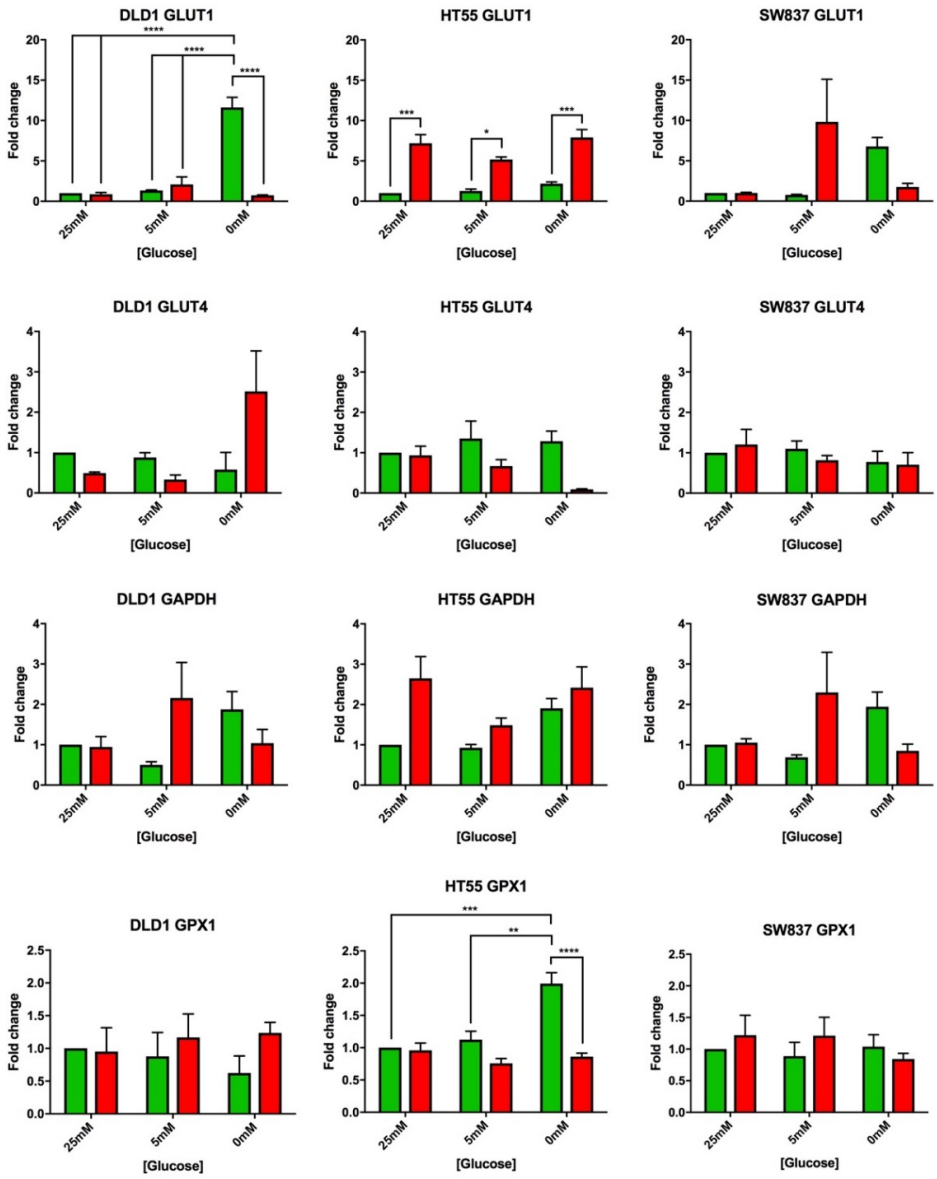

Figure A.5.1. The normalised RT-PCR data for GLUT1, GLUT4, GADPH and GPX1 expressed as fold change from cells cultured in 25mM glucose at 20.9% O_2. DLD1, HT55, SW837 cells were cultured in 25mM, 5mM or 0mM glucose then held in 20.9% or 0.2% O_2 for 48 hours. RNA was extracted and analysed via qPCR. Mean ± SEM in Table A.5.34, A.5.37, A.5.40. Two-way ANOVA was performed with Bonferroni *post hoc* test * $p < 0.1$, ** $p < 0.01$, *** $p < 0.001$ (A.5.35, A.5.36, A.5.38, A.5.39, A.5.41, A.5.42). See also Figure A.5.2,3,4,5 and 6. Glucose transporter 1 (GLUT1), glucose transporter 4 (GLUT4), glyceraldehyde 3-phosphate dehydrogenase (GAPDH), glutathione peroxidase (GPX1).

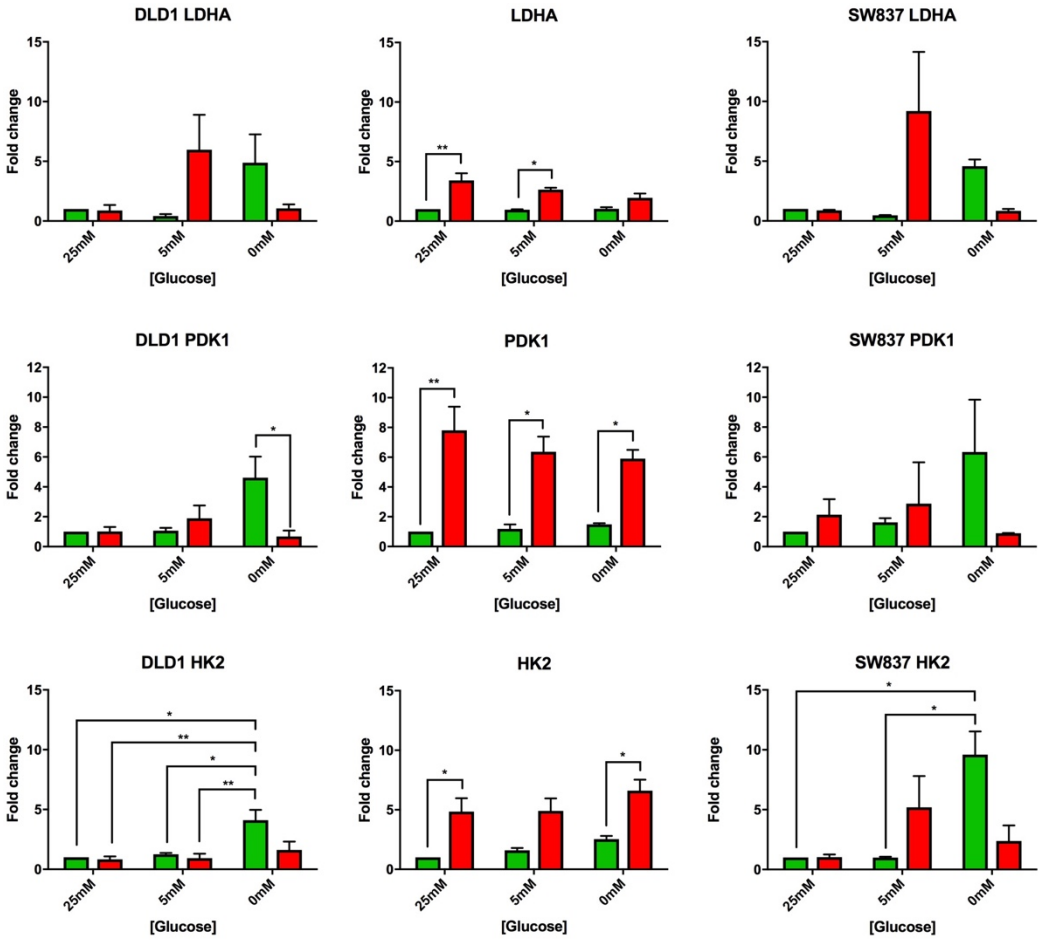

Figure A.5.2. The normalised RT-PCR data for LDHA, PDX1, and HK2 expressed as fold change from cells cultured in 25mM glucose at 20.9% O_2. DLD1, HT55, SW837 cells were cultured in 25mM, 5mM or 0mM glucose then held in 20.9% or 0.2% O_2 for 48 hours. RNA was extracted and analysed via qPCR. Mean ± SEM in Table A.5.34, A.5.37, A.5.40. Two-way ANOVA was performed with Bonferroni *post hoc* test * $p < 0.1$, ** $p < 0.01$, *** $p < 0.001$ (A.5.35, A.5.36, A.5.38, A.5.39, A.5.41, A.5.42). See also Figure A.5.1,3,4,5 and 6. Lactate dehydrogenase A (LDHA), pyruvate dehydrogenase kinase 1 (PDX1), hexokinase (HK2).

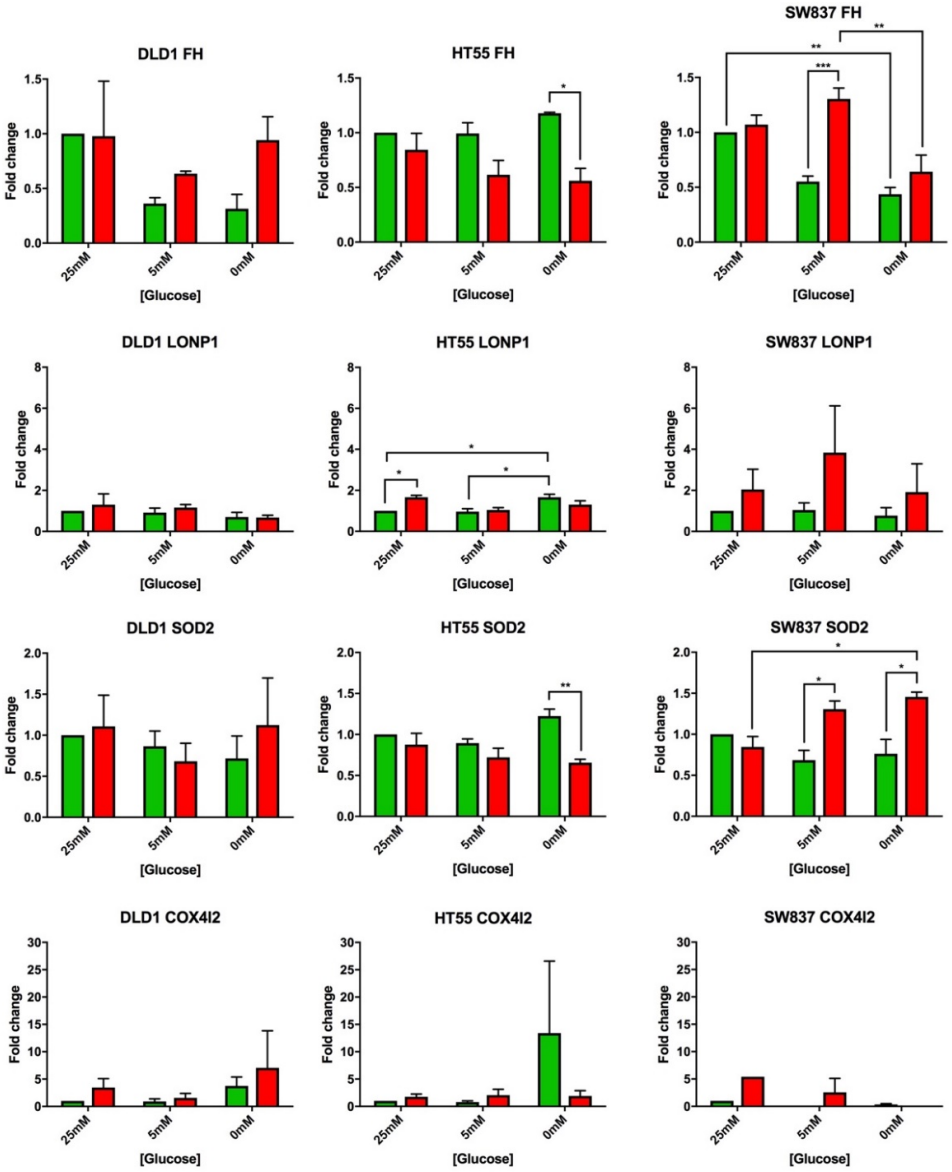

Figure A.5.3. The normalised RT-PCR data for FH, LONP1, SOD2 and COX4I2 expressed as fold change from cells cultured in 25mM glucose at 20.9% O_2. DLD1, HT55, SW837 cells were cultured in 25mM, 5mM or 0mM glucose then held in 20.9% or 0.2% O_2 for 48 hours. RNA was extracted and analysed via qPCR. Mean ± SEM in Table A.5.34, A.5.37, A.5.40. Two-way ANOVA was performed with Bonferroni *post hoc* test * $p < 0.1$, ** $p < 0.01$, *** $p < 0.001$ (A.5.35, A.5.36, A.5.38, A.5.39, A.5.41, A.5.42). See also Figure A.5.1,2,4,5 and 6. Fumarate hydratase (FH), lon peptidase 1 (LONP1), superoxide dismutase 2 (SOD2), cytochrome c oxidase subunit 4 isoform 2 (COX4I2).

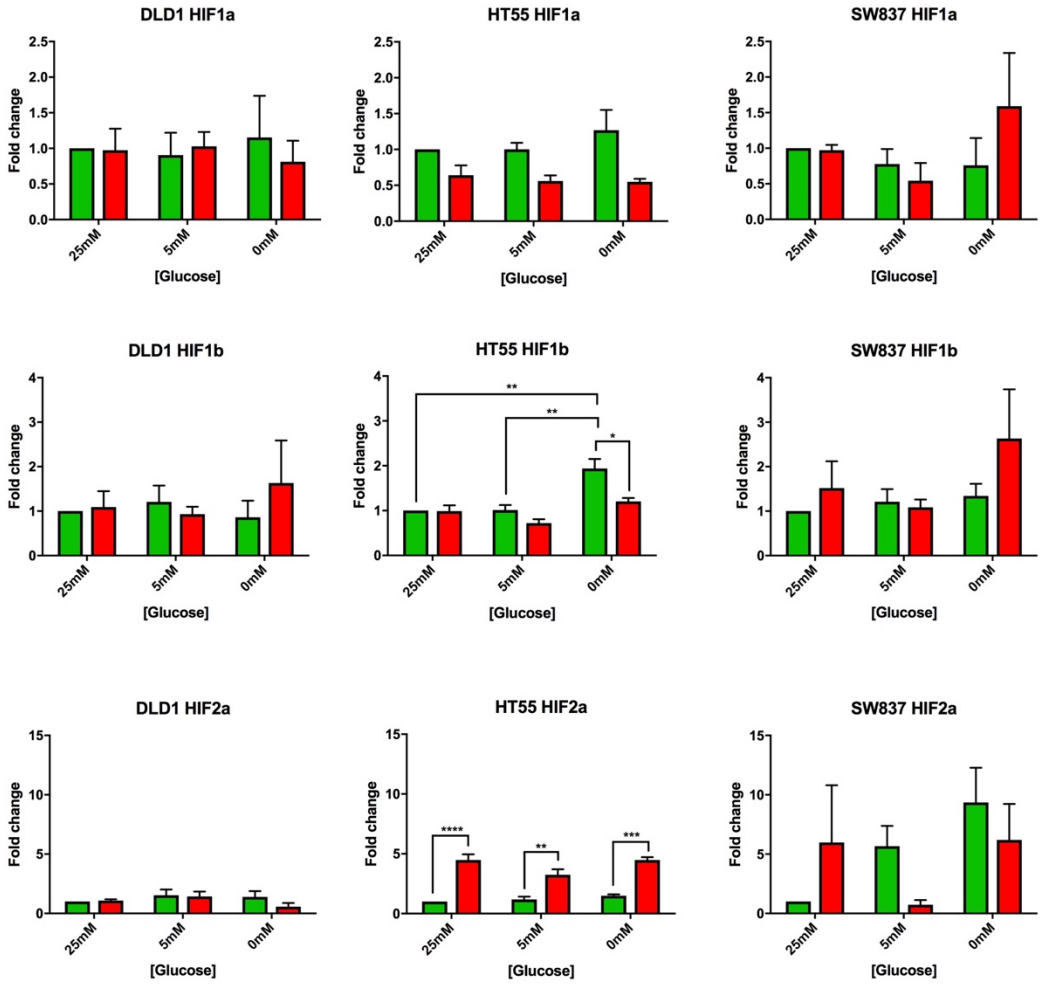

Figure A.5.4. The normalised RT-PCR data for HIF-1α, HIF-1ß and HIF-2α expressed as fold change from cells cultured in 25mM glucose at 20.9% O_2. DLD1, HT55, SW837 cells were cultured in 25mM, 5mM or 0mM glucose then held in 20.9% or 0.2% O_2 for 48 hours. RNA was extracted and analysed via qPCR. Mean ± SEM in Table A.5.34, A.5.37, A.5.40. Two-way ANOVA was performed with Bonferroni *post hoc* test * $p < 0.1$, ** $p < 0.01$, *** $p < 0.001$ (A.5.35, A.5.36, A.5.38, A.5.39, A.5.41, A.5.42). See also Figure A.5.1,2,3,5 and 6. Hypoxia inducible factor 1α (HIF-1α), hypoxia inducible factor 1ß (HIF-1ß) and hypoxia inducible factor 2α (HIF-2α).

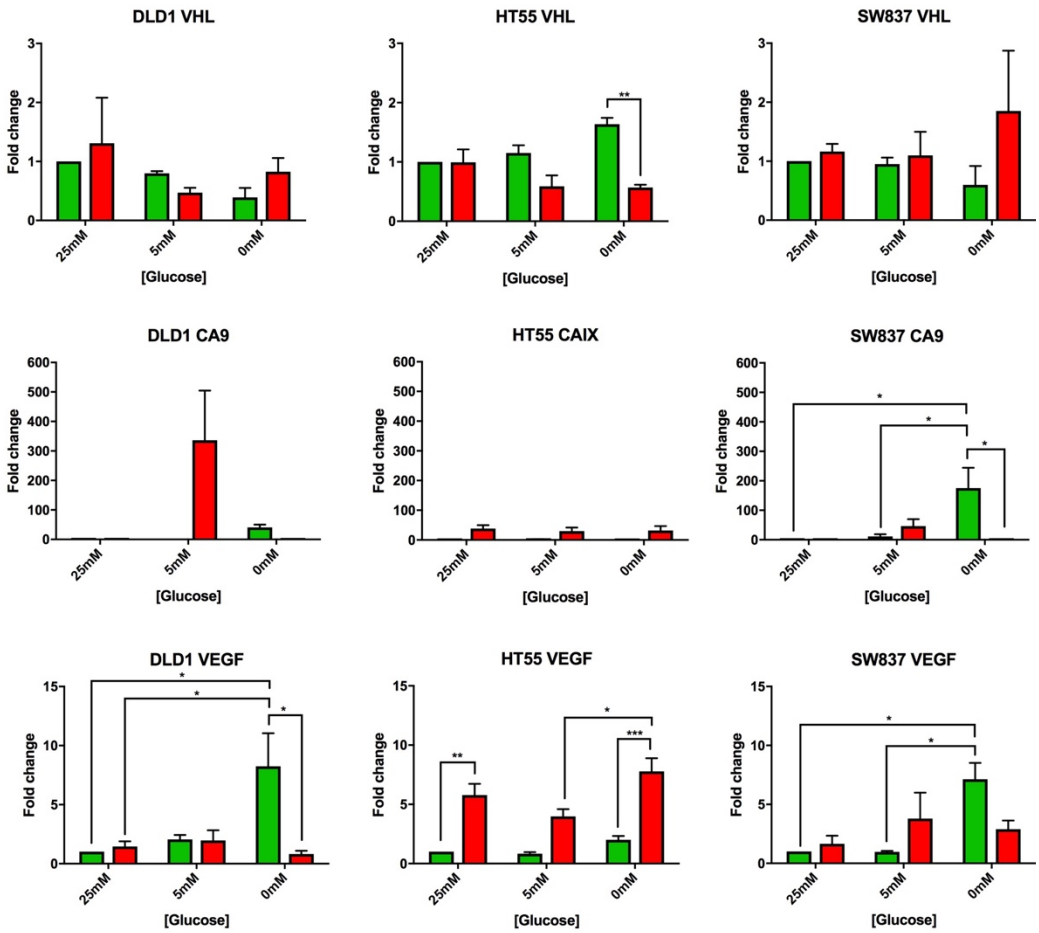

Figure A.5.5. The normalised RT-PCR data for VHL, CA9 and VEGF expressed as fold change from cells cultured in 25mM glucose at 20.9% O_2. DLD1, HT55, SW837 cells were cultured in 25mM, 5mM or 0mM glucose then held in 20.9% or 0.2% O_2 for 48 hours. RNA was extracted and analysed via qPCR. Mean ± SEM in Table A.5.34, A.5.37, A.5.40. Two-way ANOVA was performed with Bonferroni *post hoc* test * $p < 0.1$, ** $p < 0.01$, *** $p < 0.001$ (A.5.35, A.5.36, A.5.38, A.5.39, A.5.41, A.5.42). See also Figure A.5.1,2,3,4 and 6. Von Hippel-Lindau (VHL), carbonic anhydrase 9 (CA9) and vascular endothelial growth factor (VEGF).

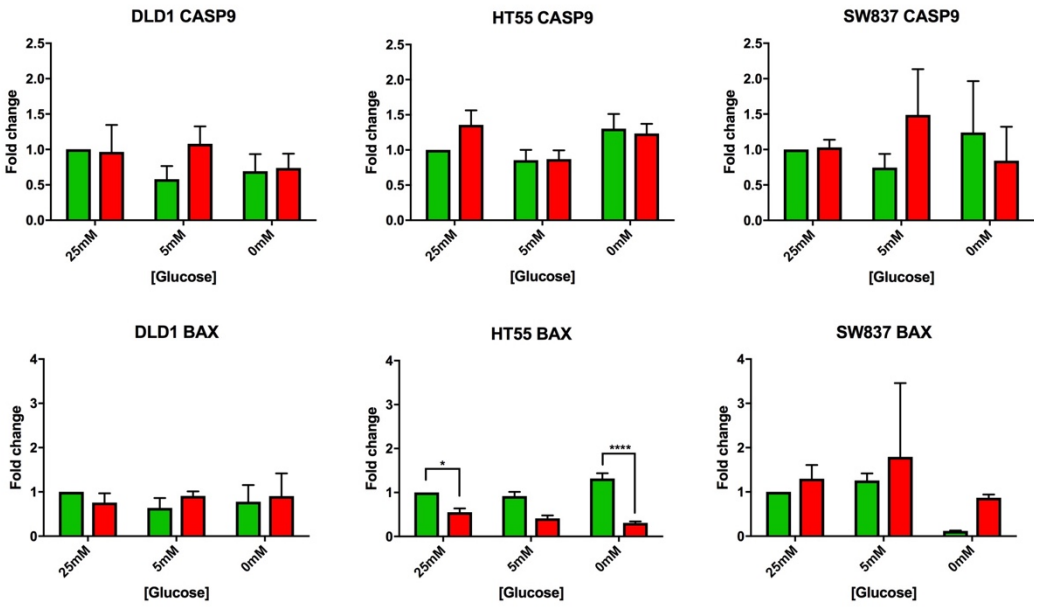

Figure A.5.6. The normalised RT-PCR data for CASP9 and BAX expressed as fold change from cells cultured in 25mM glucose at 20.9% O_2. DLD1, HT55, SW837 cells were cultured in 25mM, 5mM or 0mM glucose then held in 20.9% or 0.2% O_2 for 48 hours. RNA was extracted and analysed via qPCR. Mean ± SEM in Table A.5.34, A.5.37, A.5.40. Two-way ANOVA was performed with Bonferroni *post hoc* test * $p < 0.1$, ** $p < 0.01$, *** $p < 0.001$ (A.5.35, A.5.36, A.5.38, A.5.39, A.5.41, A.5.42). See also Figure A.5.1,2,3,4 and 5. Caspase 9 (CASP9), Bcl-2 associated X protein (BAX).

Table A.5.23. Summary of RT-PCR DLD1 data. Fold-change from 25mM glucose, shown as mean ± SEM. See also Figure A.5.1,2,3,4 and 5.

DLD1	**20.9%**		
	25mM	**5mM**	**0mM**
GLUT1	1.00±0.00	1.34±0.07	11.63±1.24
GLUT4	1.00±0.00	0.88±0.12	0.58±0.43
GAPDH	1.00±0.00	0.50±0.08	1.87±0.44
GPX1	1.00±0.00	0.88±0.37	0.62±0.26
LDHA	1.00±0.00	0.42±0.17	4.88±2.38
PDX1	1.00±0.00	1.06±0.19	4.62±0.40
HK2	1.00±0.00	1.26±0.11	4.11±0.85
FH	1.00±0.00	0.36±0.05	0.31±0.13
LONP1	1.00±0.00	0.92±0.22	0.70±0.23
SOD2	1.00±0.00	0.87±0.19	0.72±0.27
COX4I2	1.00±0.00	0.90±0.49	3.77±1.61
HIF-1α	1.00±0.00	0.90±0.32	1.15±0.59
HIF-1ß	1.00±0.00	1.21±0.37	0.86±0.37
HIF-2α	1.00±0.00	1.53±0.49	1.39±0.49
VHL	1.00±0.00	0.80±0.04	0.39±0.16
CA9	1.00±0.00	0.24±0.07	40.54±9.69
VEGF	1.00±0.00	2.05±0.37	8.23±2.80
CASP9	1.00±0.00	0.58±0.19	0.69±0.24
BAX	1.00±0.00	0.64±0.22	0.78±0.38
	0.2%		
	25mM	**5mM**	**0mM**
GLUT1	0.88±0.21	2.09±0.94	0.74±0.06
GLUT4	0.49±0.03	0.33±0.11	2.51±1.00

GAPDH	0.95±0.26	2.16±0.88	1.04±0.34
GPX1	0.95±0.36	1.17±0.36	1.24±0.16
LDHA	0.88±0.46	5.96±2.93	1.06±0.33
PDX1	1.02±0.30	1.89±0.86	0.67±0.40
HK2	0.84±0.24	0.93±0.38	1.61±0.70
FH	0.98±0.50	0.64±0.02	0.94±0.21
LONP1	1.30±0.53	1.17±0.14	0.67±0.12
SOD2	1.11±0.38	0.68±0.22	1.12±0.57
COX4I2	3.46±1.63	1.57±0.82	7.06±6.77
HIF-1α	0.97±0.03	1.03±0.20	0.81±0.30
HIF-1ß	1.09±0.36	0.93±0.17	1.63±0.95
HIF-2α	1.08±0.11	1.43±0.42	0.57±0.31
VHL	1.31±0.77	0.47±0.08	0.83±0.23
CA9	1.39±0.49	336.438±168.23	0.68±0.48
VEGF	1.46±0.44	1.97±0.86	0.82±0.27
CASP9	0.97±0.38	1.08±0.25	0.74±0.20
BAX	0.76±0.21	0.91±0.10	0.90±0.51

Table A.5.24. Summary table of two-way ANOVA for RT-PCR DLD1 fold change data. See also Figure A.5.1,2,3,4 and 5.

	ANOVA table	F (DFn, DFd)	P value	P value summary
GLUT1	Interaction	F (2, 12) = 51.21	<0.0001	****
	Glucose	F (2, 12) = 39.01	<0.0001	****
	Oxygen	F (1, 12) = 42.74	<0.0001	****
GLUT4	Interaction	F (2, 12) = 5.005	0.0263	*
	Glucose	F (2, 12) = 2.557	0.1188	ns
	Oxygen	F (1, 12) = 0.6377	0.4401	ns
GAPDH	Interaction	F (2, 12) = 4.211	0.0412	*
	Glucose	F (2, 12) = 0.6519	0.5386	ns
	Oxygen	F (1, 12) = 0.5052	0.4908	ns
GPX1	Interaction	F (2, 12) = 0.6723	0.5287	ns
	Glucose	F (2, 12) = 0.05382	0.9478	ns
	Oxygen	F (1, 12) = 1.493	0.2452	ns
LDHA	Interaction	F (2, 12) = 4.56	0.0337	*
	Glucose	F (2, 12) = 1.258	0.3191	ns
	Oxygen	F (1, 12) = 0.1783	0.6803	ns
PDK1	Interaction	F (2, 12) = 6.524	0.0121	*
	Glucose	F (2, 12) = 2.838	0.0979	ns
	Oxygen	F (1, 12) = 3.187	0.0995	ns
HK2	Interaction	F (2, 12) = 3.539	0.0619	ns
	Glucose	F (2, 12) = 9.632	0.0032	**
	Oxygen	F (1, 12) = 6.208	0.0284	*
FH	Interaction	F (2, 12) = 0.9929	0.3990	ns
	Glucose	F (2, 12) = 2.431	0.1299	ns
	Oxygen	F (1, 12) = 2.423	0.1455	ns
LONP1	Interaction	F (2, 12) = 0.2237	0.8028	ns
	Glucose	F (2, 12) = 1.706	0.2228	ns
	Oxygen	F (1, 12) = 0.6522	0.4350	ns
SOD2	Interaction	F (2, 12) = 0.4144	0.6698	ns
	Glucose	F (2, 12) = 0.3713	0.6975	ns
	Oxygen	F (1, 12) = 0.1727	0.6851	ns
COX4I2	Interaction	F (2, 12) = 0.1032	0.9027	ns
	Glucose	F (2, 12) = 1.101	0.3638	ns
	Oxygen	F (1, 12) = 0.7913	0.3912	ns

HIF-1α	Interaction	F (2, 12) = 0.2554	0.7787	ns
	Glucose	F (2, 12) = 0.002182	0.9978	ns
	Oxygen	F (1, 12) = 0.09108	0.7680	ns
HIF-1ß	Interaction	F (2, 12) = 0.6335	0.5476	ns
	Glucose	F (2, 12) = 0.1072	0.8992	ns
	Oxygen	F (1, 12) = 0.2586	0.6203	ns
HIF-2α	Interaction	F (2, 12) = 0.9099	0.4286	ns
	Glucose	F (2, 12) = 1.145	0.3508	ns
	Oxygen	F (1, 12) = 0.9285	0.3543	ns
VHL	Interaction	F (2, 12) = 0.7323	0.5011	ns
	Glucose	F (2, 12) = 1.659	0.2312	ns
	Oxygen	F (1, 12) = 0.2547	0.6229	ns
CA9	Interaction	F (2, 12) = 4.504	0.0347	*
	Glucose	F (2, 12) = 3.531	0.0622	ns
	Oxygen	F (1, 12) = 3.101	0.1037	ns
VEGF	Interaction	F (2, 12) = 6.472	0.0124	*
	Glucose	F (2, 12) = 3.975	0.0474	*
	Oxygen	F (1, 12) = 5.515	0.0368	*
CASP9	Interaction	F (2, 12) = 0.7331	0.5008	ns
	Glucose	F (2, 12) = 0.6441	0.5424	ns
	Oxygen	F (1, 12) = 0.7848	0.3931	ns
BAX	Interaction	F (2, 12) = 0.412	0.6714	ns
	Glucose	F (2, 12) = 0.0667	0.9358	ns
	Oxygen	F (1, 12) = 0.0474	0.8313	ns

Table A.5.25. Summary table for Bonferroni *post hoc* test values for qPCR on the DLD1 cell line. See also Figure A.5.1,2,3,4 and 5. Only significant values shown.

		P value	Summary
GLUT1	25mM 20.9% O_2 vs. 0mM 20.9%	<0.0001	****
	25mM 0.2% O_2 vs. 0mM 20.9% O_2	<0.0001	****
	5mM 20.9% O_2 vs. 0mM 20.9% O_2	<0.0001	****
	5mM 0.2% O_2 vs. 0mM 20.9% O_2	<0.0001	****
	0mM 20.9% O_2 vs. 0mM 0.2% O_2	<0.0001	****
PDK1	0mM 20.9% O_2 vs. 0mM 0.2% O_2	0.0293	*
HK2	25mM 20.9% O_2 vs. 0mM 20.9%	0.0111	*
	25mM 0.2% O_2 vs. 0mM 20.9% O_2	0.0074	**
	5mM 20.9% O_2 vs. 0mM 20.9% O_2	0.0214	*
	5mM 0.2% O_2 vs. 0mM 20.9% O_2	0.0093	**
VEGF	25mM 20.9% O_2 vs. 0mM 20.9%	0.0190	*
	25mM 0.2% O_2 vs. 0mM 20.9% O_2	0.0306	*
	0mM 20.9% O_2 vs. 0mM 0.2% O_2	0.0569	*

Table A.5.26. Summary of qPCR for the HT55 cell line. Fold-change from 25mM glucose, shown as mean ± SEM. See also Figure A.5.1,2,3,4 and 5.

HT55	**20.9%**		
	25mM	**5mM**	**0mM**
GLUT1	1.00±0.00	1.28±0.22	2.18±0.22
GLUT4	1.00±0.00	1.35±0.43	1.29±0.25
GAPDH	1.00±0.00	0.93±0.06	1.90±0.20
GPX1	1.00±0.00	1.12±0.13	2.00±0.17
LDHA	1.00±0.00	0.95±0.45	1.03±0.13
PDX1	1.00±0.00	1.18±0.30	1.49±0.59
HK2	1.00±0.00	1.59±0.20	2.53±0.27
FH	1.00±0.00	0.99±0.10	1.18±0.01
LONP1	1.00±0.00	0.96±0.14	1.66±0.15
SOD2	1.00±0.00	0.89±0.05	1.22±0.08
COX4I2	1.00±0.00	0.80±0.23	13.42±13.17
HIF-1α	1.00±0.00	1.00±0.09	1.27±0.04
HIF-1ß	1.00±0.00	1.01±0.11	1.99±0.21
HIF-2α	1.00±0.00	1.18±0.23	1.50±0.12
VHL	1.00±0.00	1.15±0.13	1.64±0.11
CA9	1.00±0.00	2.33±0.50	0.83±0.09
VEGF	1.00±0.00	0.83±0.14	2.00±0.33
CASP9	1.00±0.00	0.85±0.13	1.30±0.21
BAX	1.00±0.00	0.92±0.10	1.32±0.12
	0.2%		
	25mM	**5mM**	**0mM**
GLUT1	7.19±1.07	5.17±0.33	7.91±0.98
GLUT4	0.93±0.23	0.67±0.16	0.09±0.01

GAPDH	2.65±0.44	1.49±0.15	2.42±0.42
GPX1	0.96±0.11	0.76±0.07	0.86±0.06
LDHA	3.42±0.60	2.64±0.17	1.96±0.36
PDX1	7.81±1.59	6.36±1.03	5.91±0.59
HK2	4.85±1.12	4.90±1.05	6.61±0.92
FH	0.84±0.15	0.62±0.13	0.56±0.11
LONP1	1.66±0.09	1.04±0.11	1.30±0.19
SOD2	0.88±0.14	0.72±0.11	0.66±0.04
COX4I2	1.76±0.50	2.07±1.07	1.91±0.98
HIF-1α	0.64±0.14	0.56±0.08	0.55±0.04
HIF-1ß	0.99±0.13	0.72±0.09	1.21±0.08
HIF-2α	4.48±0.47	3.25±0.45	4.48±0.24
VHL	0.99±0.22	0.59±0.19	0.57±0.05
CA9	38.16±11.54	29.60±12.00	31.94±14.94
VEGF	5.78±0.94	3.98±0.61	7.78±1.12
CASP9	1.36±0.21	0.87±0.13	1.23±0.14
BAX	0.55±0.09	0.41±0.06	0.31±0.03

Table A.5.27. Summary table of two-way ANOVA data for the HT55 cell line qPCR. See also Figure A.5.1,2,3,4 and 5.

	ANOVA table	F (DFn, DFd)	P value	P value summary
GLUT1	Interaction	F (2, 12) = 1.936	0.1868	ns
	Glucose	F (2, 12) = 4.316	0.0387	*
	Oxygen	F (1, 12) = 108.8	<0.0001	****
GLUT4	Interaction	F (2, 12) = 2.936	0.0916	ns
	Glucose	F (2, 12) = 1.115	0.3598	ns
	Oxygen	F (1, 12) = 11.58	0.0052	**
GAPDH	Interaction	F (2, 6) = 1.892	0.2306	ns
	Glucose	F (2, 6) = 4.275	0.0701	ns
	Oxygen	F (1, 6) = 11.26	0.0153	*
GPX1	Interaction	F (2, 12) = 14.2	0.0007	***
	Glucose	F (2, 12) = 13.19	0.0009	***
	Oxygen	F (1, 12) = 35.69	<0.0001	****
LDHA	Interaction	F (2, 12) = 3.086	0.0829	ns
	Glucose	F (2, 12) = 2.859	0.0965	ns
	Oxygen	F (1, 12) = 46.99	<0.0001	****
PDK1	Interaction	F (2, 12) = 1.107	0.3620	ns
	Glucose	F (2, 12) = 0.4465	0.6501	ns
	Oxygen	F (1, 12) = 66.68	<0.0001	****
HK2	Interaction	F (2, 12) = 0.1384	0.8721	ns
	Glucose	F (2, 12) = 2.735	0.1050	ns
	Oxygen	F (1, 12) = 37.97	<0.0001	****
FH	Interaction	F (2, 12) = 2.563	0.1184	ns
	Glucose	F (2, 12) = 0.6748	0.5276	ns
	Oxygen	F (1, 12) = 21.19	0.0006	***
LONP1	Interaction	F (2, 12) = 8.121	0.0059	**
	Glucose	F (2, 12) = 7.381	0.0081	**
	Oxygen	F (1, 12) = 1.524	0.2406	ns
SOD2	Interaction	F (2, 12) = 4.156	0.0425	*
	Glucose	F (2, 12) = 1.598	0.2426	ns
	Oxygen	F (1, 12) = 17.44	0.0013	**
COX4I2	Interaction	F (2, 12) = 0.8937	0.4347	ns
	Glucose	F (2, 12) = 0.8916	0.4355	ns
	Oxygen	F (1, 12) = 0.5119	0.4880	ns

HIF-1α	Interaction	F (2, 12) = 0.9084	0.4292	ns
	Glucose	F (2, 12) = 0.4395	0.6543	ns
	Oxygen	F (1, 12) = 19.79	0.0008	***
HIF-1ß	Interaction	F (2, 12) = 4.496	0.0349	*
	Glucose	F (2, 12) = 19.24	0.0002	***
	Oxygen	F (1, 12) = 12.11	0.0045	**
HIF-2α	Interaction	F (2, 12) = 2.802	0.1003	ns
	Glucose	F (2, 12) = 3.384	0.0683	ns
	Oxygen	F (1, 12) = 131.7	<0.0001	****
VHL	Interaction	F (2, 12) = 7.499	0.0077	**
	Glucose	F (2, 12) = 1.446	0.2738	ns
	Oxygen	F (1, 12) = 23.82	0.0004	***
CA9	Interaction	F (2, 12) = 0.1492	0.8629	ns
	Glucose	F (2, 12) = 0.09377	0.9112	ns
	Oxygen	F (1, 12) = 18.23	0.0011	**
VEGF	Interaction	F (2, 12) = 1.983	0.1802	ns
	Glucose	F (2, 12) = 7.079	0.0093	**
	Oxygen	F (1, 12) = 70.85	<0.0001	****
CASP9	Interaction	F (2, 12) = 1.077	0.3712	ns
	Glucose	F (2, 12) = 3.851	0.0511	ns
	Oxygen	F (1, 12) = 0.6507	0.4356	ns
BAX	Interaction	F (2, 12) = 7.667	0.0072	**
	Glucose	F (2, 12) = 1.923	0.1885	ns
	Oxygen	F (1, 12) = 103.1	<0.0001	****

Table A.5.28. Summary table for Bonferroni *post hoc* test values for the HT55 cell line qPCR. See also Figure A.5.1,2,3,4 and 5. Only significant values shown.

		P value	Bonferroni *post hoc* test value summary
GLUT1	25mM 20.9% O_2 vs. 25mM 0.2% O_2	0.0002	***
	25mM 20.9% O_2 vs. 5mM 0.2% O_2	0.0069	**
	25mM 20.9% O_2 vs. 0mM 0.2% O_2	<0.0001	****
	25mM 0.2% O_2 vs. 5mM 20.9% O_2	0.0003	***
	25mM 0.2% O_2 vs. 0mM 20.9% O_2	0.0014	**
	5mM 20.9% O_2 vs. 5mM 0.2% O_2	0.0120	*
	5mM 20.9% O_2 vs. 0mM 0.2% O_2	<0.0001	****
	0mM 20.9% O_2 vs. 0mM 0.2% O_2	0.0004	***
GLUT4	5mM 20.9% O_2 vs. 0mM 0.2% O_2	0.0366	*
GPX1	25mM 20.9% O_2vs. 0mM 20.9% O_2	0.0003	***
	25mM 0.2% O_2 vs. 0mM 20.9% O_2	0.0002	***
	5mM 20.9% O_2 vs. 0mM 20.9% O_2	0.0012	**
	5mM 0.2% O_2 vs. 0mM 20.9% O_2	<0.0001	****
	0mM 20.9% O_2 vs. 0mM 0.2% O_2	<0.0001	****
LDHA	25mM 20.9% O_2 vs. 25mM 0.2% O_2	0.0015	**
	25mM 20.9% O_2 vs. 5mM 0.2% O_2	0.0335	*
	25mM 0.2% O_2 vs. 5mM 20.9% O_2	0.0012	**
	25mM 0.2% O_2 vs. 0mM 20.9% O_2	0.0017	**
	5mM 20.9% O_2 vs. 5mM 0.2% O_2	0.0272	*
	5mM 0.2% O_2 vs. 0mM 20.9% O_2	0.0382	*
PDK1	25mM 20.9% O_2 vs. 25mM 0.2% O_2	0.0011	**
	25mM 20.9% O_2 vs. 5mM 0.2% O_2	0.0088	**
	25mM 20.9% O_2 vs. 0mM 0.2% O_2	0.0175	*
	25mM 0.2% O_2 vs. 5mM 20.9% O_2	0.0015	**
	25mM 0.2% O_2 vs. 0mM 20.9% O_2	0.0022	**
	5mM 20.9% O_2 vs. 5mM 0.2% O_2	0.0116	*
	5mM 20.9% O_2 vs. 0mM 0.2% O_2	0.0232	*

	5mM 0.2% O_2 vs. 0mM 20.9% O_2	0.0184	*
	0mM 20.9% O_2 vs. 0mM 0.2% O_2	0.0373	*
HK2	25mM 20.9% O_2 vs. 25mM 0.2% O_2	0.0495	*
	25mM 20.9% O_2 vs. 5mM 0.2% O_2	0.0450	*
	25mM 20.9% O_2 vs. 0mM 0.2% O_2	0.0027	**
	5mM 20.9% O_2 vs. 0mM 0.2% O_2	0.0069	**
	0mM 20.9% O_2vs. 0mM 0.2% O_2	0.0333	*
FH	5mM 0.2% O_2 vs. 0mM 20.9% O_2	0.0315	*
	0mM 20.9% O_2 vs. 0mM 0.2% O_2	0.0161	*
LONP1	25mM 20.9% O_2 vs. 25mM 0.2% O_2	0.0465	*
	25mM 20.9% O_2 vs. 0mM 20.9% O_2	0.0475	*
	25mM 0.2% O_2 vs. 5mM 20.9% O_2	0.0326	*
	5mM 20.9% O_2 vs. 0mM 20.9% O_2	0.0333	*
SOD2	5mM 0.2% O_2 vs. 0mM 20.9% O_2	0.0184	*
	0mM 20.9% O_2 vs. 0mM 0.2% O_2	0.0070	**
HIF-1ß	25mM 20.9% O_2 vs. 0mM 20.9% O_2	0.0021	**
	25mM 0.2% O_2 vs. 0mM 20.9% O_2	0.0019	**
	5mM 20.9% O_2 vs. 0mM 20.9% O_2	0.0023	**
	5mM 0.2% O_2 vs. 0mM 20.9% O_2	0.0002	***
	0mM 20.9% O_2 vs. 0mM 0.2% O_2	0.161	*
HIF-2α	25mM 20.9% O_2 vs. 25mM 0.2% O_2	<0.0001	****
	25mM 20.9% O_2 vs. 5mM 0.2% O_2	0.0031	**
	25mM 20.9% O_2 vs. 0mM 0.2% O_2	<0.0001	****
	25mM 0.2% O_2 vs. 5mM 20.9% O_2	<0.0001	****
	25mM 0.2% O_2 vs. 0mM 20.9% O_2	0.0002	***
	5mM 20.9% O_2 vs. 5mM 0.2% O_2	0.0064	**
	5mM 20.9% O_2 vs. 0mM 0.2% O_2	<0.0001	****
	5mM 0.2% O_2 vs. 0mM 20.9% O_2	0.0228	*
	0mM 20.9% O_2 vs. 0mM 0.2% O_2	0.0002	***
VHL	5mM 0.2% O_2 vs. 0mM 20.9% O_2	0.0024	**
	0mM 20.9% O_2 vs. 0mM 0.2% O_2	0.0020	**
VEGF	25mM 20.9% O_2 vs. 25mM 0.2% O_2	0.0040	**
	25mM 20.9% O_2 vs. 0mM 0.2% O_2	0.0002	***

	25mM 0.2% O_2 vs. 5mM 20.9% O_2	0.0030	**
	25mM 0.2% O_2 vs. 0mM 20.9% O_2	0.0254	*
	5mM 20.9% O_2 vs. 0mM 0.2% O_2	0.0001	***
	5mM 0.2% O_2 vs. 0mM 0.2% O_2	0.0247	*
	0mM 20.9% O_2 vs. 0mM 0.2% O_2	0.0008	***
BAX	25mM 20.9% O_2 vs. 25mM 0.2% O_2	0.0258	*
	25mM 20.9% O_2 vs. 5mM 0.2% O_2	0.0030	**
	25mM 20.9% O_2 vs. 0mM 0.2% O_2	0.0007	***
	25mM 0.2% O_2 vs. 0mM 20.9% O_2	0.0003	***
	5mM 20.9% O_2 vs. 5mM 0.2% O_2	0.0104	*
	5mM 20.9% O_2 vs. 0mM 0.2% O_2	0.0022	**
	5mM 0.2% O_2 vs. 0mM 20.9% O_2	<0.0001	****
	0mM 20.9% O_2 vs. 0mM 0.2% O_2	<0.0001	****

Table A.5.29. Summary of qPCR SW837 cell line data. Fold-change from 25mM glucose, shown as mean ± SEM. See also Figure A.5.1,2,3,4 and 5.

SW837	**20.9%**		
	25mM	**5mM**	**0mM**
GLUT1	1.00±0.00	0.78±0.07	6.78±1.11
GLUT4	1.00±0.00	1.10±0.19	0.77±0.27
GAPDH	1.00±0.00	0.69±0.06	1.94±0.36
GPX1	1.00±0.00	0.89±0.22	1.04±0.19
LDHA	1.00±0.00	0.47±0.02	4.58±0.57
PDX1	1.00±0.00	1.62±0.28	6.33±3.51
HK2	1.00±0.00	0.99±0.08	9.59±1.95
FH	1.00±0.00	0.55±0.05	0.44±0.06
LONP1	1.00±0.00	1.04±0.35	0.77±0.39
SOD2	1.00±0.00	0.68±0.12	0.76±0.18
COX4I2	1.00±0.00	0±0	0±0
HIF-1α	1.00±0.00	0.78±0.21	0.76±0.38
HIF-1ß	1.00±0.00	1.21±0.28	1.34±0.28
HIF-2α	1.00±0.00	5.67±1.71	9.56±2.93
VHL	1.00±0.00	0.95±0.11	0.60±0.32
CA9	1.00±0.00	11.18±7.75	175.47±68.92
VEGF	1.00±0.00	0.97±0.08	7.13±1.39
CASP9	1.00±0.00	0.75±0.19	1.24±0.73
BAX	1.00±0.00	1.26±0.16	0.12±0.012
	0.2%		
	25mM	**5mM**	**0mM**
GLUT1	1.02±0.07	9.82±5.29	1.76±0.45
GLUT4	1.21±0.37	0.81±0.11	0.71±0.30

GAPDH	1.05±0.10	2.29±1.00	0.85±0.17
GPX1	1.22±0.31	1.21±0.29	0.84±0.09
LDHA	0.88±0.06	9.19±4.95	0.85±0.16
PDX1	2.13±1.04	2.88±2.77	0±0
HK2	1.04±0.22	5.20±2.61	1.39±1.29
FH	1.07±0.09	1.30±0.10	0.64±0.15
LONP1	2.04±0.98	3.83±2.28	1.92±1.38
SOD2	0.85±0.13	1.31±0.10	1.46±0.06
COX4I2	0±0	0±0	0±0
HIF-1α	0.97±0.08	0.54±0.25	1.59±0.75
HIF-1ß	1.52±0.60	1.09±0.18	2.63±1.11
HIF-2α	5.98±4.82	0.73±0.41	6.19±3.03
VHL	1.16±0.13	1.10±0.40	1.85±1.02
CA9	1.09±0.32	46.47±23.33	1.01±0.36
VEGF	1.65±0.70	3.80±2.20	2.90±0.74
CASP9	1.03±0.11	1.49±0.66	0.84±0.48
BAX	1.30±0.31	1.79±1.67	0.87±0.07

Table A.5.30. Summary table of two-way ANOVA summary data for qPCR on the SW837 cell line. See also Figure A.5.1,2,3,4 and 5.

	ANOVA table	F (DFn, DFd)	P value	P value summary
GLUT1	Interaction	F (2, 12) = 5.17	0.0240	*
	Glucose	F (2, 12) = 2.044	0.1722	ns
	Oxygen	F (1, 12) = 0.5536	0.4712	ns
GLUT4	Interaction	F (2, 12) = 0.5166	0.6092	ns
	Glucose	F (2, 12) = 1.145	0.3507	ns
	Oxygen	F (1, 12) = 0.0591	0.8120	ns
GAPDH	Interaction	F (2, 12) = 4.72	0.0307	*
	Glucose	F (2, 12) = 0.6163	0.5562	ns
	Oxygen	F (1, 12) = 0.2744	0.6099	ns
GPX1	Interaction	F (2, 12) = 0.8283	0.4603	ns
	Glucose	F (2, 12) = 0.322	0.7308	ns
	Oxygen	F (1, 12) = 0.4368	0.5211	ns
LDHA	Interaction	F (2, 12) = 4.938	0.0272	*
	Glucose	F (2, 12) = 1.83	0.2025	ns
	Oxygen	F (1, 12) = 0.9465	0.3498	ns
PDK1	Interaction	F (2, 11) = 1.634	0.2391	ns
	Glucose	F (2, 11) = 0.4935	0.6234	ns
	Oxygen	F (1, 11) = 0.3724	0.5541	ns
HK2	Interaction	F (2, 12) = 8.117	0.0059	**
	Glucose	F (2, 12) = 6.073	0.0151	*
	Oxygen	F (1, 12) = 0.712	0.4153	ns
FH	Interaction	F (2, 12) = 8.491	0.0050	**
	Glucose	F (2, 12) = 17.75	0.0003	***
	Oxygen	F (1, 12) = 22.92	0.0004	***
LONP1	Interaction	F (2, 12) = 0.3468	0.7138	ns
	Glucose	F (2, 12) = 0.494	0.6220	ns
	Oxygen	F (1, 12) = 2.973	0.1103	ns
SOD2	Interaction	F (2, 12) = 8.88	0.0043	**
	Glucose	F (2, 12) = 1.426	0.2782	ns
	Oxygen	F (1, 12) = 18.04	0.0011	**
COX4I2	Interaction	n/a	n/a	n/a
	Glucose	n/a	n/a	n/a

	Oxygen	n/a	n/a	n/a
HIF-1α	Interaction	F (2, 12) = 1.173	0.3426	ns
	Glucose	F (2, 12) = 0.9881	0.4006	ns
	Oxygen	F (1, 12) = 0.3913	0.5434	ns
HIF-1ß	Interaction	F (2, 12) = 0.8477	0.4525	ns
	Glucose	F (2, 12) = 1.397	0.2848	ns
	Oxygen	F (1, 12) = 1.597	0.2303	ns
HIF-2α	Interaction	F (2, 12) = 1.902	0.1916	ns
	Glucose	F (2, 12) = 1.785	0.2096	ns
	Oxygen	F (1, 12) = 0.2222	0.6458	ns
VHL	Interaction	F (2, 12) = 0.9011	0.4319	ns
	Glucose	F (2, 12) = 0.09492	0.9101	ns
	Oxygen	F (1, 12) = 1.835	0.2004	ns
CA9	Interaction	F (2, 12) = 7.069	0.0094	**
	Glucose	F (2, 12) = 4.447	0.0359	*
	Oxygen	F (1, 12) = 3.613	0.0816	ns
VEGF	Interaction	F (2, 12) = 5.012	0.0262	*
	Glucose	F (2, 12) = 5.538	0.0198	*
	Oxygen	F (1, 12) = 0.0722	0.7927	ns
CASP9	Interaction	F (2, 12) = 0.8151	0.4657	ns
	Glucose	F (2, 12) = 0.02722	0.9732	ns
	Oxygen	F (1, 12) = 0.1163	0.7389	ns
BAX	Interaction	F (2, 12) = 0.05282	0.9488	ns
	Glucose	F (2, 12) = 1.128	0.3556	ns
	Oxygen	F (1, 12) = 0.8642	0.3709	ns

Table A.5.31. Summary table for Bonferroni *post hoc* test values for the SW837 cell line qPCR. Only significant values shown. See also Figure A.5.1,2,3,4 and 5.

	Condition	**p value**	**Bonferroni *post hoc* test value summary**
HK2	25mM 20.9% O_2 vs. 0mM 20.9% O_2	0.0172	*
	25mM 0.2% O_2 vs. 0mM 20.9% O_2	0.0178	*
	5mM 20.9% O_2 vs. 0mM 20.9% O_2	0.0171	*
FH	25mM 20.9% O_2 vs. 0mM 20.9% O_2	0.0101	*
	25mM 0.2% O_2 vs. 5mM 20.9% O_2	0.0192	*
	25mM 0.2% O_2 vs. 0mM 20.9% O_2	0.0038	**
	5mM 20.9% O_2 vs. 5mM 0.2% O_2	0.0008	***
	5mM 0.2% O_2 vs. 0mM 20.9% O_2	0.0002	***
	5mM 0.2% O_2 vs. 0mM 0.2% O_2	0.0026	**
SOD2	25mM 0.2% O_2 vs. 0mM 0.2% O_2	0.0333	*
	5mM 20.9% O_2 vs. 5mM 0.2% O_2	0.0297	*
	5mM 20.9% O_2 vs. 0mM 0.2% O_2	0.0055	*
	0mM 20.9% O_2 vs. 0mM 0.2% O_2	0.0736	*
CA9	25mM 20.9% O_2 vs. 0mM 20.9% O_2	0.0209	*
	25mM 0.2% O_2 vs. 0mM 20.9% O_2	0.0210	*
	5mM 20.9% O_2 vs. 0mM 20.9% O_2	0.0323	*
	0mM 20.9% O_2 vs. 0mM 0.2% O_2	0.0209	*
VEGF	25mM 20.9% O_2 vs. 0mM 20.9% O_2	0.0381	*
	5mM 20.9% O_2 vs. 0mM 20.9% O_2	0.0370	*

Table A.5.32. Summary of two-way ANOVA statistics for mitochondrial foci and area per cell. See also Figure 5.14.

Measurement	ANOVA table	F (DFn, DFd)	p value	p value summary
DLD1 mitochondrial foci per cell (Figure 5.9.A)	Interaction	F (2, 12) = 19.68	0.0002	***
	Glucose	F (2, 12) = 86.35	<0.0001	****
	Oxygen	F (1, 12) = 8.261	0.0140	*
DLD1 mitochondrial area per cell (Figure 5.9.B)	Interaction	F (2, 12) = 7.364	0.0082	**
	Glucose	F (2, 12) = 61.52	<0.0001	****
	Oxygen	F (1, 12) = 4.458	0.0564	ns
SW837 mitochondrial foci per cell (Figure 5.9.C)	Interaction	F (2, 12) = 0.518	0.6084	ns
	Glucose	F (2, 12) = 17.27	0.0003	***
	Oxygen	F (1, 12) = 0.00	0.9646	ns
SW837 mitochondrial area per cell (Figure 5.9.D)	Interaction	F (2, 12) = 3.333	0.0706	ns
	Glucose	F (2, 12) = 28.49	<0.0001	****
	Oxygen	F (1, 12) = 1.331	0.2712	ns

Table A.5.33. Bonferroni *post hoc* test values for mitochondrial foci and area per cell. See also Figure 5.14**.** Only significant values shown.

Measurement	**Conditions**	**Bonferroni *post hoc* value summary**
DLD1 mitochondrial foci per cell (Figure 5.14.A)	25mM 20.9% O_2 vs. 0mM 20.9% O_2	****
	25mM 20.9% O_2 vs. 0mM 0.2% O_2	**
	25mM 0.2% O_2 vs. 0mM 20.9% O_2	****
	25mM 0.2% O_2 vs. 0mM 0.2% O_2	**
	5mM 20.9% O_2 vs. 0mM 20.9% O_2	****
	5mM 20.9% O_2 vs. 0mM 0.2% O_2	**
	5mM 0.2% O_2 vs. 0mM 20.9% O_2	****
	0mM 20.9% O_2 vs. 0mM 0.2% O_2	***
DLD1 mitochondrial area per cell (Figure 5.14.B)	25mM 20.9% O_2 vs. 0mM 20.9% O_2	****
	25mM 20.9% O_2 vs. 0mM 0.2% O_2	*
	25mM 0.2% O_2 vs. 0mM 20.9% O_2	****
	25mM 0.2% O_2 vs. 0mM 0.2% O_2	*
	5mM 20.9% O_2 vs. 0mM 20.9% O_2	****
	5mM 20.9% O_2 vs. 0mM 0.2% O_2	**
	5mM 0.2% O_2 vs. 0mM 20.9% O_2	****
	5mM 0.2% O_2 vs. 0mM 0.2% O_2	**
	0mM 20.9% O_2 vs. 0mM 0.2% O_2	*
SW837 mitochondrial foci per cell (Figure	5mM 20.9% O_2 vs. 0mM 0.2% O_2	*
	5mM 0.2% O_2 vs. 0mM 20.9% O_2	*
	5mM 0.2% O_2 vs. 0mM 0.2% O_2	**
SW837 mitochondrial area per cell (Figure 5.14.D)	25mM 20.9% O_2 vs. 0mM 0.2% O_2	**
	25mM 0.2% O_2 vs. 0mM 0.2% O_2	**
	5mM 20.9% O_2 vs. 0mM 0.2% O_2	**
	5mM 0.2% O_2 vs. 0mM 20.9% O_2	*
	5mM 0.2% O_2 vs. 0mM 0.2% O_2	***

Table A.5.34. Summary of two-way ANOVA statistics for percentage of total FH in mitochondria and cytoplasm per cell. See also Figure 5.16.

Measurement	ANOVA table	F (DFn, DFd)	p value	p value summary
DLD1 – FH in mitochondria	Interaction	F (2, 12) = 1.028	0.3873	ns
	Glucose	F (2, 12) = 18.67	0.0002	***
	Oxygen	F (1, 12) = 6.511	0.0254	*
DLD1 – FH in cytoplasm	Interaction	F (2, 12) = 1.03	0.3865	ns
	Glucose	F (2, 12) = 18.67	0.0002	***
	Oxygen	F (1, 12) = 6.516	0.0253	*
SW837 – FH in mitochondria	Interaction	F (2, 12) = 1.712	0.2218	ns
	Glucose	F (2, 12) = 2.816	0.0993	ns
	Oxygen	F (1, 12) = 3.117	0.1029	ns
SW837 – FH in cytoplasm	Interaction	F (2, 12) = 1.713	0.2215	ns
	Glucose	F (2, 12) = 2.802	0.1003	ns
	Oxygen	F (1, 12) = 3.109	0.1033	ns

Table A.5.35. Bonferroni *post hoc* test values for percentage of total FH in mitochondria and cytoplasm per cell. Only significant values shown. See also Figure 5.16**.**

Measurement	Conditions	Bonferroni *post hoc* value summary
DLD1 – FH in mitochondria	25mM 20.9% O_2 vs. 5mM 20.9% O_2	*
	25mM 0.2% O_2 vs. 5mM 0.2% O_2	**
	5mM 0.2% O_2 vs. 0mM 0.2% O_2	**
DLD1 – FH in cytoplasm	25mM 20.9% O_2 vs. 5mM 20.9% O_2	*
	25mM 0.2% O_2 vs. 5mM 0.2% O_2	**
	5mM 0.2% O_2 vs. 0mM 0.2% O_2	**

Table A.5.36. Summary of unpaired t-test data for Seahorse Mito Stress test. See also Figure 5.18.

Cell type	Test	Significant tests	P value	P value summary
DLD1 (Figure 5.18.A)	25mM vs 0mM	Spare capacity	0.0018	**
	5mM vs 0mM	Spare capacity	0.0035	**
DLD1 + 25mM (Figure 5.18.B)	25mM vs 5mM	Maximal respiration	0.0027	**
	25mM vs 0mM	Basal respiration	0.0029	**
		Proton leak	0.0073	**
SW837 (Figure 5.18.C)	25mM vs 0mM	Spare capacity	0.0004	***
		Maximal respiration	0.0021	**
		ATP production	0.0044	**
	5mM vs 0mM	Spare capacity	0.0030	**
		Maximal respiration	0.0044	**
SW837 + 25mM (Figure 5.18.D)	25mM vs 0mM	Spare capacity	<0.0001	****
	5mM vs 0mM		0.0030	**
MEFs (Figure 5.18.E)	WT vs KO	Spare capacity	<0.0001	****
		Maximal respiration	0.0002	***
		Proton leak	0.0066	**
		ATP production	0.0080	**

Table A.5.36b. Summary of two-way ANOVA statistics for seahorse fold change data.

See also Figure 5.18.

Measurement	ANOVA table	F (DFn, DFd)	p value	p value summary
DLD1 (Figure 5.18b.A)	Interaction	F (10, 34) = 2.675	0.0157	*
	Glucose	F (5, 34) = 2.775	0.0331	*
	Oxygen	F (2, 34) = 30.07	<0.0001	****
DLD1 + 25mM (Figure 5.18b.B)	Interaction	F (10, 36) = 4.416	0.0004	***
	Glucose	F (5, 36) = 7.318	<0.0001	****
	Oxygen	F (2, 36) = 11.5	<0.0001	****
SW837 (Figure 5.18b.C)	Interaction	F (10, 34) = 1.394	0.2245	ns
	Glucose	F (5, 34) = 2.878	0.0285	*
	Oxygen	F (2, 34) = 25.23	<0.0001	****
SW837 + 25mM (Figure 5.18b.D)	Interaction	F (10, 36) = 13.29	<0.0001	****
	Glucose	F (5, 36) = 33.22	<0.0001	****
	Oxygen	F (2, 36) = 20.97	<0.0001	****
MEFs (Figure 5.18b.E)	Interaction	F (5, 24) = 7.802	0.0002	****
	Glucose	F (5, 24) = 7.802	0.0002	****
	Oxygen	F (1, 12) = 2150	<0.0001	****

Table A.5.36c. Bonferroni *post hoc* test values for Seahorse data. See also Figure 5.18**.** Only significant values shown.

Cell type	Test	Significant tests	P value	P value summary
DLD1 (Figure 5.18b.A)	25mM vs 0mM	ATP production	0.0331	*
		Max resp.	0.0005	***
		Spare capacity	<0.0001	****
	5mM vs 0mM	ATP production	0.0140	*
		Maximal resp.	0.0011	**
		Spare capacity	<0.0001	****
DLD1 + 25mM (Figure 5.18b.B)	25mM vs 0mM	Proton leak	0.0082	**
		Maximal resp.	<0.0001	****
		Spare capacity	0.0017	**
	5mM vs 0mM	Maximal resp.	0.0373	*
		Spare capacity	0.0017	**
	25mM vs 5mM	Maximal resp.	0.0440	*
SW837 (Figure 5.18b.C)	25mM vs 0mM	ATP production	0.0164	*
		Maximal resp.	0.0061	**
		Spare capacity	<0.0001	****
	5mM vs 0mM	Maximal resp.	0.0243	*
		Spare capacity	0.0006	***
SW837 + 25mM (Figure 5.18b.D)	25mM vs 0mM	ATP production	0.0140	*
		Max resp.	0.0005	***
		Spare capacity	<0.0001	****
	5mM vs 0mM	Max resp.	<0.0001	****
		Spare capacity	0.0005	***
	25mM vs 5mM	Max resp.	0.0177	*
		Non-mito resp.	0.0221	*

MEFs (Figure 5.18b.E)	WT vs KO	Basal resp.	<0.0001	****
		ATP production	<0.0001	****
		Proton leak	<0.0001	****
		Maximal resp.	<0.0001	****
		Spare capacity	<0.0001	****
		Non-mito resp.	<0.0001	****

Chapter 10 - Bibliography

1. *Cancer Registration Statistics, England: 2015*. (2015).
2. Torre, L. A., Siegel, R. L., Ward, E. M. & Jemal, A. Global Cancer Incidence and Mortality Rates and Trends-An Update. *Cancer Epidemiol Biomarkers Prev* (2015). doi:10.1158/1055-9965.epi-15-0578
3. Sun, S. *et al.* Insulin-induced gene 2 expression correlates with colorectal cancer metastasis and disease outcome. *IUBMB Life* (2015). doi:10.1002/iub.1461
4. Jemal, A. *et al.* Annual report to the nation on the status of cancer, 1975-2001, with a special feature regarding survival. *Cancer* **101,** 3–27 (2004).
5. Choices, N. Bowel cancer - Symptoms - NHS Choices.
6. Kumar, Vinay, 1944-, Abbas, A. K., Fausto, N., Robbins, S. L. & Cotran, R. S. *Robbins and Cotran pathologic basis of disease*. (Philadelphia, Pa. : Elsevier Saunders, c2005, 2005).
7. Eisenberg, R. L. *Gastrointestinal Radiology*. (Lippincott Williams & Wilkins, 2003). doi:0781737060
8. Bowel cancer statistics | Cancer Research UK. Available at: http://www.cancerresearchuk.org/health-professional/cancer-statistics/statistics-by-cancer-type/bowel-cancer#heading-Two. (Accessed: 8th January 2017)
9. Fearon, E. R. & Vogelstein, B. A genetic model for colorectal tumorigenesis. *Cell* **61,** 759–767 (1990).
10. Vogelstein, B. *et al.* Cancer genome landscapes. *Science (80-.).* **339,** 1546–1558 (2013).
11. Stratton, M. R., Campbell, P. J. & Futreal, P. A. The cancer genome. *Nature* **458,** 719–724 (2009).
12. Gonzalez-Perez, A. *et al.* Computational approaches to identify functional genetic variants in cancer genomes. *Nat Methods* **10,** 723–729 (2013).
13. Nagase, H. & Nakamura, Y. Mutations of the APC (adenomatous polyposis coli) gene. *Hum Mutat* **2,** 425–434 (1993).
14. Pate, K. T. *et al.* Wnt signaling directs a metabolic program of glycolysis and angiogenesis in colon cancer. *EMBO J.* **33,** 1454–73 (2014).
15. Pollard, P. *et al.* The Apc1322T Mouse Develops Severe Polyposis Associated With Submaximal Nuclear β-Catenin Expression. *Gastroenterology* **136,** 2204–2213.e13 (2009).
16. Miller, J. R., Hocking, A. M., Brown, J. D. & Moon, R. T. Mechanism and function of signal transduction by the Wnt/β-catenin and Wnt/Ca2+ pathways. *Oncogene* **18,** 7860–7872 (2000).

17. Lamlum, H. *et al.* The type of somatic mutation at APC in familial adenomatous polyposis is determined by the site of the germline mutation: a new facet to Knudson's 'two-hit' hypothesis. *Nat. Med.* **5,** 1071–5 (1999).

18. Segditsas, S. *et al.* APC and the three-hit hypothesis. *Oncogene* **28,** (2009).

19. Christie, M. *et al.* Different APC genotypes in proximal and distal sporadic colorectal cancers suggest distinct WNT/β-catenin signalling thresholds for tumourigenesis. *Oncogene* **32,** 4675–82 (2013).

20. Albuquerque, C. *et al.* The 'just-right' signaling model: APC somatic mutations are selected based on a specific level of activation of the beta-catenin signaling cascade. *Hum Mol Genet* **11,** 1549–1560 (2002).

21. Korinek, V. *et al.* Constitutive transcriptional activation by a beta-catenin-Tcf complex in APC-/- colon carcinoma. *Science (80-.).* **275,** 1784–1787 (1997).

22. Morin, P. J. *et al.* Activation of beta-catenin-Tcf signaling in colon cancer by mutations in beta-catenin or APC. *Science (80-.).* **275,** 1787–1790 (1997).

23. Vogelstein, B. *et al.* Genetic alterations during colorectal-tumor development. *N Engl J Med* **319,** 525–532 (1988).

24. Lane, D. P. Cancer. p53, guardian of the genome. *Nature* **358,** 15–16 (1992).

25. Kandoth, C. *et al.* Mutational landscape and significance across 12 major cancer types. *Nature* **502,** 333–9 (2013).

26. Baker, S. J. *et al.* p53 gene mutations occur in combination with 17p allelic deletions as late events in colorectal tumorigenesis. *Cancer Res* **50,** 7717–7722 (1990).

27. Meek, D. W. The p53 response to DNA damage. *DNA Repair* **3,** 1049–1056 (2004).

28. Santini, D. *et al.* High concordance of KRAS status between primary colorectal tumors and related metastatic sites: implications for clinical practice. *Oncologist* **13,** 1270–1275 (2008).

29. Clarke, C. N. & Kopetz, E. S. BRAF mutant colorectal cancer as a distinct subset of colorectal cancer: clinical characteristics, clinical behavior, and response to targeted therapies. *J. Gastrointest. Oncol.* **6,** 660–7 (2015).

30. Fearon, E. R. *et al.* Identification of a chromosome 18q gene that is altered in colorectal cancers. *Science (80-.).* **247,** 49–56 (1990).

31. Riggins, G. J. *et al.* Mad-related genes in the human. *Nat Genet* **13,** 347–349 (1996).

32. Howe, J. R. *et al.* Mutations in the SMAD4/DPC4 gene in juvenile polyposis. *Science (80-.).* **280,** 1086–1088 (1998).

33. Burrell, R. A. *et al.* Replication stress links structural and numerical cancer chromosomal instability. *Nature* **494,** 492–496 (2013).

34. Andor, N. *et al.* Pan-cancer analysis of the extent and consequences of intratumor heterogeneity. *Nat. Med.* **22,** 105–113 (2016).

35. Gatenby, R. A. *et al.* Cellular adaptations to hypoxia and acidosis during somatic evolution of breast cancer. *Br. J. Cancer* **97,** 646–653 (2007).

36. Sottoriva, A. *et al.* A Big Bang model of human colorectal tumor growth. *Nat. Genet.* **47,** 209–216 (2015).

37. Baker, A.-M. *et al.* Quantification of Crypt and Stem Cell Evolution in the Normal and Neoplastic Human Colon. *Cell Rep.* **8,** 940–947 (2014).

38. Baker, A.-M. *et al.* Robust RNA-based in situ mutation detection delineates colorectal cancer subclonal evolution. *Nat. Commun.* **8,** 1998 (2017).

39. Popat, S., Hubner, R. & Houlston, R. S. Systematic review of microsatellite instability and colorectal cancer prognosis. *J Clin Oncol* **23,** 609–618 (2005).

40. Silver, A. *et al.* A distinct DNA methylation profile associated with microsatellite and chromosomal stable sporadic colorectal cancers. *Int J Cancer* **130,** 1082–1092 (2012).

41. Yokota, T. Are KRAS/BRAF mutations potent prognostic and/or predictive biomarkers in colorectal cancers? *Anticancer. Agents Med. Chem.* **12,** 163–71 (2012).

42. Suraweera, N. *et al.* Relative telomere lengths in tumor and normal mucosa are related to disease progression and chromosome instability profiles in colorectal cancer. *Oncotarget* **7,** 36474–36488 (2016).

43. Boland, C. R. & Goel, A. Microsatellite instability in colorectal cancer. *Gastroenterology* **138,** 2073–2087 e3 (2010).

44. Ionov, Y., Peinado, M. A., Malkhosyan, S., Shibata, D. & Perucho, M. Ubiquitous somatic mutations in simple repeated sequences reveal a new mechanism for colonic carcinogenesis. *Nature* **363,** 558–561 (1993).

45. Carethers, J. M. *et al.* Use of 5-fluorouracil and survival in patients with microsatellite-unstable colorectal cancer. *Gastroenterology* **126,** 394–401 (2004).

46. Toyota, M. *et al.* CpG island methylator phenotype in colorectal cancer. *Proc Natl Acad Sci U S A* **96,** 8681–8686 (1999).

47. Slattery, M. L. *et al.* A comparison of colon and rectal somatic DNA alterations. *Dis Colon Rectum* **52,** 1304–1311 (2009).

48. Georgiades, I. B., Curtis, L. J., Morris, R. M., Bird, C. C. & Wyllie, A. H. Heterogeneity studies identify a subset of sporadic colorectal cancers without evidence for chromosomal or microsatellite instability. *Oncogene* **18,** 7933–7940 (1999).

49. Chan, T. L. *et al.* Early-onset colorectal cancer with stable microsatellite DNA and near-diploid chromosomes. *Oncogene* **20,** 4871–4876 (2001).

50. Mouradov, D. *et al.* Colorectal cancer cell lines are representative models of the main molecular subtypes of primary cancer. *Cancer Res.* **74,** 3238–47 (2014).

51. Wang, J. *et al.* Colorectal Cancer Cell Line Proteomes Are Representative of Primary Tumors and Predict Drug Sensitivity. *Gastroenterology* **153,** 1082–1095 (2017).

52. Boyle, P. & Langman, J. S. ABC of colorectal cancer: Epidemiology. *BMJ* **321,** 805–808 (2000).

53. Ahnen, D. J. *et al.* The increasing incidence of young-onset colorectal cancer: a call to action. *Mayo Clin Proc* **89,** 216–224 (2014).

54. Davis, D. M. *et al.* Is It Time to Lower the Recommended Screening Age for Colorectal Cancer? *J. Am. Coll. Surg.* **213,** 352–361 (2011).

55. Valle, L. Genetic predisposition to colorectal cancer: where we stand and future perspectives. *World J. Gastroenterol.* **20,** 9828–49 (2014).

56. Papadopoulos, N. *et al.* Mutation of a mutL homolog in hereditary colon cancer. *Science (80-.).* **263,** 1625–1629 (1994).

57. Gulati, S., Gustafson, S. & Daw, H. A. Lynch Syndrome Associated With PMS2 Mutation: Understanding Current Concepts. *Gastrointest Cancer Res* **4,** 188–190 (2011).

58. Hampel, H. *et al.* Screening for the Lynch syndrome (hereditary nonpolyposis colorectal cancer). *N Engl J Med* **352,** 1851–1860 (2005).

59. Chen, S. *et al.* Prediction of germline mutations and cancer risk in the Lynch syndrome. *JAMA* **296,** 1479–1487 (2006).

60. Chung, L. *et al.* Unexpected endometrial cancer at prophylactic hysterectomy in a woman with hereditary nonpolyposis colon cancer. *Obs. Gynecol* **102,** 1152–1155 (2003).

61. Furlan, D. *et al.* Genetic progression in sporadic endometrial and gastrointestinal cancers with high microsatellite instability. *J Pathol* **197,** 603–609 (2002).

62. Meyer, L. A., Broaddus, R. R. & Lu, K. H. Endometrial cancer and Lynch syndrome: clinical and pathologic considerations. *Cancer Control* **16,** 14–22 (2009).

63. Groden, J. *et al.* Identification and characterization of the familial adenomatous polyposis coli gene. *Cell* **66,** 589–600 (1991).

64. Kinzler, K. W. *et al.* Identification of FAP locus genes from chromosome 5q21. *Science (80-.).* **253,** 661–665 (1991).

65. Nugent, K. P. *et al.* Phenotypic expression in familial adenomatous polyposis: partial prediction by mutation analysis. *Gut* **35,** 1622–3 (1994).

66. Lynch, P. M. Standards of care in diagnosis and testing for hereditary colon cancer. *Fam Cancer* **7,** 65–72 (2008).

67. Knudsen, A. L. *et al.* Attenuated familial adenomatous polyposis: results from an international collaborative study. *Color. Dis.* **12,** e243–e249 (2010).

68. Parc, Y., Piquard, A., Dozois, R. R., Parc, R. & Tiret, E. Long-term outcome of familial adenomatous polyposis patients after restorative coloproctectomy. *Ann Surg* **239,** 378–382 (2004).

69. Al-Tassan, N. *et al.* Inherited variants of MYH associated with somatic G:C-->T:A mutations in colorectal tumors. *Nat Genet* **30,** 227–232 (2002).

70. Nielsen, M. *et al.* Survival of MUTYH-associated polyposis patients with colorectal cancer and matched control colorectal cancer patients. *J Natl Cancer Inst* **102,** 1724–1730 (2010).

71. McGarrity, T. J., Amos, C. I., Frazier, M. L. & Wei, C. in *GeneReviews(R)* (eds. Pagon, R. A. et al.) (University of Washington, Seattle, 1993).

72. Hemminki, A. *et al.* A serine/threonine kinase gene defective in Peutz-Jeghers syndrome. *Nature* **391,** 184–187 (1998).

73. Sayed, M. G. *et al.* Germline SMAD4 or BMPR1A mutations and phenotype of juvenile polyposis. *Ann Surg Oncol* **9,** 901–906 (2002).

74. Palles, C. *et al.* Germline mutations affecting the proofreading domains of POLE and POLD1 predispose to colorectal adenomas and carcinomas. *Nat Genet* **45,** 136–144 (2013).

75. Rogler, G. Chronic ulcerative colitis and colorectal cancer. *Cancer Lett* **345,** 235–241 (2014).

76. Colotta, F., Allavena, P., Sica, A., Garlanda, C. & Mantovani, A. Cancer-related inflammation, the seventh hallmark of cancer: links to genetic instability. *Carcinogenesis* **30,** 1073–1081 (2009).

77. Choi, C.-H. R. *et al.* Cumulative burden of inflammation predicts colorectal neoplasia risk in ulcerative colitis: a large single-centre study. *Gut* gutjnl-2017-314190 (2017). doi:10.1136/gutjnl-2017-314190

78. Curtius, K., Wright, N. A. & Graham, T. A. An evolutionary perspective on field cancerization. *Nat. Rev. Cancer* **18,** 19–32 (2017).

79. Graham, T. A., McDonald, S. A. & Wright, N. A. Field cancerization in the GI tract. *Futur. Oncol.* **7,** 981–993 (2011).

80. CDC - Colorectal Cancer Rates by Race and Ethnicity. Available at: http://www.cdc.gov/cancer/colorectal/statistics/race.htm. (Accessed: 29th March 2016)

81. Locker, G. Y. & Lynch, H. T. Genetic factors and colorectal cancer in Ashkenazi Jews. *Fam Cancer* **3,** 215–221 (2004).

82. Ahmed, S., Banerjea, A., Hands, R. E., Bustin, S. & Dorudi, S. Microarray profiling of colorectal cancer in Bangladeshi patients. *Color. Dis.* **7,** 571–575 (2005).

83. Sengupta, N. *et al.* Analysis of colorectal cancers in British Bangladeshi identifies early onset, frequent mucinous histotype and a high prevalence of RBFOX1 deletion. *Mol. Cancer* **12,** 1 (2013).

84. Kim, E., Coelho, D. & Blachier, F. Review of the association between meat consumption and risk of colorectal cancer. *Nutr Res* **33,** 983–994 (2013).

85. Wiseman, M. The second World Cancer Research Fund/American Institute for Cancer Research expert report. Food, nutrition, physical activity, and the prevention of cancer: a global perspective. *Proc Nutr Soc* **67,** 253–256 (2008).

86. Bird, C. L. *et al.* Plasma ferritin, iron intake, and the risk of colorectal polyps. *Am. J. Epidemiol.* **144,** 34–41 (1996).

87. Aune, D. *et al.* Dietary fibre, whole grains, and risk of colorectal cancer: systematic review and dose-response meta-analysis of prospective studies. *BMJ* **343,** d6617 (2011).

88. Sinha, R. *et al.* Fecal Microbiota, Fecal Metabolome, and Colorectal Cancer Interrelations. *PLoS One* **11,** e0152126 (2016).

89. Sun, J. & Kato, I. Gut microbiota, inflammation and colorectal cancer. *Genes Dis.* **3,** 130–143 (2016).

90. Gagnière, J. *et al.* Gut microbiota imbalance and colorectal cancer. *World J. Gastroenterol.* **22,** 501–18 (2016).

91. Yu, Y.-N. & Fang, J.-Y. Gut Microbiota and Colorectal Cancer. *Gastrointest. Tumors* **2,** 26–32 (2015).

92. Shen, X. J. *et al.* Molecular characterization of mucosal adherent bacteria and associations with colorectal adenomas. *Gut Microbes* **1,** 138–47

93. Botteri, E., Iodice, S., Raimondi, S., Maisonneuve, P. & Lowenfels, A. B. Cigarette smoking and adenomatous polyps: a meta-analysis. *Gastroenterology* **134,** 388–395 (2008).

94. Zisman, A. L., Nickolov, A., Brand, R. E., Gorchow, A. & Roy, H. K. Associations between the age at diagnosis and location of colorectal cancer and the use of alcohol and tobacco: implications for screening. *Arch Intern Med* **166,** 629–634 (2006).

95. Walter, V., Jansen, L., Hoffmeister, M. & Brenner, H. Smoking and survival of colorectal cancer patients: systematic review and meta-analysis. *Ann Oncol* **25,** 1517–1525 (2014).

96. Giovannucci, E. *et al.* A prospective study of cigarette smoking and risk of colorectal adenoma and colorectal cancer in U.S. women. *J. Natl. Cancer Inst.* **86,** 192–9 (1994).

97. Fedirko, V. *et al.* Alcohol drinking and colorectal cancer risk: an overall and dose-response meta-analysis of published studies. *Ann Oncol* **22,** 1958–1972 (2011).

98. Secretan, B. *et al.* A review of human carcinogens--Part E: tobacco, areca nut,

alcohol, coal smoke, and salted fish. *Lancet. Oncol.* **10,** 1033–4 (2009).

99. Guh, D. P. *et al.* The incidence of co-morbidities related to obesity and overweight: a systematic review and meta-analysis. *BMC Public Health* **9,** 88 (2009).

100. Daniel, C. R. *et al.* Severe obesity prior to diagnosis limits survival in colorectal cancer patients evaluated at a large cancer centre. *Br J Cancer* **114,** 103–109 (2016).

101. Vazzana, N. *et al.* Obesity-driven inflammation and colorectal cancer. *Curr. Med. Chem.* **19,** 5837–53 (2012).

102. Martinez-Useros, J. & Garcia-Foncillas, J. Obesity and colorectal cancer: molecular features of adipose tissue. *J. Transl. Med.* **14,** 21 (2016).

103. Boyle, T., Keegel, T., Bull, F., Heyworth, J. & Fritschi, L. Physical activity and risks of proximal and distal colon cancers: a systematic review and meta-analysis. *J. Natl. Cancer Inst.* **104,** 1548–61 (2012).

104. Slattery, M. L. Physical activity and colorectal cancer. *Sports Med.* **34,** 239–52 (2004).

105. Sun, L. & Yu, S. Diabetes mellitus is an independent risk factor for colorectal cancer. *Dig Dis Sci* **57,** 1586–1597 (2012).

106. Erbach, M., Mehnert, H. & Schnell, O. Diabetes and the risk for colorectal cancer. *J Diabetes Complicat.* **26,** 50–55 (2012).

107. Wang, J. Y. *et al.* Risk of colorectal cancer in type 2 diabetic patients: a population-based cohort study. *Jpn J Clin Oncol* **43,** 258–263 (2013).

108. Khalili, H. & Chan, A. T. Is diabetes a risk factor for colorectal cancer? *Dig Dis Sci* **57,** 1427–1429 (2012).

109. Jurjus, A. *et al.* Inflammatory bowel disease, colorectal cancer and type 2 diabetes mellitus: The links. *BBA Clin.* **5,** 16–24 (2016).

110. Stein, K. B. *et al.* Colorectal cancer outcomes, recurrence, and complications in persons with and without diabetes mellitus: a systematic review and meta-analysis. *Dig Dis Sci* **55,** 1839–1851 (2010).

111. Yuhara, H. *et al.* Is diabetes mellitus an independent risk factor for colon cancer and rectal cancer? *Am J Gastroenterol* **106,** 1911–21; quiz 1922 (2011).

112. Choices, N. Bowel cancer - Screening - NHS Choices.

113. Shussman, N. & Wexner, S. D. Colorectal polyps and polyposis syndromes. *Gastroenterol. Rep.* **2,** 1–15 (2014).

114. Doubeni, C. A. The impact of colorectal cancer screening on the US population: is it time to celebrate? *Cancer* **120,** 2810–3 (2014).

115. Graser, A. *et al.* Comparison of CT colonography, colonoscopy, sigmoidoscopy

and faecal occult blood tests for the detection of advanced adenoma in an average risk population. *Gut* **58,** 241–248 (2009).

116. Mandel, J. S. *et al.* Reducing mortality from colorectal cancer by screening for fecal occult blood. Minnesota Colon Cancer Control Study. *N Engl J Med* **328,** 1365–1371 (1993).

117. Ouyang, D. L., Chen, J. J., Getzenberg, R. H. & Schoen, R. E. Noninvasive testing for colorectal cancer: a review. *Am J Gastroenterol* **100,** 1393–1403 (2005).

118. Forones, N. M. & Tanaka, M. CEA and CA 19-9 as prognostic indexes in colorectal cancer. *Hepatogastroenterology.* **46,** 905–8

119. Colorectal carcinoma | Radiology Reference Article | Radiopaedia.org. Available at: http://radiopaedia.org/articles/colorectal-carcinoma. (Accessed: 29th March 2016)

120. Chiche, J., Ricci, J. E. & Pouyssegur, J. Tumor hypoxia and metabolism -- towards novel anticancer approaches. *Ann Endocrinol* **74,** 111–114 (2013).

121. Van Cutsem, E., Cervantes, A., Nordlinger, B. & Arnold, D. Metastatic colorectal cancer: ESMO Clinical Practice Guidelines for diagnosis, treatment and follow-up. *Ann. Oncol.* **25 Suppl 3,** iii1-9 (2014).

122. Lipsyc, M. & Yaeger, R. Impact of somatic mutations on patterns of metastasis in colorectal cancer. *J Gastrointest Oncol* **6,** 645–649 (2015).

123. Williams, D. S. *et al.* Lymphocytic response to tumour and deficient DNA mismatch repair identify subtypes of stage II/III colorectal cancer associated with patient outcomes. *Gut* gutjnl-2017-315664 (2018). doi:10.1136/gutjnl-2017-315664

124. Sharma, A. *et al.* Colorectal cancer: Histopathologic differences in tumor characteristics between patients with and without diabetes. *Clin Color. Cancer* **13,** 54–61 (2014).

125. Andre, T. *et al.* Improved overall survival with oxaliplatin, fluorouracil, and leucovorin as adjuvant treatment in stage II or III colon cancer in the MOSAIC trial. *J Clin Oncol* **27,** 3109–3116 (2009).

126. Van Cutsem, E. *et al.* Cetuximab plus irinotecan, fluorouracil, and leucovorin as first-line treatment for metastatic colorectal cancer: updated analysis of overall survival according to tumor KRAS and BRAF mutation status. *J Clin Oncol* **29,** 2011–2019 (2011).

127. Hurwitz, H. *et al.* Bevacizumab plus irinotecan, fluorouracil, and leucovorin for metastatic colorectal cancer. *N Engl J Med* **350,** 2335–2342 (2004).

128. Douillard, J. Y. *et al.* Final results from PRIME: randomized phase III study of panitumumab with FOLFOX4 for first-line treatment of metastatic colorectal cancer. *Ann Oncol* **25,** 1346–1355 (2014).

129. Tabernero, J. *et al.* Ramucirumab versus placebo in combination with second-line

FOLFIRI in patients with metastatic colorectal carcinoma that progressed during or after first-line therapy with bevacizumab, oxaliplatin, and a fluoropyrimidine (RAISE): a randomised, double-blin. *Lancet Oncol* **16,** 499–508 (2015).

130. Van Cutsem, E. *et al.* Addition of aflibercept to fluorouracil, leucovorin, and irinotecan improves survival in a phase III randomized trial in patients with metastatic colorectal cancer previously treated with an oxaliplatin-based regimen. *J Clin Oncol* **30,** 3499–3506 (2012).

131. Grothey, A. *et al.* Regorafenib monotherapy for previously treated metastatic colorectal cancer (CORRECT): an international, multicentre, randomised, placebo-controlled, phase 3 trial. *Lancet* **381,** 303–312 (2013).

132. Primrose, J. *et al.* Systemic chemotherapy with or without cetuximab in patients with resectable colorectal liver metastasis: the New EPOC randomised controlled trial. *Lancet Oncol* **15,** 601–611 (2014).

133. Santoro, V. *et al.* Role of Reactive Oxygen Species in the Abrogation of Oxaliplatin Activity by Cetuximab in Colorectal Cancer. *J Natl Cancer Inst* **108,** (2015).

134. Bedard, K. & Krause, K.-H. The NOX Family of ROS-Generating NADPH Oxidases: Physiology and Pathophysiology. *Physiol. Rev.* **87,** 245–313 (2007).

135. Caillou, B. *et al.* Expression of Reduced Nicotinamide Adenine Dinucleotide Phosphate Oxidase (*ThoX, LNOX, Duox*) Genes and Proteins in Human Thyroid Tissues [1]. *J. Clin. Endocrinol. Metab.* **86,** 3351–3358 (2001).

136. El Hassani, R. A. *et al.* Dual oxidase2 is expressed all along the digestive tract. *AJP Gastrointest. Liver Physiol.* **288,** G933–G942 (2005).

137. Harper, R. W. *et al.* Differential regulation of dual NADPH oxidases/peroxidases, Duox1 and Duox2, by Th1 and Th2 cytokines in respiratory tract epithelium. *FEBS Lett.* **579,** 4911–4917 (2005).

138. Geiszt, M., Witta, J., Baffi, J., Lekstrom, K. & Leto, T. L. Dual oxidases represent novel hydrogen peroxide sources supporting mucosal surface host defense. *FASEB J.* **17,** 1502–4 (2003).

139. MacFie, T. S. *et al.* DUOX2 and DUOXA2 form the predominant enzyme system capable of producing the reactive oxygen species H2O2 in active ulcerative colitis and are modulated by 5-aminosalicylic acid. *Inflamm Bowel Dis* **20,** 514–524 (2014).

140. Edens, W. A. *et al.* Tyrosine cross-linking of extracellular matrix is catalyzed by Duox, a multidomain oxidase/peroxidase with homology to the phagocyte oxidase subunit gp91phox. *J. Cell Biol.* **154,** 879–91 (2001).

141. Doroshow, J. *et al.* Functional activity and tumor-specific expression of dual oxidase 2 in pancreatic cancer cells and human malignancies characterized with a novel monoclonal antibody. *Int. J. Oncol.* **42,** 1229–38 (2013).

142. Hill, T., Xu, C. & Harper, R. W. IFNγ mediates DUOX2 expression via a STAT-independent signaling pathway. *Biochem. Biophys. Res. Commun.* **395,** 270–274

(2010).

143. Kanthan, R., Loewy, J. & Kanthan, S. C. Skeletal metastases in colorectal carcinomas: a Saskatchewan profile. *Dis. Colon Rectum* **42,** 1592–7 (1999).

144. Mucaj, V., Shay, J. E. & Simon, M. C. Effects of hypoxia and HIFs on cancer metabolism. *Int J Hematol* **95,** 464–470 (2012).

145. Bertout, J. A., Patel, S. A. & Simon, M. C. The impact of O2 availability on human cancer. *Nat. Rev. Cancer* **8,** 967–975 (2008).

146. Yu, B. *et al.* Measuring tumor cycling hypoxia and angiogenesis using a side-firing fiber optic probe. *J. Biophotonics* **7,** 552–64 (2014).

147. Carmeliet, P. & Jain, R. K. Angiogenesis in cancer and other diseases. *Nature* **407,** 249–57 (2000).

148. Dunwoodie, S. L. The Role of Hypoxia in Development of the Mammalian Embryo. *Dev. Cell* **17,** 755–773 (2009).

149. Cermakova, P. *et al.* Heart failure and Alzheimer's disease. *J. Intern. Med.* **277,** 406–25 (2015).

150. Giordano, F. J. Oxygen, oxidative stress, hypoxia, and heart failure. *J. Clin. Invest.* **115,** 500–8 (2005).

151. Norouzirad, R., González-Muniesa, P. & Ghasemi, A. Hypoxia in Obesity and Diabetes: Potential Therapeutic Effects of Hyperoxia and Nitrate. *Oxid. Med. Cell. Longev.* **2017,** 5350267 (2017).

152. Eales, K. L., Hollinshead, K. E. R. & Tennant, D. A. Hypoxia and metabolic adaptation of cancer cells. *Oncogenesis* **5,** e190 (2016).

153. Dewhirst, M. W. Relationships between cycling hypoxia, HIF-1, angiogenesis and oxidative stress. *Radiat. Res.* **172,** 653–65 (2009).

154. Smith, H. *et al.* The Effects of Severe Hypoxia on Glycolytic Flux and Enzyme Activity in a Model of Solid Tumors. *J. Cell. Biochem.* **117,** 1890–901 (2016).

155. Helmlinger, G., Netti, P. A., Lichtenbeld, H. C., Melder, R. J. & Jain, R. K. Solid stress inhibits the growth of multicellular tumor spheroids. *Nat. Biotechnol.* **15,** 778–783 (1997).

156. Grimes, D. R., Kelly, C., Bloch, K. & Partridge, M. A method for estimating the oxygen consumption rate in multicellular tumour spheroids. *J. R. Soc. Interface* **11,** 20131124–20131124 (2014).

157. Brown, J. M. & Giaccia, A. J. The unique physiology of solid tumors: opportunities (and problems) for cancer therapy. *Cancer Res* **58,** 1408–1416 (1998).

158. Kizaka-Kondoh, S., Inoue, M., Harada, H. & Hiraoka, M. Tumor hypoxia: a target for selective cancer therapy. *Cancer Sci* **94,** 1021–1028 (2003).

159. Kaelin Jr., W. G. & Ratcliffe, P. J. Oxygen sensing by metazoans: the central role

of the HIF hydroxylase pathway. *Mol Cell* **30,** 393–402 (2008).

160. Dekervel, J. *et al.* Hypoxia-driven gene expression is an independent prognostic factor in stage II and III colon cancer patients. *Clin Cancer Res* **20,** 2159–2168 (2014).

161. Goldmann, E. The Growth of Malignant Disease in Man and the Lower Animals, with special reference to the Vascular System. *Proc. R. Soc. Med.* **1,** 1–13 (1908).

162. Murono, K. *et al.* SN-38 overcomes chemoresistance of colorectal cancer cells induced by hypoxia, through HIF1alpha. *Anticancer Res* **32,** 865–872 (2012).

163. Kuwai, T. *et al.* Expression of hypoxia-inducible factor-1alpha is associated with tumor vascularization in human colorectal carcinoma. *Int J Cancer* **105,** 176–181 (2003).

164. Liou, G.-Y. & Storz, P. Reactive oxygen species in cancer. *Free Radic. Res.* **44,** 479–96 (2010).

165. Fukuda, R. *et al.* HIF-1 Regulates Cytochrome Oxidase Subunits to Optimize Efficiency of Respiration in Hypoxic Cells. *Cell* **129,** 111–122 (2007).

166. Semenza, G. L. Oxygen-dependent regulation of mitochondrial respiration by hypoxia-inducible factor 1. *Biochem. J.* **405,** 1–9 (2007).

167. Harris, A. L. Hypoxia--a key regulatory factor in tumour growth. *Nat Rev Cancer* **2,** 38–47 (2002).

168. Raimundo, N., Baysal, B. E. & Shadel, G. S. Revisiting the TCA cycle: signaling to tumor formation. *Trends Mol Med* **17,** 641–649 (2011).

169. Altman, B. J., Stine, Z. E. & Dang, C. V. From Krebs to clinic: glutamine metabolism to cancer therapy. *Nat. Rev. Cancer* **16,** (2016).

170. Pescador, N. *et al.* Hypoxia promotes glycogen accumulation through hypoxia inducible factor (HIF)-mediated induction of glycogen synthase 1. *PLoS One* **5,** e9644 (2010).

171. Gatenby, R. A. & Gawlinski, E. T. Mathematical models of tumour invasion mediated by transformation-induced alteration of microenvironmental pH. *Novartis Found. Symp.* **240,** 85-96–9 (2001).

172. Obel, L. F. *et al.* Brain glycogen-new perspectives on its metabolic function and regulation at the subcellular level. *Front. Neuroenergetics* **4,** 3 (2012).

173. Gatenby, R. A. & Gillies, R. J. Why do cancers have high aerobic glycolysis? *Nat Rev Cancer* **4,** 891–899 (2004).

174. Huang, D., Li, C. & Zhang, H. Hypoxia and cancer cell metabolism. *Acta Biochim Biophys Sin* **46,** 214–219 (2014).

175. Griffiths, J. R. Causes and consequences of hypoxia and acidity in tumour microenvironments. *Bioessays* **23,** 295–6 (2001).

176. Sonveaux, P. *et al.* Targeting lactate-fueled respiration selectively kills hypoxic tumor cells in mice. *J. Clin. Invest.* **118,** 3930–42 (2008).

177. Guo, R., Gu, J., Zong, S., Wu, M. & Yang, M. Structure and mechanism of mitochondrial electron transport chain. *Biomed. J.* **41,** 9–20 (2018).

178. O. Warburg E. Negelein, K. P. Ueber den Stoffwechsel der Tumoren. *Biochem. Z.* **Vol. 152,** 319–344 (1924).

179. Warburg, O. On the origin of cancer cells. *Science (80-.).* **123,** 309–314 (1956).

180. Peppicelli, S., Bianchini, F. & Calorini, L. Extracellular acidity, a 'reappreciated' trait of tumor environment driving malignancy: perspectives in diagnosis and therapy. *Cancer Metastasis Rev.* **33,** 823–832 (2014).

181. Williams, A. C., Collard, T. J. & Paraskeva, C. An acidic environment leads to p53 dependent induction of apoptosis in human adenoma and carcinoma cell lines: implications for clonal selection during colorectal carcinogenesis. *Oncogene* **18,** 3199–204 (1999).

182. Koukourakis, M. I. Comparison of Metabolic Pathways between Cancer Cells and Stromal Cells in Colorectal Carcinomas: a Metabolic Survival Role for Tumor-Associated Stroma. *Cancer Res.* **66,** 632–637 (2006).

183. Koukourakis, M. I., Giatromanolaki, A., Simopoulos, C., Polychronidis, A. & Sivridis, E. Lactate dehydrogenase 5 (LDH5) relates to up-regulated hypoxia inducible factor pathway and metastasis in colorectal cancer. *Clin. Exp. Metastasis* **22,** 25–30 (2005).

184. Lu, H. *et al.* Reversible inactivation of HIF-1 prolyl hydroxylases allows cell metabolism to control basal HIF-1. *J. Biol. Chem.* **280,** 41928–39 (2005).

185. Lu, H., Forbes, R. A. & Verma, A. Hypoxia-inducible factor 1 activation by aerobic glycolysis implicates the Warburg effect in carcinogenesis. *J. Biol. Chem.* **277,** 23111–5 (2002).

186. Yokota, H. *et al.* Lactate, choline, and creatine levels measured by vitro 1H-MRS as prognostic parameters in patients with non-small-cell lung cancer. *J. Magn. Reson. Imaging* **25,** 992–9 (2007).

187. Walenta, S. *et al.* High lactate levels predict likelihood of metastases, tumor recurrence, and restricted patient survival in human cervical cancers. *Cancer Res.* **60,** 916–21 (2000).

188. Ward, P. S. & Thompson, C. B. Metabolic Reprogramming: A Cancer Hallmark Even Warburg Did Not Anticipate. *Cancer Cell* **21,** 297–308 (2012).

189. Pedersen, P. L. Tumor mitochondria and the bioenergetics of cancer cells. *Prog. Exp. Tumor Res.* **22,** 190–274 (1978).

190. Fan, T. W. M. *et al.* Rhabdomyosarcoma cells show an energy producing anabolic metabolic phenotype compared with primary myocytes. *Mol. Cancer* **7,** 79 (2008).

191. Vogelstein, B. *et al.* Somatic mutations of the mitochondrial genome in human colorectal tumours. *Nat. Genet.* **20,** 291–293 (1998).

192. Lee, J.-H., Hwang, I., Kang, Y.-N., Choi, I.-J. & Kim, D.-K. Genetic characteristics of mitochondrial DNA was associated with colorectal carcinogenesis and its prognosis. *PLoS One* **10,** e0118612 (2015).

193. Lin, P.-C. *et al.* Expression of β-F1-ATPase and mitochondrial transcription factor A and the change in mitochondrial DNA content in colorectal cancer: clinical data analysis and evidence from an in vitro study. *Int. J. Colorectal Dis.* **23,** 1223–1232 (2008).

194. Waris, G. & Ahsan, H. Reactive oxygen species: role in the development of cancer and various chronic conditions. *J. Carcinog.* **5,** 14 (2006).

195. Katagiri, M. *et al.* Hexokinase 2 in colorectal cancer: a potent prognostic factor associated with glycolysis, proliferation and migration. *Histol. Histopathol.* 11799 (2016). doi:10.14670/HH-11-799

196. Chan, S. Y. & Loscalzo, J. MicroRNA-210: a unique and pleiotropic hypoxamir. *Cell Cycle* **9,** 1072–1083 (2010).

197. Grandori, C., Cowley, S. M., James, L. P. & Eisenman, R. N. The Myc/Max/Mad network and the transcriptional control of cell behavior. *Annu. Rev. Cell Dev. Biol.* **16,** 653–99 (2000).

198. Baudino, T. A. & Cleveland, J. L. The Max network gone mad. *Mol. Cell. Biol.* **21,** 691–702 (2001).

199. Corn, P. G. *et al.* Mxi1 is induced by hypoxia in a HIF-1-dependent manner and protects cells from c-Myc-induced apoptosis. *Cancer Biol. Ther.* **4,** 1285–94 (2005).

200. Gordan, J. D., Bertout, J. A., Hu, C.-J., Diehl, J. A. & Simon, M. C. HIF-2alpha promotes hypoxic cell proliferation by enhancing c-myc transcriptional activity. *Cancer Cell* **11,** 335–47 (2007).

201. Dang, C. V., Kim, J., Gao, P. & Yustein, J. The interplay between MYC and HIF in cancer. *Nat. Rev. Cancer* **8,** 51–56 (2008).

202. Satoh, K. *et al.* Global metabolic reprogramming of colorectal cancer occurs at adenoma stage and is induced by MYC. *Proc. Natl. Acad. Sci.* **114,** E7697–E7706 (2017).

203. Schmid, T., Zhou, J. & Brüne, B. HIF-1 and p53: communication of transcription factors under hypoxia. *J. Cell. Mol. Med.* **8,** 423–31

204. Hammond, E. M. & Giaccia, A. J. The role of p53 in hypoxia-induced apoptosis. *Biochem. Biophys. Res. Commun.* **331,** 718–725 (2005).

205. Hammond, E. M., Denko, N. C., Dorie, M. J., Abraham, R. T. & Giaccia, A. J. Hypoxia links ATR and p53 through replication arrest. *Mol. Cell. Biol.* **22,** 1834–43 (2002).

206. Kondoh, H. *et al.* Glycolytic enzymes can modulate cellular life span. *Cancer Res.* **65,** 177–85 (2005).

207. Bensaad, K. *et al.* TIGAR, a p53-Inducible Regulator of Glycolysis and Apoptosis. *Cell* **126,** 107–120 (2006).

208. Matoba, S. *et al.* p53 regulates mitochondrial respiration. *Science* **312,** 1650–3 (2006).

209. Pollard, P. J., Wortham, N. C. & Tomlinson, I. P. The TCA cycle and tumorigenesis: the examples of fumarate hydratase and succinate dehydrogenase. *Ann Med* **35,** 632–639 (2003).

210. Koivunen, P. *et al.* Inhibition of hypoxia-inducible factor (HIF) hydroxylases by citric acid cycle intermediates: possible links between cell metabolism and stabilization of HIF. *J Biol Chem* **282,** 4524–4532 (2007).

211. Chisanga, D. *et al.* Colorectal cancer atlas: An integrative resource for genomic and proteomic annotations from colorectal cancer cell lines and tissues. *Nucleic Acids Res.* **44,** D969-74 (2016).

212. Mouse Genome Sequencing Consortium *et al.* Initial sequencing and comparative analysis of the mouse genome. *Nature* **420,** 520–62 (2002).

213. Frese, K. K. & Tuveson, D. A. Maximizing mouse cancer models. *Nat. Rev. Cancer* **7,** 645–58 (2007).

214. McIntyre, R. E., van der Weyden, L. & Adams, D. J. Cancer gene discovery in the mouse. *Curr. Opin. Genet. Dev.* **22,** 14–20 (2012).

215. Francis, J. C. *et al.* Whole-exome DNA sequence analysis of *Brca2* - and *Trp53* - deficient mouse mammary gland tumours. *J. Pathol.* **236,** 186–200 (2015).

216. McIntyre, R. E., Buczacki, S. J. A., Arends, M. J. & Adams, D. J. Mouse models of colorectal cancer as preclinical models. *Bioessays* **37,** 909–20 (2015).

217. Nguyen, T. L. A., Vieira-Silva, S., Liston, A. & Raes, J. How informative is the mouse for human gut microbiota research? *Dis. Model. Mech.* **8,** 1–16 (2015).

218. Johnson, R. L. & Fleet, J. C. Animal models of colorectal cancer. *Cancer Metastasis Rev.* **32,** 39–61 (2013).

219. Calado, R. T. & Dumitriu, B. Telomere dynamics in mice and humans. *Semin. Hematol.* **50,** 165–74 (2013).

220. Mestas, J. & Hughes, C. C. W. Of Mice and Not Men: Differences between Mouse and Human Immunology. *J. Immunol.* **172,** (2004).

221. Moser, A. R., Pitot, H. C. & Dove, W. F. A dominant mutation that predisposes to multiple intestinal neoplasia in the mouse. *Science* **247,** 322–4 (1990).

222. Su, L. K. *et al.* Multiple intestinal neoplasia caused by a mutation in the murine homolog of the APC gene. *Science* **256,** 668–70 (1992).

223. Nishisho, I. *et al.* Mutations of chromosome 5q21 genes in FAP and colorectal cancer patients. *Science* **253,** 665–9 (1991).

224. Kandoth, C. *et al.* Mutational landscape and significance across 12 major cancer types. *Nature* **502,** 333–339 (2013).

225. McIntyre, R. E., van der Weyden, L. & Adams, D. J. Cancer gene discovery in the mouse. *Curr. Opin. Genet. Dev.* **22,** 14–20 (2012).

226. Hung, K. E. *et al.* Development of a mouse model for sporadic and metastatic colon tumors and its use in assessing drug treatment. *Proc. Natl. Acad. Sci.* **107,** 1565–1570 (2010).

227. Boutin, A. T. *et al.* Oncogenic Kras drives invasion and maintains metastases in colorectal cancer. (2017). doi:10.1101/gad.293449.116

228. Galon, J. *et al.* Type, density, and location of immune cells within human colorectal tumors predict clinical outcome. *Science* **313,** 1960–4 (2006).

229. Kim, B.-G. *et al.* Smad4 signalling in T cells is required for suppression of gastrointestinal cancer. *Nature* **441,** 1015–9 (2006).

230. Flatmark, K., Mælandsmo, G. M., Martinsen, M., Rasmussen, H. & Fodstad, Ø. Twelve colorectal cancer cell lines exhibit highly variable growth and metastatic capacities in an orthotopic model in nude mice. *Eur. J. Cancer* **40,** 1593–1598 (2004).

231. Pocard, M., Tsukui, H., Salmon, R. J., Dutrillaux, B. & Poupon, M. F. Efficiency of orthotopic xenograft models for human colon cancers. *In Vivo* **10,** 463–9

232. Hackl, C. *et al.* Metronomic oral topotecan prolongs survival and reduces liver metastasis in improved preclinical orthotopic and adjuvant therapy colon cancer models. *Gut* **62,** 259–71 (2013).

233. Lavilla-Alonso, S. *et al.* Optimized Mouse Model for the Imaging of Tumor Metastasis upon Experimental Therapy. *PLoS One* **6,** e26810 (2011).

234. Julien, S. *et al.* Characterization of a large panel of patient-derived tumor xenografts representing the clinical heterogeneity of human colorectal cancer. *Clin. Cancer Res.* **18,** 5314–28 (2012).

235. Garralda, E. *et al.* Integrated next-generation sequencing and avatar mouse models for personalized cancer treatment. *Clin. Cancer Res.* **20,** 2476–84 (2014).

236. Voskoglou-Nomikos, T., Pater, J. L. & Seymour, L. Clinical predictive value of the in vitro cell line, human xenograft, and mouse allograft preclinical cancer models. *Clin. Cancer Res.* **9,** 4227–39 (2003).

237. World Health Organisation. *Global Report on Diabetes*. (2016).

238. WHO | Global status report on noncommunicable diseases 2010.

239. Pruzin, J. J., Nelson, P. T., Abner, E. L. & Arvanitakis, Z. Invited Review: Relationship of type 2 diabetes to human brain pathology. *Neuropathol. Appl.*

Neurobiol. (2018). doi:10.1111/nan.12476

240. Athauda, D. & Foltynie, T. Insulin resistance and Parkinson's disease: A new target for disease modification? *Prog. Neurobiol.* **145–146,** 98–120 (2016).

241. Leon, B. M. & Maddox, T. M. Diabetes and cardiovascular disease: Epidemiology, biological mechanisms, treatment recommendations and future research. *World J. Diabetes* **6,** 1246–58 (2015).

242. Bosetti, C. *et al.* Diabetes mellitus and cancer risk in a network of case-control studies. *Nutr Cancer* **64,** 643–651 (2012).

243. Anderson, R. J., Freedland, K. E., Clouse, R. E. & Lustman, P. J. The prevalence of comorbid depression in adults with diabetes: a meta-analysis. *Diabetes Care* **24,** 1069–78 (2001).

244. Qi, W., Li, Q., Gordin, D. & King, G. L. Preservation of renal function in chronic diabetes by enhancing glomerular glucose metabolism. *J. Mol. Med.* (2018). doi:10.1007/s00109-018-1630-0

245. Tolman, K. G., Fonseca, V., Dalpiaz, A. & Tan, M. H. Spectrum of liver disease in type 2 diabetes and management of patients with diabetes and liver disease. *Diabetes Care* **30,** 734–43 (2007).

246. Kowluru, R. A., Kowluru, A., Mishra, M. & Kumar, B. Oxidative stress and epigenetic modifications in the pathogenesis of diabetic retinopathy. *Prog. Retin. Eye Res.* **48,** 40–61 (2015).

247. Risk Factor Collaboration, N. Worldwide trends in diabetes since 1980: a pooled analysis of 751 population-based studies with 4Â·4 million participants. *Lancet* **387,** 1513–1530 (2016).

248. Cost of Diabetes. Available at: http://www.diabetes.co.uk/cost-of-diabetes.html. (Accessed: 29th March 2016)

249. Prescribing for Diabetes. Available at: http://www.hscic.gov.uk/catalogue/PUB14681/pres-diab-eng-200506-201314-rep.pdf. (Accessed: 29th March 2016)

250. Palermo, A., Maggi, D., Maurizi, A. R., Pozzilli, P. & Buzzetti, R. Prevention of type 2 diabetes mellitus: is it feasible? *Diabetes Metab Res Rev* **30 Suppl 1,** 4–12 (2014).

251. Yoon, J. W. & Jun, H. S. Autoimmune destruction of pancreatic beta cells. *Am J Ther* **12,** 580–591 (2005).

252. Ma, R. C., Tutino, G. E., Lillycrop, K. A., Hanson, M. A. & Tam, W. H. Maternal diabetes, gestational diabetes and the role of epigenetics in their long term effects on offspring. *Prog Biophys Mol Biol* (2015). doi:10.1016/j.pbiomolbio.2015.02.010

253. Pearson, E. R. *et al.* Switching from insulin to oral sulfonylureas in patients with diabetes due to Kir6.2 mutations. *N Engl J Med* **355,** 467–477 (2006).

254. Aathira, R. & Jain, V. Advances in management of type 1 diabetes mellitus. *World J Diabetes* **5,** 689–696 (2014).

255. Tuomilehto, J. The emerging global epidemic of type 1 diabetes. *Curr Diab Rep* **13,** 795–804 (2013).

256. Fradkin, J. E. & Rodgers, G. P. Diabetes research: a perspective from the National Institute of Diabetes and Digestive and Kidney Diseases. *Diabetes* **62,** 320–326 (2013).

257. Group, T. D. P. Incidence and trends of childhood Type 1 diabetes worldwide 1990-1999. *Diabet Med* **23,** 857–866 (2006).

258. Chen, L., Magliano, D. J. & Zimmet, P. Z. The worldwide epidemiology of type 2 diabetes mellitus--present and future perspectives. *Nat Rev Endocrinol* **8,** 228–236 (2012).

259. Chung, W. K., Power-Kehoe, L., Chua, M., Lee, R. & Leibel, R. L. Genomic structure of the human OB receptor and identification of two novel intronic microsatellites. *Genome Res.* **6,** 1192–9 (1996).

260. Zhang, Y. *et al.* Positional cloning of the mouse obese gene and its human homologue. *Nature* **372,** 425–32 (1994).

261. Friedman, J. M. & Halaas, J. L. Leptin and the regulation of body weight in mammals. *Nature* **395,** 763–70 (1998).

262. Cefalu, W. T. *et al.* Animal Models of Type 2 Diabetes: Clinical Presentation and Pathophysiological Relevance to the Human Condition. *ILAR J.* **47,** 186–198 (2006).

263. Bates, S. H., Kulkarni, R. N., Seifert, M. & Myers, M. G. Roles for leptin receptor/STAT3-dependent and -independent signals in the regulation of glucose homeostasis. *Cell Metab.* **1,** 169–178 (2005).

264. Shafrir, E., Ziv, E. & Mosthaf, L. Nutritionally induced insulin resistance and receptor defect leading to beta-cell failure in animal models. *Ann. N. Y. Acad. Sci.* **892,** 223–46 (1999).

265. Marzban, L., Park, K. & Verchere, C. B. Islet amyloid polypeptide and type 2 diabetes. *Exp. Gerontol.* **38,** 347–51 (2003).

266. Adam, J. *et al.* Fumarate Hydratase Deletion in Pancreatic β Cells Leads to Progressive Diabetes. *Cell Rep.* **20,** 3135–3148 (2017).

267. Fuhrmann-Benzakein, E., García-Gabay, I., Pepper, M. S., Vassalli, J. D. & Herrera, P. L. Inducible and irreversible control of gene expression using a single transgene. *Nucleic Acids Res.* **28,** E99 (2000).

268. Adam, J. *et al.* Fumarate Hydratase Deletion in Pancreatic β Cells Leads to Progressive Diabetes. *Cell Rep.* **20,** 3135–3148 (2017).

269. Klueh, U. *et al.* Continuous Glucose Monitoring in Normal Mice and Mice with Prediabetes and Diabetes. *Diabetes Technol. Ther.* **8,** 402–412 (2006).

270. Greenwood, M. & Wood, F. The Relation between the Cancer and Diabetes Death-rates. *J Hyg* **14,** 83–118 (1914).

271. Zendehdel, K. *et al.* Cancer incidence in patients with type 1 diabetes mellitus: a population-based cohort study in Sweden. *J Natl Cancer Inst* **95,** 1797–1800 (2003).

272. Shu, X. *et al.* Cancer risk among patients hospitalized for Type 1 diabetes mellitus: a population-based cohort study in Sweden. *Diabet Med* **27,** 791–797 (2010).

273. Gordon-Dseagu, V. L., Shelton, N. & Mindell, J. S. Epidemiological evidence of a relationship between type-1 diabetes mellitus and cancer: a review of the existing literature. *Int J Cancer* **132,** 501–508 (2013).

274. Zhang, P. H. *et al.* Increased risk of cancer in patients with type 2 diabetes mellitus: a retrospective cohort study in China. *BMC Public Health* **12,** 567 (2012).

275. Oberaigner, W. *et al.* Increased cancer incidence risk in type 2 diabetes mellitus: results from a cohort study in Tyrol/Austria. *BMC Public Health* **14,** 1058 (2014).

276. Szablewski, L. Diabetes mellitus: influences on cancer risk. *Diabetes Metab Res Rev* (2014). doi:10.1002/dmrr.2573

277. Duan, W. *et al.* Hyperglycemia, a neglected factor during cancer progression. **2014,** 461917 (2014).

278. Simon, D. & Balkau, B. Diabetes mellitus, hyperglycaemia and cancer. *Diabetes Metab* **36,** 182–191 (2010).

279. Brenner, H., Kloor, M. & Pox, C. P. Colorectal cancer. *Lancet* **383,** 1490–1502 (2014).

280. Ferguson, R. D., Gallagher, E. J., Scheinman, E. J., Damouni, R. & LeRoith, D. The epidemiology and molecular mechanisms linking obesity, diabetes, and cancer. *Vitam Horm* **93,** 51–98 (2013).

281. Garg, S. K., Maurer, H., Reed, K. & Selagamsetty, R. Diabetes and cancer: two diseases with obesity as a common risk factor. *Diabetes Obes Metab* **16,** 97–110 (2014).

282. Larsson, S. C., Orsini, N. & Wolk, A. Diabetes mellitus and risk of colorectal cancer: a meta-analysis. *J Natl Cancer Inst* **97,** 1679–1687 (2005).

283. Jiang, Y. *et al.* Diabetes mellitus and incidence and mortality of colorectal cancer: a systematic review and meta-analysis of cohort studies. *Eur J Epidemiol* **26,** 863–876 (2011).

284. Deng, L., Gui, Z., Zhao, L., Wang, J. & Shen, L. Diabetes mellitus and the incidence of colorectal cancer: an updated systematic review and meta-analysis. *Dig Dis Sci* **57,** 1576–1585 (2012).

285. Wu, L. *et al.* Diabetes mellitus and the occurrence of colorectal cancer: an updated meta-analysis of cohort studies. *Diabetes Technol Ther* **15,** 419–427 (2013).

286. Bu, W. J., Song, L., Zhao, D. Y., Guo, B. & Liu, J. Insulin therapy and the risk of colorectal cancer in patients with type 2 diabetes: a meta-analysis of observational studies. *Br J Clin Pharmacol* **78,** 301–309 (2014).

287. Meyerhardt, J. A. *et al.* Impact of diabetes mellitus on outcomes in patients with colon cancer. *J Clin Oncol* **21,** 433–440 (2003).

288. Jullumstro, E., Kollind, M., Lydersen, S. & Edna, T. H. Diabetes mellitus and outcomes of colorectal cancer. *Acta Oncol* **48,** 361–367 (2009).

289. Zanders, M. M., Boll, D., van Steenbergen, L. N., van de Poll-Franse, L. V & Haak, H. R. Effect of diabetes on endometrial cancer recurrence and survival. *Maturitas* **74,** 37–43 (2013).

290. Siddiqui, A. A. Metabolic syndrome and its association with colorectal cancer: a review. *Am J Med Sci* **341,** 227–231 (2011).

291. Forootan, M., Tabatabaeefar, M., Yahyaei, M. & Maghsoodi, N. Metabolic syndrome and colorectal cancer: a cross-sectional survey. *Asian Pac J Cancer Prev* **13,** 4999–5002 (2012).

292. Tran, T. T. *et al.* Hyperinsulinemia, but not other factors associated with insulin resistance, acutely enhances colorectal epithelial proliferation in vivo. *Endocrinology* **147,** 1830–1837 (2006).

293. Ye, Q., Cai, W., Zheng, Y., Evers, B. M. & She, Q.-B. ERK and AKT signaling cooperate to translationally regulate survivin expression for metastatic progression of colorectal cancer. *Oncogene* **33,** 1828–1839 (2014).

294. Stanilov, N. S., Karakolev, I. A., Deliysky, T. S., Jovchev, J. P. & Stanilova, S. A. Association of insulin-like growth factor-I receptor polymorphism with colorectal cancer development. *Mol Biol Rep* **41,** 8099–8106 (2014).

295. Papa, V. *et al.* Elevated insulin receptor content in human breast cancer. *J Clin Invest* **86,** 1503–1510 (1990).

296. Grivennikov, S. I., Greten, F. R. & Karin, M. Immunity, inflammation, and cancer. *Cell* **140,** 883–899 (2010).

297. Lee, H. *et al.* Persistently activated Stat3 maintains constitutive NF-kappaB activity in tumors. *Cancer Cell* **15,** 283–293 (2009).

298. Wei, X. *et al.* Activation of the JAK-STAT3 pathway is associated with the growth of colorectal carcinoma cells. *Oncol Rep* **31,** 335–341 (2014).

299. Greten, F. R. *et al.* IKKbeta links inflammation and tumorigenesis in a mouse model of colitis-associated cancer. *Cell* **118,** 285–296 (2004).

300. Han, L. *et al.* High glucose promotes pancreatic cancer cell proliferation via the induction of EGF expression and transactivation of EGFR. *PLoS One* **6,** e27074 (2011).

301. Cao, H. *et al.* Changes in serum IGF-1 level and tumor VEGF expression in mice with colorectal cancer under hyperglycemic conditions. *Mol Med Rep* **7,** 1361–

1365 (2013).

302. Shin, H. Y., Jung, K. J., Linton, J. A. & Jee, S. H. Association between fasting serum glucose levels and incidence of colorectal cancer in Korean men: the Korean Cancer Prevention Study-II. *Metabolism* **63,** 1250–1256 (2014).

303. Lu, J., Kunimoto, S., Yamazaki, Y., Kaminishi, M. & Esumi, H. Kigamicin D, a novel anticancer agent based on a new anti-austerity strategy targeting cancer cells' tolerance to nutrient starvation. *Cancer Sci.* **95,** 547–52 (2004).

304. Sivitz, W. I. & Yorek, M. A. Mitochondrial dysfunction in diabetes: from molecular mechanisms to functional significance and therapeutic opportunities. *Antioxid. Redox Signal.* **12,** 537–77 (2010).

305. Dabkowski, E. R. *et al.* Mitochondrial dysfunction in the type 2 diabetic heart is associated with alterations in spatially distinct mitochondrial proteomes. *AJP Hear. Circ. Physiol.* **299,** H529–H540 (2010).

306. Friederich, M., Fasching, A., Hansell, P., Nordquist, L. & Palm, F. Diabetes-induced up-regulation of uncoupling protein-2 results in increased mitochondrial uncoupling in kidney proximal tubular cells. *Biochim. Biophys. Acta - Bioenerg.* **1777,** 935–940 (2008).

307. Kelley, D. E., He, J., Menshikova, E. V & Ritov, V. B. Dysfunction of mitochondria in human skeletal muscle in type 2 diabetes. *Diabetes* **51,** 2944–50 (2002).

308. Ritov, V. B. *et al.* Deficiency of subsarcolemmal mitochondria in obesity and type 2 diabetes. *Diabetes* **54,** 8–14 (2005).

309. Choo, H.-J. *et al.* Mitochondria are impaired in the adipocytes of type 2 diabetic mice. *Diabetologia* **49,** 784–791 (2006).

310. Frizzell, N., Thomas, S. A., Carson, J. A. & Baynes, J. W. Mitochondrial stress causes increased succination of proteins in adipocytes in response to glucotoxicity. *Biochem J* **445,** 247–254 (2012).

311. Yang, H. *et al.* Adipose-Specific Deficiency of Fumarate Hydratase in Mice Protects Against Obesity, Hepatic Steatosis, and Insulin Resistance. *Diabetes* **65,** 3396–3409 (2016).

312. King, A., Selak, M. A. & Gottlieb, E. Succinate dehydrogenase and fumarate hydratase: linking mitochondrial dysfunction and cancer. *Oncogene* **25,** 4675–4682 (2006).

313. Einbeck, H. Uber quantitative versuche mit dem succinicoxydon von Battelli und Stern. *Biochem J* **95,** 296 (1919).

314. Raimundo, N. *et al.* Differential metabolic consequences of fumarate hydratase and respiratory chain defects. *Biochim. Biophys. Acta* **1782,** 287–94 (2008).

315. Yogev, O. *et al.* Fumarase: a mitochondrial metabolic enzyme and a cytosolic/nuclear component of the DNA damage response. *PLoS Biol* **8,** e1000328 (2010).

316. O'Flaherty, L. *et al.* Dysregulation of hypoxia pathways in fumarate hydratase-deficient cells is independent of defective mitochondrial metabolism. *Hum. Mol. Genet.* **19,** 3844–51 (2010).

317. Isaacs, J. S. *et al.* HIF overexpression correlates with biallelic loss of fumarate hydratase in renal cancer: novel role of fumarate in regulation of HIF stability. *Cancer Cell* **8,** 143–153 (2005).

318. Selak, M. A. *et al.* Succinate links TCA cycle dysfunction to oncogenesis by inhibiting HIF-alpha prolyl hydroxylase. *Cancer Cell* **7,** 77–85 (2005).

319. Picaud, S. *et al.* Structural basis of fumarate hydratase deficiency. *J. Inherit. Metab. Dis.* **34,** 671–6 (2011).

320. Mullen, A. R. *et al.* Reductive carboxylation supports growth in tumour cells with defective mitochondria. *Nature* **481,** 385–388 (2012).

321. Zheng, L. *et al.* Reversed argininosuccinate lyase activity in fumarate hydratase-deficient cancer cells. *Cancer Metab.* **1,** 12 (2013).

322. Tyrakis, P. A. *et al.* Fumarate Hydratase Loss Causes Combined Respiratory Chain Defects. *CellReports* **21,** 1036–1047 (2017).

323. Pollard, P. *et al.* Evidence of increased microvessel density and activation of the hypoxia pathway in tumours from the hereditary leiomyomatosis and renal cell cancer syndrome. *J. Pathol.* **205,** 41–9 (2005).

324. Pollard, P. J. *et al.* Accumulation of Krebs cycle intermediates and over-expression of HIF1alpha in tumours which result from germline FH and SDH mutations. *Hum. Mol. Genet.* **14,** 2231–9 (2005).

325. Pollard, P. J. *et al.* Targeted inactivation of fh1 causes proliferative renal cyst development and activation of the hypoxia pathway. *Cancer Cell* **11,** 311–9 (2007).

326. Jiang, Y. *et al.* Local generation of fumarate promotes DNA repair through inhibition of histone H3 demethylation. *Nat. Cell Biol.* **17,** 1158–68 (2015).

327. TANAKA, K. R. & VALENTINE, W. N. Fumarase activity of human leukocytes and erythrocytes. *Blood* **17,** 328–33 (1961).

328. Lehtonen, R. *et al.* Biallelic inactivation of fumarate hydratase (FH) occurs in nonsyndromic uterine leiomyomas but is rare in other tumors. *Am. J. Pathol.* **164,** 17–22 (2004).

329. Ashrafian, H. *et al.* Expression Profiling in Progressive Stages of Fumarate-Hydratase Deficiency: The Contribution of Metabolic Changes to Tumorigenesis. *Cancer Res.* **70,** (2010).

330. Adam, J. *et al.* Cell Reports Report A Role for Cytosolic Fumarate Hydratase in Urea Cycle Metabolism and Renal Neoplasia. *CellReports* **3,** 1440–1448 (2013).

331. Hanahan, D. & Weinberg, R. A. Hallmarks of cancer: the next generation. *Cell* **144,** 646–674 (2011).

332. Yang, M., Soga, T., Pollard, P. J. & Adam, J. The emerging role of fumarate as an oncometabolite. *Front Oncol* **2,** 85 (2012).

333. Merkley, E. D., Metz, T. O., Smith, R. D., Baynes, J. W. & Frizzell, N. The succinated proteome. *Mass Spectrom Rev* **33,** 98–109 (2014).

334. Bardella, C. *et al.* Aberrant succination of proteins in fumarate hydratase-deficient mice and HLRCC patients is a robust biomarker of mutation status. *J Pathol* **225,** 4–11 (2011).

335. Hirayama, A. *et al.* Quantitative metabolome profiling of colon and stomach cancer microenvironment by capillary electrophoresis time-of-flight mass spectrometry. *Cancer Res* **69,** 4918–4925 (2009).

336. Laukka, T. *et al.* Fumarate and Succinate Regulate Expression of Hypoxia-inducible Genes via TET Enzymes. *J. Biol. Chem.* **291,** 4256–65 (2016).

337. Alderson, N. L. *et al.* S-(2-Succinyl)cysteine: a novel chemical modification of tissue proteins by a Krebs cycle intermediate. *Arch Biochem Biophys* **450,** 1–8 (2006).

338. Blatnik, M., Frizzell, N., Thorpe, S. R. & Baynes, J. W. Inactivation of glyceraldehyde-3-phosphate dehydrogenase by fumarate in diabetes: formation of S-(2-succinyl)cysteine, a novel chemical modification of protein and possible biomarker of mitochondrial stress. *Diabetes* **57,** 41–49 (2008).

339. Nagai, R. *et al.* Succination of protein thiols during adipocyte maturation: a biomarker of mitochondrial stress. *J. Biol. Chem.* **282,** 34219–28 (2007).

340. Kensler, T. W. & Wakabayashi, N. Nrf2: friend or foe for chemoprevention? *Carcinogenesis* **31,** 90–99 (2010).

341. Zheng, L. *et al.* Fumarate induces redox-dependent senescence by modifying glutathione metabolism. *Nat. Commun.* **6,** 6001 (2015).

342. Alderson, N. L. *et al.* S-(2-Succinyl)cysteine: a novel chemical modification of tissue proteins by a Krebs cycle intermediate. *Arch Biochem Biophys* **450,** 1–8 (2006).

343. Frizzell, N., Lima, M. & Baynes, J. W. Succination of proteins in diabetes. *Free Radic Res* **45,** 101–109 (2011).

344. Adam, J., Ratcliffe, P. J. & Pollard, P. J. Novel insights into FH-associated disease are KEAPing the lid on oncogenic HIF signalling. *Oncotarget* **2,** 820–821 (2011).

345. Ternette, N. *et al.* Inhibition of Mitochondrial Aconitase by Succination in Fumarate Hydratase Deficiency. *Cell Rep.* **3,** (2013).

346. Sullivan, L. B. *et al.* The proto-oncometabolite fumarate binds glutathione to amplify ROS-dependent signaling. *Mol. Cell* **51,** 236–48 (2013).

347. Adam, J. *et al.* Renal Cyst Formation in Fh1-Deficient Mice Is Independent of the Hif/Phd Pathway: Roles for Fumarate in KEAP1 Succination and Nrf2 Signaling. *Cancer Cell* **20,** 524–537 (2011).

348. Ashrafian, H. *et al.* Fumarate is cardioprotective via activation of the Nrf2 antioxidant pathway. *Cell Metab.* **15,** 361–71 (2012).

349. Sciacovelli, M. *et al.* Fumarate is an epigenetic modifier that elicits epithelial-to-mesenchymal transition. *Nature* (2016). doi:10.1038/nature19353

350. Craene, B. De & Berx, G. Regulatory networks defining EMT during cancer initiation and progression. *Nat. Rev. Cancer* **13,** 97–110 (2013).

351. Haghikia, A., Linker, R. & Gold, R. Fumarsäure in der Therapie der Multiplen Sklerose. *Nervenarzt* **85,** 720–726 (2014).

352. Dubey, D. *et al.* Dimethyl fumarate in relapsing–remitting multiple sclerosis: rationale, mechanisms of action, pharmacokinetics, efficacy and safety. *Expert Rev. Neurother.* **15,** 339–346 (2015).

353. Sheremata, W., Brown, A. D. & Rammohan, K. W. Dimethyl fumarate for treating relapsing multiple sclerosis. *Expert Opin. Drug Saf.* **14,** 161–170 (2015).

354. Ghoreschi, K. *et al.* Fumarates improve psoriasis and multiple sclerosis by inducing type II dendritic cells. *J. Exp. Med.* **208,** 2291–303 (2011).

355. Linker, R. A. *et al.* Fumaric acid esters exert neuroprotective effects in neuroinflammation via activation of the Nrf2 antioxidant pathway. *Brain* **134,** 678–692 (2011).

356. Held, K. D., Epp, E. R., Clark, E. P. & Biaglow, J. E. Effect of dimethyl fumarate on the radiation sensitivity of mammalian cells in vitro. *Radiat. Res.* **115,** 495–502 (1988).

357. Grzegorzewska, A. P. *et al.* Dimethyl Fumarate ameliorates pulmonary arterial hypertension and lung fibrosis by targeting multiple pathways. *Sci. Rep.* **7,** 41605 (2017).

358. Rantanen, T. The cause of the Chinese sofa/chair dermatitis epidemic is likely to be contact allergy to dimethylfumarate, a novel potent contact sensitizer. *Br. J. Dermatol.* **159,** 218–221 (2008).

359. Manuel, A. M. & Frizzell, N. Adipocyte protein modification by Krebs cycle intermediates and fumarate ester-derived succination. *Amino Acids* **45,** 1243–7 (2013).

360. Zhao, H. & Chen, T. Tet family of 5-methylcytosine dioxygenases in mammalian development. *J. Hum. Genet.* **58,** 421–7 (2013).

361. Chadt, A., Scherneck, S., Joost, H.-G. & Al-Hasani, H. *Molecular links between Obesity and Diabetes: 'Diabesity'*. *Endotext* (MDText.com, Inc., 2000).

362. Ngo, H. T. *et al.* Genetic and Diet-Induced Obesity Increased Intestinal Tumorigenesis in the Double Mutant Mouse Model Multiple Intestinal Neoplasia X Obese via Disturbed Glucose Regulation and Inflammation. *J. Obes.* **2015,** 1–21 (2015).

363. INGALLS, A. M., DICKIE, M. M. & SNELL, G. D. Obese, a new mutation in the house

mouse. *J. Hered.* **41,** 317–8 (1950).

364. Chehab, F. F., Qiu, J. & Ogus, S. The use of animal models to dissect the biology of leptin. *Recent Prog. Horm. Res.* **59,** 245–66 (2004).

365. The Jackson Laboratory. JAX Mice Database—000632 B6.Cg-Lepob/J. *http://jaxmice.jax.org/strain/000632.html* (2016).

366. Lewis, A. *et al.* Severe polyposis in Apc(1322T) mice is associated with submaximal Wnt signalling and increased expression of the stem cell marker Lgr5. *Gut* **59,** 1680–1686 (2010).

367. Cormier, R. T. *et al.* Secretory phospholipase Pla2g2a confers resistance to intestinal tumorigenesis. *Nat. Genet.* **17,** 88–91 (1997).

368. MacPhee, M. *et al.* The secretory phospholipase A2 gene is a candidate for the Mom1 locus, a major modifier of ApcMin-induced intestinal neoplasia. *Cell* **81,** 957–966 (1995).

369. Gould, K. A. *et al.* Genetic evaluation of candidate genes for the Mom1 modifier of intestinal neoplasia in mice. *Genetics* **144,** 1777–85 (1996).

370. Novelli, M. R. *et al.* Tumor burden and clonality in multiple intestinal neoplasia mouse/normal mouse aggregation chimeras. *Proc. Natl. Acad. Sci. U. S. A.* **96,** 12553–8 (1999).

371. Soga, T. *et al.* Metabolomic Profiling of Anionic Metabolites by Capillary Electrophoresis Mass Spectrometry. *Anal. Chem.* **81,** 6165–6174 (2009).

372. Soga, T. *et al.* Differential Metabolomics Reveals Ophthalmic Acid as an Oxidative Stress Biomarker Indicating Hepatic Glutathione Consumption. *J. Biol. Chem.* **281,** 16768–16776 (2006).

373. Livak, K. J. & Schmittgen, T. D. Analysis of Relative Gene Expression Data Using Real-Time Quantitative PCR and the 2−ΔΔCT Method. *Methods* **25,** 402–408 (2001).

374. Yang, M. *et al.* The Succinated Proteome of FH-Mutant Tumours. *Metabolites* **4,** 640–654 (2014).

375. Yang, M., Soga, T. & Pollard, P. J. Oncometabolites: linking altered metabolism with cancer. *J Clin Invest* **123,** 3652–3658 (2013).

376. Hutton, J. E. *et al.* Oncogenic KRAS and BRAF Drive Metabolic Reprogramming in Colorectal Cancer. *Mol. Cell. Proteomics* **15,** 2924–2938 (2016).

377. Dong, G. *et al.* Genetic variations in genes of metabolic enzymes predict postoperational prognosis of patients with colorectal cancer. *Mol. Cancer* **14,** 171 (2015).

378. Stolze, B., Reinhart, S., Bulllinger, L., Fröhling, S. & Scholl, C. Comparative analysis of KRAS codon 12, 13, 18, 61 and 117 mutations using human MCF10A isogenic cell lines. *Sci. Rep.* **5,** 8535 (2015).

379. Lovly, C. M. *et al.* Routine Multiplex Mutational Profiling of Melanomas Enables Enrollment in Genotype-Driven Therapeutic Trials. *PLoS One* **7,** e35309 (2012).

380. Souglakos, J. *et al.* Prognostic and predictive value of common mutations for treatment response and survival in patients with metastatic colorectal cancer. *Br. J. Cancer* **101,** 465–472 (2009).

381. Di Nicolantonio, F. *et al.* Wild-Type *BRAF* Is Required for Response to Panitumumab or Cetuximab in Metastatic Colorectal Cancer. *J. Clin. Oncol.* **26,** 5705–5712 (2008).

382. Benvenuti, S. *et al.* Oncogenic Activation of the RAS/RAF Signaling Pathway Impairs the Response of Metastatic Colorectal Cancers to Anti-Epidermal Growth Factor Receptor Antibody Therapies. *Cancer Res.* **67,** 2643–2648 (2007).

383. Wan, P. T. C. *et al.* Mechanism of activation of the RAF-ERK signaling pathway by oncogenic mutations of B-RAF. *Cell* **116,** 855–67 (2004).

384. Chan, E. C. *et al.* Metabolic profiling of human colorectal cancer using high-resolution magic angle spinning nuclear magnetic resonance (HR-MAS NMR) spectroscopy and gas chromatography mass spectrometry (GC/MS). *J Proteome Res* **8,** 352–361 (2009).

385. Denkert, C. *et al.* Metabolite profiling of human colon carcinoma – deregulation of TCA cycle and amino acid turnover. *Mol. Cancer* **7,** 72 (2008).

386. Vander Heiden, M. G., Cantley, L. C. & Thompson, C. B. Understanding the Warburg effect: the metabolic requirements of cell proliferation. *Science* **324,** 1029–33 (2009).

387. Boland, M. L., Chourasia, A. H. & Macleod, K. F. Mitochondrial dysfunction in cancer. *Front. Oncol.* **3,** 292 (2013).

388. Lehtonen, R. *et al.* Biallelic Inactivation of Fumarate Hydratase (FH) Occurs in Nonsyndromic Uterine Leiomyomas but Is Rare in Other Tumors. *Am. J. Pathol.* **164,** 17–22 (2004).

389. Weaver, T. & Banaszak, L. Crystallographic studies of the catalytic and a second site in fumarase C from Escherichia coli. *Biochemistry* **35,** 13955–65 (1996).

390. Mescam, M., Vinnakota, K. C. & Beard, D. A. Identification of the catalytic mechanism and estimation of kinetic parameters for fumarase. *J. Biol. Chem.* **286,** 21100–9 (2011).

391. Scheffzek, K. *et al.* The Ras-RasGAP complex: structural basis for GTPase activation and its loss in oncogenic Ras mutants. *Science* **277,** 333–8 (1997).

392. Andreyev, H. J. N. *et al.* Kirsten ras mutations in patients with colorectal cancer: the 'RASCAL II' study. *Br. J. Cancer* **85,** 692–696 (2001).

393. Ogino, S. *et al.* CpG island methylator phenotype, microsatellite instability, BRAF mutation and clinical outcome in colon cancer. *Gut* **58,** 90–96 (2009).

394. Yun, J. *et al.* Glucose Deprivation Contributes to the Development of KRAS

Pathway Mutations in Tumor Cells. *Science (80-.).* **325,** (2009).

395. Toda, K. *et al.* Metabolic Alterations Caused by KRAS Mutations in Colorectal Cancer Contribute to Cell Adaptation to Glutamine Depletion by Upregulation of Asparagine Synthetase. *Neoplasia* **18,** 654–665 (2016).

396. Weinberg, F. *et al.* Mitochondrial metabolism and ROS generation are essential for Kras-mediated tumorigenicity. *Proc. Natl. Acad. Sci. U. S. A.* **107,** 8788–93 (2010).

397. Miyo, M. *et al.* Metabolic Adaptation to Nutritional Stress in Human Colorectal Cancer. *Sci. Rep.* **6,** 38415 (2016).

398. Davidson, S. M. *et al.* Environment Impacts the Metabolic Dependencies of Ras-Driven Non-Small Cell Lung Cancer. *Cell Metab.* **23,** 517–28 (2016).

399. Yogev, O. *et al.* Fumarase: A Mitochondrial Metabolic Enzyme and a Cytosolic/Nuclear Component of the DNA Damage Response. *PLoS Biol* **8,** (2010).

400. Davis, H. *et al.* Aberrant epithelial GREM1 expression initiates colonic tumorigenesis from cells outside the stem cell niche. *Nat. Med.* **21,** 62–70 (2015).

401. Dominguez Rieg, J. A. *et al.* Regulation of intestinal SGLT1 by catestatin in hyperleptinemic type 2 diabetic mice. *Lab. Invest.* **96,** 98–111 (2016).

402. Mao, J. *et al.* Overnutrition stimulates intestinal epithelium proliferation through β-catenin signaling in obese mice. *Diabetes* **62,** 3736–46 (2013).

403. O'Flaherty, L. *et al.* Dysregulation of hypoxia pathways in fumarate hydratase-deficient cells is independent of defective mitochondrial metabolism. *Hum. Mol. Genet.* **19,** 3844–51 (2010).

404. Yang, Y. *et al.* UOK 262 cell line, fumarate hydratase deficient (FH-/FH-) hereditary leiomyomatosis renal cell carcinoma: in vitro and in vivo model of an aberrant energy metabolic pathway in human cancer. *Cancer Genet. Cytogenet.* **196,** 45–55 (2010).

405. Frezza, C. *et al.* Haem oxygenase is synthetically lethal with the tumour suppressor fumarate hydratase. *Nature* **477,** 225–228 (2011).

406. Blatnik, M., Thorpe, S. R. & Baynes, J. W. Succination of proteins by fumarate: mechanism of inactivation of glyceraldehyde-3-phosphate dehydrogenase in diabetes. *Ann N Y Acad Sci* **1126,** 272–275 (2008).

407. Ioannou, M. *et al.* HIF-1α in colorectal carcinoma: review of the literature. *J. BUON.* **20,** 680–9

408. Nijhuis, A. *et al.* Remodelling of microRNAs in colorectal cancer by hypoxia alters metabolism profiles and 5-fluorouracil resistance. *Hum. Mol. Genet.* **26,** 1552–1564 (2017).

409. Nordsmark, M., Overgaard, M. & Overgaard, J. Pretreatment oxygenation predicts radiation response in advanced squamous cell carcinoma of the head and neck. *Radiother. Oncol.* **41,** 31–9 (1996).

410. Movsas, B. *et al.* Hypoxic regions exist in human prostate carcinoma. *Urology* **53,** 11–8 (1999).

411. Koong, A. C. *et al.* Pancreatic tumors show high levels of hypoxia. *Int. J. Radiat. Oncol. Biol. Phys.* **48,** 919–22 (2000).

412. Dunst, J. *et al.* Tumor volume and tumor hypoxia in head and neck cancers. The amount of the hypoxic volume is important. *Strahlenther. Onkol.* **179,** 521–6 (2003).

413. Cancer Genome Atlas Network, T. Comprehensive molecular characterization of human colon and rectal cancer. *Nature* **487,** (2012).

414. Smith, H. *et al.* The Effects of Severe Hypoxia on Glycolytic Flux and Enzyme Activity in a Model of Solid Tumors. *J. Cell. Biochem.* **117,** 1890–1901 (2016).

415. Pippitt, K., Li, M. & Gurgle, H. E. Diabetes Mellitus: Screening and Diagnosis. *Am. Fam. Physician* **93,** 103–9 (2016).

416. Iori, E. *et al.* Glucose and Fatty Acid Metabolism in a 3 Tissue In-Vitro Model Challenged with Normo- and Hyperglycaemia. *PLoS One* **7,** e34704 (2012).

417. Yang, C. *et al.* Glutamine oxidation maintains the TCA cycle and cell survival during impaired mitochondrial pyruvate transport. *Mol. Cell* **56,** 414–24 (2014).

418. Lacey, J. M. & Wilmore, D. W. Is glutamine a conditionally essential amino acid? *Nutr. Rev.* **48,** 297–309 (1990).

419. Hien, T. T. *et al.* Elevated Glucose Levels Promote Contractile and Cytoskeletal Gene Expression in Vascular Smooth Muscle via Rho/Protein Kinase C and Actin Polymerization. *J. Biol. Chem.* **291,** 3552–68 (2016).

420. Barati, M. T. *et al.* Influence of Acute High Glucose on Protein Abundance Changes in Murine Glomerular Mesangial Cells. *J. Diabetes Res.* **2016,** 3537863 (2016).

421. Zieseniss, A. Hypoxia and the modulation of the actin cytoskeleton - emerging interrelations. *Hypoxia (Auckland, N.Z.)* **2,** 11–21 (2014).

422. Wilson, C. & González-Billault, C. Regulation of cytoskeletal dynamics by redox signaling and oxidative stress: implications for neuronal development and trafficking. *Front. Cell. Neurosci.* **9,** 381 (2015).

423. Kikuchi, H., Pino, M. S., Zeng, M., Shirasawa, S. & Chung, D. C. Oncogenic KRAS and BRAF Differentially Regulate Hypoxia-Inducible Factor-1 and -2 in Colon Cancer. *Cancer Res.* **69,** 8499–8506 (2009).

424. Tammali, R., Saxena, A., Srivastava, S. K. & Ramana, K. V. Aldose reductase inhibition prevents hypoxia-induced increase in hypoxia-inducible factor-1alpha (HIF-1alpha) and vascular endothelial growth factor (VEGF) by regulating 26 S proteasome-mediated protein degradation in human colon cancer cells. *J. Biol. Chem.* **286,** 24089–100 (2011).

425. Adekola, K., Rosen, S. T. & Shanmugam, M. Glucose transporters in cancer

metabolism. *Curr. Opin. Oncol.* **24,** 650–654 (2012).

426. Huang, S. & Czech, M. P. The GLUT4 Glucose Transporter. *Cell Metab.* **5,** 237–252 (2007).

427. Zhang, J.-Y. *et al.* Critical protein GAPDH and its regulatory mechanisms in cancer cells. *Cancer Biol. Med.* **12,** 10–22 (2015).

428. Miao, P., Sheng, S., Sun, X., Liu, J. & Huang, G. Lactate dehydrogenase a in cancer: A promising target for diagnosis and therapy. *IUBMB Life* **65,** 904–910 (2013).

429. Tan, V. P. & Miyamoto, S. HK2/hexokinase-II integrates glycolysis and autophagy to confer cellular protection. *Autophagy* **11,** 963–964 (2015).

430. Gagliardi, P. A., di Blasio, L. & Primo, L. PDK1: A signaling hub for cell migration and tumor invasion. *Biochim. Biophys. Acta - Rev. Cancer* **1856,** 178–188 (2015).

431. Liu, Z. *et al.* Direct Activation of Bax Protein for Cancer Therapy. *Med. Res. Rev.* **36,** 313–341 (2016).

432. Cheng, C.-W. *et al.* Overexpression of Lon contributes to survival and aggressive phenotype of cancer cells through mitochondrial complex I-mediated generation of reactive oxygen species. *Cell Death Dis.* **4,** e681 (2013).

433. Cyr, A. R., Hitchler, M. J. & Domann, F. E. Regulation of *SOD2* in Cancer by Histone Modifications and CpG Methylation: Closing the Loop Between Redox Biology and Epigenetics. *Antioxid. Redox Signal.* **18,** 1946–1955 (2013).

434. Semenza, G. L. Oxygen-dependent regulation of mitochondrial respiration by hypoxia-inducible factor 1. *Biochem. J.* **405,** 1–9 (2007).

435. Shanmugasundaram, K. *et al.* The oncometabolite fumarate promotes pseudohypoxia through noncanonical activation of NF-kappaB signaling. *J Biol Chem* **289,** 24691–24699 (2014).

436. Labrecque, M. P., Prefontaine, G. G. & Beischlag, T. V. The aryl hydrocarbon receptor nuclear translocator (ARNT) family of proteins: transcriptional modifiers with multi-functional protein interfaces. *Curr. Mol. Med.* **13,** 1047–65 (2013).

437. Yoshimura, H. *et al.* Prognostic impact of hypoxia-inducible factors 1alpha and 2alpha in colorectal cancer patients: correlation with tumor angiogenesis and cyclooxygenase-2 expression. *Clin. Cancer Res.* **10,** 8554–60 (2004).

438. Gossage, L., Eisen, T. & Maher, E. R. VHL, the story of a tumour suppressor gene. *Nat Rev Cancer* **15,** (2015).

439. Supuran, C. T. & Winum, J.-Y. Carbonic anhydrase IX inhibitors in cancer therapy: an update. *Future Med. Chem.* **7,** 1407–1414 (2015).

440. Matsumoto, K. & Ema, M. Roles of VEGF-A signalling in development, regeneration, and tumours. *J. Biochem.* **156,** 1–10 (2014).

441. Kim, B., Srivastava, S. K. & Kim, S.-H. Caspase-9 as a therapeutic target for treating cancer. *Expert Opin. Ther. Targets* **19,** 113–127 (2015).

442. Brigelius-Flohé, R. & Maiorino, M. Glutathione peroxidases. *Biochim. Biophys. Acta - Gen. Subj.* **1830,** 3289–3303 (2013).

443. Katkoori, V. R. *et al.* Bax expression is a candidate prognostic and predictive marker of colorectal cancer. *J Gastrointest Oncol* **1,** 76–89 (2010).

444. Bensellam, M. *et al.* Glucose-induced O(2) consumption activates hypoxia inducible factors 1 and 2 in rat insulin-secreting pancreatic beta-cells. *PLoS One* **7,** e29807 (2012).

445. Tafreshi, N. K., Lloyd, M. C., Bui, M. M., Gillies, R. J. & Morse, D. L. Carbonic anhydrase IX as an imaging and therapeutic target for tumors and metastases. *Subcell. Biochem.* **75,** 221–54 (2014).

446. Vander Heiden, M. G., Cantley, L. C. & Thompson, C. B. Understanding the Warburg Effect: The Metabolic Requirements of Cell Proliferation. *Science (80-.).* **324,** (2009).

447. Technologies, A. Agilent Seahorse XF Cell Mito Stress Test Kit User Guide Kit 103015-100 Notices Manual Part Number Kit Part Number Technology Licenses Restricted Rights Legend.

448. Tatum, J. L. *et al.* Hypoxia: importance in tumor biology, noninvasive measurement by imaging, and value of its measurement in the management of cancer therapy. *Int. J. Radiat. Biol.* **82,** 699–757 (2006).

449. Koukourakis, M. I., Giatromanolaki, A., Simopoulos, C., Polychronidis, A. & Sivridis, E. Lactate dehydrogenase 5 (LDH5) relates to up-regulated hypoxia inducible factor pathway and metastasis in colorectal cancer. *Clin. Exp. Metastasis* **22,** 25–30 (2005).

450. Hagland, H. R. & Søreide, K. Cellular metabolism in colorectal carcinogenesis: Influence of lifestyle, gut microbiome and metabolic pathways. *Cancer Lett.* **356,** 273–280 (2015).

451. Yeh, C. S. *et al.* Significance of the glycolytic pathway and glycolysis related-genes in tumorigenesis of human colorectal cancers. *Oncol Rep* **19,** 81–91 (2008).

452. Kawada, K., Toda, K. & Sakai, Y. Targeting metabolic reprogramming in KRAS-driven cancers. *Int. J. Clin. Oncol.* (2017). doi:10.1007/s10147-017-1156-4

453. Yun, J. *et al.* Glucose deprivation contributes to the development of KRAS pathway mutations in tumor cells. *Science* **325,** 1555–9 (2009).

454. Vernieri, C. *et al.* Targeting Cancer Metabolism: Dietary and Pharmacologic Interventions. *Cancer Discov.* **6,** 1315–1333 (2016).

455. Gill, K. S. *et al.* Glycolysis inhibition as a cancer treatment and its role in an anti-tumour immune response. *Biochim. Biophys. Acta - Rev. Cancer* **1866,** 87–105 (2016).

456. Granchi, C. & Minutolo, F. Anticancer agents that counteract tumor glycolysis. *ChemMedChem* **7,** 1318–50 (2012).

457. Losi, L., Baisse, B., Bouzourene, H. & Benhattar, J. Evolution of intratumoral genetic heterogeneity during colorectal cancer progression. *Carcinogenesis* **26,** 916–922 (2004).

458. Muñoz-Pinedo, C., Ruiz-Ruiz, C., Ruiz de Almodóvar, C., Palacios, C. & López-Rivas, A. Inhibition of glucose metabolism sensitizes tumor cells to death receptor-triggered apoptosis through enhancement of death-inducing signaling complex formation and apical procaspase-8 processing. *J. Biol. Chem.* **278,** 12759–68 (2003).

459. Graham, N. A. *et al.* Glucose deprivation activates a metabolic and signaling amplification loop leading to cell death. *Mol. Syst. Biol.* **8,** 589 (2012).

460. Zhao, Y., Wieman, H. L., Jacobs, S. R. & Rathmell, J. C. Mechanisms and methods in glucose metabolism and cell death. *Methods Enzymol.* **442,** 439–57 (2008).

461. Wise, D. R. & Thompson, C. B. Glutamine addiction: a new therapeutic target in cancer. *Trends Biochem. Sci.* **35,** 427–33 (2010).

462. Fan, J. *et al.* Glutamine-driven oxidative phosphorylation is a major ATP source in transformed mammalian cells in both normoxia and hypoxia. *Mol. Syst. Biol.* **9,** 712 (2013).

463. Kwon, S. J. & Lee, Y. J. Effect of Low Glutamine/Glucose on Hypoxia-Induced Elevation of Hypoxia-Inducible Factor-1 in Human Pancreatic Cancer MiaPaCa-2 and Human Prostatic Cancer DU-145 Cells. *Clin. Cancer Res.* **11,** 4694–4700 (2005).

464. Vordermark, D. *et al.* Glucose requirement for hypoxic accumulation of hypoxia-inducible factor-1α (HIF-1α). *Cancer Lett.* **230,** 122–133 (2005).

465. Semenza, G. L. HIF-1: upstream and downstream of cancer metabolism. *Curr Opin Genet Dev* **20,** 51–56 (2010).

466. Hammond, E. M., Kaufmann, M. R. & Giaccia, A. J. Oxygen sensing and the DNA-damage response. *Curr. Opin. Cell Biol.* **19,** 680–4 (2007).

467. Lees-Miller, S. P. Fumarate in DNA repair. *Nat. Cell Biol.* **17,** 1096–1097 (2015).

468. Wentzel, J. F. *et al.* Exposure to high levels of fumarate and succinate leads to apoptotic cytotoxicity and altered global DNA methylation profiles in vitro. *Biochimie* **135,** 28–34 (2017).

469. Paddenberg, R. *et al.* Essential role of complex II of the respiratory chain in hypoxia-induced ROS generation in the pulmonary vasculature. *Am. J. Physiol. - Lung Cell. Mol. Physiol.* **284,** (2003).

470. Tseng, C.-P., Yu, C.-C., Lin, H.-H., Chang, C.-Y. & Kuo, J.-T. Oxygen- and Growth Rate-Dependent Regulation of Escherichia coli Fumarase (FumA, FumB, and FumC) Activity. *J. Bacteriol.* **183,** 461–467 (2001).

471. Takeuchi, T., Schumacker, P. T. & Kozmin, S. A. Identification of fumarate hydratase inhibitors with nutrient-dependent cytotoxicity. *J. Am. Chem. Soc.* **137,**

564–7 (2015).

472. Rossignol, R. *et al.* Energy substrate modulates mitochondrial structure and oxidative capacity in cancer cells. *Cancer Res.* **64,** 985–93 (2004).

473. Boohaker, R. J., Zhang, G., Carlson, A. L., Nemec, K. N. & Khaled, A. R. BAX supports the mitochondrial network, promoting bioenergetics in nonapoptotic cells. *Am. J. Physiol. Cell Physiol.* **300,** C1466-78 (2011).

474. McIntyre, A. *et al.* Carbonic anhydrase IX promotes tumor growth and necrosis in vivo and inhibition enhances anti-VEGF therapy. *Clin. Cancer Res.* **18,** 3100–11 (2012).

475. Courtnay, R. *et al.* Cancer metabolism and the Warburg effect: the role of HIF-1 and PI3K. *Mol. Biol. Rep.* **42,** 841–851 (2015).

476. Ionov, Y., Yamamoto, H., Krajewski, S., Reed, J. C. & Perucho, M. Mutational inactivation of the proapoptotic gene BAX confers selective advantage during tumor clonal evolution. *Proc. Natl. Acad. Sci.* **97,** 10872–10877 (2000).

477. Karbowski, M., Norris, K. L., Cleland, M. M., Jeong, S.-Y. & Youle, R. J. Role of Bax and Bak in mitochondrial morphogenesis. *Nature* **443,** 658–662 (2006).

478. Youle, R. J. & van der Bliek, A. M. Mitochondrial Fission, Fusion, and Stress. *Science (80-.).* **337,** (2012).

479. Rossignol, R. *et al.* Energy Substrate Modulates Mitochondrial Structure and Oxidative Capacity in Cancer Cells. *Cancer Res.* **64,** (2004).

480. Bayley, J. P., Launonen, V. & Tomlinson, I. P. The FH mutation database: an online database of fumarate hydratase mutations involved in the MCUL (HLRCC) tumor syndrome and congenital fumarase deficiency. *BMC Med Genet* **9,** 20 (2008).

481. Gillies, R. J., Robey, I. & Gatenby, R. A. Causes and Consequences of Increased Glucose Metabolism of Cancers. *J. Nucl. Med.* **49,** 24S–42S (2008).

482. Solaini, G., Baracca, A., Lenaz, G. & Sgarbi, G. Hypoxia and mitochondrial oxidative metabolism. *Biochim. Biophys. Acta - Bioenerg.* **1797,** 1171–1177 (2010).

483. Wang, Z. *et al.* mTOR Co-Targeting in Cetuximab Resistance in Head and Neck Cancers Harboring PIK3CA and RAS Mutations. *JNCI J. Natl. Cancer Inst.* **106,** dju215-dju215 (2014).

484. Amendt, C., Staub, E., Friese-Hamim, M., Störkel, S. & Stroh, C. Association of EGFR expression level and cetuximab activity in patient-derived xenograft models of human non-small cell lung cancer. *Clin. Cancer Res.* **20,** 4478–87 (2014).

485. Karapetis, C. S. *et al. K-ras* Mutations and Benefit from Cetuximab in Advanced Colorectal Cancer. *N. Engl. J. Med.* **359,** 1757–1765 (2008).

486. Prewett, M. *et al.* Tumors established with cell lines selected for oxaliplatin resistance respond to oxaliplatin if combined with cetuximab. *Clin Cancer Res* **13,** 7432–7440 (2007).

487. Balin-Gauthier, D. *et al.* Cetuximab potentiates oxaliplatin cytotoxic effect through a defect in NER and DNA replication initiation. *Br. J. Cancer* **98,** 120–128 (2008).

488. Tabernero, J. *et al.* Phase II trial of cetuximab in combination with fluorouracil, leucovorin, and oxaliplatin in the first-line treatment of metastatic colorectal cancer. *J Clin Oncol* **25,** 5225–5232 (2007).

489. Sobrero, A. F. *et al.* EPIC: phase III trial of cetuximab plus irinotecan after fluoropyrimidine and oxaliplatin failure in patients with metastatic colorectal cancer. *J. Clin. Oncol.* **26,** 2311–9 (2008).

490. Van Cutsem, E. *et al.* Cetuximab and Chemotherapy as Initial Treatment for Metastatic Colorectal Cancer. *N. Engl. J. Med.* **360,** 1408–1417 (2009).

491. Bokemeyer, C. *et al.* Fluorouracil, Leucovorin, and Oxaliplatin With and Without Cetuximab in the First-Line Treatment of Metastatic Colorectal Cancer. *J. Clin. Oncol.* **27,** 663–671 (2009).

492. Peeters, M. *et al.* Randomized Phase III Study of Panitumumab With Fluorouracil, Leucovorin, and Irinotecan (FOLFIRI) Compared With FOLFIRI Alone As Second-Line Treatment in Patients With Metastatic Colorectal Cancer. *J. Clin. Oncol.* **28,** 4706–4713 (2010).

493. Cunningham, D. *et al.* Cetuximab Monotherapy and Cetuximab plus Irinotecan in Irinotecan-Refractory Metastatic Colorectal Cancer. *N. Engl. J. Med.* **351,** 337–345 (2004).

494. Maughan, T. S. *et al.* Addition of cetuximab to oxaliplatin-based first-line combination chemotherapy for treatment of advanced colorectal cancer: results of the randomised phase 3 MRC COIN trial. *Lancet (London, England)* **377,** 2103–14 (2011).

495. Tveit, K. M. *et al.* Phase III Trial of Cetuximab With Continuous or Intermittent Fluorouracil, Leucovorin, and Oxaliplatin (Nordic FLOX) Versus FLOX Alone in First-Line Treatment of Metastatic Colorectal Cancer: The NORDIC-VII Study. *J. Clin. Oncol.* **30,** 1755–1762 (2012).

496. Nordlinger, B. *et al.* Perioperative chemotherapy with FOLFOX4 and surgery versus surgery alone for resectable liver metastases from colorectal cancer (EORTC Intergroup trial 40983): a randomised controlled trial. *Lancet* **371,** 1007–1016 (2008).

497. Dahan, L., Sadok, A., Formento, J.-L., Seitz, J. F. & Kovacic, H. Modulation of cellular redox state underlies antagonism between oxaliplatin and cetuximab in human colorectal cancer cell lines. *Br. J. Pharmacol.* **158,** 610–20 (2009).

498. Yamaguchi, H. *et al.* Caspase-independent cell death is involved in the negative effect of EGF receptor inhibitors on cisplatin in non-small cell lung cancer cells. *Clin. Cancer Res.* **19,** 845–54 (2013).

499. Orcutt, K. P. *et al.* Erlotinib-mediated inhibition of EGFR signaling induces

metabolic oxidative stress through NOX4. *Cancer Res.* **71,** 3932–40 (2011).

500. Hussain, S. P., Hofseth, L. J. & Harris, C. C. Radical causes of cancer. *Nat. Rev. Cancer* **3,** 276–285 (2003).

501. Hamanaka, R. B. & Chandel, N. S. Warburg Effect and Redox Balance. *Science (80-.).* **334,** 1219–1220 (2011).

502. Giannoni, E., Parri, M. & Chiarugi, P. EMT and oxidative stress: a bidirectional interplay affecting tumor malignancy. *Antioxid. Redox Signal.* **16,** 1248–63 (2012).

503. Szatrowski, T. P. & Nathan, C. F. Production of Large Amounts of Hydrogen Peroxide by Human Tumor Cells. *Cancer Res.* **51,** (1991).

504. Meitzler, J. L. *et al.* NADPH Oxidases: A Perspective on Reactive Oxygen Species Production in Tumor Biology. *Antioxid. Redox Signal.* **20,** 2873–2889 (2014).

505. Lander, H. M. An essential role for free radicals and derived species in signal transduction. *FASEB J.* **11,** 118–24 (1997).

506. Itoh, T. *et al.* Cisplatin induces production of reactive oxygen species via NADPH oxidase activation in human prostate cancer cells. *Free Radic. Res.* **45,** 1033–1039 (2011).

507. Mahajan, K. & Mahajan, N. P. Cross talk of tyrosine kinases with the DNA damage signaling pathways. *Nucleic Acids Res.* **43,** 10588–10601 (2015).

508. Yang, X. *et al.* Cetuximab-mediated tumor regression depends on innate and adaptive immune responses. *Mol. Ther.* **21,** 91–100 (2013).

509. Douillard, J.-Y. *et al.* Randomized, Phase III Trial of Panitumumab With Infusional Fluorouracil, Leucovorin, and Oxaliplatin (FOLFOX4) Versus FOLFOX4 Alone As First-Line Treatment in Patients With Previously Untreated Metastatic Colorectal Cancer: The PRIME Study. *J. Clin. Oncol.* **28,** 4697–4705 (2010).

510. Kulkarni, R. A. *et al.* A chemoproteomic portrait of the oncometabolite fumarate. *bioRxiv* 285759 (2018). doi:10.1101/285759

511. Atlas, H. P. FH Pathology. Available at: https://www.proteinatlas.org/ENSG00000091483-FH/pathology. (Accessed: 4th March 2018)

512. Cardel, M., Jensen, S. M., Pottegard, A., Jorgensen, T. L. & Hallas, J. Long-term use of metformin and colorectal cancer risk in type II diabetics: a population-based case-control study. *Cancer Med* **3,** 1458–1466 (2014).

513. Song, C. W. *et al.* Metformin kills and radiosensitizes cancer cells and preferentially kills cancer stem cells. *Sci Rep* **2,** 362 (2012).

514. Villarreal-Garza, C. *et al.* Impact of diabetes and hyperglycemia on survival in advanced breast cancer patients. *Exp Diabetes Res* **2012,** 732027 (2012).